NCHRP
REPORT 461

NATIONAL COOPERATIVE HIGHWAY RESEARCH PROGRAM

Static and Dynamic Lateral Loading of Pile Groups

TRANSPORTATION RESEARCH BOARD

NATIONAL RESEARCH COUNCIL

NATIONAL COOPERATIVE HIGHWAY RESEARCH PROGRAM

NCHRP REPORT 461

Static and Dynamic Lateral Loading of Pile Groups

D. A. BROWN
Auburn University
Auburn, AL

M. W. O'NEILL
University of Houston
Houston, TX

M. HOIT
M. MCVAY
University of Florida
Gainesville, FL

M. H. EL NAGGAR
University of Western Ontario
Ontario, Canada

AND

S. CHAKRABORTY
Auburn University
Auburn, AL

SUBJECT AREAS
Bridges, Other Structures, and Hydraulics and Hydrology • Soils, Geology, and Foundations

Research Sponsored by the American Association of State Highway and Transportation Officials
in Cooperation with the Federal Highway Administration

TRANSPORTATION RESEARCH BOARD — NATIONAL RESEARCH COUNCIL

NATIONAL ACADEMY PRESS
WASHINGTON, D.C. — 2001

NATIONAL COOPERATIVE HIGHWAY RESEARCH PROGRAM

Systematic, well-designed research provides the most effective approach to the solution of many problems facing highway administrators and engineers. Often, highway problems are of local interest and can best be studied by highway departments individually or in cooperation with their state universities and others. However, the accelerating growth of highway transportation develops increasingly complex problems of wide interest to highway authorities. These problems are best studied through a coordinated program of cooperative research.

In recognition of these needs, the highway administrators of the American Association of State Highway and Transportation Officials initiated in 1962 an objective national highway research program employing modern scientific techniques. This program is supported on a continuing basis by funds from participating member states of the Association and it receives the full cooperation and support of the Federal Highway Administration, United States Department of Transportation.

The Transportation Research Board of the National Research Council was requested by the Association to administer the research program because of the Board's recognized objectivity and understanding of modern research practices. The Board is uniquely suited for this purpose as it maintains an extensive committee structure from which authorities on any highway transportation subject may be drawn; it possesses avenues of communications and cooperation with federal, state and local governmental agencies, universities, and industry; its relationship to the National Research Council is an insurance of objectivity; it maintains a full-time research correlation staff of specialists in highway transportation matters to bring the findings of research directly to those who are in a position to use them.

The program is developed on the basis of research needs identified by chief administrators of the highway and transportation departments and by committees of AASHTO. Each year, specific areas of research needs to be included in the program are proposed to the National Research Council and the Board by the American Association of State Highway and Transportation Officials. Research projects to fulfill these needs are defined by the Board, and qualified research agencies are selected from those that have submitted proposals. Administration and surveillance of research contracts are the responsibilities of the National Research Council and the Transportation Research Board.

The needs for highway research are many, and the National Cooperative Highway Research Program can make significant contributions to the solution of highway transportation problems of mutual concern to many responsible groups. The program, however, is intended to complement rather than to substitute for or duplicate other highway research programs.

Note: The Transportation Research Board, the National Research Council, the Federal Highway Administration, the American Association of State Highway and Transportation Officials, and the individual states participating in the National Cooperative Highway Research Program do not endorse products or manufacturers. Trade or manufacturers' names appear herein solely because they are considered essential to the object of this report.

NCHRP REPORT 461

Project E24-9 FY'97

ISSN 0077-5614

ISBN 0-309-06712-X

Library of Congress Control Number 2001-135525

Price $34.00

NOTICE

The project that is the subject of this report was a part of the National Cooperative Highway Research Program conducted by the Transportation Research Board with the approval of the Governing Board of the National Research Council. Such approval reflects the Governing Board's judgment that the program concerned is of national importance and appropriate with respect to both the purposes and resources of the National Research Council.

The members of the technical committee selected to monitor this project and to review this report were chosen for recognized scholarly competence and with due consideration for the balance of disciplines appropriate to the project. The opinions and conclusions expressed or implied are those of the research agency that performed the research, and, while they have been accepted as appropriate by the technical committee, they are not necessarily those of the Transportation Research Board, the National Research Council, the American Association of State Highway and Transportation Officials, or the Federal Highway Administration, U.S. Department of Transportation.

Each report is reviewed and accepted for publication by the technical committee according to procedures established and monitored by the Transportation Research Board Executive Committee and the Governing Board of the National Research Council.

Published reports of the

NATIONAL COOPERATIVE HIGHWAY RESEARCH PROGRAM

are available from:

Transportation Research Board
National Research Council
2101 Constitution Avenue, N.W.
Washington, D.C. 20418

and can be ordered through the Internet at:

http://www.national-academies.org/trb/bookstore

Printed in the United States of America

FOREWORD

By Staff
Transportation Research Board

This report contains the findings of a study to develop and validate an improved design method for pile groups under static and dynamic lateral loads. The report includes recommendations for estimating the distribution of load to piles in a group and provides guidance on analytical methods for predicting dynamic response. The material in this report will be of immediate interest to bridge engineers and geotechnical engineers involved in designing pile and drilled shaft foundations to resist lateral loads.

The principal force experienced in transportation structures during an earthquake, a hurricane, or a vessel impact is transient horizontal loading. These loads must be transmitted to the structure's foundation. State-of-the-practice design for lateral loading of pile and drilled shaft foundations uses beam-on-elastic-foundation analysis. In this analysis, load shedding from a pile to the soil is represented by "*p-y* springs" in which the soil response is modeled as a series of discrete nonlinear springs. The *p-y* springs currently used in these analyses were developed primarily to determine the load-shedding behavior of single piles subjected to static loads. The use of *p-y* springs in the analyses of pile groups subjected to static and dynamic lateral loads had not been validated.

The objective of this research was to evaluate and extend current design methods for groups of piles and groups of drilled shafts subjected to lateral loads associated with earthquakes, hurricanes, and vessel impacts. Under NCHRP Project 24-09, Auburn University conducted experimental and analytical studies of pile groups. Through a series of field tests, the researchers determined the distribution of lateral loads to the individual piles in a group and verified that the pile-group response can be predicted analytically using *p-y* springs. Experimentally determined multipliers are used to adjust the magnitude of load carried by each row of piles in the group. The findings from this research could significantly increase confidence in and reduce the cost of foundations subjected to dynamic loads.

CONTENTS

AUTHOR ACKNOWLEDGMENTS

The research reported herein was performed under NCHRP Project 24-9 by Auburn University. Dr. Dan A. Brown was principal investigator and senior author of this report. Subcontractors were the University of Florida, where Dr. Marc Hoit was research supervisor and co-author of this report; the University of Western Ontario, where Dr. Hesham El Naggar was research supervisor and co-author of this report; and the University of Houston, where Dr. Michael O'Neill was co-principal investigator and co-author of this report. The authors are grateful to Dr. Donald Anderson of CH2M Hill for providing technical review; to Dr. An-Bin Huang of the National Chao-Tung University of Hsinchu, Taiwan, for providing the data for the Taiwan load tests; to Xianfeng Zhang for performing the analysis of the Taiwan load tests; to Mark Williams of the University of Florida for his work with FLPIER; and to Lijun Sin of Auburn University for her assistance with data analysis.

STATIC AND DYNAMIC LATERAL LOADING OF PILE GROUPS

SUMMARY

Groups of piles, commonly used to support bridge structures, are frequently subjected to lateral loadings during extreme events, such as vessel impacts and earthquakes. There is evidence that during past extreme-event loadings, pile group foundations have undergone lateral translations severe enough to cause loss of bearing support for superstructure elements and, on rare occasions, structural failure in the piles. Current design methods for deep foundations for highway structures most often involve making an estimate of the ratio of shear load to lateral deflection for the group as a whole and using this constant stiffness ratio as an input to model the foundation in linear modal analysis computer codes to analyze the structural response, especially for seismic loading. The code also outputs the dynamic loads on the foundations. For critical structures, nonlinear pushover analyses are then conducted on the substructure and foundation to ensure that there is adequate ductile reserve at these loads to preclude complete collapse.

However, lateral pile foundation response to static or dynamic loading is nonlinear, often considerably so. It is therefore more desirable to analyze the foundation and substructure considering this nonlinearity and either to couple such a nonlinear analysis method with a nonlinear superstructure analysis code, or to use a nonlinear foundation analysis code independently, iterating with the superstructure analysis code until the loads assumed to act on the foundation for determining equivalent linear foundation stiffnesses equal the loads exerted on the foundation from the superstructure analysis.

In this project, several full-scale field tests were conducted on pile groups of 6 to 12 piles, both bored and driven, in relatively soft cohesive and cohesionless soils. All of the groups were loaded laterally statically to relatively large deflections, and groups of instrumented pipe piles were also loaded dynamically to large deflections, equivalent to deflections that might be suffered in major ship impact and seismic events. Dynamic loading was provided by a series of impulses of increasing magnitude using a horizontally mounted Statnamic device. Although such loading did not capture the aspects of lateral loading and ground shaking that may generate high pore water pressures, it did capture the damping that occurs at very large pile deflections and the inertial effects of the problem.

A dynamic version of the computer code FLPIER (the Florida Pier program)—FLPIER(D)—was developed in parallel with the field tests. This program has the capa-

bility of modeling complete hysteresis in the soil surrounding the piles via *p-y* curves, as well as cracking and hysteresis in the structural components of the pile group, inertia in the structural components, viscous damping in the soil, lateral group action by the application of adjustment factors for the *p-y* curves (termed "*p*-multipliers"), loading of the piles directly through vibrating soil, and simple superstructure feedback (i.e., inertia) loads. FLPIER(D) was used mainly to interpret the results of the field tests. The results of this interpretation can be used in similar codes that simulate the dynamic behavior of systems of piles and coupled pile-structure systems.

Simultaneously with the development of FLPIER(D), separate analytical solutions were also developed for dynamic *p-y* curves and simplified dynamic *p*-multipliers for piles in cohesionless soils, as well as for frequency-dependent damping in the soil. These solutions were programmed into FLPIER(D). The *p-y* curves, however, were non-hysteretic. Although the option to use the *p-y* curves is available in FLPIER(D), the curves were not used in the interpretation of the dynamic field load tests. Through analysis of the full-scale field load tests with FLPIER(D), it was found that use of both (1) *p-y* curves that are prescribed in standard programs for static (i.e., noncyclic) loading, modified to simulate unloading, reloading, and gap development, and (2) default values of static *p*-multipliers that were derived from a review of many historical static lateral group loading tests and given in the help files of FLPIER were reasonably accurate in simulating the initial load-deformation response and subsequent free vibration of groups of piles loaded with the Statnamic impulse device to large lateral deflections. In general, the computed group response was in reasonable agreement with the measured response.

FLPIER(D), or any other program that uses *p*-multipliers that are defined row-by-row, outputs shear and moment diagrams that are constant from pile to pile in each row. That is, the shear and moment diagrams are averages for piles in a given row. However, measurements of shear and moment, while indicating average row-wise values that were near those predicted by FLPIER(D), were quite variable. This variability was apparently caused by point-to-point variations in lateral stiffness of the soil within the pile groups and other random factors such as inadvertent minor batter of plumb piles. In order to account for these random effects, a load factor of approximately 1.2 should be applied to the computed maximum bending moments in the piles when the piles are designed structurally.

It is also suggested that, for assessing pile group stiffness, it is quite acceptable to use an average *p*-multiplier for all piles in the group, rather than defining *p*-multipliers row-by-row, as is the standard practice. Use of a single average group effect parameter (i.e., *p*-multiplier) is justified for seismic loading on the basis that the direction of loading changes, constantly and often unpredictably, during the loading event and that load reversals occur, converting "leading" rows of piles (i.e., high *p*-multipliers) instantaneously into "trailing rows" (i.e., low *p*-multipliers).

In regard to the testing method and load test components, impulse loading by the Statnamic device was found to be a feasible way to test the pile groups economically by applying dynamic loads that produced large deflections and by inducing vibrations in the pile groups at natural periods of 2 to 4 Hz. It is recommended that in future tests, the piles be tied together at their heads by cast-in-place reinforced concrete caps rather than by the steel frame first envisioned by the research team. The Statnamic device and the instrumented test piles used on this research project are available for future use to assist state departments of transportation in the design of laterally loaded pile groups on production-level projects.

CHAPTER **1**

INTRODUCTION AND RESEARCH APPROACH

INTRODUCTION

A key concern of bridge engineers is the design and performance of pile group foundations under lateral loading events, such as ship or ice impacts and earthquakes. This report documents a research program in which the following were developed: (1) a numerical model to simulate static and dynamic lateral loading of pile groups, including structural and soil hysteresis and energy dissipation through radiation; (2) an analytical soil model for nonlinear unit soil response against piles (i.e., *p-y* curves) for dynamic loading and simple factors (i.e., *p*-multipliers) to permit their use in modeling groups of piles; (3) experimental data obtained through static and dynamic testing of large-scale pile groups in various soil profiles; and (4) preliminary recommendations for expressions for *p-y* curves, damping factors, and *p*-multipliers for analysis of laterally loaded pile groups for design purposes. The report also describes experimental equipment for performing site-specific, static, and dynamic lateral load tests on pile groups.

Background

Observations made during two recent earthquakes in California, the 1989 Loma Prieta and the 1994 Northridge events, as well as during the 1995 Hanshin-Awaji earthquake near Kobe, Japan, and the 1999 Chi-Chi earthquake in central Taiwan, provide clear evidence of the types of damage that occur in pile foundations and in the structures that they support.

Bridge Performance—Loma Prieta Earthquake

During the Loma Prieta earthquake of October 17, 1989, significant damage occurred to bridges located in the five-county area near the earthquake epicenter south of San Francisco. Of the approximately 1,500 bridges located in the five-county area, more that 80 suffered minor damage, 10 needed temporary supports, and 10 were closed because of major structural damage (*1*). The cost to restore these structures to their pre-earthquake operational capacity was estimated at between $1.8 and $2.0 billion.

The greatest bridge damage occurred to older structures on soft ground. Collapses of the Cypress Street viaduct and a link span for the San Francisco–Oakland Bay Bridge are the most well-known examples of this damage. The death toll from the Cypress Street viaduct collapse was 42. It is also reported that other bridges of similar design would have collapsed if the ground shaking had lasted longer.

Ground motions for the bridges damaged in Loma Prieta were often surprisingly low (e.g., less than 0.2 g). Typically, the bridges were supported on pile foundations (e.g., cast-in-drill-hole [CIDH] and timber piles). It was inferred from discussions with Caltrans' engineers that many of the bridge foundations were supported by groups of piles located at spacing ratios of three-to-five pile diameters.

Structural damage to the pile foundation systems for bridges during the Loma Prieta event was apparently limited. Shear failure occurred near the heads of some piles in the Struve Slough bridges near Watsonville. This failure was attributed to large ground deformation resulting from liquefaction. In most cases, however, amplification of the bedrock acceleration and relative displacement of the ground and bridge structure were generally the principal causes of damage. Some pile group foundations, particularly at the Port of Oakland, showed evidence of structural distress when a few batter piles were used. The bents attracted lateral load, evidently because the batter piles were stiff with respect to lateral loading compared with the vertical piles in the group.

Bridge Performance—Northridge Earthquake

During the Northridge earthquake (in the Los Angeles metropolitan area) of January 17, 1994, 7 highway bridges suffered partial collapses, and another 170 bridges suffered damage ranging from minor cracking to the slumping of abutment fills. One life was lost, and several injuries were the direct consequence of these failures (*2, 3*). The total repair cost for the damaged bridges was estimated to be about $150,000,000 (*4*). Most of the damaged bridges had been designed with pre-1971 design standards.

Peak ground accelerations were much higher for the Northridge event than were those for the Loma Prieta event, exceeding 1 g close to the epicentral area. Soils were, however, typically stronger than the soils associated with damage during the Loma Prieta event. The damaged bridges were supported on piles (e.g., primarily 406- to 610-mm- [16- to 24-in.-] diameter CIDH piles, but including H-piles and drilled shafts up to

3.66 m [12 ft] in diameter) or combinations of piles and spread footings.

The only bridge where pile damage was possibly noted was the Los Virgenes Bridge on U.S. Route 101. Most of the damage seemed to result from span displacements that exceeded girder seat widths or excessive forces in columns that supported the bridge deck. At one bridge location, the S.R. 14/ I-5 separation and overhead structure, spatial variation in ground motion from support to support was suspected of being a contributor to bridge damage.

Bridge Performance—Hanshin-Awaji Earthquake

The Hanshin-Awaji earthquake occurred on January 17, 1995, near the city of Kobe, Japan. This earthquake caused more than 5,000 deaths and extensive property damage in a highly urbanized area of Japan (*5*). On the order of 27 highway bridges sustained major damage, and many more suffered moderate-to-minor damage. One estimate of the cost of the damage to one of the agencies operating freeways in the Hanshin area was U.S. $5 billion. Most of the damage was confined to structures built more than 30 years ago and before the introduction of modern seismic codes.

Typical damage sustained by the bridge structures included shear and flexural failures in nonductile concrete columns, flexural and buckling failures in steel columns, steel bearing failures under lateral load, and foundation failures caused by liquefaction. Costantino (*6*) reports that geotechnical observations suggested pile-supported facilities faired well during the event, although some damage was noted, and that significant damage occurred to dock facilities as well, as at connections to pile-supported structures. The caisson-supported seawall on Port Island showed lateral movement at some locations and extensive collapse of pavements immediately in front of the wall. Most of the observations of pile foundation damage were associated with lateral ground displacement (i.e., soil flow).

According to Buckle (*5*), many of the bridges were founded (on piles) and installed in sand-gravel terraces (alluvial deposits), which overlie gravel-sand-mud deposits at depths of less than 10 m. Liquefiable soils were present along the shoreline and in most ports and channels above those founding deposits.

Ishihara (*7*) concluded that some serious damage occurred where bridges were supported on groups of large-diameter (i.e., typically 1 m or greater) bored piles (i.e., drilled shafts) during the Hanshin-Awaji event, which had a Richter magnitude of 7.2 and whose epicenter was less than 10 km from the sites of heavily damaged bridges. The most damaging condition by far was a combination of liquefaction and lateral spreading of the ground surface. Permanent lateral movement of the soil surrounding grouped bored pile foundations in the order of 0.5 to 2.0 m occurred where the groups were located within about 100 m of quay walls that yielded during the earthquake. The permanent lateral movements of the pile heads, which were nominally fixed to the pile caps, were about one-half of the reported permanent ground movements; some were as high as 0.5 m. After the earthquake, the damaged piles were cored, subjected to pulse-echo testing, and excavated partially for examination by remote television cameras. The most severe structural damage in the piles, as evidenced by severe cracking, was found at three locations: (1) at the bottom of the liquefied zone; (2) at the depth at which the reinforcement schedule or cross-section changed; and (3) at the pile heads, where the bending moments were theoretically the highest because the piles were fixed into their caps. Although the piles suffered damage, the structures experienced little damage when the piles were more than 12 m long. Presumably, such piles penetrated well below the zone of liquefaction and lateral soil movement.

Matsui et al. (*8*), who investigated these and other pile group foundations after the Hanshin-Awaji earthquake, stated that pile groups located away from areas in which liquefaction and lateral spreading occurred behaved well structurally, with the exception of the development of tension cracks, which reflect high bending moments, in some concrete piles below the ground surface, especially near the contact between soil zones of high soil stiffness contrast.

Bridge Performance—Chi-Chi Earthquake

An earthquake of Richter magnitude 7.3 struck the central mountain region of Taiwan, near the town of Chi-Chi, on September 21, 1999, causing widespread damage and more than 2,400 deaths. One hundred twenty-one buildings of five stories or higher were damaged so severely that they had to be torn down. Of 457 structures with damaged foundations that were surveyed (i.e., bridges and buildings), 27 percent were discerned to have been damaged by direct movement of one of two causative faults immediately next to or beneath the structure; 15 percent were damaged as the result of ground liquefaction; and 58 percent were damaged because of "superstructure interface" failure—for example, shear failure of plinths and columns or rotation of substructures to the extent that beams and joists fell from their seats or were buckled (*9*). Most of the damaged bridges were near or across the fault breaks and appeared to have been damaged because of superstructure interface problems (*10*).

In the four counties nearest the epicenter, approximately 20 percent of the bridge inventory suffered minor-to-major damage. Damage modes that could possibly be associated with foundation performance included displaced bearings; unseated girders; shear failure in columns, abutment walls, and caissons (i.e., drilled shafts); foundation failures caused by slope movements; joint failures in column-to-girder connections; and liquefaction (*11*). Of 183 distinct damage patterns noted in highway bridges damaged in the Chi-Chi event, 14 (i.e., 8 percent) were identified as structural failures of foundations (*11*), although many of the superstructure failures may have been caused at least partially by excessive movements of founda-

tions. Most of the bridges with major damage were very close to the epicenter, and many even crossed the Chelungpu Fault, one of the two causative faults for this earthquake. In such a case, permanent displacement or rotation of the bent or abutment, or both, were frequently noted. Only two bridges, both at river crossings, were reported to have clearly been damaged because of liquefaction (although the foundations for others may have suffered excessive movement because of elevated pore water pressures in the fine sand and silt alluvium typical in the four-county area). For severely damaged bridges that were not close to a causative fault, failure most often occurred because of loss of seating for girders in simple-span bridges.

Significance of Damage Observations

Bardet et al. (*12*) state that the structural performance of the pile foundations during the Loma Prieta, Northridge, and Hanshin-Awaji (i.e., Kobe) earthquakes appeared to be quite good, with few if any examples of damage being mentioned, except in places in the Kobe area in which there were significant liquefaction and lateral ground spreading. In fact, where there was liquefaction but no lateral spreading of the ground, piles suffered little or no structural damage.

However, although the piles may have survived the earthquakes with little or no damage, many bridge structures in the four earthquakes did not. Forces in and displacements of the damaged structures exceeded allowable values, in some cases leading to collapse of the structures. Because the forces and displacements are directly related to the stiffness of the foundation systems, it is likely that at least some of the observed damage to the structures could have been prevented or minimized by improved modeling of the deformability of the pile foundations during the design process. Many of the pile foundations in the four earthquakes consisted of groups of piles with center-to-center spacing ratios of three-to-five diameters.

A significant cause of bridge failures in the Chi-Chi event was a lack of horizontal restraints at the girder seats, which allowed the girders to slide off their supports. This factor may have also reduced inertial loads on the foundations, which, in turn, may have prevented some structural failures of foundations.

A significant factor contributing to the apparent lack of structural damage in the pile foundations in the California events is Caltrans' design philosophy of limiting maximum design loads applied to the foundation in order to preclude severe inelastic behavior (e.g., without development of plastic hinges within the foundation). This is often achieved by limiting the maximum moment at the connection of the column to the bent cap or to the piled footing (e.g., forcing the plastic hinge to occur there), thereby providing a limiting maximum load to the pile system. Although this approach "protects" the pile system, it does not limit the inertial forces or the displacement that can develop in the structure and therein is an apparent cause of past superstructure damage. Recognizing that foundation systems have, in general, performed well in earthquakes, suggestions have been made that recommend that the next generation of AASHTO seismic design guidelines allows the foundation system to carry more load. If this approach is adopted, it is possible that, following future earthquakes, evidence of at least some structural damage in the pile system will become more prevalent unless design methods are improved.

In order to minimize future damage to bridges during seismic events, a two-step approach to design likely will be included in the AASHTO guidelines. This two-step approach will involve linear dynamic response analyses of the structure at a lower level of earthquake loading—for example, ground response corresponding to return periods of 150 to 200 years (Step 1) and a quasi-static "pushover" or collapse analysis at a higher level of loading, which is currently identified as an event with a return period of approximately 2,500 years (Step 2). For both analyses, the modeling of the foundation system will have a direct effect on the capacity demands within the structural system. The accuracy of the foundation model will, therefore, have direct relevance to the improvement or optimization of bridge performance during seismic loading.

Bardet et al. (*12*), after considering the first three seismic events summarized above, identified several productive areas for research concerning pile foundations in seismic events. At the top of their list were the following:

1. Develop a better understanding of the way the soil is modeled, including the effects of pile-soil-pile interaction in soft ground, including
   - "*p-y*" and "*t-z*" response of soil (which will be defined later) or liquefied ground under extreme event loading conditions;
   - Relations between lateral ground pressures, *p-y* curves, and free-field ground displacements;
   - Lateral loads imposed on pile foundations by lateral ground spreading, including the effects of nonliquefied crustal soil sliding laterally upon layers of liquefied ground; and
   - The influence of site stratigraphy.
2. Evaluate systematically methods of analysis against case histories and refine design and analysis methods.
3. Evaluate design philosophy; specifically, should inelastic behavior of the piles be permitted to occur?

Current Design Practice

1997 Survey of Practice

The interim report for this project (*13*) provided a general overview of current design practice for laterally loaded pile groups, primarily for seismic loading. A brief review of current practice is presented here. First, seismic loads are viewed as being primarily horizontal. Budek et al. (*14*) indicate that common current department of transportation (DOT) practice

for the quasi-elastic lateral-load design of pile foundations and bridge columns for seismic loading is to (1) estimate the lateral stiffness of the foundation (i.e., pile group) under a selected load, so that deflections under that load can be computed; (2) replace the foundation with an extension of the bridge column and select a depth to fixity for that column, assuming linearity, that will give the same lateral displacement at the top of the foundation as that of the foundation; and (3) determine the expected deflections and rotations at the top of the column through appropriate analysis. In order to analyze for stresses in the superstructure, a dynamic, linear modal analysis of the extended column and the structure it supports may be performed. The piles that support the column are then analyzed under the computed loads at the foundation level to ensure that they do not yield structurally, which is usually the desired situation. This may be viewed as Step 1 in the analysis of a foundation for seismic loading. A second step, Step 2, is then sometimes performed to determine the capacity of the foundation at the time plastic failure fully develops. This plastic capacity should exceed the loadings computed from Step 1 by some prescribed amount in order to ensure that adequate ductility is available to prevent total collapse.

At one level of practice, lateral pile group stiffness for a Step 1 analysis is estimated by performing static, elastic subgrade reaction analyses (see Davisson [*15*] for an example) on typical piles within the group using factors that reduce the lateral stiffnesses of the individual piles in the group below the stiffnesses estimated for single, isolated piles in order to account for overlapping strains in the mass of soil in which all of the piles are embedded. The group stiffness is then the sum of the individual pile stiffnesses, and the group stiffness is inserted as a boundary constraint in a linear superstructure modal analysis program without formally computing a depth of fixity for an equivalent column.

Pile stiffness reduction for group action for this approach to design is accomplished in a variety of ways. Many DOT designers use the recommendations given in the U.S. Navy's *Foundations and Earth Structures—Design Manual 7.2 (DM-7)* (*16*) and in the 1985 edition of the *Canadian Foundation Engineering Manual (CFEM)* (*17*). These documents recommend a factor, *R*, to reduce the lateral subgrade modulus acting against group piles (not pile stiffness). AASHTO (*18*) recommends the same reduction factors for drilled shafts, but not explicitly for driven piles. The *DM-7* and *CFEM* factors, which are summarized in Table 1, along with factors recommended by ASCE and the U.S. Army Corps of Engineers (*19*), are not specific to the installation method; the factors are also strictly valid only for static loading conditions, and their origins can be traced to traditions of practice and to small-scale model tests. The most recent edition (1992) of the *CFEM* refers to procedures to estimate group-pile stiffness, based on theory of elasticity, that are suggested by Poulos and Davis (*20*) and others.

On the other hand, PoLam and Martin (*21*) suggested neglecting group effects during seismic loading for sandy soils and introducing as much as a 50-percent reduction in lateral pile stiffness for piles spaced at three diameters on centers or less in soft clays. That recommendation is somewhat inconsistent with Section C4.5.5 of a recent Applied Technology Council report, which states "in view of the uncertainties, it is recommended that group effects be neglected for earthquake loading at three-diameter center-to-center spacing or higher" (*22*, p. 123).

A listing of specific methods for analyzing pile groups statically as linear systems, with and without batter piles, in which the reduced soil or pile stiffness values are used, is given in the interim report (*13*).

Commentary on Current Practice

The conventional design procedure discussed above, although relatively easy to apply, is based on the assumption of linear elasticity in both the superstructure and the foundation; hence, modal analyses are possible. The procedure ignores the fact that both piles and soil can behave in a non-

TABLE 1 Subgrade modulus reduction factors from *DM-7*, *CFEM-1985*, and ASCE

Pile Spacing in Direction of Loading, *D* = Pile Diameter	*DM-7* and *CFEM* Subgrade Reaction Reduction Factors, *R*	U.S. Army Corps of Engineers/ASCE Group Reduction Factor, *R*
8D	1.00	1.00
6D	0.70	0.56
4D	0.40	0.38
3D	0.25	0.33

NOTE: $E_{subgrade}$ (lateral soil subgrade modulus) for a group pile = $R\ E_{subgrade\ isolated\ pile}$

linear manner during an extreme event. Williams et al. (*23*) indicate that linear modal analyses can result in significant errors in the moments and shears in bridge pier columns for certain configurations of piles and certain types of soil. Sometimes, these errors are unconservative. It can be inferred from the paper authored by Williams et al. that linear modal analyses for both the structure and the foundation should be replaced with nonlinear time-domain analyses. This philosophy, however, has not yet been incorporated in design practice, except on occasion for major structures in which designers have redefined iteratively the stiffness of pile foundations based on either the load or displacement computed in the structural analysis at the level of the foundation. The computational model that will be described in this report has the capability of modeling both soil and structural nonlinearities.

Although present design practice presumes to keep group piles from experiencing the development of plastic hinges in order to force structural failures to occur and ductility to develop in the superstructure, design philosophy is turning more toward allowing plastic hinge development in grouped piles during seismic events, specifically at the points at which the pile heads are fixed into the pile footing or bent cap, with secondary hinges at the depth of maximum subsurface bending moment (*14*). Plastic hinge development in piles profoundly affects the piles' stiffness and energy dissipation capacities. It also affects the natural frequencies of the superstructure-foundation system and, thus, the way the structure responds to seismic loading. Budek et al. (*14*) describe the phenomenon of migration of the secondary (i.e., below pile-head) plastic hinges in fixed-headed pile groups from the depth at which the hinges initially develop toward the surface, which can materially affect structural response during a seismic event. This observation again suggests that analyses that consider both the nonlinear behavior of the structural elements (i.e., piles, substructure, and superstructure) and the nonlinear behavior of the supporting soils should be performed if accurate predictions of both pile and structure performance are to be obtained.

Considering the nonlinear nature of soils during extreme events, PoLam et al. (*24*) recommend *p-y* methods for defining the stiffnesses of laterally loaded piles and pile groups for seismic loading. The lateral secant stiffnesses of pile heads (for either single piles or groups) can be developed as functions of head deformations using the *p-y* method. In an iterative Step 1 analysis, the deformations computed from the linear modal analysis of the structure at the top of the foundation (i.e., pile heads) can be matched to a specific linear (i.e., secant) stiffness for the piles that was developed through a nonlinear *p-y* analysis. If that value of stiffness differs from the one assumed in the linear structural analysis, the stiffness is changed and the linear model analysis for the structure is repeated, several times if necessary, until closure is achieved. The *p-y* method models the bending behavior of the pile by either finite difference or finite element techniques and models the soil reaction using nonlinear reaction "springs" (i.e., nonlinear Winkler subgrade springs), which have been derived for static loading in many types of soil and rock semi-empirically (see Reese and Wang [*25*] for an example).

Detailed ways of handling the effects of cyclic soil degradation and the velocity of the pile relative to that of the soil for extreme event loading using a *p-y* soil model are described by PMB Engineering, Inc. (*26*). For example, consider the "backbone" (i.e., static) *p-y* curve (Figure 1). A set of such *p-y* curves for a given pile may be obtained from published criteria or can be measured at a specific site. Values of *p* can then be adjusted tentatively for cyclic degradation using Equation 1:

$$p_c = 10^{\left(\frac{\log 2}{1-N_{50}}\right)}\left(p_p - p_d\right) + p_d \qquad (1)$$

where

p_c = degraded value of *p;*
N_{50} = number of cycles required to degrade the shear strength by 50 percent, which could be estimated from cyclic triaxial tests or similar soil tests;
p_p = *p* on the degraded *p-y* curve for the previous cycle of loading; and
p_d = fully degraded shear strength of the soil, which can also be estimated from triaxial or similar soil tests.

Hysteretic damping can be considered in the *p-y* model by allowing the unloading path to differ from the loading path and to discount soil resistance whenever the pile displacement relative to that of the soil is less than the displacement that

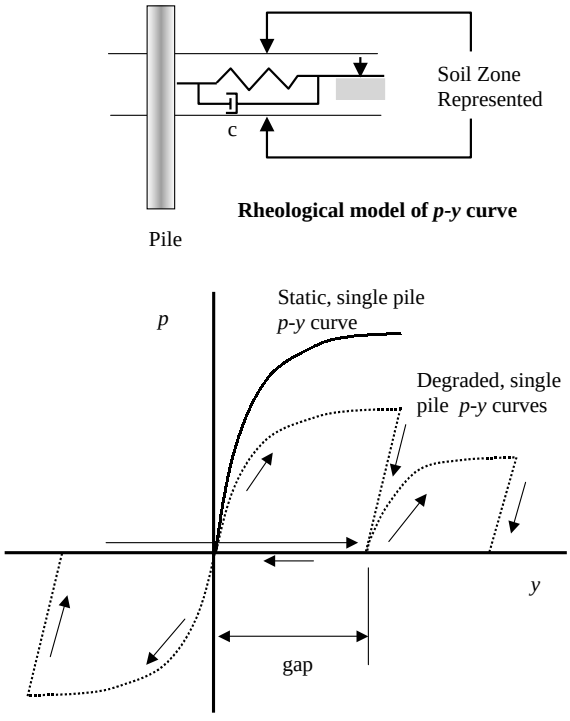

Figure 1. p-y *Method for modeling cyclic degradation and hysteretic damping in soil.*

occurred during the last unloading cycle. This model is also illustrated in Figure 1. Radiation damping can be simulated using a viscous damper (i.e., dashpot) that may be dependent on frequency, displacement, or both.

In the mathematical model of the pile-soil system, the instantaneous velocity of the pile relative to that of the soil is multiplied by c (the damping value) (see Figure 1) to obtain a resisting force per unit length of the pile that is added to the displacement-dependent value of p (i.e., degraded p-y curve). One way of estimating c in Figure 1 is to use Equation 2:

$$c = 2D\frac{\gamma}{g}(v_s + v), \tag{2}$$

where

D = pile diameter,
γ = total unit weight of the soil,
g = acceleration of gravity,
v_s = shear wave velocity of the soil, and
v = average of shear wave and compression wave velocity of the soil.

The p-y method, with consideration of both soil degradation and viscoelastic strength gain, has long been used successfully in the design of piles for offshore structures.

Washington State DOT Method. A more advanced level of design, which is not yet customary in U.S. DOTs, is illustrated by Washington State's DOT (WashDOT) procedure (*27*). This procedure incorporates the p-y method of analysis in a rational way that involves a linear-iterative superstructure analysis. A detailed summary of the development of that procedure, developed for WashDOT by Geospectra, Inc., is given below to serve as a definition of the current high-level state of the practice. The WashDOT procedure recognizes implicitly that the piles in a pile group are loaded along their lengths by the lateral translation of the soil via upward-propagating shear waves produced by seismic motion of the earth at a large depth and at the piles' heads by inertial effects from the vibrating structure that is supported by the piles. These two modes of loading are sometimes referred to as "kinematic" loading and "inertial" loading. The WashDOT method is intended primarily for use in Step 1 of the two-step design approach mentioned earlier.

The WashDOT method includes only stiffness and does not explicitly address foundation damping. The method simplifies and standardizes the procedures for designers by assuming standard earthquake spectra, site conditions, pile types, and layouts. Whether, in standardizing the design process, important effects of differences in these factors at actual construction sites may tend to be overlooked in the interest of simplicity of design remains to be seen.

The WashDOT method recognizes that soil reactions against the piles and the pile cap in the lateral direction occur only when there is relative movement between the piles and the soil in the free field. The free-field motion, as well as the equivalent, strain-based elastic stiffness of the soil, is controlled by base motion in bedrock and details of the soil profile.

The procedure used to develop the stiffness terms for pile groups in this method was as follows:

1. Select seven typical soil profiles that are common in Washington State.
2. Develop 500-year-return-period rock spectra corresponding to peak horizontal ground accelerations of 0.2, 0.3, and 0.4 g and match appropriate recorded acceleration time histories to these spectra.
3. Select six typical foundation types used for typical bridges in the state of Washington and combine these with the seven typical soil profiles to arrive at specific analysis cases. Some of these foundations were single-pile foundations, and some were grouped-pile foundations.
4. Use the computer program SHAKE (*28*) to determine the one-dimensional free-field site response above the elevation of the vibrating rock for all seven soil profiles and for the acceleration time histories determined above that corresponded to the various rock spectra.
5. From the SHAKE analysis, which yields shear strain profiles, determine strain-compatible soil properties (e.g., shear and Young's moduli, shear strength) and establish average soil properties for each of the seven standard soil profiles and for each seismic spectrum.
6. Compute the horizontal stiffnesses (i.e., load/deformation) for a typical single pile as a function of pile-head translation in each foundation group in each typical soil profile for a pinned- or fixed-head condition. The p-y method, referenced above, was used to develop these stiffness values. The pile-head stiffness was defined as shear load/lateral displacement for each of several magnitudes of displacement (i.e., secant stiffness) and is deflection dependent.
7. Compute the vertical stiffness for the typical single pile as a function of pile-head settlement in each foundation group in each typical soil profile. The t-z method, which is similar to the p-y method but for axial loading, was used to develop the pile-head stiffness values. This stiffness was defined as thrust load/axial displacement for each magnitude of axial displacement (i.e., secant stiffness) and is also deflection dependent.
8. Model the lateral and vertical dynamic response of the typical piles and groups using a finite-element program (i.e., SASSI) in order to determine how the loading of one pile affected the stiffness of other piles in a group. These analyses were elastic, but they were also dynamic and so included inertia and stress-wave propagation effects. The software allowed for the consideration of pile-soil-pile interaction during dynamic loading. Individual pile stiffness reduction

factors for static loading were then obtained using elastic methods (see Poulos and Davis [*20*] for an example) for horizontal and vertical loading for every pile in each typical group in each typical soil profile. The dynamic single-pile stiffness terms (i.e., shear/ lateral displacement and thrust/axial movement) computed from the finite element analysis were then modified by these stiffness reduction factors. It was found that the group pile stiffnesses obtained by using the simple static stiffness reduction factors were similar to the pile stiffnesses computed from the finite element program for a period of motion, *T*, exceeding 0.5 s (frequency < 2 Hz). For shorter periods or higher frequencies, the stiffnesses determined for group piles from the linear dynamic finite element analyses differed somewhat from the single-pile dynamic stiffnesses that were modified by the static stiffness reduction factors. A complete set of the dynamic stiffness reduction factors obtained in this step is documented in the referenced report (*27*).

9. Compute the horizontal stiffnesses of the pile group by summing the reduced stiffnesses of the individual piles in the group determined in the above step. Similarly, compute the vertical stiffness of the group by summing the reduced stiffnesses axial stiffnesses for the individual piles determined in the above step.
10. Compute the rocking stiffnesses and torsional stiffness of the group from the stiffness values for the individual piles and their geometric coordinates. (No description is given of how coupling was between lateral and rotational modes; however, cross-coupling values are given in the completed design charts for groups. Norris [*29*] suggests that relatively accurate analyses can be made by neglecting such cross-coupling if the group is small and the piles are slender.)
11. Compute the stiffness of the pile cap versus lateral deflection of the cap by assuming a passive condition against the pile cap (limit equilibrium method).
12. Sum the cap and pile stiffnesses to obtain the overall lateral translational group stiffness.
13. Tabulate the stiffnesses at zero (or very small) displacement and graph the ratios of the stiffnesses of the various groups to the zero-deflection stiffness as a function of pile-cap displacement. These stiffness tables become the design aids, and they are given in *Design Manual for Foundation Stiffnesses Under Seismic Loading* (*27*) in detail for all of the typical foundations for all of the typical soil profiles for each of the typical free-field ground deformations. (This approach allows the designer to vary the stiffness of the pile foundation based on pile-cap deflections computed in the modal analysis of the superstructure, so that displacement-compatible stiffness is achieved in the foundation, even though the analysis is linear.)
14. Use the "strain wedge method" (*30, 31*) to estimate the ground deflections around the group piles that are produced by the lateral translations of the piles. These are compared with the free-field deformation patterns in each soil profile for each base acceleration time. The group stiffness values for lateral translation are then truncated at lateral pile group deflections corresponding to the free-field ground deflections. There are two case scenarios. The horizontal stiffnesses are taken in design as the values corresponding to the target deflection for the pile cap if that target deflection is equal to or greater than the free-field deflection computed by SHAKE (Case 1). If the computed free-field deflection exceeds the deflection targeted for design, the stiffness is evaluated based on the assumption that the pile-cap (and therefore pile-head) displacement is equal to the estimated free-field displacement (Case 2). This decision process allows for approximate consideration of inertial loading (Case 1) and kinematic loading (Case 2).

The linear superstructure analysis is then performed using the resulting stiffnesses at the connection between the column and the pile cap, and the connection deformations are compared with the target deformations from which the pile stiffnesses were developed. If deformations are approximately equal, the computed pile group stiffnesses are satisfactory. If not, they are modified according to the computed values of deflection, using the design tables, and a revised superstructure analysis is made.

Norris (*29*) questions the use of standard *p-y* criteria for developing lateral stiffness terms for the individual piles, citing the fact that pile shape and the presence of the pile cap may affect the *p-y* curves. However, he states that the effects of soil degradation and pile-soil-pile interaction may have a greater effect than do the pile shape and surface conditions; it was therefore considered reasonable from a design perspective to use the *p-y* approach in the research described here.

The WashDOT method also provides normalized bending moment and shear diagrams for typical piles for each of the cases considered. If analysis beyond this step is not required, these diagrams can provide the basis for checking the adequacy of structural capacity of the piles.

For major structures, however, AASHTO requires that the ductility of the structure be shown to be adequate under extreme event loading; this includes the ductility of the foundation system. Methods for performing a ductility evaluation are documented in the interim report (*13*). The computer code FLPIER (the Florida Pier program), developed during the current research project, has the capability of performing a ductility analysis of the substructure.

The *p*-Multiplier Method. In lieu of using dynamic or static soil stiffness reduction factors based on elastic solutions, as was done in the development of the WashDOT procedure, PoLam et al. (*24*) now recommend that pile groups be modeled by applying *p*-multipliers, ρ, which are defined in Figure 2, of 0.5 to static *p-y* curves for piles or drilled shafts in cohesionless or cohesive soils to reflect both group action

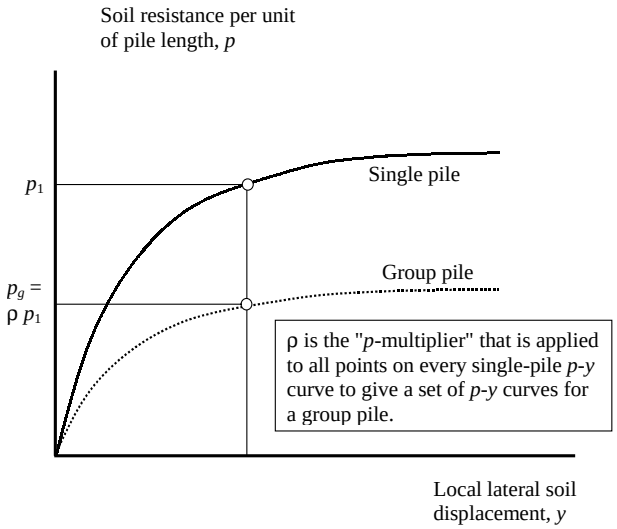

Figure 2. Definition of the p-y *curve and the* p*-multiplier.*

(i.e., stress overlaps) and cyclic degradation of soil around the piles for seismic loading in deposits that do not liquefy. This can be a simple alternative to the explicit PMB Engineering, Inc. method described previously. In addition, this factor takes into account the effects of stress overlaps that occur among the piles in a group because of loading of neighboring piles. Table 2 summarizes typical *p*-multipliers that are used presently for static analyses of pile groups (*32,* p. 223; *33*). On the average, these values are quite close to the value of 0.5 recommended by PoLam et al., indicating that for dynamic, cyclic loading, the combined effects of soil degradation and temporary strength and stiffness gain caused by radiation damping approximately offset one another.

PoLam et al. (*24*) also conclude that the effects of pile-head fixity, variations in bending stiffness in the piles during lateral loading, scour, soil liquefaction, and the formation of gaps between piles and soil during cyclic loading are major issues that need to be considered in pile-group design. That is, the use of *p*-multipliers is only one detail that is significant in the design of laterally loaded pile groups.

Alternative Analysis Methods. Alternative methods for the analysis of laterally loaded pile groups are used by some consultants to state DOTs (*13*). Some of these methods, like the WashDOT method, take account of the effects of stress waves that are generated in the soil by laterally vibrating piles on the stiffness of their neighboring piles. These waves in theory can affect both the stiffness and damping in the soil supporting a given pile in the group. Current practice, however, generally concedes that these effects are small for extreme event loading, in which considerable energy is dissipated through hysteresis rather than through radiation, because only radiation produces stress waves. The model that is proposed in this report does not directly consider stress wave interaction effects.

Liquefaction. In the event that soil in the free field is determined through separate geotechnical analysis to have the potential to liquefy during a loading event such as an earthquake, PoLam et al. (*24*) recommend that *p*-multipliers smaller than 0.5 be used. Such values would come from the evaluation of the strength loss in the soil from free-field pore pressures. Some guidance on these factors is available through small-scale centrifuge experiments on the behavior of piles in liquefied soil (see Dobrey et al. [*34*] or Wilson et al. [*35*] as examples). Ashford and Rollins (*36*) conducted very informative large-scale, slow-cyclic, field lateral-load tests on single piles and pile groups within zones of liquefied sand (which was produced by controlled blasting). For a four-pile (2×2) group of free-headed, 324-mm-diameter steel pipe piles in liquefied soil, the lateral stiffness of the group on the first cycle of loading was reduced to a value of about 0.2 times its stiffness in the same soil prior to liquefaction. For a nine-pile (3×3) group of the same piles, the lateral stiffness of the group in the liquefied soil on the first cycle was reduced to about 0.15 times its stiffness in the same soil mass before liquefaction. These data suggest, as PoLam et al. indi-

TABLE 2 *p*-Multipliers commonly used for static loading

Pile Row	***p*-Multipliers from Peterson and Rollins (*32*)** ***S / D* = 3**	**Default *p*-Multipliers from FLPIER (*33*)** ***S / D* = 3**
Lead	0.6	0.8
First Trail	0.4	0.4
Second Trail	0.4	0.2
Third Trail	0.4	0.3
Average	*0.45*	*0.43*

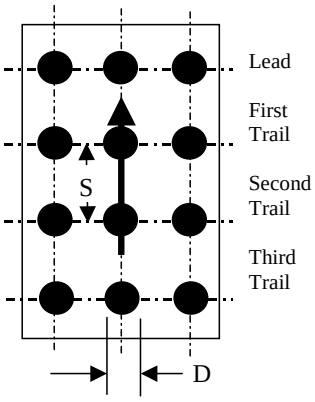

cate, not only that liquefaction has a profound effect on lateral stiffness of the soil-supporting piles in groups, but also that such stiffness does not decrease to zero.

The analysis method that will be pursued in this report, which is based on the *p-y* method, will not explicitly consider liquefied soils. The information from the Chi-Chi earthquake and similar studies has indicated that far less than half of the damaged foundations and superstructure damage resulting from excessive foundation movements occurred in liquefied soils. However, soil strength in the proposed method can be degraded, and *p*-multipliers can be modified empirically to account for the designer's best estimate of loss of soil support because of liquefaction.

Axial Pile Stiffness Modeling. Proper modeling of axial pile response is very important in the analysis of laterally loaded pile groups. Lateral forces applied to the superstructure mobilize axial loads in piles in two ways. First, the forces produce moments about the pile cap that produce rotation of the cap and, therefore, axial compression and tension thrusts in the piles. Second, even if the resultant of loads passes through the centroid of the pile group, any lateral component will cause the cap to translate. If the piles are fixed into the cap with any degree of fixity, "fixing" moments will be produced at the pile heads that will cause the cap to rotate, thus inducing axial thrusts in the piles. The extent to which such cap rotation can produce axial thrusts depends on the axial stiffness of the piles (*37*). In turn, these axial forces affect the pile-head moments, which affect the lateral response (i.e., stiffness) of the pile group.

Norris (*29*) stated that the axial stiffness of piles is different in compression and uplift so that when a pile group rotates under extreme lateral loads, the center of rotation migrates because the piles acting in compression have a different axial stiffness than those acting on the uplifting side of the group. One-half cycle later, the piles that were in compression go into uplift and vice versa, which causes a shift in the location of the axis of rotation. If the migration of the center of rotation is not taken into account in the analysis, the motion of the pile group and the loads on the piles will be computed incorrectly. This is not easily done in a Step 1 analysis unless the method used in the analysis can incorporate different values of stiffness for axial compression and uplift loading. Most current design procedures ignore this effect, and many ignore axial stiffness altogether.

Summary

The realization that nonlinear structural and soil behavior affect the stiffness of laterally loaded pile groups during extreme events, which in turn affects the response of the structure, suggests that an improved, user-friendly, nonlinear model should be developed and employed for designing laterally loaded pile groups for DOT structures in the future. That development and employment effort was the overall goal of this research project. Because of the successful experiences of designers of offshore structures in the use of the *p-y* method, the *p-y* method was selected as the basis of nonlinear soil modeling for the pile-group-superstructure analysis method that was developed for this project. In order for that method to improve practice significantly, it must have the capability of simulating yielding of piles during the extreme event being modeled and simulating the effects of axial loads in piles in the group on lateral behavior, and, per the recommendations of Bardet et al. (*12*), it should permit loads to be applied to the pile-structure system through the soil. It will be possible to model liquefaction implicitly and empirically through user-supplied modifications to the *p-y* curves; however, the computational model will not be developed to analyze the effects of laterally spreading ground.

In order to facilitate the use of this computational model, or similar models that now exist that could conceivably be used for the same purpose, it was desirable to develop a means of defining *p-y* curves and correction factors for *p-y* curves to take account of group action, dynamic loading, and similar effects. That was a major effort in this research project. The *p-y* curves and correction factors such as *p*-multipliers were developed through a combination of analytical modeling and full-scale dynamic field testing, and a means for deriving such factors on a site-specific basis was also devised.

RESEARCH OBJECTIVES

The underlying objective of the research reported herein was to advance the state of design-level practice for laterally loaded pile groups, with a strong focus on extreme-event loading by using and improving upon the current concepts that were described in the previous section. Specific objectives were as follows:

1. Determine experimentally the effect of method of pile installation on *p*-multipliers.
2. Determine appropriate *p-y* curves analytically, including damping factors and *p*-multipliers for harmonic, dynamic loading.
3. Develop a specific, user-friendly numerical model for static and dynamic loading of pile groups. This model will incorporate the capability of using the dynamic *p-y* curves and *p*-multipliers from Objectives 1 and 2 and be capable of modeling (a) extreme nonlinear structural behavior of the piles within the group and full or partial restraint at the pile heads; (b) loading of the piles through the pile cap (as for ship or ice impact loading) and from the pile cap (as for feedback from seismic loading of the foundation); (c) loading of the piles kinematically by the seismically excited soil; and (d) the presence of batter piles in the group.
4. Design, develop, and deploy a reusable pile group that can be installed at various sites by state DOTs to determine directly site-specific and pile-type-specific dynamic stiffness, site-specific and pile-type-specific dynamic *p-y* curves and *p*-multipliers, or both.

5. Perform repetitive impact loading tests upon the pile group (i.e., Objective 4) at two geologically diverse sites and with two geometric configurations for the purposes of evaluating the performance of the group piles and other features of the portable system, and derive experimental *p-y* curves and *p*-multipliers from those tests.

These objectives address the recommendations of the report by Bardet et al. (*12*), except for providing a better understanding of the behavior of laterally loaded pile groups in liquefied soil and the means for modeling the effects of laterally spreading soils.

RESEARCH APPROACH

The research objectives were accomplished by performing the following tasks:

1. Reviewing the literature on design and analysis of laterally loaded pile groups.
2. Reviewing the state of the practice in designing laterally loaded pile groups for extreme events, and developing an initial design for the reusable pile group referred to in Objective 4 in the preceding section.
3. Writing an interim report covering Tasks 1 and 2 (*13*). The salient points in the interim report, except for the design of the reusable test pile group, are summarized in the introduction to Chapter 1 of this report. Drawings of the reusable test pile group are provided in this report.
4. Selecting and testing a numerical model that can be modified to meet Objective 3. Use that model to infer *p*-multipliers for new static lateral loading tests on pile groups—for example, a set of massive group tests conducted recently in Taiwan. The model chosen was FLPIER, developed at the University of Florida, which employs a time-domain analysis of a pile-soil-cap-pier system.
5. Modifying FLPIER to include dynamic loading. The modifications are illustrated in Figure 3. Included in the FLPIER modification are two capabilities. The first is the capability to excite the piles by exciting the supports of *p-y* curves according to time histories of free-field soil motion predicted off-line by SHAKE (*28*) or similar methods; to include mass effects in the piles, pile cap, and supported pier; and to include nonlinearity and hysteretic damping in the *p-y* curves (i.e., soil) and the *M*-Φ relations (piles and other structural elements). The second is the capability to model the development of gaps both in the soil adjacent to a pile after lateral movement of the pile has thrust the soil away from the pile and in the piles, in which, for example, cracks in concrete piles may need to be closed before the section can begin to develop a higher resisting moment. Test the modified version of FLPIER against well-controlled experiments, and validate it against ADINA, a well-known, comprehensive finite element program (*38*).

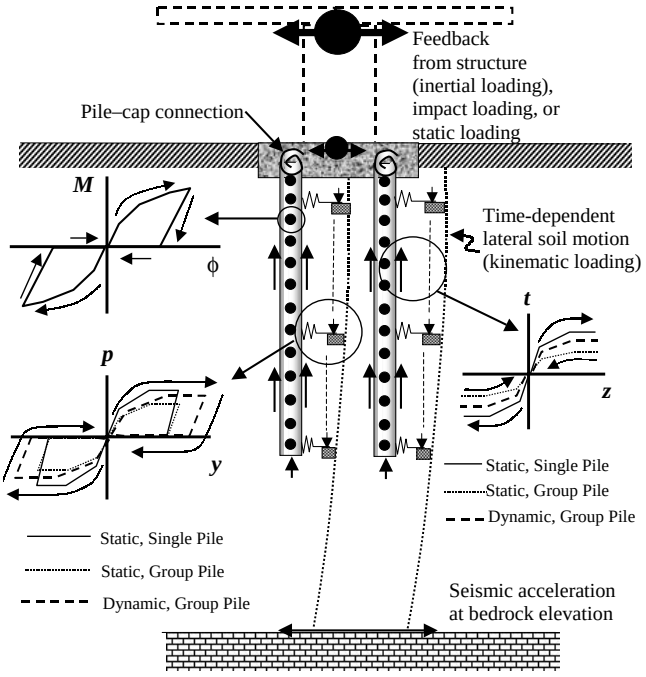

Figure 3. Schematic model for laterally loaded pile groups for this project.

6. Performing field load tests with the reusable pile group. First, construct an instrument and calibrate the piles; then, construct a portable cap (i.e., frame). Second, select sites for testing. The sites chosen were the U.S. 17 bypass over the northeast Cape Fear River, near Wilmington, North Carolina (which is a soft-soil location), and the Spring Villa National Geotechnical Experimentation Site near Auburn, Alabama (which is a stiffer-soil location). Third, conduct the load tests by performing static and Statnamic® load tests on single reference piles and then upon the test groups. Statnamic tests applied a single-direction impulse load through an increasing sequence of load amplitudes. Fourth, reduce and analyze the test data to infer *p-y* curves and *p*-multipliers under repeated impulse loading (for use in FLPIER or similar software), and comment on the future use of the portable pile group for site-specific testing.
7. Developing the final report (i.e., this document).

CHAPTER **2**

FINDINGS

INTRODUCTION

The findings for this research are given in detail in Appendixes A–F. This chapter provides a summary of those findings.

EFFECT OF INSTALLATION METHOD ON *p*-MULTIPLIERS

Current typical modifications for *p-y* curves for group action using *p*-multipliers were reviewed in Table 2. These factors were developed from analysis of full-scale pile group tests and from centrifuge tests on pile groups. They modify *p-y* curves on a row-by-row basis, rather than on a pile-by-pile basis, mainly because analysis of test results did not yield a clear pattern of shear resistances among the individual pile heads within any group, but it did reveal clear patterns of average head shears on each row, from leading to trailing. Trailing rows tend to attract less load than do leading rows because the strength of the soil mass against which a trailing row of piles pushes has been reduced by the movement of the piles in a leading row away from that soil mass. This physical effect is not reflected in elastic solutions for pile-soil interaction without artificial manipulation of elastic constants for the soil, but it is directly reflected in the *p*-multipliers.

One factor that may affect the values of *p*-multipliers is the manner in which the piles are installed. For example, the installation of a group of bored piles tends to reduce the effective stresses, and thereby the strength and stiffness, in soils surrounding piles already in place. For driven piles, the opposite effect may prevail. The values in Table 2 do not reflect installation method. During the performance of this research project, the research team had the opportunity to acquire and analyze data from a major static lateral pile group testing program in predominantly loose to medium-dense silty sand; the testing program was conducted for the Taiwan High Speed Rail Authority near the city of Chaiyi, Taiwan. Details of the test program and soil conditions are given in Appendix A.

Two pile groups were installed and tested as illustrated in Figures 4 and 5. The first group (Figure 4) was a group of 6 (3×2) bored piles 1.5 m in diameter. The second group (Figure 5) was a group of 12 (4×3) driven, circular displacement piles 0.8 m in diameter. The spacing in both groups in both directions was three-diameter on centers. Companion, isolated piles were also installed adjacent to the test groups to serve as references. Because of the manner in which the group piles were attached to the pile caps (i.e., thick, cast-in-place reinforced concrete caps), the bored piles were considered as being fixed (i.e., having full moment connections), while the driven piles were considered as being pinned to the cap.

In both groups, the installation order was generally from the leading row (i.e., first) to the last trailing row (i.e., last), although there were some variations in this pattern (see Figures 4 and 5 for documentation of installation order). After all of the group piles were installed, but before they were loaded, cone penetration tests (CPTs) and dilatometer tests (DMTs) were performed in the soil between the group piles and compared with the CPT and DMT readings before the piles were installed. These tests indicated that in the zone in which lateral soil response is important, installation of the bored pile group generally caused the strength and stiffness indicators to decrease, while the opposite observation was made of the driven pile group.

Site-specific *p-y* curves were determined through back-analysis of the results of the lateral load tests on the reference piles, using the computer code LPILE (*25*). These *p-y* curves then were input into an early (i.e., static) version of FLPIER (*33*), and the deformations of the group caps were predicted. The version of FLPIER that was used had the capacity to model nonlinear structural behavior in the piles.

Meanwhile, the group caps had been loaded to a maximum load of 1000 metric tons (1,100 tons) each by one-way jacking, and the deformations of the pile caps and individual piles were measured. The loads were applied as ground-line shears in several increments of increasing load, with unloading after every increment.

The predicted and measured load-deformation relations did not match without modification of the *p-y* curves that had been developed for single piles at the site. *p*-Multipliers had to be applied to both sets of *p-y* curves (i.e., bored and driven piles) in order for an acceptable match in predicted and measured results to be obtained. These *p*-multipliers were quite different for the bored and driven pile groups—lower for the bored piles than for the driven piles, which reflects, at least qualitatively, the changes in CPT and DMT readings observed in the soil within the groups before they were loaded. The values for the *p*-multipliers that were required to affect acceptable matches in load-deformation behavior are shown in Table 3.

On average, the *p*-multipliers for the bored pile group were slightly lower than those recommended by Peterson and

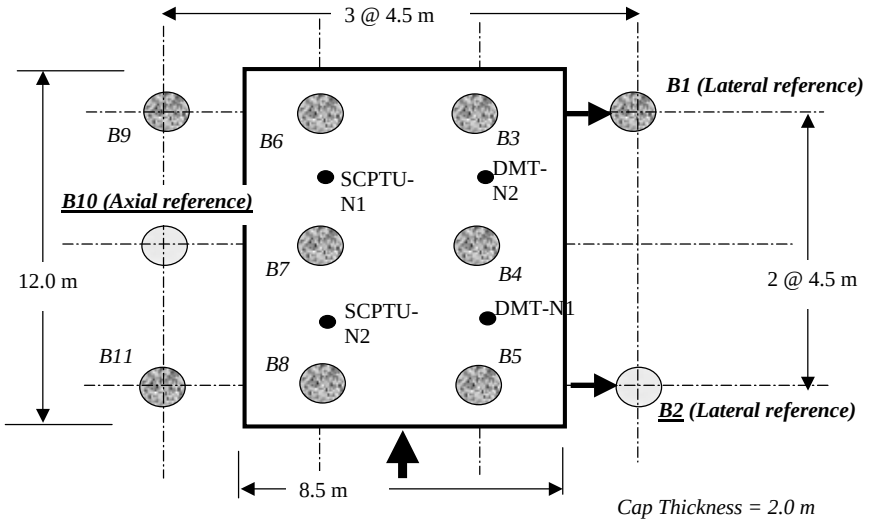

(a) Bored pile group layout.

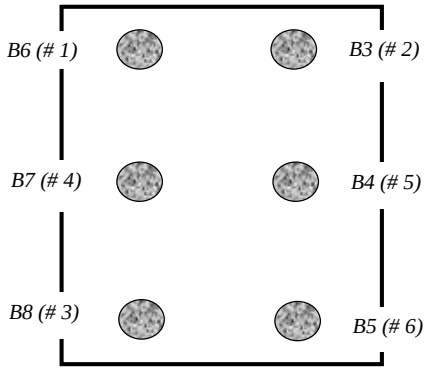

(b) Order of installation for bored piles in test group.

Figure 4. Plan view of test group for bored piles and reference piles (not to scale).

Rollins (*32*) or by FLPIER (*33*). As for the other methods, the *p*-multipliers were found to be larger for the first row than for the subsequent trailing rows. For the driven pile group, however, the *p*-multipliers were higher on average than those recommended by Peterson and Rollins or by FLPIER. This may have been caused to some extent by the fact that the driven piles were modeled as pinned-headed. Had they been modeled as having partially restrained heads at the level of the pile cap, the *p-y* curves that would have been required to match the measured behavior would be softer, and the *p*-multipliers, therefore, would be lower. There was no evidence in the test results, however, that the piles were restrained by the pile cap.

It can be concluded from the Chaiyi tests that lower *p*-multipliers should be used in loose to medium-dense cohesionless silty sand for modeling groups of bored piles rather than for modeling groups of driven, displacement piles, in the general pattern shown in Table 3. Further research on this issue is warranted. This effect may not be true at sites at which cohesion exists in the granular soil. It is also noted that the *p*-multipliers for these very large-scale static tests were in the general order of magnitude of the *p*-multipliers that PoLam et al. (*24*) recommend for seismic analysis of laterally loaded pile groups.

ANALYTICALLY DERIVED *p-y* CURVES AND *p*-MULTIPLIERS

The development of *p-y* curves and *p*-multipliers for dynamic (e.g., seismic) loading involved several sub-studies, which are documented in Appendix B.

Kinematic Loading of Pile Groups

First, in order to investigate the effects of kinematic loading (i.e., loading of the piles by the soil) versus inertial loading (i.e., loading of the piles from inertial feedback from the super-

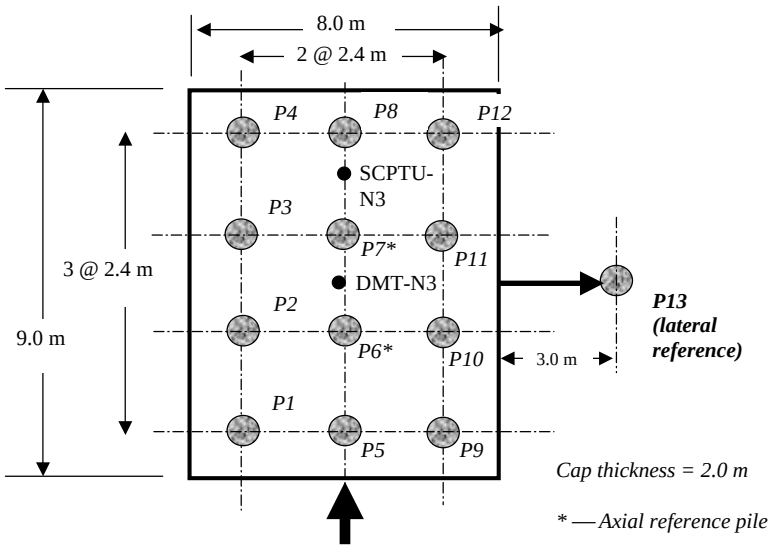

(a) Driven pile group layout.

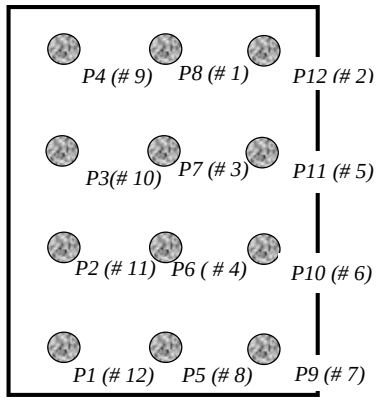

(b) Order of installation for driven piles in test group.

Figure 5. Plan view of test group for driven piles and reference piles (not to scale).

structure), single piles and pile groups embedded in soil were modeled using the computer code ANSYS (*39*) by imposing seismic motion from a simulated bedrock base located either at the elevation of the pile toes (simulating socketed piles) or below the elevation of the pile toes (simulating floating or "friction piles"). ANSYS is a three-dimensional finite element code that permits the use of nonlinear soil stiffness, including damping and gapping between the soil and the piles. The piles had mass, but supported no superstructure with mass or stiffness when modeling only kinematic action.

The salient results of this sub-study were that

- Pile-head response resembles free-field response at low predominant earthquake frequencies;
- Pile-soil-pile interaction (pspi) is not important in the frequency range of interest for seismic loading (0–10 Hz); and
- Based on limited evidence, pspi is important in the frequency range of interest for seismic loading (0–10 Hz) when inertial feedback occurs, but pspi appears not to be dependent on the frequency of loading in this frequency range.

Inertial Loading of Pile Groups

Inertial (i.e., pile-head) loading of both individual piles and pile groups under harmonic conditions was analyzed using a computational model addressed in an article by El Naggar and Novak (*40*). A schematic of that model is shown in Figure 6. Hysteretic, hyperbolic *p-y* curves are used in the near field, in the vicinity of the pile, to capture the nonlinear stiffness of the soil and the hysteretic energy dissipation that occurs in the soil near a pile. This stiffness model is placed in parallel with a damper, which is frequency dependent. The

TABLE 3 *p*-Multipliers for Chaiyi lateral group load tests

Pile Row	Inferred *p*-Multipliers from Chaiyi Load Tests		*p*-Multipliers from Peterson and Rollins (*32*) $S/D = 3$	Default *p*-Multipliers from FLPIER (*33*) $S/D = 3$	Dynamic *p*-Multipliers from Figure 9	
	Bored Pile Group	Driven Pile Group			Bored Pile Group ($y/D = 0.013$)	Driven Pile Group ($y/D = 0.075$)
Lead	0.5	0.9	0.6	0.8	0.28	0.67
First Trail	0.4	0.7	0.4	0.4	0.18	0.61
Second Trail	0.3	0.5	0.4	0.2 (0.3)[1]	0.28	0.61
Third Trail	–	0.4	–	0.3	–	0.67
Average	*0.40*	*0.63*	*0.47*	*0.43 (0.50)*[1]	*0.25*	*0.64*

[1] Value is 0.2 for a 4-row group and 0.3 for a 3-row group; average is 0.43 for a 4-row group and 0.50 for 3-row group.

soil in the far field, away from the pile, is modeled by a separate linear spring and dashpot to represent the stiffness of the soil in the far field (which, in a group, is the soil between piles) and its radiational damping characteristics. The stiffness and damping parameters were evaluated from methods referenced in Appendix B. The piles were modeled with a numerical version of the dynamic bending stiffness equation. The piles remained elastic, had mass, and, for computational purposes, were circular and vertical.

The basic near-field soil stiffness relation was taken to be the static *p-y* curve recommended by the American Petroleum Institute (*41*). Both clay criteria and sand criteria were used to develop these curves. The soil and computational models were validated by modeling Statnamic tests on piles.

Using the computational model, dynamic *p-y* curves were developed for a typical single pile in clay and sand profiles. Soil parameters and pile properties used in the various runs are documented in Table B-1 of Appendix B. Cyclic degradation of the soil was permitted using the Idriss δ method (see Appendix B), and gapping was modeled. The pile was considered to be a solid circular pile with mass. Results (after five cycles of harmonic pile-head loading at various frequencies) are represented by Figure 7 (i.e., soft clay) and Figure 8 (i.e., medium-dense sand). The dynamic *p-y* curves were stiffer and stronger than the static *p-y* curves.

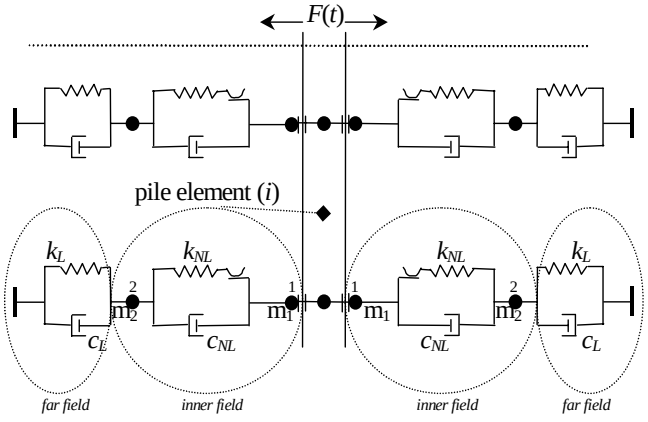

Figure 6. Schematic of model used for deriving dynamic p-y *curves and* p-*multipliers.*

Simplified Dynamic *p-y* Expressions

The dynamic, single-pile *p-y* curves were fit with an analytical expression, which appears to be valid for soft to stiff clay and loose to dense sand. That expression is given in Equation 3.

$$p_d = p_s\left[\alpha + \beta a_o^2 + \kappa a_o\left(\frac{\omega y}{D}\right)^n\right],$$

$$p_d \le p_u \text{ at depth of } p\text{-}y \text{ curve}, \qquad (3)$$

where

p_d = dynamic value of p on the p-y curve at depth x (e.g., in N/m);
p_s = corresponding reaction on the static p-y curve at depth x (N/m);
a_o = frequency of loading, expressed in dimensionless terms $\omega r_o/V_s$;
r_o = pile radius equals $D/2$ (m);
ω = circular frequency of loading equal to $2\pi f$, where f equals the actual frequency of loading (rad/s);
y = lateral pile deflection relative to the soil at depth x, when the soil and pile are in contact (m); and
D = pile diameter (m);
α, β, κ and n = constants determined from curve fitting Equation 3 to the dynamic p-y curves such as those shown in Figures 7 and 8. Values are given for various soil types in Table 4.

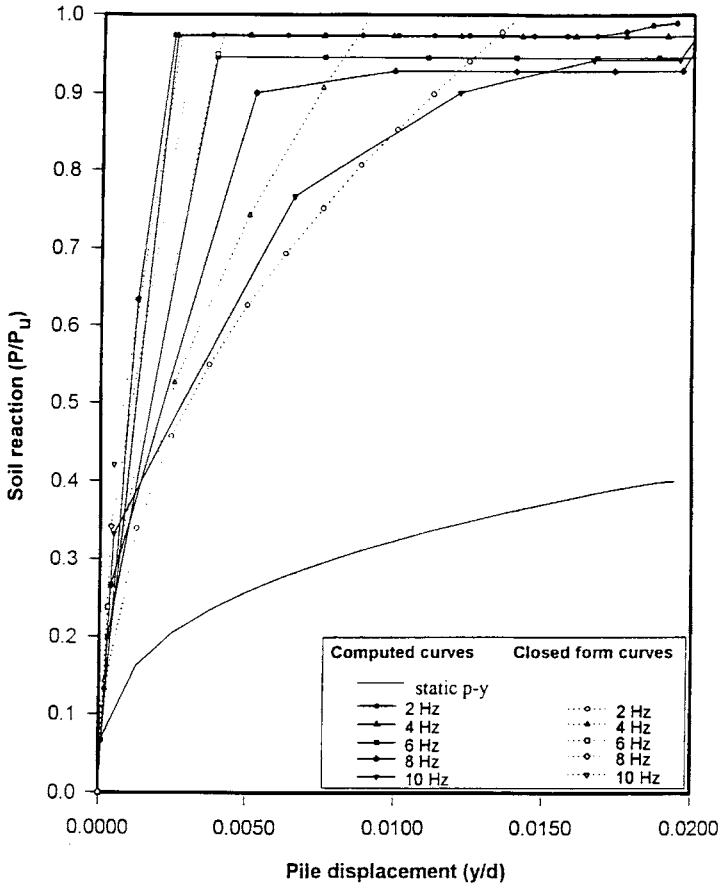

Figure 7. Static and dynamic p-y *curves for soft clay (1-m depth).*

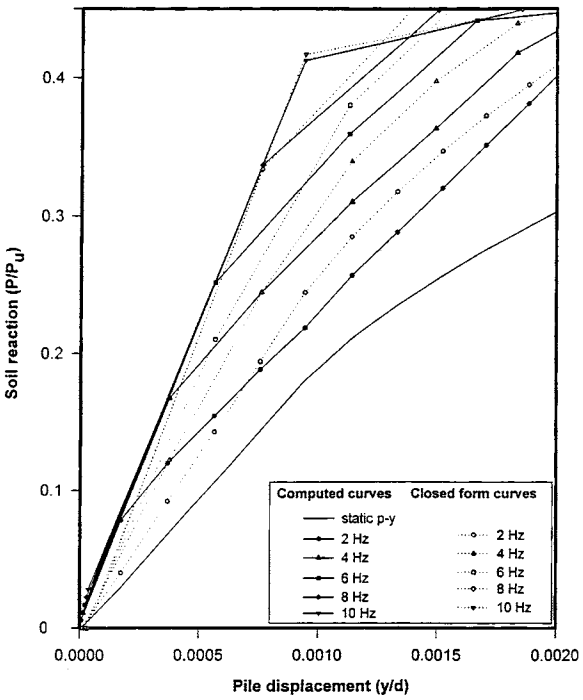

Figure 8. Static and dynamic p-y *curves for medium-dense sand (1.5-m depth).*

The fitted expressions are shown as dotted lines in Figures 7 and 8.

Equation 3 can be separated into two parts: a secant stiffness that is exactly equal to the secant stiffness to the static *p-y* curve at a given value of *y* and a damping term that is used to multiply the lateral velocity of the pile at depth *x*. That is,

$$p_d = ky + c\dot{y}, \tag{4}$$

where

k = secant modulus to the static *p-y* curve at pile deflection y,
c = damping value given by Equation 5, and
$\dot{y}$ = velocity of the pile at the depth of the *p-y* curve.

The damping constant c is given by

$$c = \frac{p_s\left(\beta a_o^2 + \kappa a_o\left(\frac{\omega y}{D}\right)^n\right)}{\omega y}, \tag{5}$$

where the factors are as defined previously. This *p-y* curve formulation has been incorporated as an option in FLPIER, which is discussed in the next section and in Appendix C. For

TABLE 4 Dynamic *p-y* curve parameter constants for a range of soil types*

SOIL TYPE	DESCRIPTION	α	β		κ	*N*
			$a_o < 0.025$	$a_o > 0.025$		
Soft clay	$C_u < 50$ kPa $V_s < 125$ m/s	1	–180	–200	80	0.18
Medium clay	$50 < C_u < 100$ kPa $125 < V_s < 175$ m/s	1	–120	–360	84	0.19
Stiff clay	$C_u > 100$ kPa $V_s > 175$ m/s	1	–2900	–828	100	0.19
Medium-dense sand (saturated)	$50 < D_r < 85$ % $125 < V_s < 175$ m/s	1	3320	1640	–100	0.1
Medium-dense sand (unsaturated)	$50 < D_r < 85$ % $125 < V_s < 175$ m/s	1	1960	960	–20	0.1
Dense sand (saturated)	$D_r > 85$ % $V_s > 175$ m/s	1	6000	1876	–100	0.15

*($D = 0.25$ m; $L/D = 40$; $0.015 < a_o = \omega r_o/V_s < 0.225$); $P_d = P_s\left[\alpha + \beta a_o^{\,2} + \kappa a_o\left(\frac{\omega y}{d}\right)^n\right]$

use in FLPIER, or any similar program, ω can be taken as 2π times the predominant frequency of the earthquake for which the foundation is being designed, not to exceed 10 Hz. The dynamic *p-y* curve expressions, Equations 4 and 5, are most accurate for $a_o > 0.02$ because the plane strain dynamic stiffness model used to develop the far-field stiffness terms tends to become inaccurate as static conditions are approached ($a_o = 0$).

Dynamic *p*-Multipliers

p-Multipliers for dynamic pile-head (i.e., inertial) loading were developed using the model described by El Naggar and Novak (*40*) by comparing the response of two identical parallel piles at a given center-to-center spacing, *S*, with that of a single pile under comparable harmonic, pile-head loadings. In this set of computations, only sand *p-y* curves (loose, medium, and dense) were used as backbone relationships. Nonlinear near-field soil behavior, gapping, and soil degradation were modeled, but the piles remained linear. The dynamic *p-y* curve *p*-multiplier is expected to depend upon several parameters, indicated in Equation 6 below, in which θ is the angle between the direction of movement of a pile for which *p-y* curves are being computed and a line connecting the center of that pile with the center of a neighboring pile that influences the stiffness and strength of the soil surrounding the pile for which *p-y* curves are being calculated.

$$p\text{-multiplier} = f(S/D, y/D, a_0, \theta) \quad (6)$$

The analytical work did not directly address the effect of θ; however, preliminary analyses indicated that θ had only a small effect on the *p*-multiplier. That is, group interaction for two side-by-side piles with this model was similar to that for two in-line piles at a comparable spacing, and the *p*-multiplier was not strongly dependent upon direction of loading. That is, the *p*-multiplier for the effect of a leading pile on a trailing pile was about the same as for the effect of a trailing pile on a leading pile. The effect of direction of loading was not strong—the *p*-multipliers were determined after five cycles of loading, after which the model could not distinguish "shadowing" in a trailing pile from "plowing" in a leading pile.

The *p*-multipliers that were obtained for a medium-dense sand using this model are shown in Figure 9 for several values of dimensionless spacing, *S/D,* dimensionless displacement, *y/D,* and dimensionless frequency, a_o, for in-line loading (θ = 0). The soil and pile properties were identical to those used to obtain the dynamic, single-pile *p-y* curves (Figures 7 and 8) and are given in Table B-1 of Appendix B.

Figures similar to Figure 9 for loose and dense sand are shown in Appendix B. The values for the dynamic *p*-multipliers vary very little among loose, medium, and dense sand profiles. It is also clear by comparing the various panels in Figure 9 that the *p*-multipliers are almost independent of the frequency of loading. To date, similar factors have not been developed for clay soils.

The *p*-multipliers were developed through a series of analyses of two interacting piles with varying spacing and varying frequency. Varying values of *y* were produced by varying the amplitude of applied load. The manner in which the derived *p*-multipliers can be used to analyze a pile group under seismic or impact loading is illustrated in Figure 10. For any given pile, its *p*-multiplier is obtained by successively multiplying the

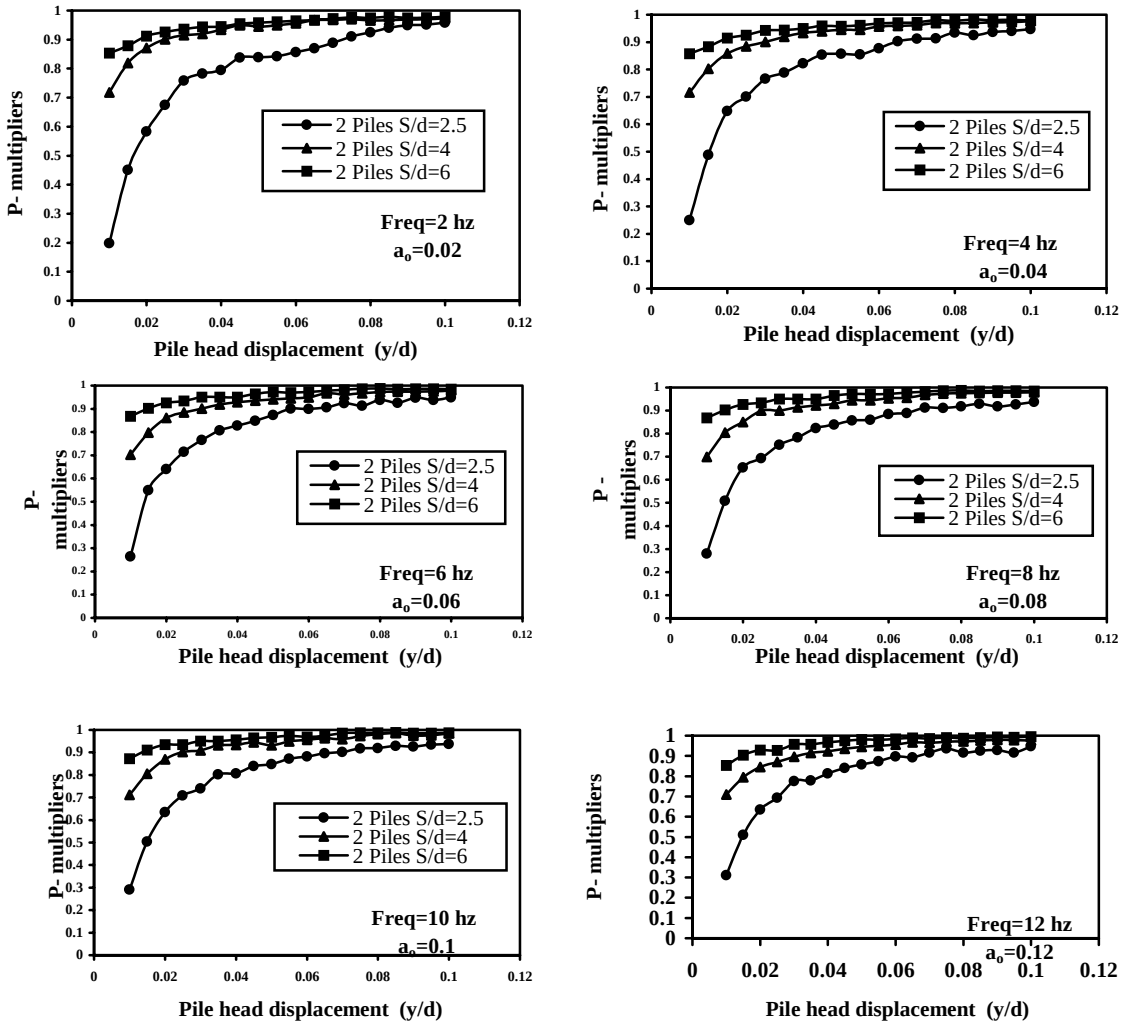

Figure 9. Dynamic p*-multipliers versus pile-head displacement for medium-dense sand.*

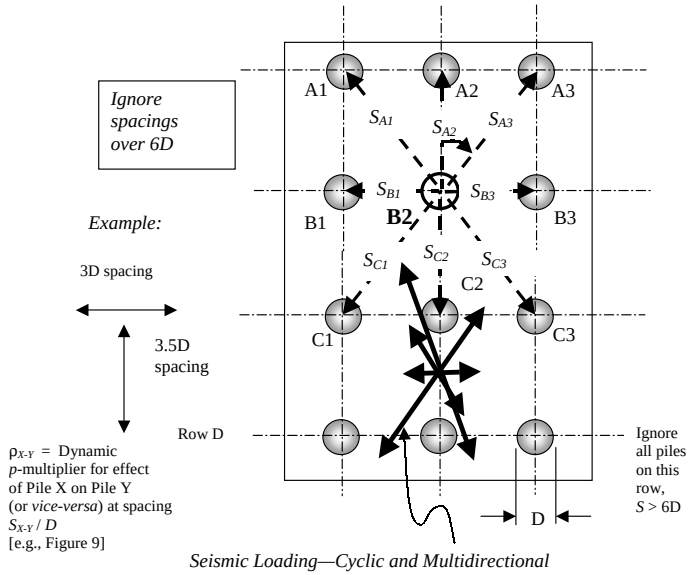

p-multiplier for Pile B2 = $[\rho_{A1\text{-}B2}]\,[\rho_{A2\text{-}B2}]\,[\rho_{A3\text{-}B2}]\,[\rho_{B1\text{-}B2}]\,[\rho_{B3\text{-}B2}][\rho_{C1\text{-}B2}]\,[\rho_{C2\text{-}B2}]\,[\rho_{C3\text{-}B2}]$

Figure 10. Calculation of dynamic p*-multiplier for typical pile in group.*

p-multipliers for surrounding piles (not to exceed a spacing of six diameters) together. θ is not considered in the determination of the *p*-multiplier; however, the *p*-multiplier is dependent on pile displacement, *y*, especially at close spacings. In theory, therefore, the computer code that uses these *p*-multipliers must vary the *p*-multiplier according to the computed lateral pile displacement. However, the dynamic *p*-multiplier can be evaluated approximately as a constant at the target value of pile-head (i.e., soil-surface) deflection for practical purposes.

The analytical results, which show very little dependence of the *p*-multiplier on θ, along with the observation that seismic motion is multidirectional as indicated in Figure 10, suggest that an acceptable approach to analysis of laterally loaded pile groups using the *p-y* method with *p*-multipliers would be to calculate the average *p*-multiplier from among all piles in the group and to use that average *p*-multiplier for each pile in the group when executing FLPIER or similar numerical models.

It is of value to compare the dynamic *p*-multipliers given in Figure 9 with the static *p*-multipliers obtained from the large-scale pile group tests at the Chaiyi site in Taiwan. The comparisons are made in Table 3. For the bored pile group, the dynamic *p*-multipliers were determined at a value of *y* corresponding to 20 mm, the largest value measured at the cap elevation in the load test, and for a value of $a_o = 0.06$. This corresponded to $y/D = 20/1500 = 0.013$, which might reasonably be taken as a lower bound to the limiting deflection of this group in an earthquake. Much larger deflections were achieved in the driven pile group, and the limiting deflection for seismic action for the purpose of computing the *p*-multipliers was arbitrarily set at 60 mm ($y/D = 60/800 = 0.075$). Again, $a_o = 0.06$ was assumed (although very similar values would have been obtained for a_o varying from 0.02 to 0.12). It is observed in Table 3 that the dynamic *p*-multipliers were somewhat lower than the static values determined from the load test on the leading two rows and were somewhat higher on the trailing two rows. However, the average values were nearly equal. Because the *p*-multipliers in Figure 9 are relatively constant beyond $y/D = 0.075$, it can by hypothesized that the average static *p*-multiplier that is measured in static load tests such as the ones performed at Chaiyi is a reasonable approximation of the average dynamic *p*-multiplier in soil that can be characterized as a medium-dense to loose sand at relatively large pile displacements that may occur in a severe extreme event. For the bored pile group, the match of average *p*-multipliers was not as close. This difference may be because the physical piles were much larger than the piles modeled analytically on an absolute scale basis ($D = 1500$ mm versus $D = 250$ mm).

FLORIDA PIER (FLPIER[D])

A computational model for the nonlinear dynamic analysis of pile groups, group caps, and supported superstructures was produced as part of this research project. The computer code is called FLPIER(D). FLPIER has been developed to its current state through a 10-year evolutionary process under sponsorship of the Florida DOT, FHWA, and NCHRP. In developing the current dynamic version of FLPIER, special attention was given to nonlinear modeling of the reinforced concrete members of the pile-cap-pier system as cracking and yielding occur during a seismic or impact event. FLPIER(D) also includes nonlinear soil response in the axial and lateral directions along all piles in the system using *p-y* curves and *t-z* curves (see Figure 3) and has the provision for specifying the parameters for the simplified dynamic *p-y* curves that are described in the previous section and *p*-multipliers that are selected by the user. Although explicit values for dynamic *p*-multipliers based in Figure 9 are not determined internally in FLPIER, the user can select values from Figure 9, based on pile spacings and target deflections, and input the values into the code. It should be noted that the dynamic *p*-multipliers in Figure 9 have only been developed for sand profiles (i.e., soils whose initial stiffness increases in proportion to depth). The applicability of these factors to clay sites is unknown.

The material models and general computational methods used in FLPIER are documented in Appendix C. FLPIER runs in a Windows® environment and was written in such a way that it can be used readily by designers. For information on obtaining copies of the code and instructions for its use, the reader should contact the Bridge Software Institute at the University of Florida (www.ce.ufl.edu/~bsi/).

One potential advantage of FLPIER(D) (i.e., the dynamic version of FLPIER) is that it is capable of modeling the softening effects that occur in any component of the soil-pile-cap-pier system as an impact or seismic event progresses. By appropriate future application of FLPIER(D) (to model the nonlinear dynamic behavior of the soil-pile-cap-pier system), FLPIER(D) can be used iteratively with other computer codes that model the nonlinear behavior of the detailed superstructure and adjoining bridge piers. By using this simulation method in the design approach, it will not be necessary to compute the feedback loads on the pile caps computed in a linear modal analysis of the superstructure and to divide those loads by a factor (in the range of 1.5 to 5), as is currently done, to reflect structural nonlinearity before analyzing the piles structurally. Because both the foundation-pier program (FLPIER[D]) and a nonlinear superstructure program will capture nonlinear effects (cracking, yielding, and plastic hinges), the loads that are determined to occur in the piles will be the correct ones to be used for structural detailing.

However, FLPIER, as well as other appropriate computer pile foundation codes, can be used in the current two-step design process to compute displacement- and velocity-dependent pile group stiffness for use in analyzing the supported structure in a modal analysis process (i.e., Step 1). The forces and moments computed at the column–cap connection by modal analysis of the structure can then be reduced by the appropriate structural ductility factors and applied back to the founda-

tion, using FLPIER to compute the axial thrusts, shears, and bending moments in all of the piles to permit structural detailing in such a manner that appropriate ductility will be provided. The simplified dynamic *p-y* model for laterally loaded pile groups described in the previous section and the dynamic *p-y* curves and *p*-multipliers inferred from the full-scale test data reviewed in the following section are intended to improve the accuracy of FLPIER, or other nonlinear foundation analysis software, for the purpose of this design application.

The version of FLPIER(D) that has been developed for this project contains the following specific improvements relative to earlier versions of FLPIER:

- A fiber model for modeling nonlinear bending of reinforced concrete cross sections, including hysteresis with gapping in cracked regions;
- Distributed mass models for the piles, cap, and pier for modeling dynamic loads;
- The facility to impose dynamic loads at the level of the pile cap or motion time histories at some prescribed elevation in the soil, usually the top-of-rock elevation, for which the acceleration time history is either known or can be estimated for a given design seismic event;
- The capability to input estimated ground acceleration time histories into the piles within the pile group at the support points of all *p-y* curves (equally in all piles);
- Extension of the existing *p-y* models for the soil to consider unloading and gapping, to include effects of radiation damping through user-prescribed values of a dashpot constant attached in series to each *p-y* curve (e.g., Equation 5), and to include forced movement of the reference points (i.e., supports) for the family of *p-y* curves needed to implement the algorithm for Equation 4; and
- The specific formulation for *p-y* curves under dynamic loading given in Appendix B.

None of the *p-y* models currently implemented in FLPIER(D) explicitly considers soil liquefaction or lateral spreading of ground resulting from liquefaction.

FLPIER(D) was validated against a sophisticated finite element code, ADINA (*38*), for the case of linear piles and nonlinear soil. Details are provided in Appendix C.

Application of the new version of FLPIER(D) to structural load tests reported in the literature indicates that the proposed model for concrete is in reasonable agreement with a number of reported test results. Several comparisons of predicted and measured nonlinear structural behavior are thoroughly documented in Appendix C. A "fiber" model incorporated into FLPIER(D) (see Figure 3) to consider nonlinear bending and hysteresis in reinforced concrete seems to be effective in modeling steel as well as circular and square reinforced concrete sections.

It is clear from laboratory test results that are reviewed in Appendix C that anchorage slip of reinforcement is an important concern when analyzing reinforced concrete members under cyclic loading, which is typical in earthquakes. Anchorage slip is not explicitly included in the reinforced concrete model for FLPIER(D); however, it is shown in Appendix C that it is possible to model anchorage slip effects by decreasing the values of the moduli of elasticity for both concrete and steel. The reduced-modulus model can be calibrated for a specific structure by performing physical tests for different structural sections and by adopting the corrected value for the moduli of elasticity in the analytical model. Others performed physical tests on rectangular-shaped cross sections under various modes of loading. Those tests are modeled numerically in Appendix C, and the same values of corrected moduli of elasticity for steel and concrete gave the best results for each test on a given section, showing that anchorage slip is a function of the cross-sectional details rather than of the type of loading.

A concrete gap was introduced into the fiber model to replicate the stiffness degradation of the section. This appeared to work very well when compared with cyclic load tests on reinforced concrete members. However, it is clear from the hysteresis diagrams for all of the tests that a steel model that includes strain hardening, and possibly cyclic degradation, should be used in addition to the modeling of anchorage slip. Strain hardening of reinforcing steel is available as an option in FLPIER(D).

The dynamic version of FLPIER (i.e., FLPIER[D]) was used to model two dynamic pile group tests in which soil was present around the piles (see Appendix C). Although the computational results were generally reasonable, procedures for specifying the dynamic group effect were not well understood at the time that these tests were modeled, and factors such as dynamic *p-y* curves and pspi were modeled arbitrarily. However, the approximations for *p-y* curves that were made in the analysis of centrifuge tests and full-scale tests using FLPIER(D) (see Examples 6 and 7, Appendix C) gave reasonable estimates for the displacements and forces acting in the structures from very simple soil parameters.

The dynamic field tests described in the next section of this chapter and in Appendixes D, E, and F provide additional insight into modeling the dynamic group effect. These new field tests were performed in parallel with the development of the new version of FLPIER(D), and analysis of these new test results using FLPIER(D) (documented in the following section) provided valuable guidance in modeling dynamic group effects.

FIELD TESTING PROGRAM

Objectives

The major effort in this research project was the performance of field tests on full-scale, instrumented pile groups at two sites in the United States in order to accomplish the following four objectives:

1. Evaluate group effects on lateral soil response against piles, specifically observing the differences between group effects that occur during static loading, which are reasonably well documented, and between those for large-magnitude dynamic loading, which are not;
2. Measure and assess the effects of the rate of loading on the lateral response of pile groups;
3. Develop data from these tests in such a way that these test results can be used to evaluate or provide a basis for a dynamic model for laterally loaded pile groups that employs the *p-y* approach to soil modeling, such as FLPIER(D) (see Appendix C); and
4. Develop and evaluate the benefits of a reusable pile group for possible applications at future field test sites.

In order to accomplish these objectives, a group of instrumented steel pipe piles were constructed, complete with a steel frame that was designed to serve as a both driving template and loading cap. Thirteen piles were instrumented internally with strain gauges that were designed to survive and function after repeated installation by driving and extraction of the piles. The system worked generally as intended, although the frame proved to be somewhat time consuming to erect and dismantle. The future use of this part of the system will be discussed in more detail.

The tests completed for this project include both static and dynamic lateral loading tests at sites with a range of soil conditions, along with static tests on single piles that serve as controls for comparison of group effects. Static tests were performed by hydraulic jacking of the instrumented pile group against a reaction foundation. Dynamic tests were performed by using the Statnamic loading system to impart a sequence of rapid load pulses against the test group. Tests were performed at two locations at each of two sites.

Overview of the Load Testing Program

The first of the two sites was in Wilmington, North Carolina, at the proposed location of the Cape Fear River Bridge. The use of the test pile system was incorporated into a design phase load-testing program with the cooperation of the North Carolina DOT (NCDOT). Static and dynamic load tests were performed at a location composed of very soft clay underlain by sand, and dynamic load tests were done at a second location with a depth of almost 2 m of water underlain by loose sand.

The second site was near Opelika, Alabama, at the Spring Villa National Geotechnical Experimentation Site (NGES) operated by Auburn University. Static and dynamic tests were performed on pile groups installed at different spacings between piles in a silty residual soil.

The following is a summary of the lateral loading tests performed for this project:

1. Wilmington static test on 3 (column) × 4 (row) group at three-diameter center-to-center (3D c-c) pile spacing in both directions in soft clay;
2. Wilmington dynamic test on 3 × 4 group at 3D c-c spacing in soft clay;
3. Wilmington static test on single pile in soft clay;
4. Wilmington static test on single pile over water in loose sand;
5. Wilmington dynamic test on 3 × 4 group at 3D c-c spacing over water in loose sand;
6. Spring Villa static test on 3 × 4 group at 3D c-c spacing in silt;
7. Spring Villa dynamic test on 3 × 4 group at 3D c-c spacing in silt;
8. Spring Villa static tests (at two separate locations) on single pile in silt;
9. Spring Villa static test on 3 × 3 group at 4D c-c spacing in silt; and
10. Spring Villa dynamic test on 3 × 3 group at 4D c-c spacing in silt.

The dynamic tests were generally performed by loading the pile group in the direction opposite to that of the static loading and after the static loading test was completed. Exceptions were the Wilmington test over water in sand, which did not have a static load test, and the Spring Villa 3 × 4 group test, in which the Statnamic loading was performed first, followed by the static loading in the opposite direction.

In the interest of producing a readable report, the details of the testing and test results at each site are provided in Appendix D (the Wilmington tests), Appendix E (the Auburn tests), and Appendix F (the instrument calibrations) of this report. A summary of the test results is provided in the following sections of this chapter, along with illustrations and comparisons with computational models; these serve to provide a general sense of the observations and support the conclusions that are derived from these observations.

Load Testing System and Methodology

The reusable load testing system is composed of the instrumented piles, a reusable frame, the loading systems, the external instrumentation, and the data-acquisition system. The instrumented piles and frame were constructed explicitly for this project. The loading systems (i.e., hydraulic jack and Statnamic device) were rented, and the external instrumentation and data-acquisition system used equipment that is the property of Auburn University.

Instrumented Piles

The most critical part of the load testing system is the instrumented steel pipe piles. These piles were selected to be large enough to represent field-scale piles, with an outside diameter of 273 mm (10.75 in.) and a length of approximately 12 m (40 ft). The piles had a wall thickness of 12.7 mm (½ in.) and a yield strength of approximately 300 MPa (43 ksi) so that the piles can be loaded repeatedly to relatively large displace-

ments and bending stresses without yielding the piles. The piles consisted of straight seam pipe rather than spiral welded pipe so that the fabrication process would have minimal influence on the instrumentation. All strain gauges were installed with the seam at 90° from the direction of loading and strain measurement.

Each of the 13 piles was instrumented with strain sensors on opposite sides of the pile at various levels. Seven of the piles were instrumented at seven elevations (i.e., 14 instruments) designed to measure the distribution of stresses along the portion of the length of the pile likely to be affected by lateral bending stresses; the other six piles were instrumented at three elevations (i.e., 6 instruments) near the top of the pile.

The strain sensors were constructed using a system of strain transducers welded to the inside of the pile. The strain sensors consisted of a square tube approximately 12 mm wide and 300 mm long that was instrumented on two opposite sides with a pair of electrical resistance strain gauges in T-rosette configuration on each side. These four gauges composed a single strain sensor, which provided a full-bridge strain gauge circuit that was stable, automatically thermal compensating, and unaffected by the resistance of lead wires. The electrical resistance gauges were used to allow for high-frequency measurements during dynamic loading; vibrating wire gauges were not suitable in such conditions.

Each strain sensor was positioned over two alignment holes drilled into the face of the pile at a distance approximately 200 mm apart at the appropriate elevation, and TIG (i.e., gas tungsten arc) welded through these holes from the outside face of the pile. The hole left on the pile face was then filled with epoxy so that the strain indicator had no effect on the shape of the pile. These strain sensors were thus entirely within the enclosed steel pipe and were protected from damage by the soil during installation.

The lead wires for the sensors were routed up through the pile and attached to a hook inside the pile near the top so that the lead wires were entirely inside the pile during driving. The leads were connected to a quick connect–type plug so that a separate, independent cable could be attached from the data-acquisition system after completion of pile driving.

At each measurement elevation, a strain sensor was positioned on each opposite side of the pile, with the sensor positions aligned with the direction of load. The piles had an external marking so that the pile could be aligned properly for a given loading direction. Because each sensor was a full-bridge circuit, each one provided a measure of tensile or compressive strain as a stand-alone device. Bending moments could be computed from the difference in strain between gauges on opposite sides, and axial forces could be computed from the average strain reading from gauges on opposite sides.

The completed piles with internal strain sensors were calibrated in the structures laboratory at Auburn University. This calibration was accomplished using a three-point loading system, in which the two ends of the 12-m-long pile were clamped to the strong floor and the center of the pile lifted via a cable equipped with a tension load cell. In this manner, the bending moment at each gauge location was known, and the associated strains were compared with the gauge output. The piles were loaded multiple times in opposite directions in order to exercise the gauges and to verify that the signal was repeatable in both compression and tension. Details of the pile calibration are provided in Appendix F.

It is of interest to note that the gauge calibrations varied significantly from the theoretical values, with output signals smaller than anticipated by a factor of as much as 2. The signals were reproducible, reversible, and otherwise completely consistent in every case, and the calibration of the load cell was checked to verify that the calibration process was accurate and reliable. The field measurements of bending versus depth from the single-pile test results agreed with the expected trend near the top of the pile after adjustment of the sensors for the calibration factors. It is not clear why the gauge calibrations were variable. It is possible that the welding of the tubes to the pile on one side of the tube induced some bending in the tubes so that the strain measured on the sensor tube was not precisely that of the pipe to which the tube was attached. This is only a hypothesis for the observation, however, as the actual mechanism was not known. In any event, so long as the strain sensor members behave elastically and the measurements are repeatable, this strain measurement system appears to provide reliable data. The strain sensors on the piles have survived four installations and three extractions with only a few lost gauges (and these generally appear to be caused by wire damage near the top of the pile).

Loading Frame and Pile Installation

The steel loading frame was constructed of steel H and wide flange sections with attached steel cutouts welded to the frame to provide a guide for each pile. Dywidag bars (i.e., high tension–capacity threaded-steel rods) passed through the frame to allow the frame to be clamped down onto the piles after installation. Angle steel cross bracing on either side was provided to add stiffness. A schematic and a photo of the frame are provided, respectively, in Figures 11 and 12.

For the typical arrangement of four rows of three piles, the center portion of the frame was erected, and cross braces were tack welded into position for the two center piles to be driven. The outside piles on the two center rows were driven next, and the central portion of the frame was tightened onto the piles with cross braces welded to the frame in these two bays. The leading and trailing row members of the frame were positioned next, and the center piles on these two outside rows were driven, followed by the four corner piles. Finally, the outermost frame members were tightened, Dywidag bars were adjusted, and cross-brace members were welded.

After the first such installation was completed and the system was examined and evaluated, the decision was made that the piles should be tack welded to the frame guides. This decision was the result of concern that some slippage might occur if the axial loads in the pile during rotation of the group

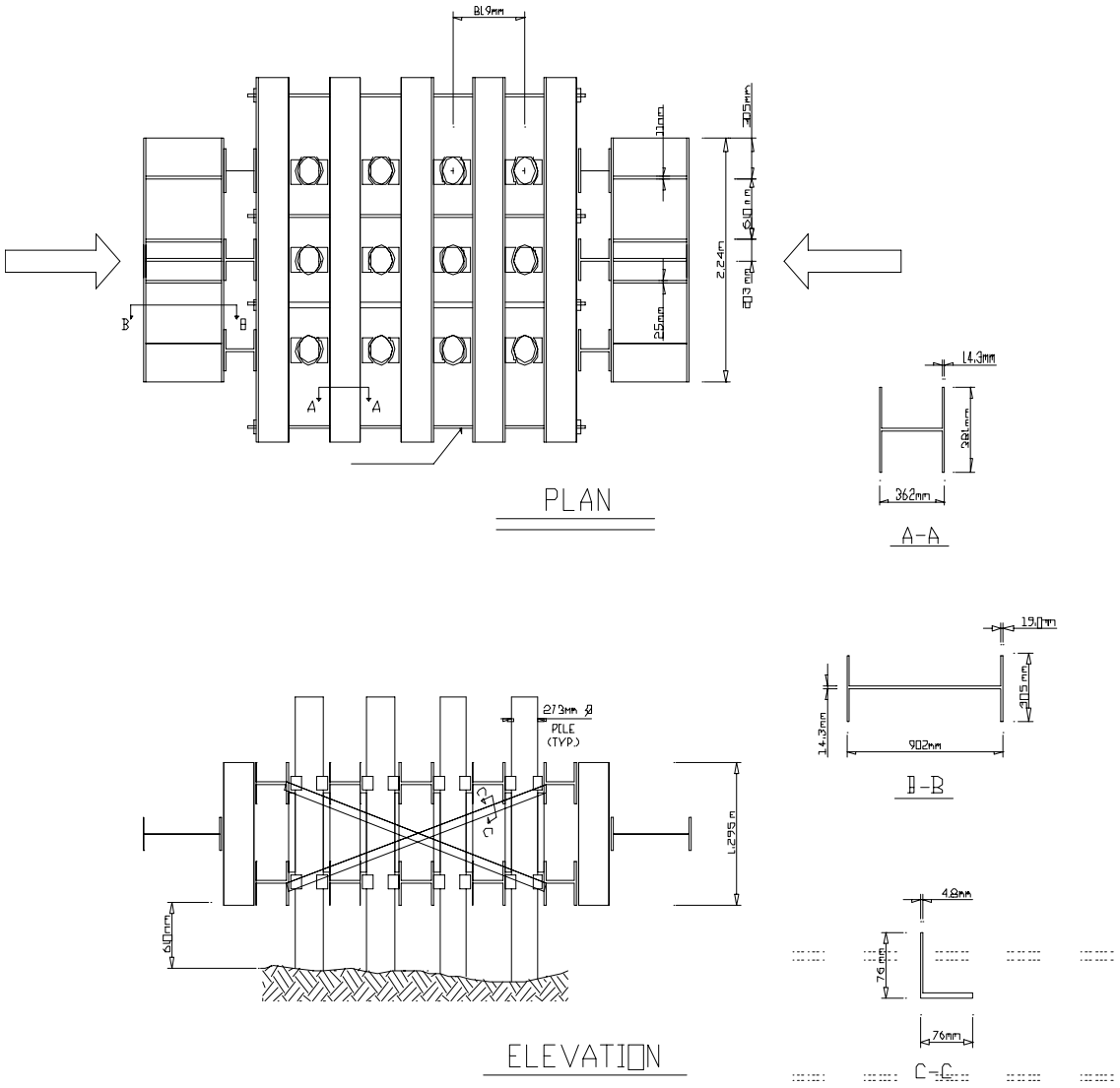

Figure 11. Schematic of loading frame with pile group.

Figure 12. Photograph of loading frame at the Wilmington site.

became high. Without welding the piles to the frame, the only mechanism available to transfer axial forces through the frame would be friction at the guide contacts on the top and bottom of the frame. These guide contacts did not appear to fit so snugly as to eliminate concern that the axial forces might exceed the friction available at these points. The welding of the piles to the frame then required that these welds be cut and ground upon demobilization of the system; after three rounds of cutting and demobilization, the pile guides appear ragged and will need to be refabricated prior to another use.

External Instrumentation

Other instrumentation used during the testing program included linear potentiometers for displacement measure-

ment of the frame, piezoelectric accelerometers mounted on the frame for measurement of acceleration during Statnamic loading, and electronic load cells during all static and Statnamic loading operations. The potentiometers were mounted at four different locations on the face of the frame so that the overall displacements, pitching rotations, and torsional rotations could be determined. Accelerometers were mounted similarly. During single-pile tests, two potentiometers were mounted with the lower one at the elevation of the point of loading and a second one at a higher elevation, so that the slope of the top of the pile could be determined. Electronic load cells were used in every case to monitor load, with backup provided for static tests by observation of fluid pressure in the calibrated hydraulic jack. Details of the instrumentation setup and measurement locations for each test are provided in the appendixes, which describe the specific load tests. Although each test was arranged similarly, the actual location of each instrument was measured and recorded for each individual load test.

Data-Acquisition System

The acquisition of all instrumentation during the testing was accomplished using a Megadac® data-acquisition system. This system provides the needed capability to monitor more than 100 channels of data at a frequency of up to 2,000 samples/s. The system is controlled using a laptop computer; data storage on the device is downloaded, using an Institute of Electrical and Electronics Engineers (IEEE) interface, to the computer hard drive immediately after completion of the test. For static testing, the system was typically set to monitor and record all channels of data at an interval of 2 to 10 s. For the dynamic tests (i.e., Statnamic loading), the system was set to record each channel at a frequency of 2,000 samples/s, with a recording trigger off the load cell and storage of 0.5 s of pre-trigger and 4 s of post-trigger data. This time interval proved more than adequate to capture the pile group response during the dynamic loading events. Data stored using the Megadac test control software were exported to ASCII files for storage and subsequent analysis. Matlab® software was generally used for data presentation and analysis of test results.

Static-Load Application

Static loads were applied to the instrumented pile groups using a hydraulic jack with a load cell, pushing between the test foundation and a reaction foundation. In the case of the Wilmington Site 1 (i.e., Ratt Island) test, the load was applied to the back side of the frame by pushing against a beam that was connected to the reaction foundation via tension cables. For the Auburn (i.e., Spring Villa) tests, the reaction and test foundations were pushed apart. In every case, hemispherical bearings were used on either side of the jack to avoid eccentricity in the load cell-and-jack system. Single-pile tests were performed in a similar manner.

Loads were applied and maintained at increments of load in order to include 6 to 12 load increments during the load application and to define a load-versus-displacement response to the static loading. At the Auburn site, some unload-reload cycles were included to measure the stiffness in such application. Each load was maintained for a duration of approximately 5 min. It was difficult to maintain the load precisely by pumping the jack because smooth application of load in very precise amounts was not possible. Instead, the pressure valves from the jack were simply closed, and the creep displacement and load was monitored. A static test was performed in typically 1.0 to 1.5 h. The data-acquisition system monitored all instrumentation and was set to record data every few seconds.

Statnamic Loading

The Statnamic loading method allows for generating large loads on foundations by "launching" a heavy reaction mass away from the foundation at an acceleration that can approach 20 g. Figure 13 illustrates the typical test arrangement. The energy for the test is generated by burning special fuel pellets in a combustion chamber inside the Statnamic device and allowing the resulting high-pressure gas to vent at a controlled rate, which in turn controls the rate at which the foundation is loaded. The reaction mass is initially set up against the side of the foundation and imparts a load that ramps up to its maximum value in a finite amount of time, usually between 0.1 and 0.3 s, and then gradually decreases as the mass is propelled away from the foundation and physical contact between the foundation and the reaction mass ceases. The load is not a sharp impact, but builds rapidly as a function of the gas pressure generated by fuel burning. The Statnamic loading provides a test that is quick, provides energy in a frequency band close to the fundamental frequency of the foundation, and produces significant inertial forces in the system that allows the determination of dynamic system properties. Successive Statnamic loadings with increasing load amplitudes were intended to approximate roughly the nonlinear soil response against the piles that would be experienced during a seismic event in nonliquefiable soils.

Basic Interpretation of Statnamic Test Measurements

Because the Statnamic loading involves inertial forces, the direct measurement of load and the measurements of foundation response must be considered with regard to a dynamic system. For a simple initial examination of the test data, evaluation of the dynamic response of each foundation group tested with the Statnamic loading device has been modeled

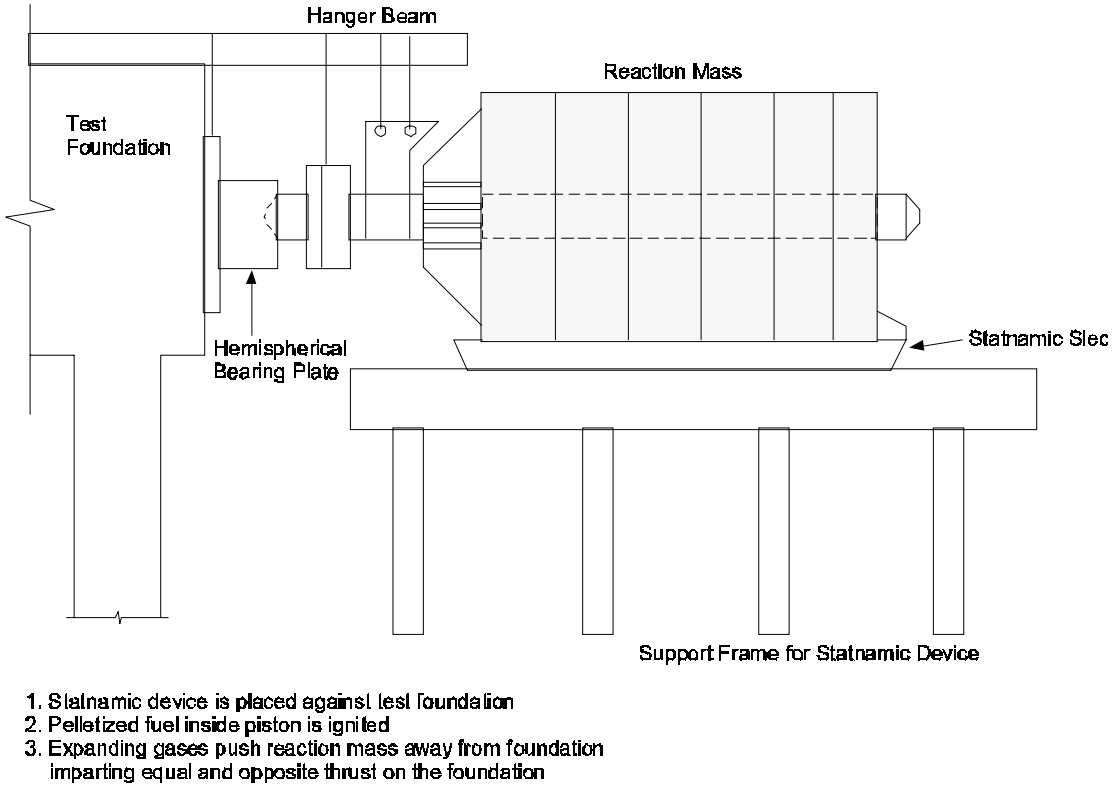

Figure 13. Schematic of Statnamic load test.

using an equivalent single-degree-of-freedom (SDOF) system. The dynamic response of a SDOF system is governed by the following differential equation:

$$Mu'' + Cu' + Ku = \mathbf{F}(t), \tag{7}$$

where u'', u', and u represent the acceleration, velocity, and displacement of the system, respectively, and define the physical state of the system at any instant of time, t. $\mathbf{F}(t)$ represents the forcing function vector; actual values of applied force in the load cell are measured with the data-acquisition system at a frequency of 2,000 samples/s. M, C, and K are the generalized mass, damping, and stiffness coefficients of the SDOF system. The mass and the damping coefficient are generally considered constant during a single loading event. Because soil load-displacement response to lateral loading at large strains is known to be highly nonlinear, the stiffness coefficient K is modeled with a nonlinear stiffness term that decreases as a function of displacement, u within a single loading event. Equation 7 may also be expressed as follows:

$$\mathbf{F}_{\text{inertia}} + \mathbf{F}_{\text{damping}} + \mathbf{F}_{\text{static}} = \mathbf{F}_{\text{Statnamic}}, \tag{8}$$

where

$\mathbf{F}_{\text{inertia}}$ = inertial resistance from effective mass of the foundation,
$\mathbf{F}_{\text{damping}}$ = effective viscous damping resistance,
$\mathbf{F}_{\text{static}}$ = effective static soil resistance, and
$\mathbf{F}_{\text{Statnamic}}$ = measured force on the Statnamic load cell.

The Newmark-β integration algorithm is used to solve the dynamic equation of motion numerically. Assuming the acceleration varied linearly between consecutive time steps, the response at any time could be computed using a total force balance and the state of the system at the previous step. The solution was implemented using a Matlab program with a graphic user interface, the input of which consisted of the measured Statnamic load vector $\mathbf{F}(t)$ and the values of the system parameters M, C, and K. The response of the system was obtained by interactively changing the values of M, C, and K until a good match was observed between the measured displacement time history (i.e., signals from the displacement transducers) and the simulated response (which was computed by the model). The goodness of match between the model response and the measured response is judged by eye by plotting the time histories simultaneously on the same graph. In most cases, it is possible to arrive at a good match between the two with a relatively small number of trials.

The effective mass M is composed of the total mass of the pile cap and portions of individual piles that contribute inertially to the response. The latter is usually restricted to the mass of the piles above the mud line or ground line, but it may vary slightly depending on the magnitude of displacement and the degree of nonlinearity of the system. As such, this is the parameter that is easiest to define for SDOF analysis. The mass term

affects the amplitude and form of the forced-vibration part of the response (i.e., duration of Statnamic load) and the frequency of oscillation for the post-loading response, in which the system undergoes damped free vibration.

The numerical value of the viscous dashpot, *C*, has relatively little effect on the response magnitude during the actual loading event, but is significant in determining the amplitude decay and the damped free vibration frequency for post-loading response. In order to relate *C* more meaningfully to a system damping parameter, the damping constant may also be expressed as a percent of the critical damping C_c as follows:

$$\xi = C/C_c = C/\left[2(KM)^{1/2}\right], \quad (9)$$

where ξ = the damping ratio, and

$$\mathbf{F}_{\text{damping}} = 2\,\xi\,(KM)^{1/2}u' \quad (10)$$

The term *C* is required to capture all of the rate-of-loading effects in the soil, which can be considered to result in energy dissipation in the soil through radiation, the material damping in the piles and pile cap, and the displacement-dependent hysteretic damping in the soil. Therefore, while Equations 7 and 8 are useful in visualizing the general performance of a dynamically laterally loaded pile group, a model, such as FLPIER(D) (see Appendix C), is desirable to separate these distinct effects.

The magnitude of the first peak in the simulated displacement time history is sensitive to the value of the effective stiffness parameter chosen, *K*. The stiffness term also affects the frequency of damped free vibration at the end of the Statnamic loading event. *K* is also used to back-calculate a derived static load-displacement response, which may be compared with the load-displacement function obtained from a conventional static test.

The simple SDOF model has been found to be extremely useful in comparing the results of Statnamic loading tests with more conventional static tests and in visualizing the dynamic and rate-of-load effects that are present during such a test. This model is described further in Appendix D.

Test Results and Static Evaluation

This section provides a brief overview of the static evaluation of the Statnamic loading tests at each site, followed by an examination of all of the test data in comparison with the FLPIER(D) model (see Appendix C). Greater details of the test measurements are provided in Appendixes D and E. Complete test data are voluminous, but they are available from Auburn University on CD-ROM.

Wilmington Tests

The test pile program on the Cape Fear River in Wilmington, North Carolina, was the first use of the test piles. Two test areas were identified and used: Test Area 1 was on the shore of a land area known as Ratt Island, and Test Area 2 was in the water along the eastern edge of the channel in relatively deep water. For purposes of this evaluation, Test Area 1 data will be considered in greater detail because the test provides both static and dynamic measurements to large displacements at a soft-soil site. Test Area 2 included only Statnamic loading, and the great depth to the mud line resulted in the domination of the behavior of the pile group by structural characteristics of the system above the mud line, not soil behavior. At both locations, the piles were driven at a spacing of 3D c-c, with four rows of three piles per row. These tests are described in detail in Appendix D.

Soil Conditions. The soil profile at Test Area 1 (i.e., Ratt Island) consists of an upper layer of soft organic clay, 2.5 m thick, underlain by a 7.5-m-thick layer of loose, alluvial sandy silts and silty sands. Below this layer is a thin layer of very soft alluvial clay just above the top of a dense, silty sand, constituting the locally termed "Peedee Formation." The test piles were entirely within the organic clay and alluvial sand. Standard penetration test (SPT) values in the upper 6 m were generally 0, with 11 to 12 blows per 0.3 m (1 blow per foot [bpf]) in the lower portions of the alluvial sand. Cone penetration (CPT) tip resistance in the organic clay was close to 0 (at the lower limit of the instrument), around 3 to 5 MPa in the 3-to-7-m depth range, and above 10 MPa below 7 m. Some pressuremeter tests (PMTs) were performed at this location, and these data indicate a modulus of deformation of around 2 to 3 MPa in the upper 2.5 m, around 20 MPa for the alluvial sand at the 3-to-5-m depths, and around 60 MPa for the lower portion of the alluvial sand.

Subsurface conditions at Test Area 2 (i.e., the east side of the river) consisted of 2 m of water depth at high tide and 0.3 to 0.6 m of water depth at low tide. The upper 13.5 m consisted of loose, alluvial silty sands and loose-to-dense sands. The top of the Peedee Formation was encountered around elevation –15.5 m. The piles were entirely within the alluvial sands. These sands had SPT values of 0 to 4 blows per 0.3 m (bpf) in the elevation range of –2 to –7 m, and in the range of 10 to 20 blows per 0.3 m (bpf) below. CPT tip resistance was less than 1 MPa above elevation –6 m and rose steadily to a value of around 15 MPa at a depth of around –9 m. The PMT modulus was 3 to 4 MPa in the five tests performed above elevation –7 m, rising to around 65 MPa at elevation –9 m. Dilatometer modulus values ranged from 1 to 10 MPa above elevation –7 m and from 50 to 130 MPa below that elevation.

Load-Deflection Response. The static loading at Test Area 1 was completed first, followed by Statnamic loading in the opposite direction in four successively larger increments. Presented in Figure 14 is the general load-versus-displacement response from the static and the derived static and total (static + damping) soil resistance from the Statnamic loading. For Test Area 2, only Statnamic results are available as no static

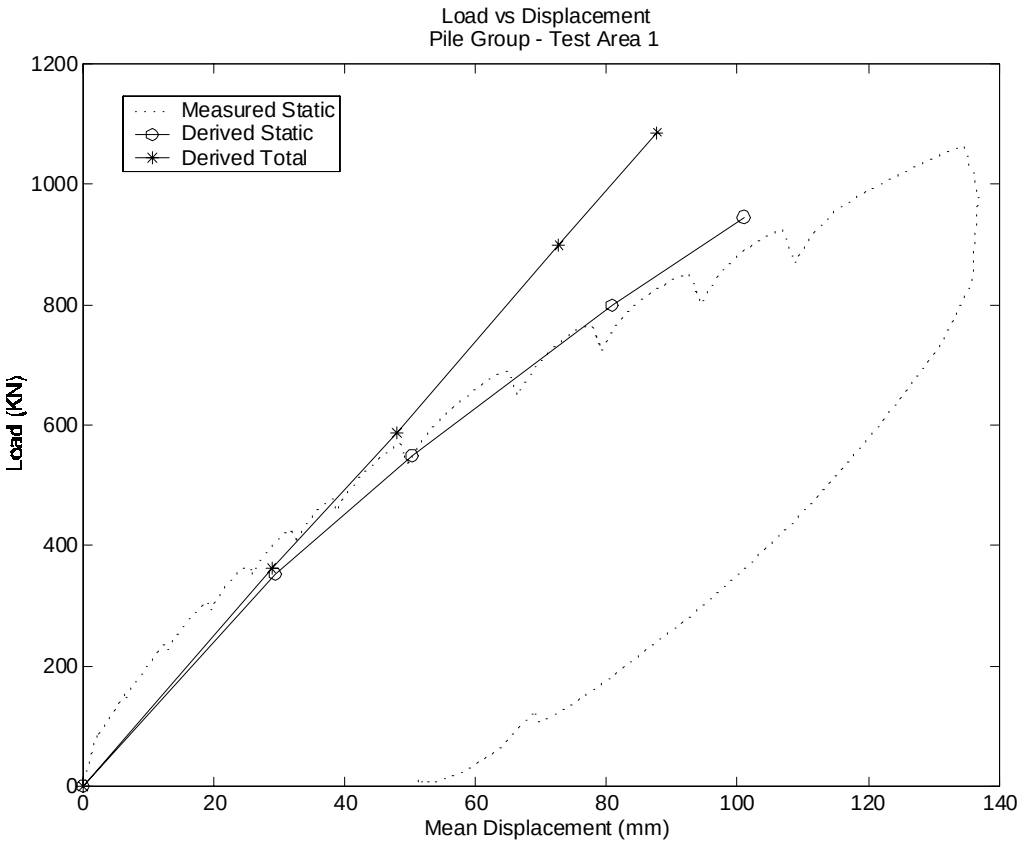

Figure 14. Derived static load-deflection response, Wilmington Test Area 1.

test was performed. These results are presented in Figure 15. In each case, the group was obviously loaded to very large lateral displacements, approximately equal to 50 percent of the diameter of an individual pile. The static behavior and static behavior derived from the Statnamic loading using the SDOF model compare exceptionally well for these test data. The initial loading point on the Statnamic result at Test Area 1 is likely to be softer than would be the case for a virgin loading because of residual displacement from the preceding static test in the opposite direction. The Statnamic test data indicate that a considerable damping contribution was present in the soil resistance for the two largest Statnamic loads (as indicated by the separation between the derived static and derived total load versus displacement points). This was likely a result of large hysteretic (i.e., displacement-dependent) soil damping at those loads, which could potentially represent relatively severe seismic loading.

Interpretation of Strain Measurements. Examples of the bending moment versus depth measurements are provided in Figures 16 and 17, for two load levels on Piles 8 and 11 during the static loading at Test Area 1. Pile 8 was in the lead row for this load, and Pile 11 was in the trailing row. One can see that the maximum positive bending moment for the trailing-row pile occurs deeper than for the leading-row pile.

At and above the ground line, the slope of the bending moment versus the depth relationship should provide an indication of the shear force transmitted to each pile. This interpretation of pile-head shear provides an estimate of the load distribution to the piles in the group. The load distribution estimated in this manner should be considered approximate as measurement errors are greatly magnified when comparing differences between measurements (each of which has an associated measurement error).

Evaluations of the test data to estimate shear force distribution to the piles in the group indicate that the expected general distribution by row position was observed in these tests, with the greatest shear distributed to the leading-row piles and lesser amounts to trailing rows. However, any conclusions regarding the spatial distribution of shear force must be tempered by the fact that large variations between individual piles were observed, by a factor on the order of a magnitude of 2. These variations appeared to be random and associated with spatial variations in soil resistance. In general, the piles, which were soft during the static loading, were also soft during the Statnamic loading in the opposite direction. There was no apparent pattern relating to installation order, position within a row, or any other obvious geometric factor other than row position; row position is only obvious when examining the average shear to the piles by row. The averages of

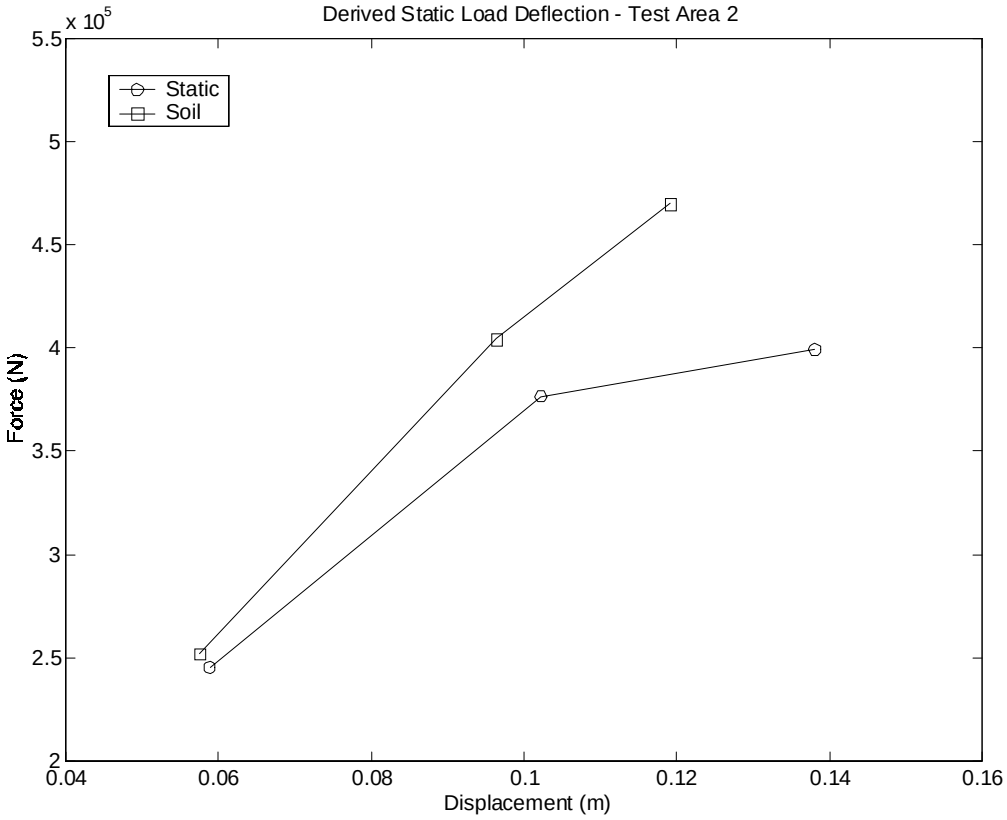

Figure 15. Derived static load-deflection response, Wilmington Test Area 2.

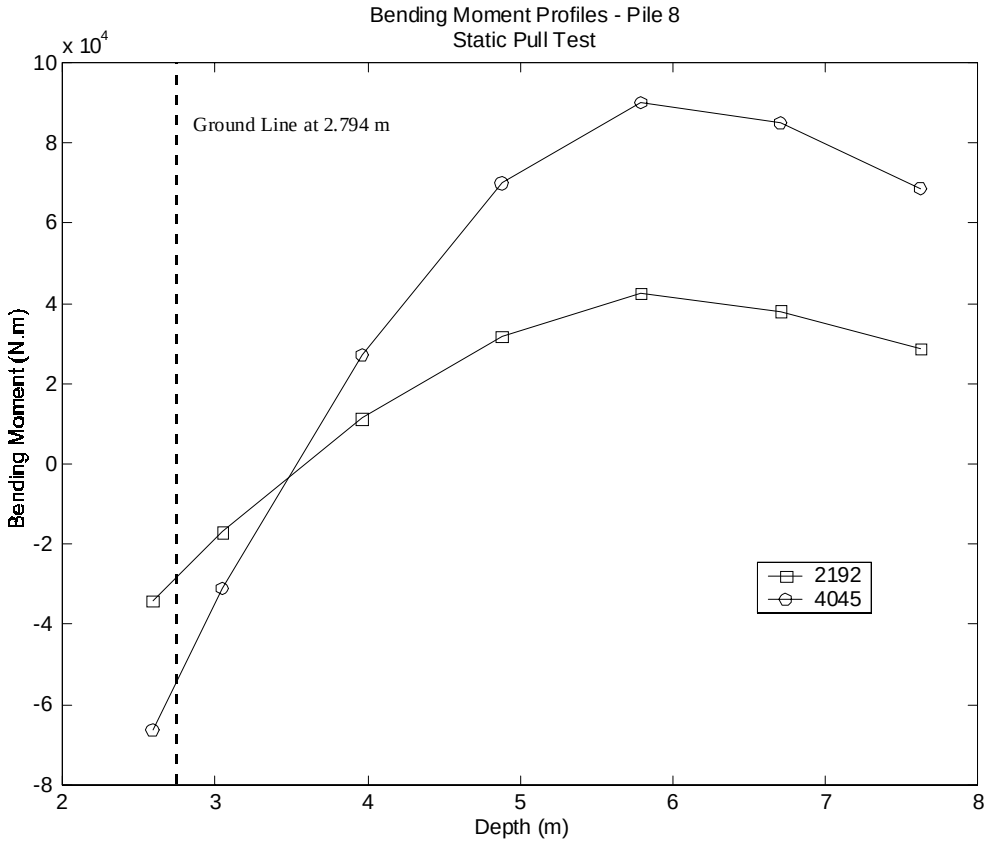

Figure 16. Bending moment profiles, leading-row pile, Wilmington Test Area 1.

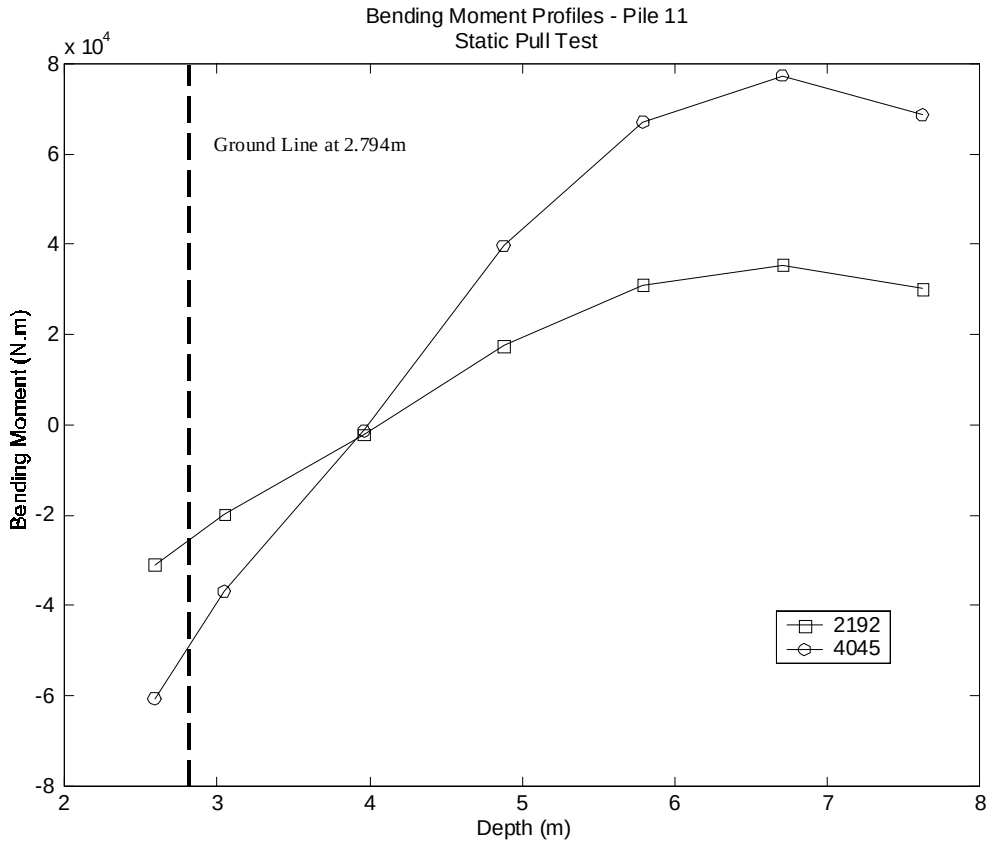

Figure 17. Bending moment profiles, trailing-row pile, Wilmington Test Area 1.

the shear distribution to piles by row position for the loadings at Test Area 1 were (by percentage of the total) as follows:

- Row 1 (lead) = 29% (static) = 33% (Statnamic)
- Row 2 = 25% (static) = 23% (Statnamic)
- Row 3 = 21% (static) = 21% (Statnamic)
- Row 4 (trail) = 25% (static) = 23% (Statnamic)

One conclusion that might derive from these observations is that random variability relating to soil variations is at least as important as any other factor. Other factors such as locked-in moments in the piles caused by lateral drift during driving might also affect this phenomenon.

Rotation of the group was also measured and was significant as were axial forces in the piles. The measurement of axial-force distributions to the piles is not considered particularly reliable because of the large bending strains superimposed on the strains caused by axial thrust. In principle, one can average the strain measurements across the pile cross section (there were two such measurements at each gauge level), but in practice the strains caused by bending are so much larger that the derivation of axial force from such measurements cannot be taken as entirely reliable. In effect, such a measure is an attempt to use a pipe with two strain sensors as a load cell under conditions of severe bending. Even a carefully manufactured load cell will not provide a very reliable indication of axial force under such conditions. Although there is scatter in the data, the axial forces measured appeared reasonable on the whole.

Comparison with FLPIER Static Model. It is instructive to evaluate the test data using a three-dimensional group model such as FLPIER in order to compare the observed group effects with those typically used for design. In order to isolate the group effects from other factors relating to modeling errors in predicting soil behavior, it is necessary to "calibrate" the group model using the results of tests on a single control pile. Any model prediction of group response without calibration to a single-pile control is of limited use because the errors associated with group effects are not separated from general errors associated with predicting soil response at a particular site. The results of the static load tests on the single "control" pile (see Appendix D) were used to develop soil properties such as *p-y* curves that accurately and reliably capture the response of the single pile–loading test. Of course, there can be errors associated with spatial variability in soil response between the control and the group, so no control data set is perfect. The *p-y* curve profile used at Test Area 1 is com-

posed of "soft clay" (i.e., according to Matlock criterion [*42*]) *p-y* curves overlying "sand" (i.e., according to Reese, et al. criterion [*43*]) *p-y* curves. The calibration of the *p-y* curves to the single pile–test data matched not only the load versus displacement at the loading point, but also the bending moment distribution with depth. The latter provides assurance that the general distribution of soil resistance below grade used to formulate the *p-y* curves is reasonable.

The FLPIER model of the pile group matched the as-built configuration, with the cap modeled as a flexural element having a stiffness roughly equal to that of a ½-m-thick concrete cap. This cap is *not* perfectly rigid, but is thought to approximately match the stiffness of the frame. The axial stiffness of the piles proved relatively important in matching the rotational stiffness of the group, but axial loading test data were not available with which to "calibrate" the single pile–axial response. The axial stiffness was simply estimated using default soil parameters within the FLPIER code and proved to match the observations reasonably well. No piles were observed to fail during static loading or during the first three Statnamic loadings. Some slippage at the pile/frame connection appeared to occur during the fourth Statnamic loading as evidenced by popping sounds from the tack welds and jerks in the strain data while the measurements were being taken. The fourth Statnamic loading therefore may have higher rotation than would be estimated by a model in which no pile yielding occurs.

The FLPIER model for a rectangular pile group with piles spaced at 3D c-c uses *p*-multiplier values according to row position to account for group effects. By default, these values are 0.3, 0.2, 0.4, and 0.8 for trailing to leading row, respectively, for a four-row group. The default *p*-multiplier values in FLPIER are based on historical static load test experiments performed both in the field and in the geotechnical centrifuge. Using these default values and the *p-y* soil models developed from evaluation of the single-pile test, FLPIER computed load versus displacement and rotation, which is compared with the static test measurements in Figure 18. This model is seen to provide excellent overall agreement with the measured group response. The FLPIER analysis was performed again using a common *p*-multiplier for all piles equal to the weighted average for the four rows of piles in the group. The results of that analysis are also shown in Figure 18. This exercise was performed to evaluate a much more simple computational procedure. It appears that the overall response is captured reasonably well with this approach.

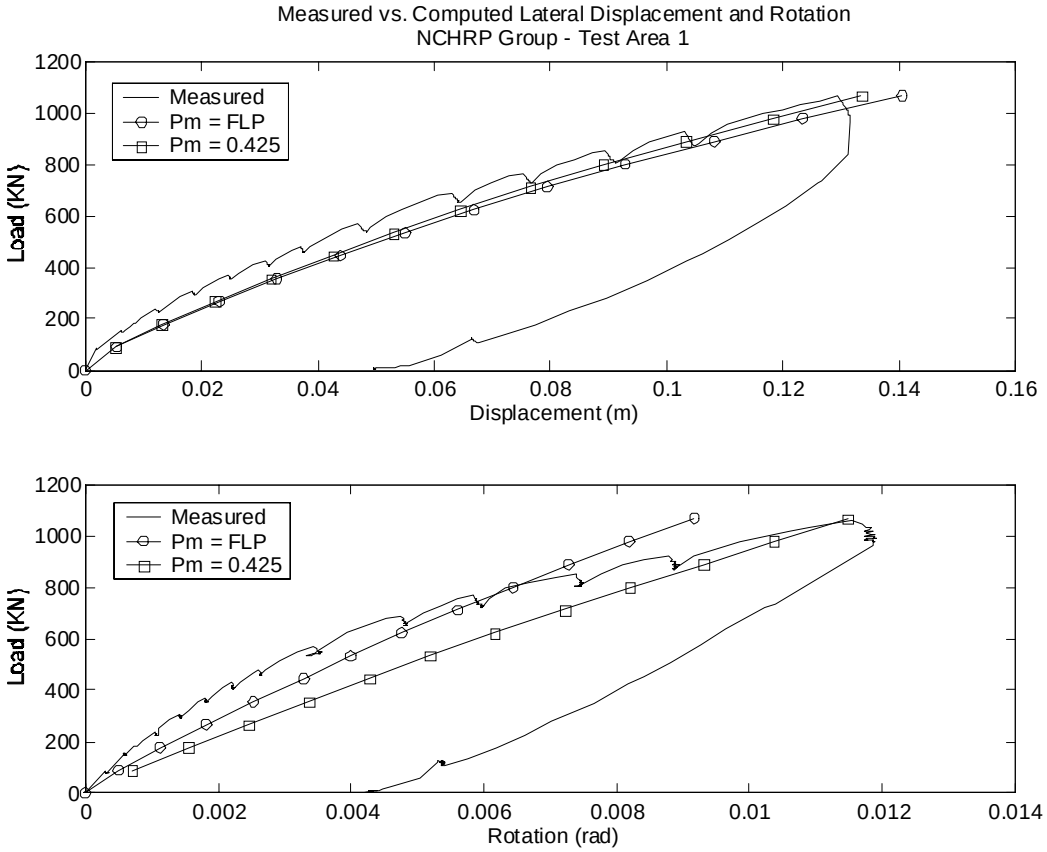

Figure 18. Measured versus computed lateral displacement and rotation, Wilmington Test Area 1.

Continuing with the average *p*-multiplier concept, data are presented in Figure 19 that provide a comparison of bending moments versus depth for the two FLPIER simulations with those measured on two piles. Pile 12 is in the trailing row, and Pile 8 is in the leading row. The symbols labeled "Pm = FLP" represent the FLPIER model with the aforementioned default row-wise *p*-multiplier values; the "Pm = 0.425" represents the FLPIER model with a single averaged *p*-multiplier applied uniformly to all piles. Both simulations appear to capture the bending moments in the piles within the general range of acceptance for engineering-design purposes. Considering the wide variations among shear distributed to piles that was unrelated to row position (and was apparently random), these computed results appear acceptable for design purposes.

The distribution of shear to the piles by row position computed by the FLPIER model was as follows (compared with the measured average shear by row position):

- Row 1 (lead) = 34% (FLPIER) = 29% (static)
  = 33% (Statnamic)
- Row 2 = 26% (FLPIER) = 25% (static)
  = 23% (Statnamic)
- Row 3 = 19% (FLPIER) = 21% (static)
  = 21% (Statnamic)
- Row 4 (trail) = 21% (FLPIER) = 25% (static)
  = 23% (Statnamic)

It appears that the default row-wise *p*-multiplier values slightly overestimate the variations by row position for this test. Of course, the model using the uniform average *p*-multiplier computes uniformly distributed shear to the piles (i.e., 25 percent to each row).

Auburn University (Spring Villa NGES) Tests

The test pile program at the Spring Villa NGES was performed in January and February, 2000, after shipment of the piles and frame from North Carolina. Two test foundations were constructed using the NCHRP pipe piles about a central reaction foundation as shown in Figure 20. The test groups consisted of a group of 12 piles at a spacing of 3D c-c (i.e., similar to the Wilmington test) and a test group of 9 piles at a spacing of 4D c-c. Static lateral tests on each group were conducted by hydraulic jacking, as shown in Figure 20. Dynamic loading of each pile group was achieved in the direction opposite to the static loading using the Statnamic device. Static lateral tests were also carried out on single piles at locations adjacent to each group as shown in Figure 20.

The 12-pile group was constructed first, using the steel frame as a template. After the previous uses of this frame with tack welding of piles and welding and cutting of cross braces each time, the pipe guides and cross-bracing locations had

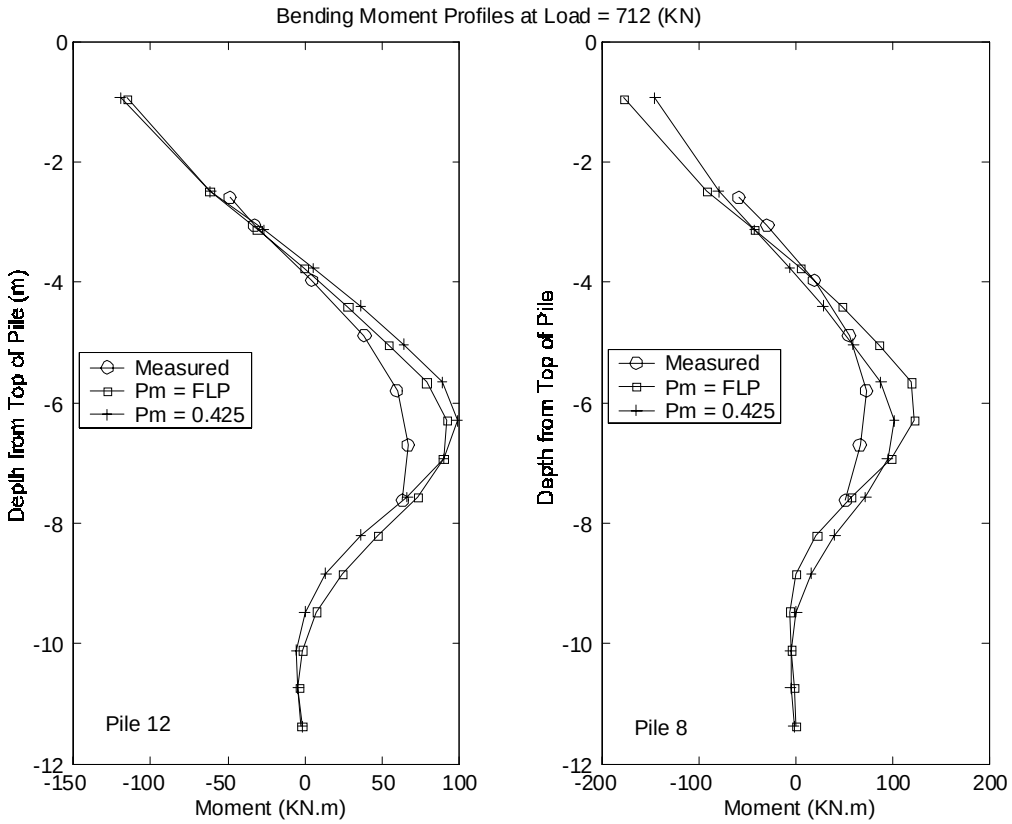

Figure 19. Bending moment profiles at load = 712 kN, Wilmington Test Area 1.

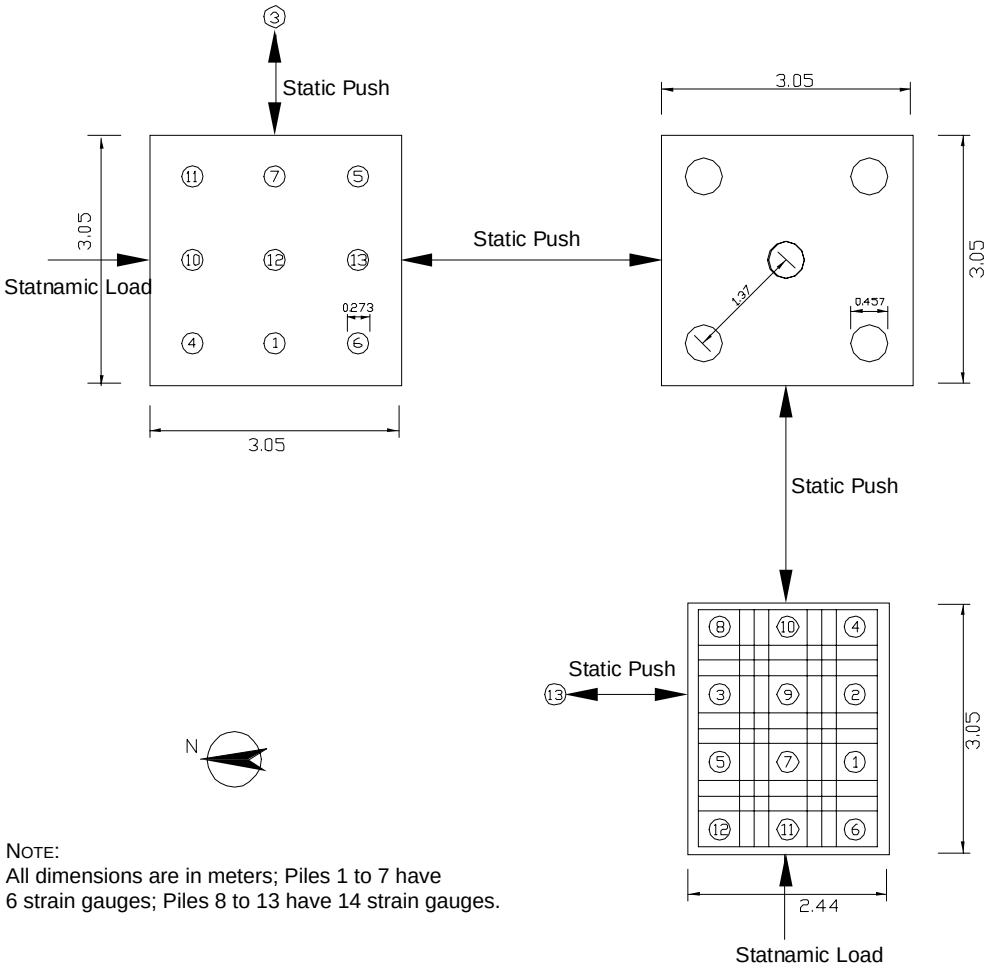

Figure 20. Site plan of testing, Spring Villa Test Site.

become ragged and required a large amount of cutting and grinding to match components together. The pile installation was completed, and the piles were welded to the frame at the contact points; however, these contact points required some additional small pieces of steel plate to be inserted to fill voids, and the process of completing this installation was very time consuming. In addition, the cross braces were placed on the outside of the panels, as shown in Figure 11, rather than internally within each bay, as shown in Figure 12, in an attempt to expedite completion of the test setup. The 12-pile group was tested first using the Statnamic device, followed by static loading in the opposite direction by pushing against the reaction foundation. The Statnamic loading was performed with a procedure similar to that used for Wilmington, although the sled for the device rested directly on the ground rather than on steel runner beams or a barge deck.

After completion of testing of the 3D c-c, 12-pile group, the piles were extracted and redriven for the 4D c-c, 9 pile–group configuration. The extraction proved to be exceedingly difficult because of the large axial tension capacity of the piles. Note that the Wilmington tests over water had available a huge floating crane (i.e., 4-MN lifting capacity), which was able to pull the piles directly. At the Spring Villa site with a typical construction-site crawler crane having approximately 0.7-MN lifting capacity, it was not possible to pull the piles statically. A vibratory hammer was obtained, but in order to "grab" the piles with the hammer, it was necessary to weld a rather large plate to the tops of the piles. This entire process necessitated cutting about ½ m off the top of each pile to remove the damaged portion relating to the plate welding.

Because of the difficulties with using the frame for the 12-pile group, the fact that the frame would need to be reconfigured for the 4D arrangement, concerns that the construction time schedule had overrun the budget (the contractor was unwilling to stay on-site to refabricate the frame), and concerns that the frame had not proven to be as nearly rigid as anticipated, a decision was made to complete the 9 pile–group test using a conventional cast-in-place concrete cap. Formwork was available from the 3-×-3-m reaction foundation construction, and this was suitable for a 3-×-3 group of piles at 4D c-c spacing. The piles were driven, and the cap cast around them after completion of the installation process. The

0.9-m-thick, heavily reinforced concrete cap was formed above grade using a plywood floor, and the supports for the floor were removed after the concrete was set. The piles were lubricated with form oil to facilitate future removal of the concrete cap, but this did not seem to result in slippage of the piles within the cap during the load tests.

The tests on the 9-pile group were performed by first applying static loading against the reaction foundation, and subsequently applying Statnamic loading in the opposite direction. The concrete cap proved to provide a very stable platform for instrumentation during the Statnamic loading. No indications of pile/cap slippage, cracking, or inelastic flexure in the cap were detected.

Soil Conditions. The two test locations at the Auburn University site were within 20 m of each other, with no detectable differences in soil conditions between the two locations. The soil at the Spring Villa site is a residual soil typical of the Piedmont Plateau of the southeastern United States between the Atlantic Coastal Plains and the Blue Ridge Mountains and extending from Alabama to Pennsylvania. These soils are derived from weathering of metamorphic rocks, predominantly gneisses and schists of early Paleozoic Age or older (*44*), and are composed of micaceous sandy silts. Commonly referred to as "saprolite," these residual soils retain the foliation and structural features of the parent rock, but have the texture and appearance of soil. As is common in this geology, the clay content of the soil is higher in the upper meters because of the more advanced state of weathering. Unified soil classification is typically CL/ML, with some soils below the 3-m depth classified as SM, as the sand content is very close to 50 percent. Groundwater is typically at a depth of 3 to 4 m below the surface and varies seasonally.

Strength data include a wide range of in situ tests as well as lab tests on undisturbed samples. SPT *N*-values were typically 10 to 18 blows per 0.30 m in the upper 2 m, 8 to 12 in the 3-to-6-m depth range, and 10 to 15 below 6 m. Average CPT resistance was 2 to 4 MPa in the upper 10 m, with friction ratio values in the 4-to-6-percent range (generally higher at shallower depths). Undrained shear strengths from unconsolidated, undrained triaxial tests indicated considerable variability, with strengths ranging from 50 to 150 kPa. The scatter in these data at shallow depths likely is due to variations in clay content and the effects of negative pore water pressures at depths above the groundwater table. Results from consolidated undrained and consolidated drained triaxial tests (mostly from samples in the 3-to-12-m depth range) suggest that the soil has an effective cohesion, $c' = 17$ kPa, and an effective friction angle, $\phi = 31°$. A more complete presentation of the site geotechnical data, along with pressuremeter, dilatometer, and other test results, are presented in Appendix E and the Appendix E references.

The many borings and in situ tests on the site suggest that the soil properties are spatially variable within small (i.e., cm) distances. On the whole, the site appears to have consistent soil properties (as indicated by the CPT and SPT soundings) with the high local variability superimposed on the general pattern. The soils exhibit a trend of higher stiffness and strength in the upper 3 m, apparently caused by higher clay content and negative pore water pressures above the groundwater level.

Load-Deflection Response. The measured load-displacement response from the static test, along with the derived static and total soil resistances from the Statnamic testing, is provided in Figure 21. Note that in this case the Statnamic test was performed prior to the static load test. It appears that the Statnamic loading has a more significant effect on the subsequent static loading in the opposite direction, which is due to a recoil from the inertial effects of the group during the dynamic loading that produces some prior loading in the opposite direction. Thus, the initial slope of the measured static response relationship is thought to be softer than would occur for a virgin test, and the derived static curve likely is to be more representative of an initial loading curve. The two static curves appear to converge at large displacements. Note also that large damping (indicated by the separation between the total and derived static resistance from the Statnamic loading) was present only at large loads and displacements. Most of the increased resistance mobilized by the fourth and final Statnamic loading over that of the third loading appears to be related to damping as only very small additional static resistance was generated.

The static load versus displacement response for the tests on the 9-pile group at 4D c-c spacing are provided in Figure 22. In this case, the static load test was performed prior to the Statnamic loading. It appears that the initial Statnamic load response is probably too soft and was affected by the residual displacement from the prior static loading in the opposite direction. At large displacements, these two curves appear to merge. By comparing Figures 21 and 22, it is clear that the magnitude of the load required to achieve large lateral displacement was much higher for this test foundation than for the Auburn 12-pile group. At a load of around 1600 kN, the reaction foundation failed by yielding during the static loading, so this represents the maximum static load that could be achieved.

Interpretation of Strain Measurements—12-Pile Group. Examples of the bending moment versus depth measurements for the 12-pile group are provided in Figures 23 and 24 for each of the four peak-load levels during the Statnamic loading on Piles 8 and 12. Pile 8 was in the lead row for this loading, and Pile 12 was in the trailing row. As was the case for the Wilmington data, the maximum positive moment occurs deeper in the trailing-row pile than in the leading-row pile. However, compared with the Wilmington data, these bending moment curves indicate smaller negative bending moments at the base of the frame and much larger positive moments *at depth.* The applied loads at Spring Villa were much larger than at Wilmington because of the stronger soil, and these data suggest that more bending in the frame occurred

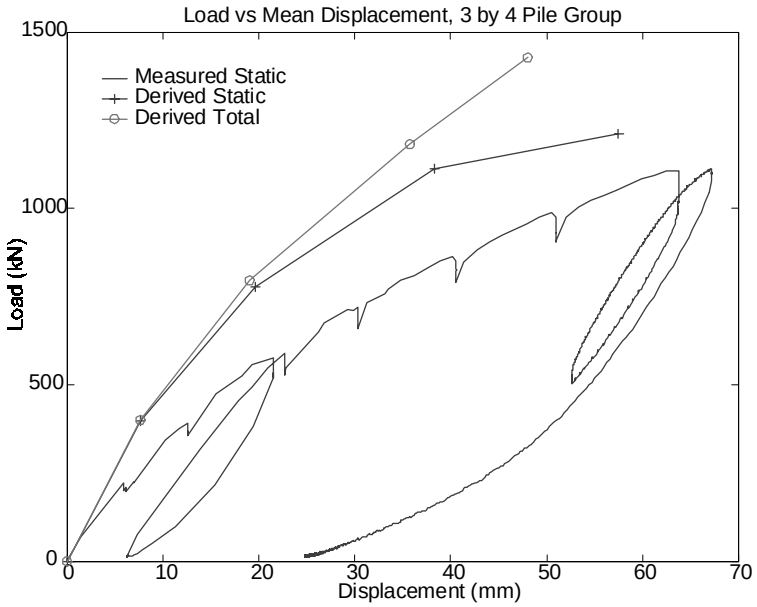

Figure 21. Load versus displacement, 3 × 4 pile group at Spring Villa Site.

at the Auburn site. In fact, postmortem inspection revealed that several of the welded connections between the piles and frame had broken. Every indication suggests that there may have been some internal racking in the frame (between rows of piles) during these tests, such that the condition of restraint at the pile heads was less than full fixity to a rigid pile cap. The frame was fully intact and gave no outward appearance of any distortion, but these measurements suggest that the piles were not fully fixed at their heads.

As was the case for the Wilmington tests, there was a general pattern of shear distribution in which the leading-row piles exhibited higher head shear than did other rows, but there was large spatial variability in head shear between piles within the group that has no apparent explanation other than

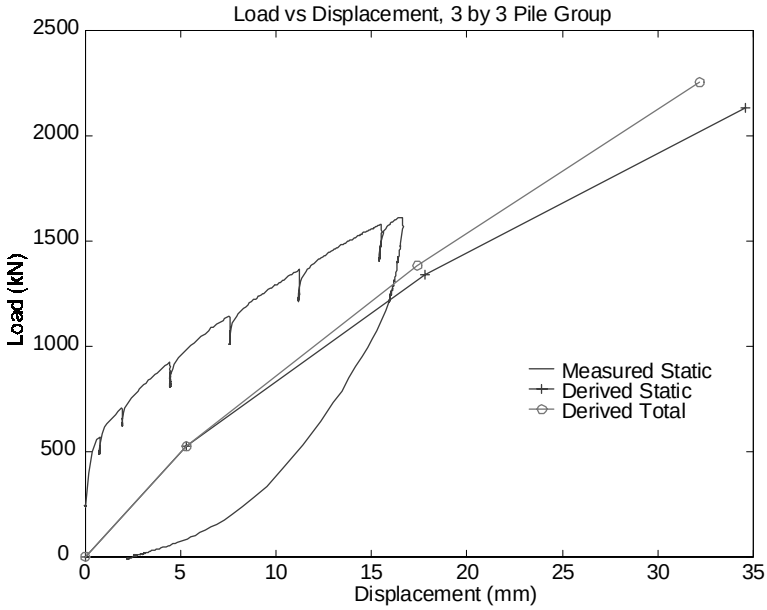

Figure 22. Load versus displacement, 3 × 3 pile group at Spring Villa Site.

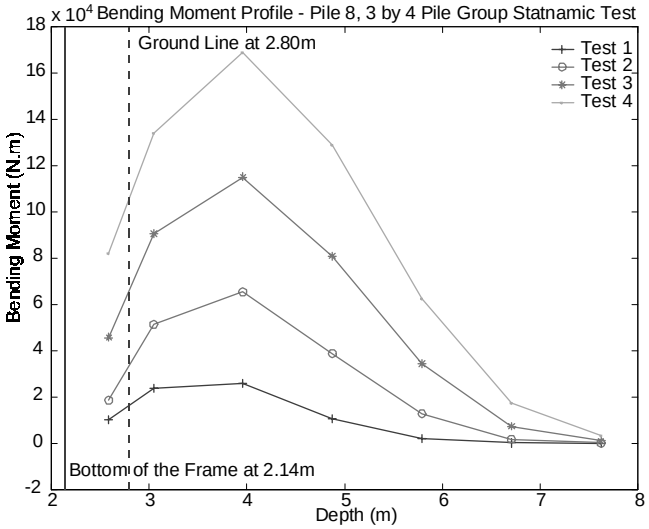

Figure 23. Bending moment profiles, leading-row pile, 3 × 4 pile group at Spring Villa Site.

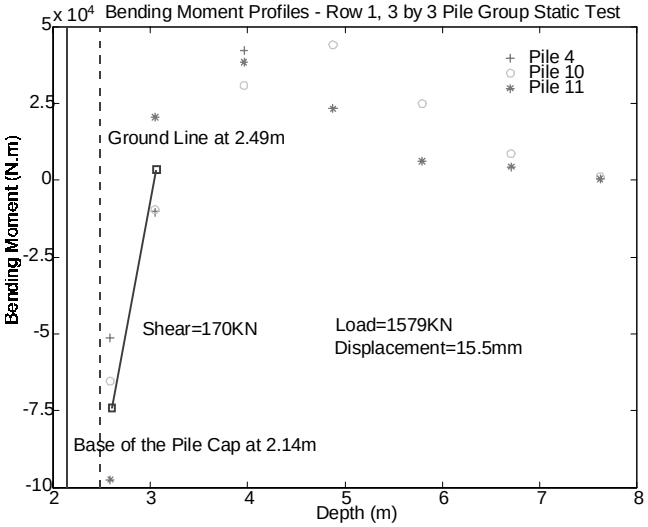

Figure 25. Bending moment profiles, leading-row pile, 3 × 3 pile group at Spring Villa Test Site.

random soil variations. The averages of the shear distribution to piles by row position for the loadings on the 12-pile group were (by percentage of the total) as follows:

- Row 1 (lead) = 29% (static) = 27% (Statnamic)
- Row 2 = 23% (static) = 23% (Statnamic)
- Row 3 = 21% (static) = 26% (Statnamic)
- Row 4 (trail) = 27% (static) = 25% (Statnamic)

The proportion of load distributed to the lead row at this site is less extreme than was observed at Wilmington (e.g., the distribution here is more uniform). However, the actual variation in head shear among individual piles at this site was more extreme. It should also be noted that interpretation of shear force from the bending moment versus depth relation is sensitive to small measurement errors and, at this site, is less reliable than at Wilmington because of the stiff soil at shallow depth. At Wilmington, the near-surface soils were extremely soft, so the initial slope of the bending moment versus the depth curve (which determines the shear at the top of the pile) could be determined more accurately.

Interpretation of Strain Measurements—9-Pile Group. Examples of the bending moment versus depth measurements for the 9-pile group are provided in Figures 25 and 26 for the leading-row and trailing-row piles at the maximum

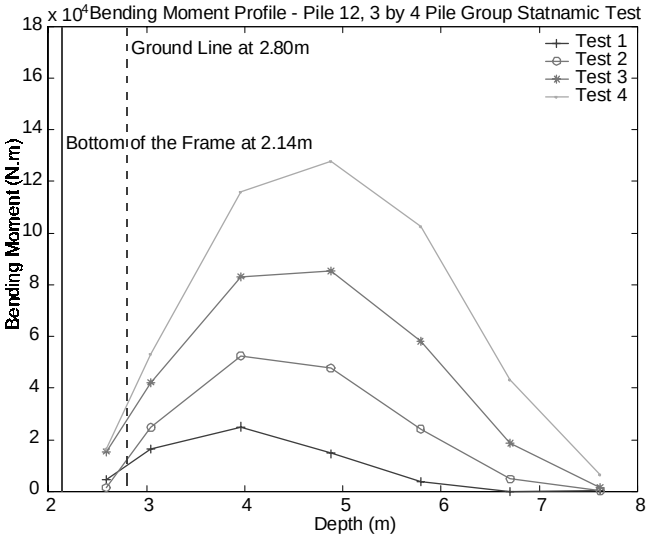

Figure 24. Bending moment profiles, trailing-row pile, 3 × 4 pile group at Spring Villa Test Site.

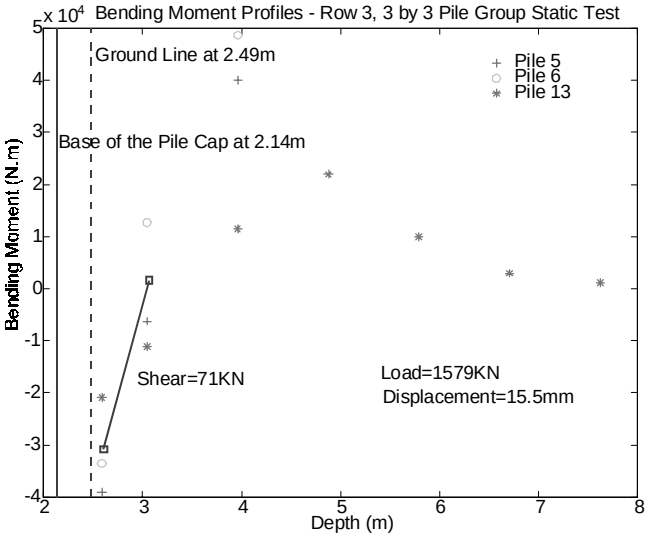

Figure 26. Bending moment profiles, trailing-row pile, 3 × 3 pile group at Spring Villa Test Site.

load level during the static loading. Note the large negative bending moments at the tops of the piles and the variability between piles in a given row. The large negative bending moments at the tops of the piles suggest that the piles were strongly fixed to the concrete cap and that the cap rotation was minimal (i.e., measurements of rotation of the cap indicated very small rotation). Because the ground surface was located at a small distance below the base of the cap and the shallow soils were stiff and strong, the determination of shear from these bending-moment measurements is subject to considerable uncertainty. Interpreted average values for the leading and trailing rows of piles at this load are shown in Figures 25 and 26, respectively. The averages of the head shear distribution to piles by row position for the loadings on the 9-pile group were (by percentage of the total) as follows:

- Row 1 (lead) = 45% (static) = 31% (Statnamic)
- Row 2 = 36% (static) = 35% (Statnamic)
- Row 3 (trail) = 19% (static) = 34% (Statnamic)

Note that the variation between rows observed with the static test is substantial from front to back, but this pattern did not repeat during the Statnamic loading. The third and final Statnamic loading exhibited this trend, and this load produced displacements far beyond any that may have been affected by the earlier static loading; thus, the influence of the prior static loading cannot adequately explain this head shear distribution. In addition, the head shear variation among individual piles for this group of piles was at least as large as with any other test group, and this group test used the concrete cap cast after pile installation. It appears, therefore, that variability in shear distribution to individual piles was not affected substantially by structural details within the loading frame. On the other hand, it appears that the piles in the row that made up the lead row for static loading (and Row 3, the trailing row, for Statnamic loading in the opposite direction) were simply installed into stiffer soil relative to the average and that the piles in the row that made up Row 3 for static loading (and Row 1 for Statnamic loading in the opposite direction) were in softer soil relative to the average. If one averages the two cases (thus averaging out some of the random variability), the variation by row position is 38 percent to 35 percent to 27 percent from leading to trailing row, respectively.

These data suggest that the trend observed throughout all of the testing for this project is confirmed by this final test configuration: for actual field conditions, random variability relating to soil variations is as important as any other factor influencing head shear distribution to the piles in a group.

Comparison with FLPIER Static Model. As discussed with respect to the Wilmington data, the soil parameters for the generation of *p-y* curves in FLPIER were calibrated to the single pile–test results in order to isolate the group effects from other factors relating to modeling errors in predicting soil behavior. The results of the two static load tests on the single control piles (see Appendix E) were similar and were used to develop a soil profile that accurately captures the response of the single-pile loading tests. The *p-y* curve profile that was used consisted of the Reese et al. (*43*) static stiff clay criterion with a higher shear strength near the surface and lower strengths below the 3-m depth. The calibration to the single pile–test data matched not only the load versus displacement at the loading point, but also the bending moment distribution with depth. The latter provides assurance that the general distribution of soil resistance below grade is reasonable.

The FLPIER model of the 12-pile group was similar to the model used at Wilmington, with adjustments for ground surface elevation and soil characteristics (i.e., *p-y* curve profiles). Because the pile bending-moment data and observations suggest that some internal rotation occurred within the steel frame, the piles were not modeled as completely fixed to the cap. This "partial fixity" between the piles and the frame introduces some additional degree of uncertainty in the interpretation of the results. However, FLPIER has a provision to model partial fixity, and this provision was exercised with these test results. A partial fixity factor of 0.1 was used at the pile–cap connection to release some of the moment that occurs at this connection.

The 9-pile group was modeled using nine similar piles, with the pile cap modeled using shell elements, each 0.85 m in thickness and with an elastic modulus of concrete (3×10^7 kPa, or 4400 ksi). The piles were modeled as fixed to the cap.

The input parameters for the axial soil model (i.e., *t-z* curves) were based on the CAPWAP (Case Pile Wave Analysis Program) analyses of a restrike blow on one of the piles after installation and also on the default parameters suggested in FLPIER. Observations of the test results suggest that none of the piles yielded (either geotechnically or structurally) in the axial direction, so the axial pile stiffness is the only relevant parameter. The shear modulus (used for construction of the default *t-z* curves) used for the 12-pile group was at the lower range of the FLPIER default parameters and was less than that used for the 9-pile group, in order to reduce the axial stiffness to account for axial group effects caused by the closer pile spacing. The value for the 9-pile group is consistent with the guidelines provided in the FLPIER help manual.

FLPIER Results—12-Pile Group at 3D Spacing. The FLPIER model for a 12-pile group spaced at 3D c-c uses *p*-multiplier values according to row position to account for group effects. By default, these values are 0.3, 0.2, 0.4, and 0.8 for trailing to leading row, respectively. Using these default values and the *p-y* soil models developed from evaluation of the single-pile test, the load versus displacement and rotation relations computed by FLPIER are compared with the static test measurements in Figure 27. The computed results are stiffer than the measured response, although not by a large amount. In order to match the measurements more, the *p*-multipliers were scaled down by a uniform value. The computed displacements and rotations are shown to be very

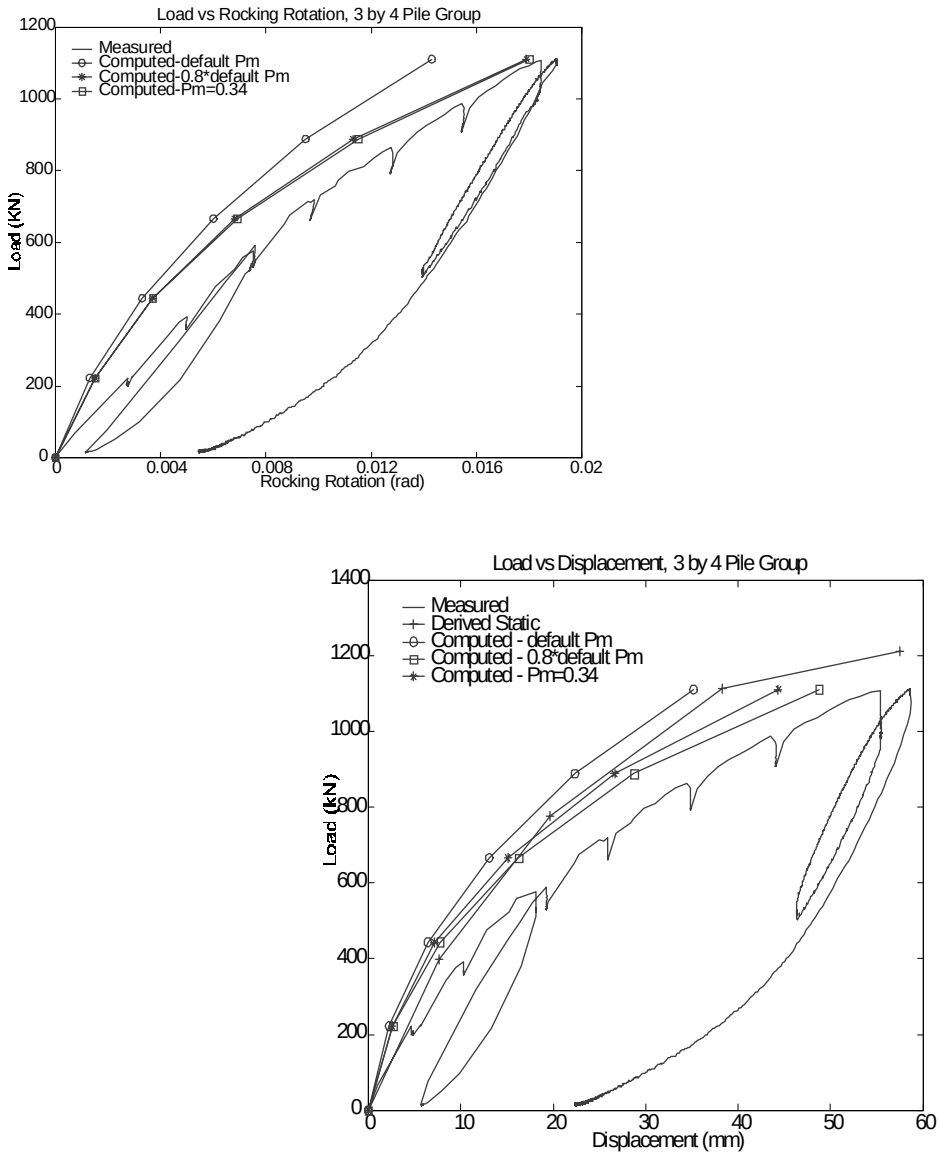

Figure 27. Measured versus computed displacement and rotation, 3 × 4 pile group at Spring Villa Test Site.

close to the measurements with an additional scaling factor of 0.8 applied, giving *p*-multipliers by row of 0.24, 0.16, 0.32, and 0.64. There is no special significance to this factor of 0.8 other than to define the magnitude of the error in the prediction for this test using default values. It appears that the default values are generally within the range of engineering accuracy for most applications. One possible explanation for this overestimation of stiffness may be related to the soil profile at the site. This profile includes a stiffer crust over a weaker underlying stratum, and this type of profile may tend to amplify the group effects because the group is influenced more strongly by the deeper soils than is an isolated pile.

In order to evaluate the effects of a simpler model, additional analyses were performed using a uniform *p*-multiplier. An additional plot of lateral displacement is shown in Figures E-17 (see Appendix E) for a FLPIER analysis with the *p*-multiplier for all 12 piles set at 0.34 (i.e., the average of 0.24, 0.16, 0.32, and 0.64). The overall response with this simple model appears to be sufficiently close to the distribution obtained using row-wise *p*-multipliers for general engineering and design purposes. A simple, uniform *p*-multiplier may have advantages for some seismic analyses in which load reversals occur in multiple directions and the consideration of directional effects makes the analysis much more complex.

Figures 28 through 30 provide plots of the computed and measured bending moments as functions of depth for two piles. Piles 8 and 10 are in the trailing row; Pile 12 is in the leading row. There is general agreement in the trend of the measured and computed bending moment profiles, but there

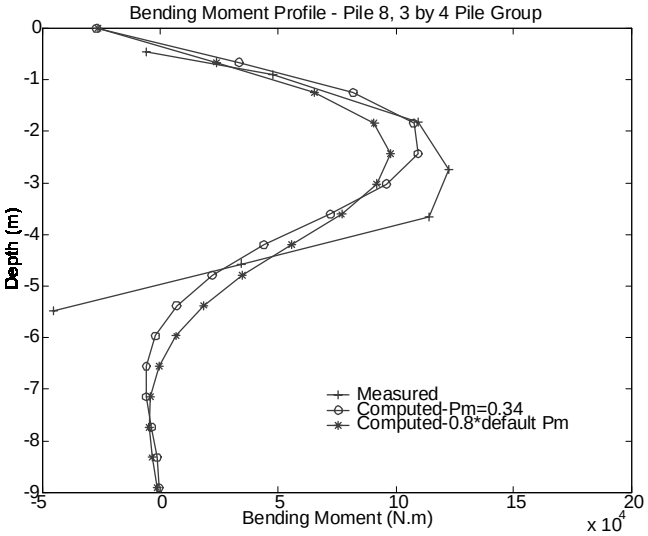

Figure 28. Bending moment profile, trailing-row pile, 3 × 4 pile group at Spring Villa Test Site, group load = 1111 kN.

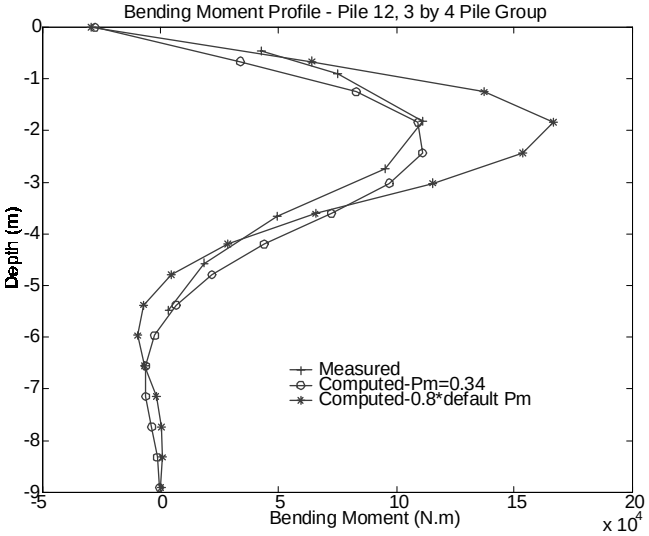

Figure 30. Bending moment profile, leading-row pile, 3 × 4 pile group at Spring Villa Test Site, group load = 1111 kN.

is a wide variation in the magnitude of the maximum moment values. The computed maximum moments in Pile 12 are somewhat less than those measured on Pile 8, but significantly more than those measured on Pile 10. Piles 8 and 10 are in the same row, so the computed values are identical. The results shown demonstrate the wide measured variations observed within the physical group. However, there is excellent overall agreement with the measured group shear load versus displacement relationship. Also shown in Figures 28 through 30 are the results of static analyses with FLPIER in which all 12 piles were assigned a *p*-multiplier value that was equal to the weighted average for the four rows of piles in the group. This exercise was performed to evaluate a simple approach to estimating bending moments in piles within the group. It appears that the overall measured bending moment response is captured well with this approach.

The distribution of shear to the heads of the piles by row position computed by the FLPIER static model (with row-wise default *p*-multipliers) was as follows, compared with measured averages by row position:

- Row 1 (lead) = 38% (FLPIER) = 29% (static) = 27% (Statnamic)
- Row 2 = 25% (FLPIER) = 23% (static) = 23% (Statnamic)
- Row 3 = 16% (FLPIER) = 21% (static) = 26% (Statnamic)
- Row 4 (trail) = 21% (FLPIER) = 27% (static) = 25% (Statnamic)

It appears that the default *p*-multiplier values overestimate the variations by row position for this test. Of course, when the piles are assigned the uniform average *p*-multiplier, uniformly distributed pile head shears are obtained with FLPIER (25 percent to each row).

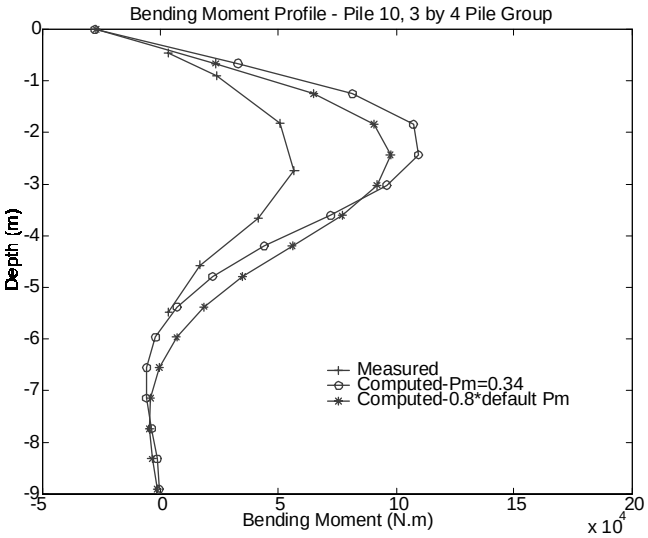

Figure 29. Bending moment profile, trailing-row pile, 3 × 4 pile group at Spring Villa Test Site, group load = 1111 kN.

FLPIER Results—9-Pile Group at 4D Spacing. The *p*-multipliers used for the initial analysis of the 9-pile group were the default values recommended by the help file in FLPIER for a pile group with three rows. Values used for the spacing of 4D c-c were interpolated between the values given in the help file for 3D spacing and 5D spacing, as values are not given for 4D spacing. These interpolated values are 0.50, 0.625, and 0.90, starting with the trailing row and ending with the leading row. As was the case for the 12-pile group, these default values produce a response that is slightly too stiff, and better agreement with the overall load-deflection

behavior was again obtained by scaling the *p*-multipliers down by a factor of 0.8. The resulting *p*-multipliers are 0.4, 0.5, and 0.72 for the trailing to leading rows, respectively. The computed lateral load displacement response at the base of the cap using these values is shown in Figure 31, along with the measured static response and the static response derived from the Statnamic test using the SDOF procedure outlined previously. Note that the static test was performed prior to the Statnamic test for this pile group; therefore, the measured initial derived equivalent static test data may be slightly too soft because of the permanent set that occurred in the earlier loading in the opposite direction. In addition, the initial stiffness of the measured static response may be too stiff because of a residual load in the jack that appeared to be in place when the instrumentation was zeroed. (This was discovered upon unloading.)

As was the case for the 12-pile group, the computed lateral displacement at the pile heads using the default *p*-multipliers was too stiff. The adjusted *p*-multipliers appear to lead to slightly soft responses at small displacements (i.e., less than 5 to 8 mm), but appear to match the measured data well at larger displacements, which are of most interest for extreme

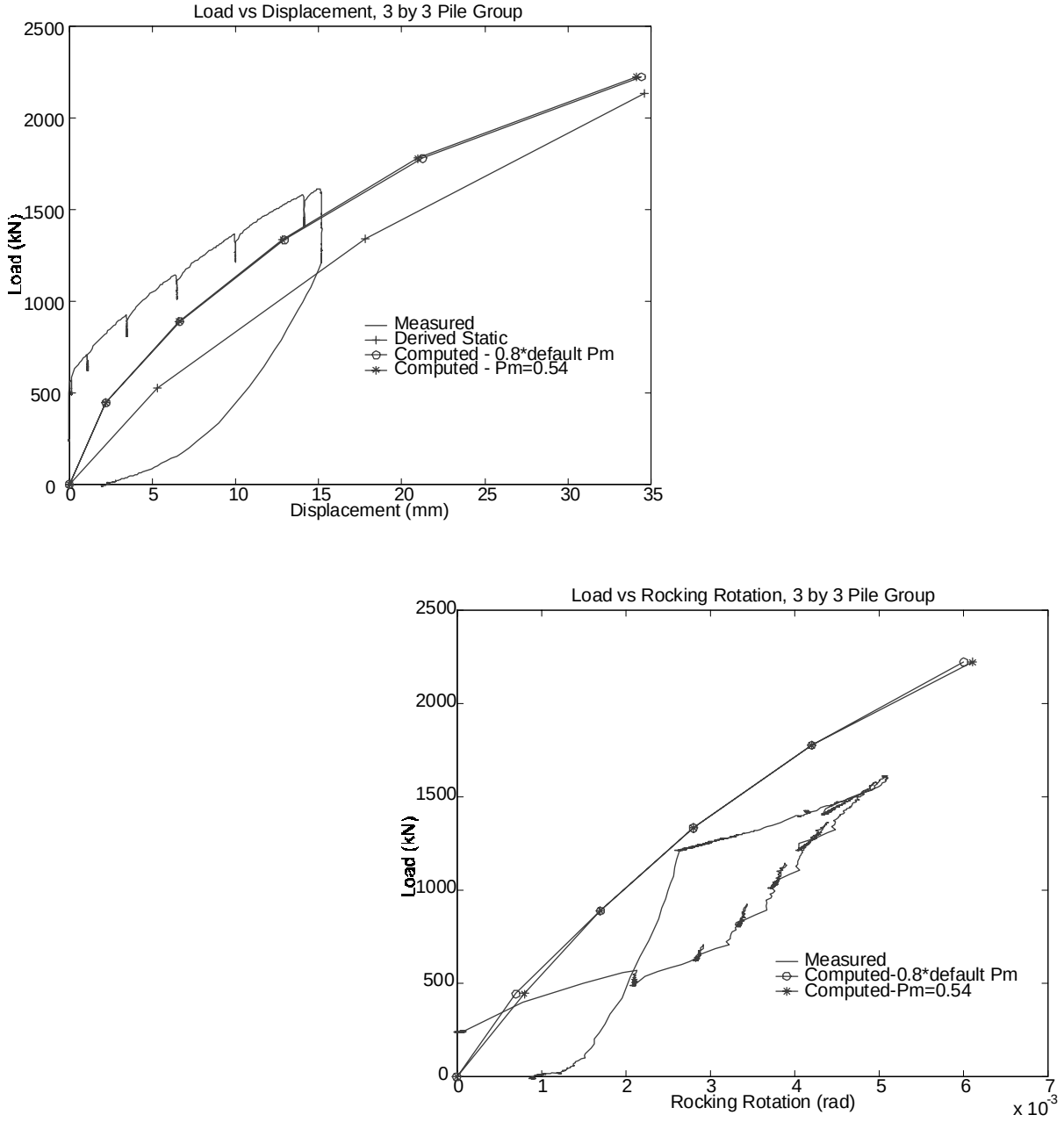

Figure 31. Measured versus computed lateral displacement and rotation, 3 × 3 pile group at Spring Villa Test Site.

event loadings. The stratigraphy (i.e., stiff crust over softer soil) at the location of the 9-pile group was similar to that at the location of the 12-pile group, which was situated a few meters away.

As with the 12-pile group, analyses were also performed using a uniform *p*-multiplier. The plot in Figure 31 of lateral displacements with the *p*-multiplier for all 9 piles set at 0.54 (i.e., the average of 0.4, 0.5, and 0.72) appears to be sufficiently close to the more realistic distribution for general engineering and design purposes, for reasons advanced for the 12-pile group.

Figures 32 through 34 provide plots of the computed and measured bending moments as functions of depth for three piles. Piles 10 and 11 are in the lead row; Pile 13 is in the trailing row. There is general agreement in the trend of the measured and computed bending-moment profiles, but the magnitude of the maximum moment values do not match. Some error in the maximum measured moment values may be attributed to the strains superimposed from the axial pile forces.

The distribution of shear to the pile heads by row position computed by the FLPIER model was as follows (compared with measured average by row position):

- Row 1 (lead) = 45% (FLPIER) = 45% (static) = 31% (Statnamic)
- Row 2 = 36% (FLPIER) = 36% (static) = 35% (Statnamic)
- Row 3 (trail) = 19% (FLPIER) = 19% (static) = 34% (Statnamic)

Note that the agreement between FLPIER and the static test measurements (average by row) appears to be excellent. However, this result is likely to be fortuitous, as there is a distinct lack of agreement between FLPIER and the results from the third and final Statnamic loading. As for all of the previous pile group tests in this study, the measurements are influenced by apparently random variations within the group attributed to variations in soil response unrelated to spatial position.

In summary, the group effects on the 9-pile group were substantial and slightly greater than those predicted using FLPIER with default *p*-multipliers. The stratigraphy of stiff crust over softer underlying soil is thought to have contributed to the more significant group effects. After calibration using the single pile–test data, the FLPIER model for static response of the 9-pile group appeared to capture the general load-deformation behavior well for engineering-design purposes, especially when the row-wise *p*-multipliers were reduced by a constant

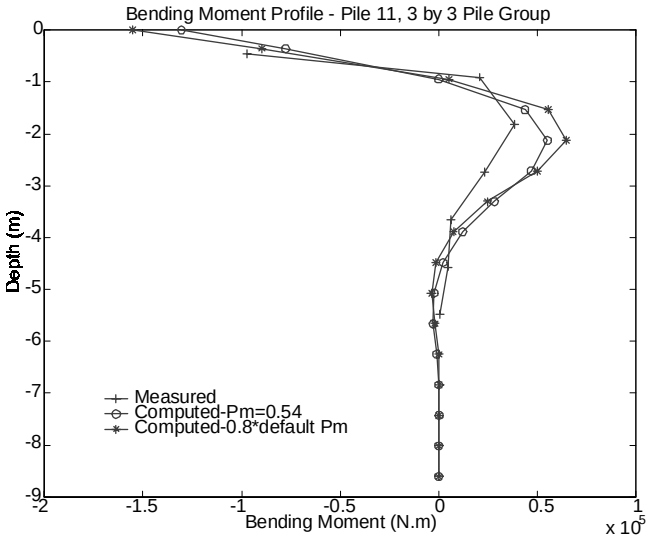

Figure 33. Bending moment profile, leading-row pile, 3 × 3 pile group at Spring Villa Test Site, group load = 1333 kN.

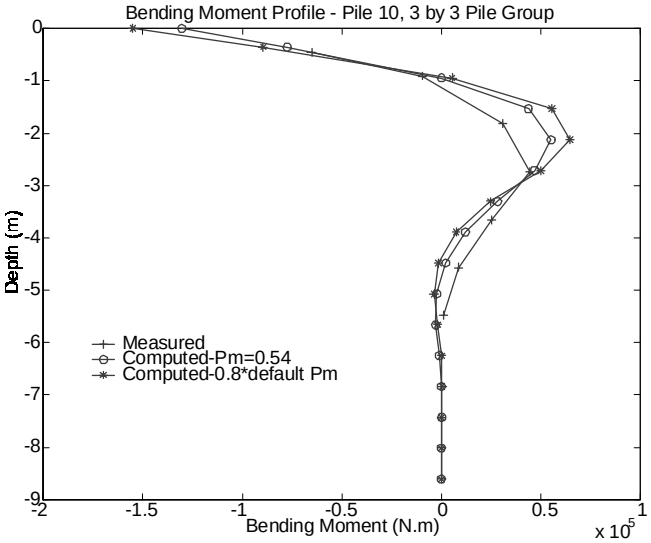

Figure 32. Bending moment profile, leading-row pile, 3 × 3 pile group at Spring Villa Test Site, group load = 1333 kN.

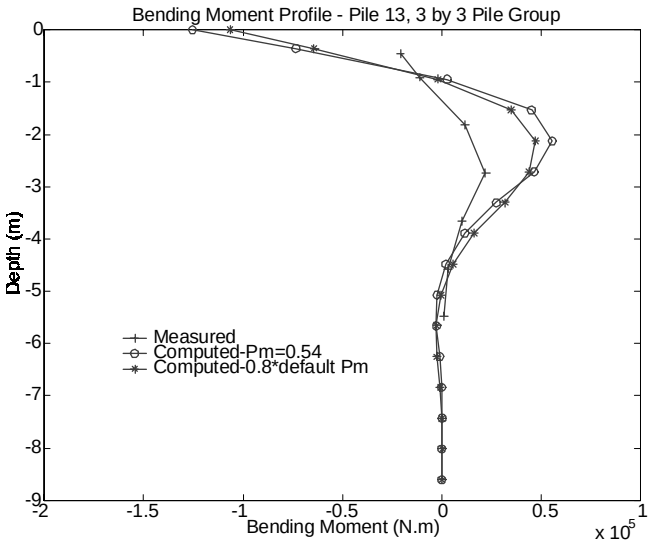

Figure 34. Bending moment profile, trailing-row pile, 3 × 3 pile group at Spring Villa Test Site, group load = 1333 kN.

factor of 0.8. The measured distribution of head shear from pile to pile was more variable than predicted by FLPIER, owing to apparently random variations in soil response that appear unrelated to spatial position of a pile in the group. The use of an averaged *p*-multiplier does not reproduce the measured head shear distribution pattern, but it appears to provide overall load-displacement results, as well as maximum moments and shear, that are suitable for design purposes. The deviation of the computed pile-by-pile head shears and maximum bending moments from the measured values will require a relatively high load factor to be used when using FLPIER or similar software to design the piles structurally to account for the uncertainty in the pile stresses that are unrelated to geometric positions of the piles.

Dynamic Response of Test Foundations

This section provides a brief summary of the dynamic characteristics of the test foundations that were measured during the Statnamic loading and an interpretation of the results. The Statnamic loadings, described in the previous section, represent a rapidly applied push to the foundation as gas pressure builds during the rapid burn of the propellant within the device. As the inertial mass is accelerated away from the test foundation, the gas pressure is diminished and finally vented. An example of the measured force time histories for Statnamic loading of the test foundations is provided in Figure D-30 (see Appendix D); these plots represent the force measured in the load cell between the Statnamic cylinder and the foundation during the four test loadings at Test Area 1 in Wilmington. Other test loadings are similar although the load amplitudes varied in magnitude (the Auburn [i.e., Spring Villa] loads were larger).

Evaluation of Dynamic Response Using Simple SDOF Model

The simple SDOF model for the Statnamic loading event was described earlier. This model provides a simple framework for capturing the components of dynamic motion of the test foundation in terms of inertia (i.e., force proportional to acceleration), damping (i.e., force proportional to velocity), and nonlinear static stiffness (i.e., force proportional to displacement). Although this model (in the form used for this study) does not have provisions to capture permanent set, gapping, hysteresis in the soil, combined rotation and translation, and so forth, the advantage of the use of the SDOF model is its simplicity and utility in placing the test results in a meaningful form for ready, direct comparison with static test results.

A direct comparison of the foundation stiffness at the rate of loading applied in the Statnamic tests is provided by comparing the total soil resistance versus the equivalent static soil resistance for each test foundation as shown in Figures 14, 15, 21, and 22. These plots demonstrate that the damping resistance observed during the Statnamic load event was small until large displacements were mobilized as is evident by the close tracking of these two curves. At large displacements (i.e., those generally exceeding 10 percent of the pile diameter), the damping resistance contributed significantly. The velocity was much higher at these larger displacements than it was at small displacements, but the soil supporting the pile was also subjected to considerably more hysteretic damping (resulting in energy loss) near the ground surface than would have occurred at lower displacements when the soil was still semielastic. Whether the damping effect is due to elastic energy dissipation or soil hysteresis or a combination thereof, it is impossible to tell from the observation that damping increases with increasing deflection, which also corresponds to increasing velocity.

In order to place the test observations into a useful form, however, the SDOF model may be used to derive a "rate effect" parameter to estimate the overall stiffness of the foundation at different rates of loading. This parameter can be considered a surrogate for the physical soil hysteresis and elastic wave dissipation effects, but it will be analyzed in conjunction with the SDOF model as if it relates only to velocity. Consider that for each Statnamic load event, the effective static stiffness is defined as the soil resistance (i.e., measured force corrected for inertia) divided by the maximum displacement (at which point the velocity is zero). The average rate of displacement, *V*, during this loading event is defined as the peak displacement divided by the time required to achieve this displacement from the initiation of loading. The total stiffness of the foundation is defined as the peak total resistance force (i.e., static spring force + viscous damping force) divided by the displacement at which this peak force occurs. So, the total stiffness compared with the static stiffness is a measure of the increase in stiffness caused by the viscous damping component derived using the SDOF model. A foundation could have a relatively large damping coefficient (i.e., force as a function of velocity), but if the velocity (or displacement) is not high during the loading event, the total stiffness will not be substantially increased above the static stiffness.

Using this concept and the average velocity for each loading event, the total dynamic stiffness normalized by the static stiffness from all of the Statnamic tests performed during this research is plotted as a function of displacement rate (i.e., average velocity) on a single plot as shown in Figure 35. This relationship is not meant to be an exact representation of the dynamic foundation resistance, but is rather meant to serve as a guideline for estimating the resistance that might be mobilized by a forcing function that induces the system to react at different rates (or to different deflections).

The data in Figure 35 reveal some interesting aspects regarding foundation resistance to dynamic applied loads. First, the test data from a range of soils and foundation geometries suggest similar effects of loading rate for steel piles. Larger damping at low displacement rates might be expected for drilled shafts because of structural cracking of the reinforced concrete at these smaller displacement rates.

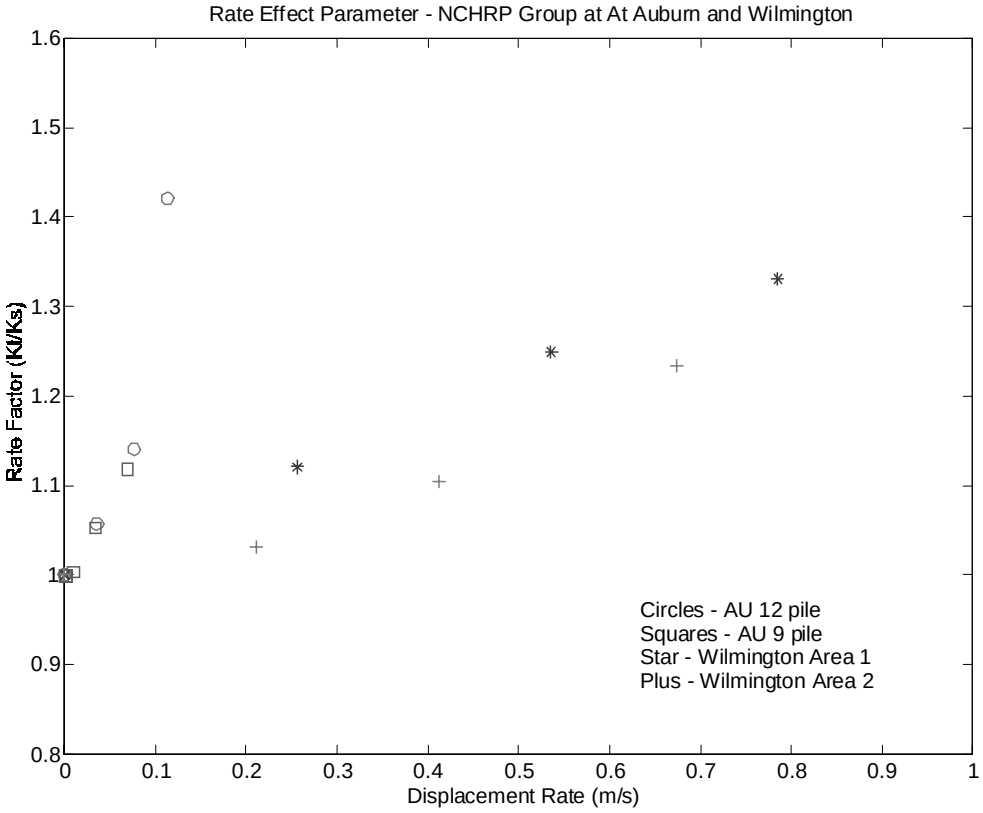

Figure 35. Effects of displacement rate on foundation stiffness.

Second, these data could be used to infer which cases of loading might include a significant component of damping resistance such that the overall foundation stiffness computed using a static model might be low. Consider the case of a barge impacting a pile foundation group: the barge causes the foundation to deflect laterally by 0.15 m (about 6 in.). Assuming that the barge causes this displacement to occur within approximately 3 s after initiation of loading, the average rate of displacement is approximately 0.05 m/s. The data in Figure 35 suggest that the total foundation stiffness for such a rate of displacement is not more than 5 percent greater than the static stiffness, a trivial amount considering normal engineering practice in estimating foundation stiffness for design. For all practical purposes, such a problem can be analyzed as a static problem from the standpoint of the foundation response (but obviously not from the standpoint of the barge, as the effective load is a function of the inertial forces generated as the barge momentum is altered).

Consider also the case of a seismic load with a frequency of around 0.5 Hz and a force that produces peak foundation displacements on the order of 0.1 m relative to the at-rest position. An average displacement rate from such a loading is on the order of 0.8 m/s (i.e., 0.2 m peak to peak divided by 0.25 seconds for ½ cycle). The data in Figure 35 suggest that the foundation stiffness might be on the order of 30 percent greater than the static stiffness for such high rates of loading, an amount that is certainly not trivial.

Of course, for cyclic loads such as seismic shaking, there may be other factors such as cyclic degradation, buildup of free-field pore pressures, and so forth. The data and discussion provided above serve (1) as a guideline for the implication of the data from this research on the magnitude of the differences in static and dynamic response under certain conditions and (2) to help identify circumstances in which dynamic analyses may be in order.

Dynamic Response Using FLPIER(D)

In order to evaluate the dynamic version of FLPIER that was developed for this project, FLPIER(D), the site-calibrated static *p-y* curves, pile geometries, cap properties, *p*-multipliers adjusted to average uniform static values (as described above), and the Statnamic force measurements from the load cell were sent to the computational research team at the University of Florida. In each case, the pile group model arrangement that was used was identical to the arrangement for the static tests, except for the load time history provided as input. For the Spring Villa 12-pile group, the partial fixity at the pile–cap connection was used exactly as it was in the static analyses. The model used includes both velocity-dependent damping and hysteretic damping in the *p-y* curves (as described in Appendix C). Some minor structural damping was included, in the form of proportional damping equal to (0.015 × cap

mass) + (0.01 × cap stiffness) + N [0.01 × pile mass + 0.01 × pile stiffness], where N is the number of piles in the group. Some other parameters were varied for one test case that will be discussed. The results of these computations were returned in the form of the FLPIER(D) output files. The plots provided in this section of the report were generated from those files by the experimental research team at Auburn University.

Presented in Figure 36 are the computed and measured displacement time histories for the four Statnamic loadings of the 12-pile group at Test Area 1 (i.e., Ratt Island) at Wilmington, North Carolina. The computed displacement for the initial peak is somewhat larger than the measured value for all four Statnamic loadings, and the model appears to have a frequency response that is too high after the initial peak. Note that the oscillations from the linear variable differential transformer (LVDT) measurements are thought to be the result of measurement errors related to vibration of the reference beam. Although the reference system was founded on piles, the ground was so soft that movements of this system could be visibly detected; the integrated accelerometer measurements are shown to indicate fairly high damping of the test foundation.

For the 12-pile group at Spring Villa, the inputs to FLPIER(D) were similar to those for the Wilmington test for Test Area 1, except for the differences in site-calibrated *p-y* curves caused by the soil differences and the partial-fixity parameter. Presented in Figure 37 are the computed and measured displacement time histories for the 12-pile group at the Spring Villa test site. For this test case, FLPIER(D) is seen to match well with the measured displacement data in terms of both amplitude and frequency. Note that the LVDT and accelerometer data are similar for this test, indicating little movement of the reference beam. It is not immediately apparent why the model appears to provide such good agreement at this site, but fares so poorly for the Wilmington data. Analyses were performed for these two test cases with the radiation damping set to zero; this made virtually no difference in the computed response as the damping component appears to be dominated by hysteretic damping.

The FLPIER(D) model for the 9-pile group are thought to provide the most realistic computed response because of the excellent measurements obtained on the concrete cap and the confidence that this cap provides a rigid and well-defined end condition. Presented in Figure 38 are the computed and measured displacement time histories for the second Statnamic loading of the 9-pile group. The computed initial peak displacement is relatively near the measured value (although somewhat low), and the frequency response is similar. Presented in Figure 39 are the FLPIER(D) results for the third Statnamic loading of the 9-pile group, computed using dyna-

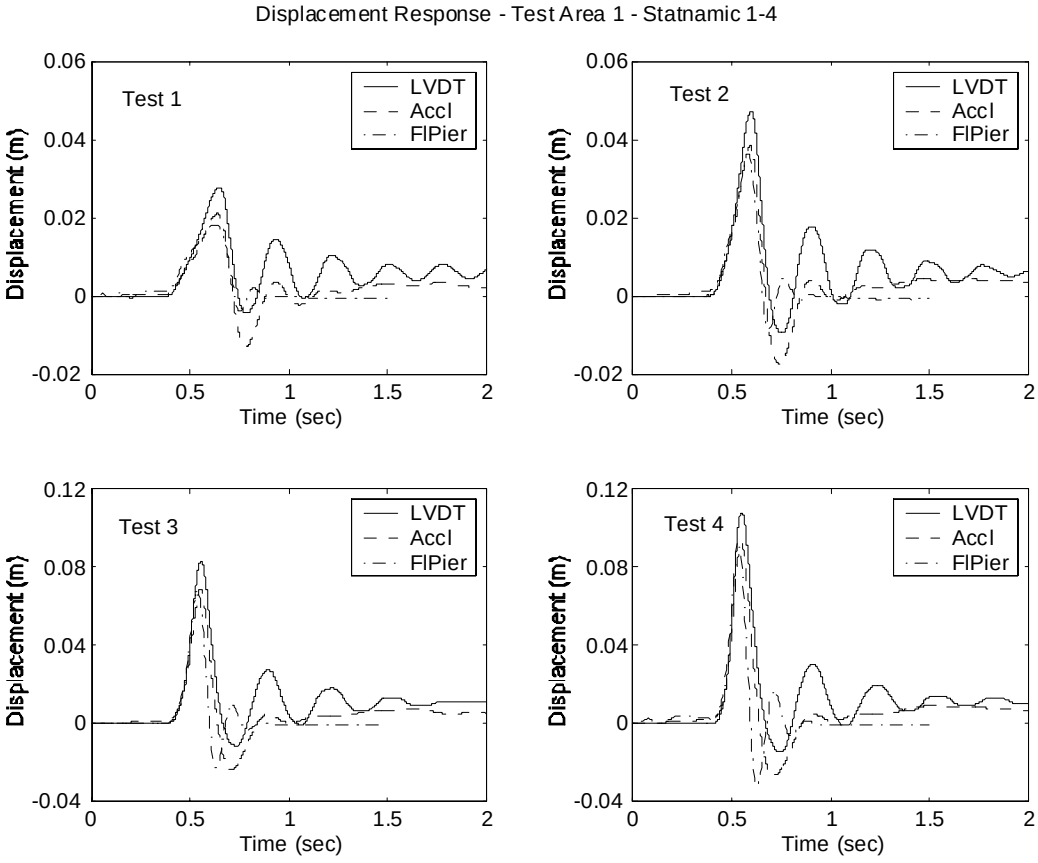

Figure 36. Computed and measured dynamic response, Wilmington Test Area 1.

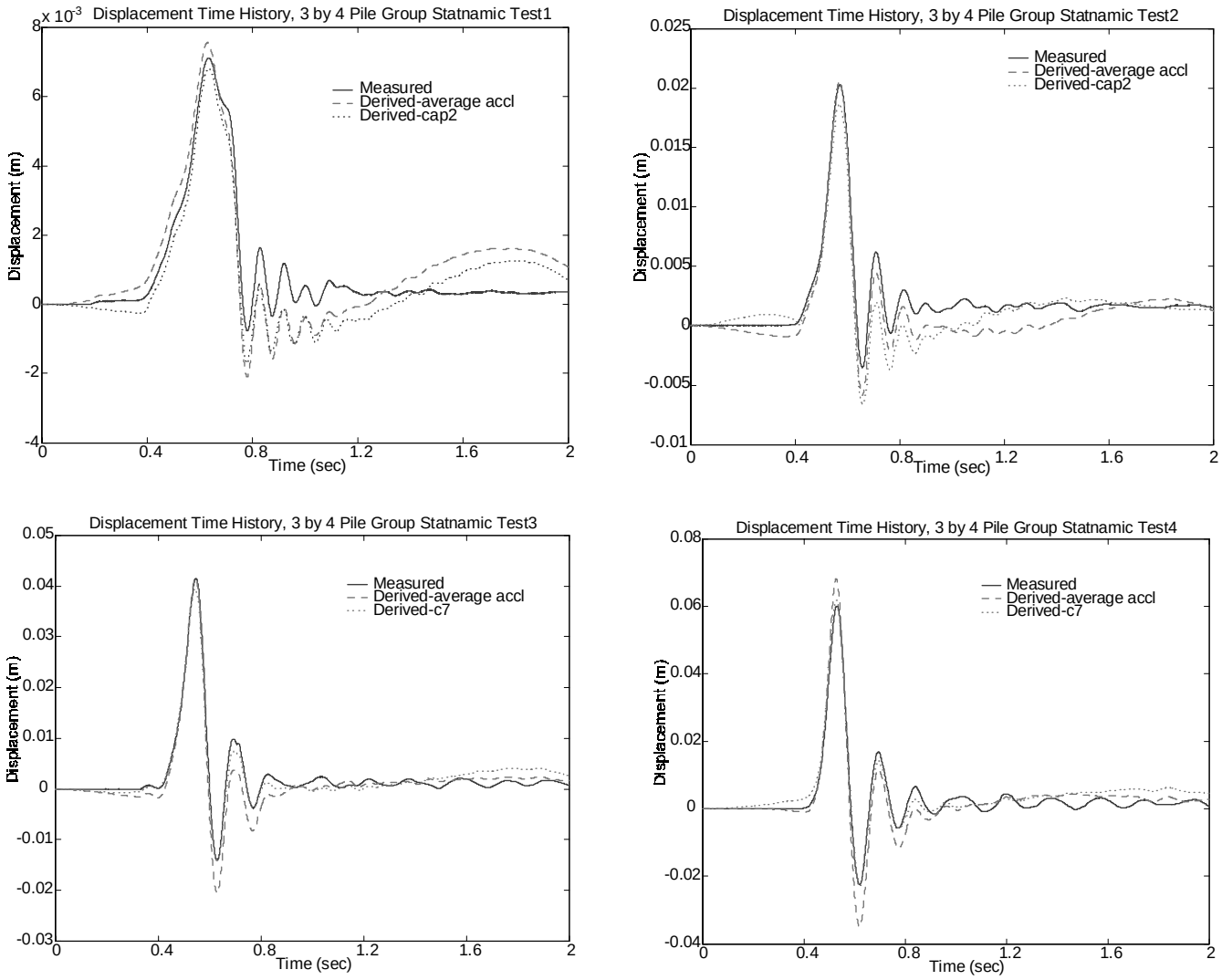

Figure 37. Computed and measured dynamic response, 3 × 4 pile group at Spring Villa Test Site.

mic soil parameters similar to the previous runs. These computed data are also close to the measured response.

The third Statnamic loading of the 9-pile group was used to evaluate the effects of various input soil parameters within FLPIER(D) in order to develop some sense of the relative importance. Also shown in Figure 39 is a computed response for which a dynamic rate effect has been added to the soil *p-y* curves. This effect has been included as outlined in Appendix C, with a soil factor F2 of 0.07 and a baseline (i.e., static) loading rate of 7E-6 m/s (1 in./h). The effect of loading rate using these parameters is seen to be negligible, as the two computed curves are virtually identical.

FLPIER(D) was performed with mass added to the *p-y* curves in order to represent some contribution of participating soil mass within the pile group. Data are presented in Figure 40 that illustrate the effect of adding mass equal to ½ of the soil mass within the group, distributed evenly to the *p-y* curves on the group piles. The effect is seen to be most significant in extending the period of oscillation. The effect on the amplitude of motion is fairly small for this group.

Data are presented in Figure 41 to illustrate the effect of radiation damping on the overall computed response. The influence of this parameter is seen to be minor; the computed damping in this foundation is clearly dominated by hysteresis.

The conclusion resulting from these parametric runs using FLPIER(D) is that the dynamic response of the model of the test foundation is dominated by the static stiffness, the overall mass of the system, and the hysteresis in the *p-y* curves.

SUMMARY

The findings from the test program in Chaiyi, Taiwan, the analytical modeling; the numerical modeling; and the testing programs in Wilmington, North Carolina, and in Auburn, Alabama, can be summarized as follows:

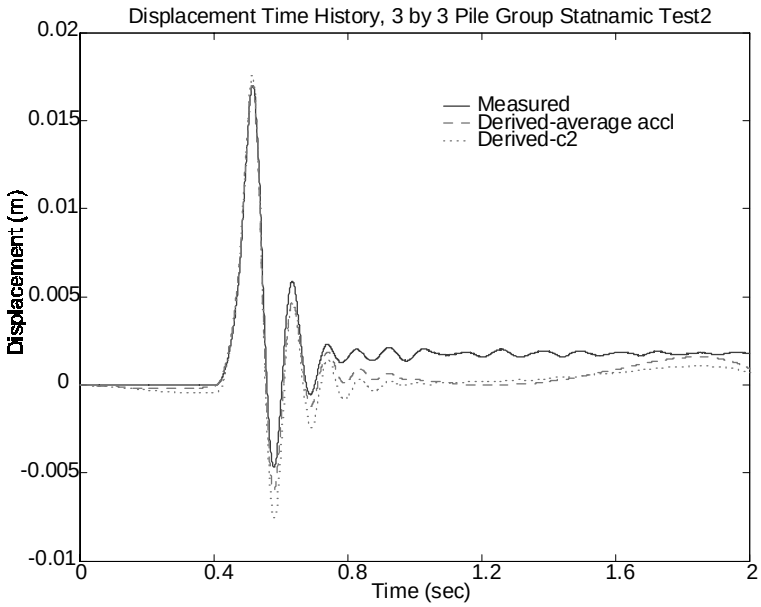

Figure 38. Computed and measured dynamic response, 3 × 3 pile group at Spring Villa Test Site.

1. Analysis of static lateral load tests of a 2 × 3 × 3D–spaced group of large-diameter bored piles and a 3 × 4 × 3D–spaced group of large-diameter driven displacement piles in silty to clayey fine, saturated sand on the western Taiwan coastal plain indicated that *p*-multipliers for groups of bored piles are lower than those for groups of driven piles, particularly in the front or leading row. Comparative values are given along with default values from FLPIER in Table 3.
2. Layered continuum analyses of the dynamic lateral loading of a single pile and of two parallel piles at varying spacings and harmonic frequencies in cohesionless soil were conducted. These analyses indicated that the harmonic dynamic lateral response of a single pile

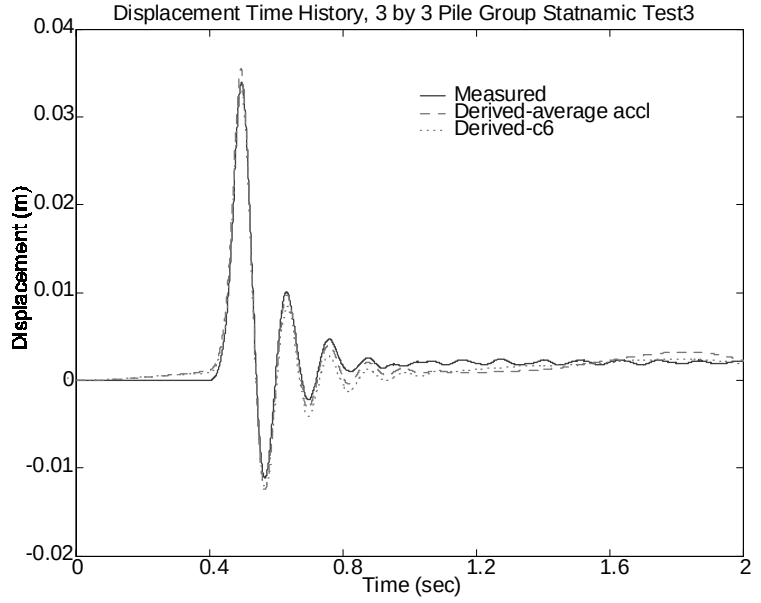

Figure 39. Computed and measured dynamic response, 3 × 3 pile group at Spring Villa Test Site.

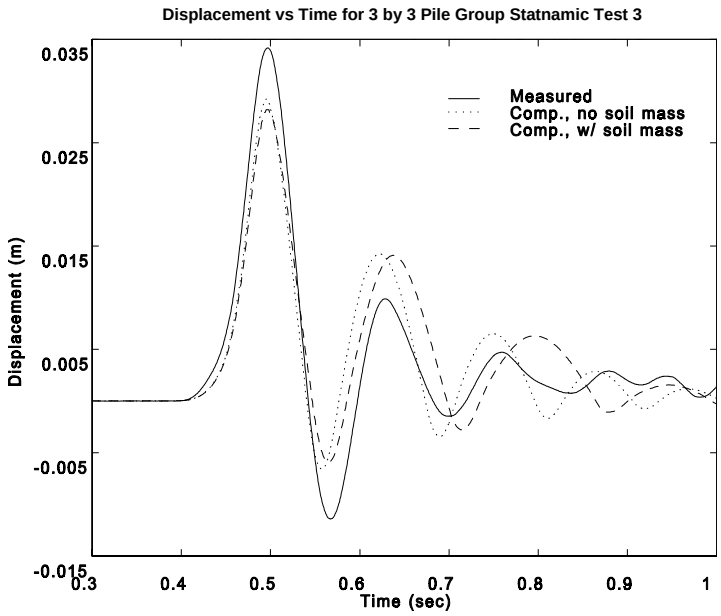

Figure 40. Effect of adding soil mass to computer model.

could be simulated well using static *p-y* curves, in particular those recommended for sands by the American Petroleum Institute (*41*), provided a velocity-dependent resistance is added to the static resistance at a given local pile displacement, *y*. The velocity-dependent stiffness can be expressed through a damping parameter, *c*, that is a function of several other parameters, including the frequency of vibration. This concept is expressed mathematically in Equations 4 and 5. Dynamic *p*-multipliers for piles in a group for cohesionless soil derived from analytical two-pile interaction analyses are given in Figure 9. With the mathematical formulation that was used, there is no difference in the *p*-multiplier, ρ, based on the relative position of the pile

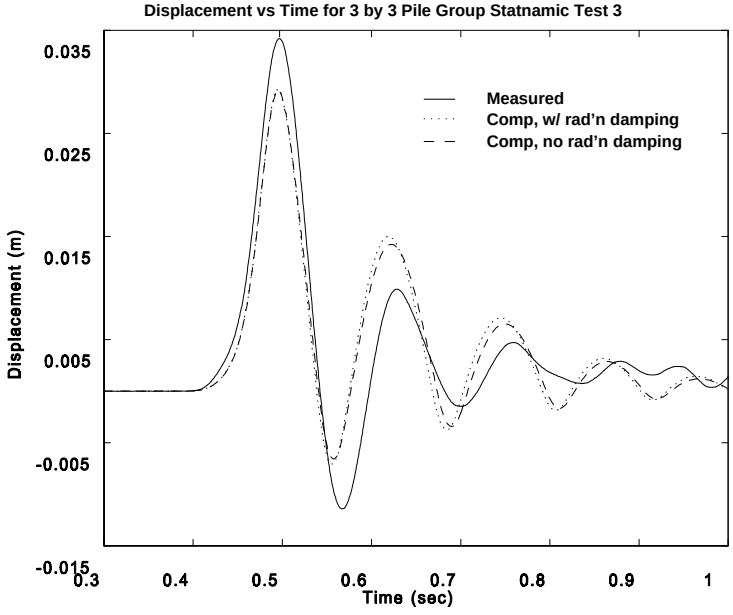

Figure 41. Effect of radiation damping on computer response.

within the group relative to another pile (e.g., leading, trailing, in-between, side-by-side, or skewed). Only the c-c spacing, pile-head displacement, and frequency of loading affect ρ. In a group of more than two piles, ρ is obtained for a given pile by multiplying together the ρ values for all surrounding piles. For a series of dimensionless frequencies, $0.02 < a_o < 0.12$ ($a_o = \pi fD/V_s$, in which f is the frequency of harmonic pile motion, D is pile diameter or equivalent diameter for a noncircular pile, and V_s is the shear wave velocity of the soil), ρ is expressed in Figure 9. This figure applies to medium-dense sands, in terms of relative head displacement, y/D, and c-c pile spacing. Similar graphs for soils of different density are provided in Appendix B. For relative pile-head displacements of interest for extreme event loading—for example, 0.075 for the more flexible driven pile group in Taiwan, and for $0.02 < a_o < 0.12$, which may be typical for seismic loading as long as the soil does not liquefy—the computed values of ρ are less dispersed row by row than was measured during static testing, but the average analytical ρ-value was about equal to the average measured value of ρ (see Table 3). However, for the more rigid bored pile group tested in Taiwan, in which the maximum y/D was only 0.013, the row-by-row and average analytical ρ values were smaller than the measured static ρ values (see Table 3). This "*p*-multiplier" effect appears to be less dependent on frequency than on pile deformation (according to the analytical model) and method of construction (according to the test program in Taiwan; see Appendix A). It appears tentatively, therefore, that values of ρ obtained from static load testing of pile groups or inferred from static *p-y* criteria and criteria for ρ for static design can be used to analyze pile groups undergoing low-frequency, large-displacement dynamic (i.e., extreme-event) loading, provided the relative head displacements are in the order of 0.05 to 0.10 D during the extreme event. During static loading, the ρ values did not appear to be highly dependent on y/D, as shown in Table A-2 (see Appendix A), so the use of values of ρ obtained from static lateral group tests or from published criteria to model low-frequency, low-displacement ($0 < y/D < 0.05$, approximately) extreme-event loading was not established in this study. In any event, damping must also be included in the *p-y* model (e.g., using Equations 4 and 5 or through explicit modeling of soil or structural material hysteresis, or both [see below]).

3. The analytical layered, continuum model (see Appendix B) referred to above does not consider soil hysteresis, nor does it consider nonharmonic or kinematic loading directly. To provide the designer with a versatile, user-friendly computational tool, FLPIER(D) (see Appendix C), a dynamic version of the FLPIER program, was written to model dynamic laterally loaded pile groups in the time domain with hysteretic soil and structural material (i.e., cap and piles) damping, along with gapping. The value of c proposed for application to static *p-y* curves in Equation 5 can be input into FLPIER(D), which uses several standard static *p-y* models for clay and sand. FLPIER(D) also permits the modeling of both inertial loading (i.e., from the cap) and kinematic loading (i.e., through the soil), although the latter was not verified. FLPIER can consider various levels of fixity of the pile to the cap and considers nonlinear axial behavior, which affects the lateral behavior of the group if there is any fixity between the piles and the pile cap. It appears that FLPIER(D) may exhibit difficulty converging under some conditions when there is partial fixity at the pile heads, but this did not occur for the field tests that were analyzed here. Overall, FLPIER(D) provided reasonable simulations of the impulse (i.e., Statnamic) tests on full-scale pile groups that are summarized below.
4. This comment and the following comments apply to the field-testing program carried out with driven pipe piles in North Carolina and Alabama. The Statnamic loading sequence (i.e., a series of lateral impulses with increasing amplitude) was used to simulate dynamic extreme-event loading, such as barge impact and seismic loading. Although the relatively long time lapse between pulses did not allow for simulation of the response of soils in which high pore water pressures build up during the extreme event (e.g., liquefiable soil), it did allow for the simulation of the effect of loading rates and displacement amplitudes produced in the soil by the movements of the piles.
5. With only a few small exceptions, the instrumentation and measurements appear to provide reliable indications of the pile group behavior. The strain gauge pairs within each pile provided reliable bending-moment measurements; however, the superposed axial forces appeared to contribute to some measurement errors in converting the measured strains to bending moment. Conversely, the superposed bending strains made the measured axial forces in the piles subject to large measurement errors. In essence, steel pipe piles do not make very good load cells when large bending stresses are imposed and measurements are obtained using only an averaged pair of strain sensors. Previous field loading tests that use a pinned connection avoid some of these measurement problems because axial and bending forces are not superposed on the piles; however, such tests are less realistic foundation models than are the fully coupled foundation tests performed as part of this research.
6. The group effects were substantial for all foundations tested, including the tests in Taiwan, and were slightly larger than expected at the Spring Villa site using the default *p*-multipliers for both the 3D and 4D c-c spac-

ing. The default *p*-multipliers used by the FLPIER code provided excellent agreement with the observed test results. Close agreement at the Spring Villa site was obtained between measured and computed results when *p*-multipliers were scaled down by a factor of 0.8. This reduction factor appears to be associated with a stiff-over-soft soil profile. The differences in overall group performance (i.e., shear load versus lateral deformation and rotation) between the 3D and 4D c-c spacing predicted by using the interpolated *p*-multipliers in the FLPIER code appear to be approximately correct.

7. The axial stiffnesses in the piles for the 4D spacing appeared to be higher than was the case for the 3D spacing. It is suggested that designers may apply judgment and use softer *t-z* curves for closely spaced groups of piles (which is accomplished by using a smaller shear modulus within FLPIER), but the measurements of group rotation for these two test cases are insufficient to develop specific design guidelines. No piles were observed to yield either structurally or geotechnically in the axial direction during these tests.
8. The measured distribution of shear loads to the piles in the group *by average row position* was generally less extreme than was computed using the row-by-row *p*-multipliers in FLPIER.
9. The measured distribution of shear loads to the individual piles within the group was more extreme than was computed using the row-by-row *p*-multipliers in FLPIER. There appeared to be significant and substantial variation in individual pile stiffness that was unrelated to geometric position alone. Random spatial variability in soil response caused by stratigraphic variations, installation effects, or other uncontrolled variables was at least as important as geometric position of the pile within the group in determining the actual shear distribution to an individual pile within the group. The general pattern of greater load to the leading row and less to trailing rows could only be discerned by observing average response for piles in a given row. This behavior was observed not only for the piles driven within the frame template, but also for piles driven in the free field for the 9-pile group, which had a suspended, cast-in-place concrete cap constructed after pile driving was completed. Therefore, for purposes of designing the piles and pile–pile cap connections structurally, the average row-wise moments and shears computed using a code such as FLPIER should be multiplied by a load factor. Figures 19, 28 through 30, and 32 through 34 suggest that this factor should be on the order of 1.2 for bending moment. Further tests of grouped piles at other sites are clearly justified for purposes of defining this factor more accurately.
10. The use of the steel frame for pile group testing proved to be difficult and time consuming and led to uncertainties relating to small connection details. Although the difficulties with the use of this frame could be resolved, the use of a cast-in-place concrete cap proved to be much more reliable and cost effective and provided better measurements. The use of the frame on future projects is not recommended.
11. The static FLPIER computer model using a single average *p*-multiplier (which was equal to the weighted average of all the *p*-multipliers by row position) provided a good prediction of overall static load-deformation behavior. Given the many other uncertainties in the actual distribution of shear and moment, this simple approach may be sufficient for many engineering design applications, provided an appropriate load factor (which was discussed in Item 9) is applied to the results.
12. The rotation of the cap and, to a lesser degree, the lateral stiffness in translation were sensitive to the axial stiffness of the piles. When there is any degree of fixity of the pile heads to the pile cap, attention must be paid to axial pile stiffness when experimentally deconvolving *p-y* curves or *p*-multipliers, or both, for the pile group.
13. The interpretation of the Statnamic loading using the simple SDOF model appears to provide a good correlation with static test results for load versus lateral translation and natural frequency of vibration. The rate of loading effects with the Statnamic loading appear to be relatively modest although they increase with increasing displacements. The Statnamic device provided the capability to push the 9-pile group to large lateral displacements after the reaction foundation failed during the static testing and so was a very valuable part of the test program.
14. At the rates of loading achieved in the field (which were similar to rates of loading in seismic events), static soil stiffness was the dominant component of soil resistance to lateral load. Damping adds significant additional stiffness only at a relatively high displacement rate (i.e., velocity)—an increase on the order of 30 to 40 percent from the static resistance at a velocity of around 0.8 m/s.
15. In general, the static version of FLPIER was successful in modeling the test results. The partial fixity at the pile–frame connection appears to be modeled appropriately using this feature of FLPIER. The dynamic version did a reasonable job of modeling the Statnamic loadings of the 12- and 9-pile groups at Spring Villa, capturing the peak displacements and frequency of motion well. This agreement was achieved by (1) using as inputs to the model static *p-y* curves for the soil, such as the Reese et al. (*43*) *p-y* curve formulation for stiff clay with small changes to calibrate the *p-y* curves to the behavior of reference or "control" piles at the test site; (2) defining (internally) unloading branches to the *p-y* curves in which hysteretic damping was included in the system by allowing the *p-y* curves to "loop" (see

Appendix C); (3) including modest material damping (as proportional damping), as defined in this chapter, for the piles and cap; and (4) using a uniform average of the default static *p*-multipliers. The Wilmington model was less effective at modeling the measured response, with a computed frequency of motion that was too high. The reasons for this poor correlation are as yet unknown, but additional evaluations of the FLPIER(D) model for this case are ongoing.

16. Sensitivity studies conducted using the FLPIER(D) model for the 9-pile group suggest that the most important parameters controlling the computed dynamic response to inertial lateral loading are the static soil stiffness (including axial stiffness of individual piles), the overall mass of the foundation, and the hysteresis damping provided by the *p-y* curves. Radiation damping, structural damping, rate effects in soil stiffness (as defined using the default parameters outlined in Appendix C), the use of uniform average *p*-multipliers in lieu of row-by-row values, and the addition of a modest amount of soil mass had relatively small effects on the computed response.

CHAPTER **3**

INTERPRETATION, APPRAISAL, AND APPLICATION

INTERPRETATION

The primary reason for initiating this study was to develop guidelines and computational vehicles for designing laterally loaded groups of piles for transportation structures. The emphasis was on extreme-event dynamic loading, such as ship impact and seismic loading. As the research developed, it appeared that this type of loading would be amenable to analysis by means that have been well developed in the past for modeling the static behavior of laterally loaded pile groups. That is, by applying inertial effects to the structural elements; using static stiffness relationships for the soil (in the form of *p-y* curves); adding soil damping through either a viscous damping factor or hysteresis and gapping in the *p-y* model; using *p*-multipliers developed from previous, full-scale and centrifuge static load testing; and employing minor structural material damping, solutions to inertial loading events (i.e., loading through the pile cap) could be obtained that are sufficiently accurate for design purposes.

A computational model, a dynamic version of FLPIER, was developed to include the characteristics listed above. This model was then verified against a series of full-scale static and impulse-type dynamic tests performed in the field at two sites. The impulse loading events used in the field tests can be classified as "inertial," in the sense that loading was applied through the cap, rather than "kinematic," in which the loading would be applied to the piles to the soil. Seismic loading is a combination of inertial and kinematic loading. Although FLPIER was not verified for the case of loading through the soil, it was programmed with the capability to model such loading through time-domain motion of the supports for the *p-y* curves; the motion mimics free-field ground motion.

Although it should be possible to include a liquefaction model in the *p-y* curve formulation, in neither the field tests nor FLPIER was any attempt made to model explicitly the effects of liquefying soil.

This approach to modeling the test groups appeared to give results that are sufficiently accurate for the design of pile groups in nonliquefying soils at a limited number of sites and generally should be applicable to the design of pile groups in nonliquefying soil as the number of sites at which the method has been calibrated increases. It should be pointed out that this approach is not limited to the code used here (i.e., FLPIER), but should apply to any structural program that includes the inertia of structural elements and uses hysteretic *p-y* curves that can be modified by *p*-multipliers.

APPRAISAL

Using the general inputs described above and without using viscous damping factors for the soil, the computational tool FLPIER(D) provided reasonable predictions of the field test behavior, with two exceptions. First, the program did not give reasonable results when the pile heads were specified to be partially fixed (i.e., rotation permitted with some resisting moment developing) to the pile cap. Second, the program did not predict accurately the distribution of either head shears or bending moments among the various piles. The first deficiency likely is due to a "bug" in the program that has not yet been located. In due time, it is expected that this problem will be solved, but it could not be solved in the time frame available to the research team. The second deficiency appears not to be a deficiency in the program, but rather to be a result of spatial variations in lateral soil resistance among the locations of the individual piles in the group that is not associated with group action. For example, it was shown that extreme differences in the installation method (e.g., boring and casting piles in place versus driving displacement piles) produced rather large differences in soil resistance against both individual piles and pile groups at an independent test site in Taiwan. For this reason, it is recommended that the ideal (computed) maximum shears and moments in the various piles be multiplied by a load factor before the piles are designed structurally.

The field test program included only two sites that, although dissimilar, did not represent geotechnically all of the soil types of concern in designing laterally loaded pile groups for extreme events. When using the approach described here, it is expected that the most accurate designs for impact or seismic loading will be achieved when full-scale pile group tests are tested at the site of interest. In the event that large, portable inertial vibrators become available in the future, using vibrators instead of the Statnamic device will undoubtedly prove more appropriate for simulating seismic loading. The test piles that were developed for this project would be appropriate for future field studies; however, the steel frame should be abandoned in favor of using a cast-in-place concrete cap.

APPLICATION

The results and analyses of the field load test program suggest the following engineering guidelines for the design of pile groups subject to lateral loading.

Pile-Soil-Pile Interaction and Group Effects

The use of *p*-multipliers derived from static testing, as implemented in FLPIER, is an effective means of modeling the effects of group action on the soil resistance. In granular soils, consideration should be given to reducing the default values of the *p*-multipliers (see Table 3) when bored piles (i.e., drilled shafts) are used by (1) about 40 percent on the leading row if row-by row *p*-multipliers are used or (2) about 20 percent if a single, average *p*-multiplier is used for all rows of piles. The default values provided in FLPIER (see Table 3) from the soils at the field test sites for 3D and 4D c-c pile spacing appeared appropriate when the piles were driven displacement piles. For the rare case in which closer spacings (2.5D) are used and granular soil is present near the ground surface, the *p*-multipliers that are approximated from Figure 9 are recommended for use.

Although the general trend of distribution of shear and moment to the piles within a group is similar by row position to the trend predicted by the row position–based *p*-multipliers in Table 3, the actual distribution of shear and moment that might be expected among the piles in the row considered on a realistic, full-sized pile group foundation is subject to significant random variations because of variations in soil properties. This unpredictable variability is at least as significant as any geometric variability; therefore, designers should provide accommodations for variability of computed maximum bending moments in the piles by multiplying the computed average maximum moment for a pile in a given row by a load (i.e., moment multiplication) factor of about 1.2 before completing the structural design of the piles.

The use of a simple average *p*-multiplier for all piles in the group based on a computed weighted average of the individual piles based on row position provides a computed response that is equally suitable for design purposes. Given the uncertainties related to the above-noted variability and to the unknown, reversible, and likely variable direction of loading from a seismic event, it appears sufficient for design purposes to use this simplified approach.

The test data and the modeling efforts both indicate strong coupling between lateral and rotational stiffness. The axial pile stiffness has a major influence on the rotation of the cap, and this stiffness is strongly coupled to the lateral stiffness. The use of group models such as FLPIER or other computer codes that include axial stiffness of the piles are recommended. The use of uncoupled analyses could significantly underestimate or overestimate the lateral stiffness, particularly if the pile cap is assumed not to rotate.

Dynamic Behavior

The lateral dynamic response for large lateral loads that are similar to extreme-event loading is strongly nonlinear, even when the structural response of the piles and cap is within the linear elastic range. The damped resonant frequency is reduced and the damping increases with increasing displacement amplitudes; therefore, damping needs to be included in the design model (e.g., FLPIER).

If funds are available at a bridge site, Statnamic loading of a test group should be strongly considered, especially in the case of critical structures. The Statnamic loading device provides a mechanism to apply large lateral loads to a test foundation with a force time history that is close to the resonant frequency of a full-scale test foundation. Except for the largest pile groups, this system is effective at inducing large-amplitude dynamic motions in test foundations and provides a means of obtaining meaningful dynamic measurements of the system response. The Statnamic loading mechanism is limited in producing the cyclic degradation in soil strength and stiffness that might be expected during a seismic or repeated loading event and could be replaced with a portable vibrator. At present, however, inertial vibrators with force amplitudes large enough to produce lateral deformations in the piles equivalent to those that are expected in major seismic events in full-scale pile groups are not available. When the vibrators become available, they may be employed in place of the Statnamic device.

A simple SDOF model for evaluating the dynamic response of a pile group to Statnamic impulse loading, however, can be very useful for identifying fundamental system properties and extracting nonlinear static stiffness, which is the most important parameter in predicting dynamic response. SDOF modeling can be done independently of computer simulations and may, in certain circumstances, be sufficient for evaluating the response of the pile group.

For more in-depth analysis, FLPIER(D) or a similar code should be used to simulate the behavior of the group. Modeling the dynamic response of the soil using hysteretic, static *p-y* curves and static *p*-multipliers seems to capture well the most important aspects of foundation behavior during dynamic loading. The inertial effects of the structure above grade are straightforward and must be included in the simulation because they are important to the overall system response. Some small amount of system damping, which can be modeled with additional participating mass, may be considered, but this damping does not appear to be a major influence on the foundation. Compared with the static response, the most important elements in the dynamic soil response are the gapping and hysteretic damping and the rate effects in cohesive soils. Radiation damping may contribute to overall damping, but it is difficult to separate the effects of radiation damping from that of hysteretic damping. For this reason, all damping for low-frequency, large-displacement (i.e., $y/D > 0.05$) loading is modeled as hysteretic for seismic loading conditions.

The static stiffness is the dominant component of resistance to lateral load for the low-frequency motion characteristic of a full-scale group of piles or shafts (in the range of 2 to 4 Hz). Damping adds significantly to the resistance at higher amplitudes of motion (e.g., in excess of 20 to 30 mm), with increasing effect at larger amplitudes. For vessel impact loads, which

may occur at a much lower rate of loading than seismic loading (e.g., load times on the order of several seconds to peak), the static response is likely to dominate most cases, and static analyses should be only slightly conservative (unless inertial components of the structure are substantial).

APPLICATION OF FLPIER(D) TO THE ANALYSIS AND DESIGN FOR SEISMIC LOADING

FLPIER(D), the dynamic version of FLPIER, was developed in this study to facilitate interpretation of the field test results and to serve as a design tool for those who wish to use it. It is emphasized that FLPIER(D) is one of many suitable tools that can be used to analyze pile groups under lateral loading.

The following is a summary of the process used to analyze a bridge pier for earthquake loading. This process assumes that the reader is familiar with FLPIER and how to develop models of bridge piers using the FLPier_Gen graphics generator. FLPier_Dyn_Gen is the equivalent generator in the new code, FLPIER(D). Some hand editing may be necessary because all of the capabilities for the FLPier_Dyn engine are not available in the FLPier_Dyn_Gen generator.

Before executing the program, users should download the program from www.ce.ufl.edu/nchrpdemo.html. A help file and a sample data file can be found on this download. This program will be disabled after December 31, 2001, as a precaution against propagating a new program that may have bugs. If the program has never been installed before, the user should understand that the graphics interface uses a font that most Windows 98 and new NT systems do not have. Users are encouraged to go to the software link at www.ce.ufl.edu/ and download the font for their operating system, following the instructions given at that site.

In order to illustrate the use of FLPIER(D), the following example is given. The analysis process is based on the results from the Statnamic field tests for this project and the ensuing dynamic model results using FLPIER(D).

Consider the following soil properties, which are assumed to apply to all of the piles at the location of the pier to be analyzed.

Example:

Layer	Thickness (in.)	Modulus (k/in.^{2})	Unit Weight (k/in.^{3})	Undrained Shear Strength (k/in.^{2})	ϵ_{50}	ϵ_{100}	Shear Modulus (k/in.^{2})	Poisson's Ratio	τ_f (k/in.^{2})	Tip Bearing Capacity (k/in.^{2})
1	360	0.5	0.000066	0.003	0.020	—	1.5	0.3	0.15	
2	480	0.5	0.000071	0.030	0.005	0.03	1.5	0.3	0.15	
Tip							1.5	0.3		0.27

NOTE: 1 k = 4.45 kN; 1 in. = 25.4 mm.

These properties were taken from soil borings near the subject pile group. The soil profile is similar to that at the Wilmington site (i.e., Cooper River Bridge) described earlier in this report and elaborated upon in Appendix D. From these data, an initial pile system was developed. Note that the parameter τ_f is the ultimate unit side resistance used by FLPIER or FLPIER(D) to produce axial unit load transfer curves. A very high value was used in this example analysis to force the response of the pile group to be translational in the lateral direction of loading, rather than both translational and rotational. In most cases, this value would be the estimated value of maximum unit side resistance.

The following step-by-step procedure is then followed to develop the input file.

Step 1: *Estimate an equivalent static load for initial sizing of the piles.*

Use 10 percent of the pier + bridge weight. For this example, 2,000 kips (8.9 MN) was used.

Step 2: *Create a pier model with a trial size and number of piles.*

The "Pseudo Dynamic Curve" option is used. This option requires an approximate fundamental period of the structure (17 cycles/s was chosen for this example) and the shear velocity of each soil layer. For this example, 2,000 in./s (50.8 m/s) was used for soil shear wave velocity.

Step 3: *Run this pseudo-dynamic option and iterate on the size and number of piles until the displacements of the pile head and the pile and pier moments are within design tolerance.*

Set the piles to "linear" with "properties," obtain convergence on the soil, change the pile to "nonlinear," and finalize the pile configuration. The file used for this analysis is included with the example files as part of the FLPier_Dyn install and is named "design_stdyn.in." (Note that the "nonlinear" option of the program automatically checks the moment capacity of the piles and pier elements because of the nonlinear bending. If the program converges, the pile sections have sufficient capacity.)

During the execution of this pseudo-dynamic phase of the analysis, FLPIER(D) used the following:

- The default *p-y* curves for the soil types encountered (Matlock soft-clay criteria [*42*] in Layer 1 and Reese et al. stiff-clay below-water-table criteria [*43*] in Layer 2).
- The simplified pseudo-dynamic reduction (i.e., damping) model in Appendix B for the *p-y* curves, which was turned on for the pseudo-static analysis (i.e., the preliminary sizing of the piles achieved in this phase). This model provides an estimate of damping and was assumed to apply to clay *p-y* curves (conditions in this case) as well as to sand *p-y* curves (conditions assumed in Appendix B). A different approach was used in the next phase, as described subsequently.
- A pile cap that was assumed to be flexible, but elastic. It was assigned a Young's modulus of 4,400 ksi (30.3 GPa).

Cap–soil interaction was not modeled. The piles were rigidly framed into the pile cap. (Note that at this time, only rigid framing and pinned connections should be assumed at the pile heads in FLPIER[D] because FLPIER[D] may have difficulty converging when partial pile-head fixity is specified.)

- The default *p*-multipliers. That is, values of 0.8, 0.4, 0.3, 0.2, and 0.3 were used from front row to back row in the 5-row × 4-column group that was finally developed. (Note that these would be appropriate for a driven pile group, but possibly not for a drilled shaft group in cohesionless sands below the water table, as is demonstrated in Appendix A. Because the shear wave velocity of the soft clay at this site is low, the natural frequency of the bridge is high, and the pile radii are large, a_o is very high [i.e., > 1]. Thus, the *p*-multipliers that are given for sand with value of a_o up to 0.12 in Figure B-41 and ahead in Figures B-42 and B-43 are not appropriate.)
- For axial loading, the maximum unit skin friction (t_f) and unit tip resistance are specified as shown in the example table on the previous page, and the default *t-z* curves in FLPIER for clay are applied automatically. No damping was assumed to occur because of axial loading of the piles as the cap rotates in response to a lateral load.

The pile group that was found to be satisfactory was a 5-row × 4-column group of steel pipe piles, each with a diameter of 60 in. (1.524 m), a wall thickness of 1.5 in. (38.1 mm), and a c-c spacing of 3D in both directions. A layout of this group is shown in Figure 42.

For that group, the final displacements given below were obtained. *X* is the displacement in the loading direction; *Y* is the transverse displacement; *Z* is the vertical displacement.

Summary of Displacements at Pile Heads Only

NODE	*X* (in.)	*Y* (in.)	*Z* (in.)
1	4.9487	–0.0001	–0.5371
2	4.9484	0.0001	–0.0060
3	4.9479	0.0002	0.5431
4	4.9487	0.0001	–0.5371
5	4.9484	–0.0001	–0.0060
6	4.9479	–0.0002	0.5431

NOTE: 1 in. = 25.4 mm.

Because the problem converged using the "nonlinear" option, the piles have sufficient capacity. The preliminary design has now been completed. The full time domain analysis using an actual or assumed earthquake record can be run next to provide a final check on the pile group system.

Please note that alternative approaches could have been taken in this step, which results in preliminary sizing of the group. Static codes such as FLPIER, or, for example, a simple program known as PIGLET (*45*), could have been employed using an estimated peak dynamic load. However, use of FLPIER(D) in this step is expected to save time in the overall design process.

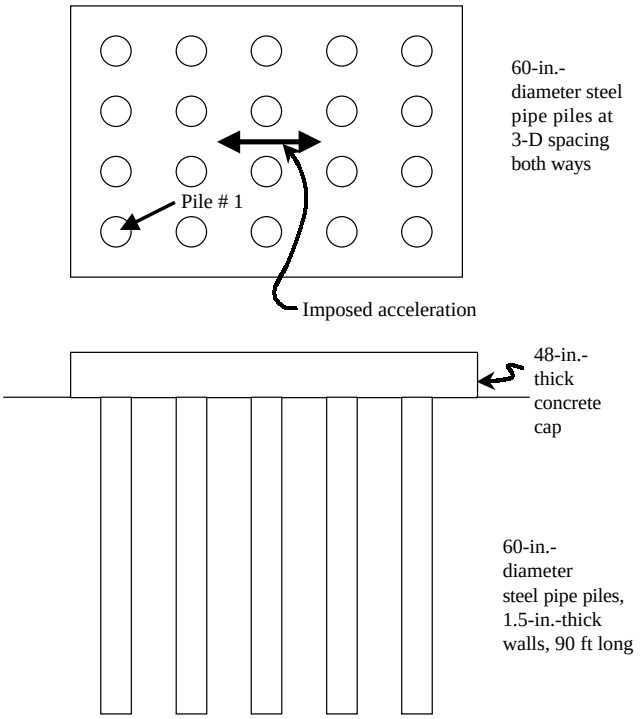

Note: 1 in. = 25.4 mm

Figure 42. Layout of pile group for FLPIER(D) example problem.

Step 4: *Convert the static model to a time-domain dynamic model by adding damping, mass, and an earthquake record.*

The file used for this analysis is included with the example files as part of the FLPier_Dyn install and is named "design_dyn_gap.in." In this phase of the analysis (i.e., the time-domain analysis), damping is handled differently from the way in which it was handled in the previous phase (i.e., the pseudo-dynamic analysis [Step 3]). In the pseudo-dynamic analysis, soil damping was handled in FLPIER(D) by using the approximation developed in Appendix B. In this step, however, hysteretic damping in the soil under lateral loading (with the *p-y* curves) was modeled in FLPIER(D) using the gap model described in Appendix C. There is no hysteretic damping associated with axial loading of the piles as the cap rotates in this example. Radiation damping in this step, for both lateral and axial loading of the piles, was handled in FLPIER(D) by specifying Raleigh damping (*45*). The axial load-movement curves were generated in FLPIER(D) using McVay's (*33*) driven pile model for unit load transfer curves.

In this phase, an earthquake record (i.e., the acceleration time history) was input as a discrete time history at the origin of coordinates (i.e., the middle of the top of the pile cap). The acceleration time history used in this example was the El Centro, California, record of 1940. Any saved

acceleration record can be captured by the user interface for FLPIER(D) and placed in the input file. At present, two records are saved for use by the program: El Centro and Northridge, California.

The results of the field Statnamic tests summarized in Chapter 2 and covered in detail in Appendixes D and E were used to infer input parameters for this phase of the analysis. From the field Statnamic tests, the following parameters appear to work well in the FLPIER(D) model:

- **Damping:** Raleigh damping can be used to replicate radiation damping in the pile group system. Such damping is expressed in FLPIER(D) by ($\alpha \times$ mass of the cap and pile system + $\beta \times$ lateral group stiffness). In the field tests conducted with steel piles, good matching was found with FLPIER(D) using the following, with the exception (for soil) described in the following:

	α	β
Structure (pier)	0.04	0.01
Piles	0.001 (steel)	0.001 (steel)
Soil	0.015	0.015

In the analysis of earthquake motion, additional damping is required that was not found in the Statnamic tests because the Statnamic device applies a short pulse of energy followed by a period of free vibration response. An earthquake acceleration record, however, causes continuous energy input, and the response is more sensitive to damping.

It is estimated that the soil damping is about 10 times that of a steel pile. As a result of Step 3, the damping values shown in the preceding table were used, and the pier and pile group shown in Figure 42 was analyzed.

- **Additional Input Options:** For the dynamic time domain analysis, the following options were specified:
  - **P = 2, 1, 4:** Print displacements for the analysis for Nodes 1 and 4 (i.e., the pile heads). This will create the name.DS1 and name.DS2 files, which contain the six displacements at Nodes 1 and 4, respectively, for each time step. These are text files and are best viewed using a spreadsheet such as Microsoft Excel.
  - **W = 1, 1, 1:** Print the forces for Pile 1, Element 1, and Node 1 (the bottom of the element) for each time step. Only one end of a single element can be printed per run. The forces are saved in the file *name*.DFO.

  All the plots in the list given below were executed using Excel. To read the result files in Excel, do the following:
  1. Start Excel by using the File->Open command;
  2. Change to all files (*.*);
  3. Select the file to read (name.DS1 or name.DFO, etc.); and
  4. On the pop-up dialog, select finish (to read the data).

  All data are now in columns and can be plotted using normal Excel functions.
- **Principal Results from Time-Domain Analysis:** From the dynamic time-domain analysis, plots were made for the pile-head translation in the direction of loading (*X*) and for the induced bending moment in the direction of loading for Pile 1 for the time window of the analysis. These plots are given in Figures 43 and 44, respectively. In both of these figures, time is expressed in seconds.

The maximum displacement in the analysis is a little more than 2 in. (51 mm). Notice that the earthquake response has several significant peaks during the modeled time window of response. Unlike the free vibration response from the Statnamic test, the response does not decay. The moment at the head of Pile 1 is given in Figure 44. Similarly, several peaks occur, and the maximum moment is slightly more than 15,000 in.-K (1695 kN-m),

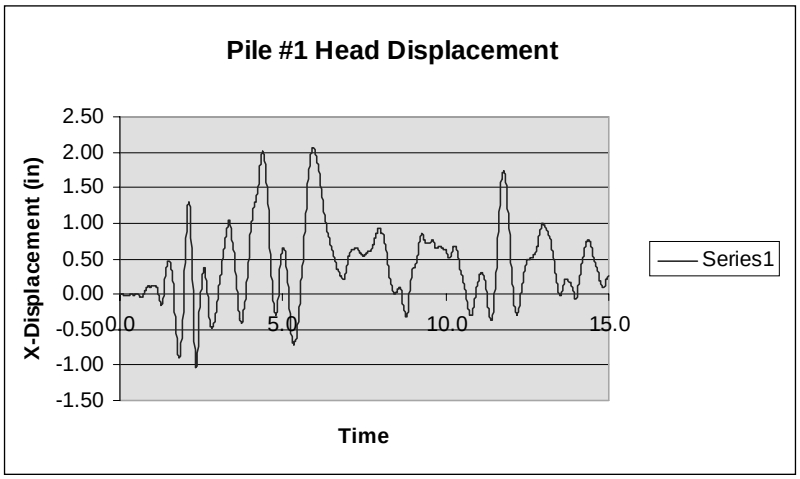

Figure 43. Lateral displacement time history for Pile 1 computed by FLPIER(D).

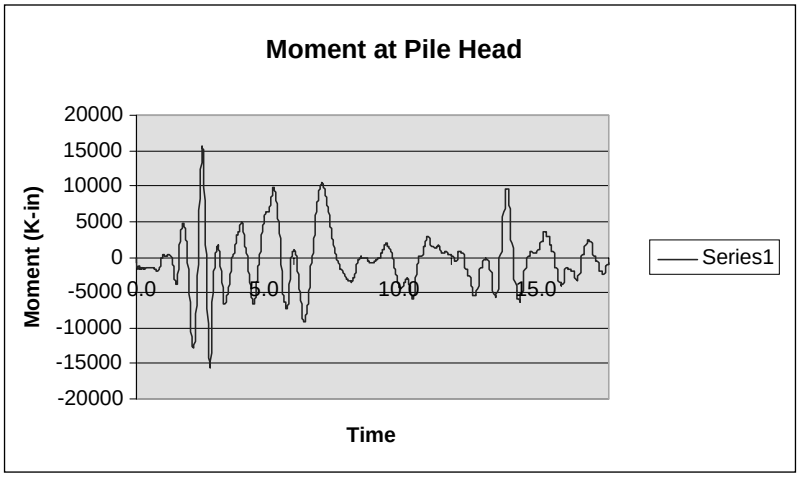

Figure 44. Time history of bending moment computed at the head of Pile 1 by FLPIER(D).

which is less than the moment at which plastic behavior occurs.

Because convergence occurs in FLPIER(D), the piles have sufficient moment capacity. The gap model causes the structure flexibility to increase as time increases because less and less of the soil is in contact with the piles.

- **Completing the Design Process:** This analysis should be conducted *using a range of values* of soil properties that covers the associated uncertainties, including damping and *p*-multipliers. For example, it would be prudent to vary the default *p*-multipliers by about ± 25 percent and to reduce the front-row values to as low as 0.5 for bored piles in cohesionless soil. For critical structures, the design process should include site-specific dynamic pile group loading tests with a large-force exciter to calibrate the program to site conditions.

CHAPTER **4**

CONCLUSIONS AND RECOMMENDATIONS

CONCLUSIONS

The research confirmed the viability of the reusable pile-testing system with the Statnamic activator; however, the original plans for a steel-frame cap proved infeasible for repeated use, and cast-in-place caps are recommended in any future experiments.

From a design perspective, the research demonstrated that laterally loaded pile groups in nonliquefying soil that are exposed to low-frequency (2 to 4 Hz), high-displacement-amplitude (≥ 20 mm) loading, or both, can be simulated using a code such as FLPIER(D), which models the soil with hysteretic, static, *p-y* curves and which uses *p*-multipliers that are derived from static tests (such as the default values in FLPIER or FLPIER[D]). Evidence was presented that the average *p*-multipliers were about 10 percent lower for bored piles in cohesionless soil than the average default values given in FLPIER or FLPIER(D). Inertial effects must be included in the method; however, structural damping has a minor effect on pile group behavior and may be included and omitted, as the designer chooses.

Random variations from the maximum bending moments and shears that were computed for each row of piles by FLPIER(D) were observed in the field experiments. This behavior appeared to derive from random variations in soil stiffness within the group and from other random factors, such as random small batters in the piles. This variability should be accounted for in designing the piles structurally by applying a load factor of approximately 1.2 to the computed maximum moments and shears.

RECOMMENDATIONS FOR FURTHER STUDY

Some modifications to FLPIER—to create the dynamic version FLPIER(D)—are in order:

1. The default parameters in FLPIER(D) tend to overestimate damping, based on comparisons with the impact-type field tests in this study. Adjustments to the unloading branches of *p-y* curves may improve modeling of hysteretic damping for this type of loading. Further studies of the effects of high-amplitude, cyclic dynamic loading should be undertaken to determine whether the FLPIER(D) damping model is suitable for seismic loading without modification.
2. FLPIER(D) gives unexpected results at certain times when the displacement is large and when the piles are prescribed to have partial fixity with the cap. This effect appears to be due to convergence of the mathematical solution and to the sensitivity of the solution to the value of the rotational restraint at the pile head. Corrections have been made in the program to minimize this effect; however, users should proceed with caution when analyzing piles with partial head fixity. This behavior should be investigated further, and the formulations should be corrected, if necessary.
3. FLPIER(D) has not been verified for the case in which loading is generated against the piles from the soil (i.e., kinematic loading with inertial feedback from the superstructure). Further physical data should be collected, perhaps using shaking-table tests or full-scale tests with significant explosive charges, against which to verify FLPIER(D) for this application.
4. An appropriate *p-y* model should be developed to handle liquefying soil.
5. A formal research project should be undertaken to evaluate methods for determining pile-head shear accurately from bending sensors in the piles or by other means and to evaluate the flexural stiffness of pile heads for piles of differing types (e.g., pipe, prestressed concrete, H, circular reinforced concrete) with varied procedures for attaching the piles to the caps. This project, if successful, should make it easier to perform and interpret the results of field tests on laterally loaded pile groups.

With respect to the field testing program, it is noted that the test piles that were instrumented and developed for this study, as well as the Statnamic testing device (which is the property of FHWA) are available for further testing on other sites. The major conclusions of this research, stated above, should be verified by further field tests in other geologic settings (e.g., stiff clay; loose, clean water-bearing sand; loose, dry sand; and soft-over-stiff soil layering). This verification can be accomplished most conveniently in conjunction with highway-construction projects.

The applicability of this research to seismic loading can be enhanced by repeating these experiments, using a large vibra-

tor, to correlate damping inferred from Statnamic tests with damping under continuous loading with nonlinear displacements. Such a vibrator should be designed, constructed, and deployed.

IMPLEMENTATION PLAN

A brief plan for the implementation of this research is as follows:

1. The appropriate federal agency should identify state DOT design projects in which seismic or vessel–ice impact is a major concern in the design of the foundations.
2. Two to four such projects should be selected for research implementation. The selected projects should cover a variety of soil sites (e.g., saturated sand, soft clay, very stiff clay or rock) and more than one type of loading event (e.g., seismic and vessel impact).
3. The custodian of the testing equipment from this project should then be directed to make such equipment available to the state DOTs whose design projects are selected, and those states should conduct full-scale field tests with a Statnamic device, as was employed in this project, or with a very large vibrator.
4. The state DOTs or their consultants should, in parallel with the field tests, perform mathematical modeling of the test pile group using either FLPIER(D) or other suitable software, taking advantage initially of the recommendations developed in this report and modifying the input parameters as necessary to affect acceptable matches with the observations. The same software should then be used to design the pile foundations for the subject structure.
5. During this process, the responsible federal agency should compile the results of the field tests and of the designers' interpretations for input parameters (i.e., damping values, *p*-multipliers, etc.) and should make the information available to the national community of DOT structural and geotechnical engineers through a sponsored conference or short course.
6. The use of the field testing system developed for the current project and the software that is used in the above process should then be evaluated by a select panel of experts, and a decision should be made by the responsible federal agency, with the advice of the panel of experts, whether to continue with further field experiments, to standardize the input parameters (so as to use them without field testing), or take some other approach to the design of laterally loaded pile groups.

REFERENCES

1. Earthquake Engineering Research Institute. "Loma Prieta Earthquake Reconnaissance Report," Chapter 6: Bridge Structures in *Earthquake Spectra, Supplement to Volume 6* (1990); pp. 151–187.
2. Buckle, I. G. *The Northridge, California, Earthquake of January 17, 1994: Performance of Highway Bridges.* Technical Report NCEER-94-0008, National Center for Earthquake Engineering Research (1994).
3. Earthquake Engineering Research Institute. "Northridge Earthquake of January 17, 1994, Reconnaissance Report," Chapter 6: Highway Bridges and Traffic Management in *Earthquake Spectra, Supplement to Volume 11* (1995); pp. 287–372.
4. Kiremidjian, A. A., and N. Basoz. "Evaluation of Bridge Damage Data from Recent Earthquakes," *NCEER Bulletin*, National Center for Earthquake Engineering Research, Vol.11, No. 2 (1997); pp. 1–7.
5. Buckle, I. G. "Report from the Hanshin-Awaji Earthquake: Overview of Performance of Highway Bridges," *NCEER Bulletin*, National Center for Earthquake Engineering Research, Vol. 9, No. 2 (1995); pp. 1–6.
6. Costantino, C. "Report from the Hanshin-Awaji Earthquake: Overview of Geotechnical Observations," *NCEER Bulletin*, National Center for Earthquake Engineering Research, Vol. 9, No. 2 (1995); pp. 7–10.
7. Ishihara, K. "Geotechnical Aspects of the 1995 Kobe Earthquake," *Proceedings, XIV International Conference on Soil Mechanics and Foundation Engineering*, Vol. 4, Hamburg; Balkema (1997); pp. 2047–2073.
8. Matsui, T., M. Kitazawa, A. Nanjo, and F. Yasuda. "Investigation of Damaged Foundations in the Great Hanshin Earthquake Disaster," *Seismic Behavior of Ground and Geotechnical Structures*, P. S. Sêco e Pinto (ed.); Balkema (1997); pp. 235–242.
9. Lin, M.-L. *Geotechnical Hazard Caused by Chi-Chi Earthquake*. Department of Civil Engineering, National Taiwan University (2000).
10. *Chi-Chi Earthquake Database Analysis and Management System (CEDAMS)*. Taiwan's National Center for Research and Earthquake Engineering, Taipei (2000).
11. Chang, K.-C., D.-W. Chang, M.-H. Tsai, and Y-C. Sung. "Seismic Performance of Highway Bridges," *Earthquake Engineering and Engineering Seismology*, Vol. 2, No. 1 (2000); pp. 55–77.
12. Bardet, J. P., N. Adachi, I. M. Idriss, M. Hamada, T. O'Rourke, and K. Ishihara. Chapter 7: Performance of Pile Foundations in *Proceedings, North America–Japan Workshop on the Geotechnical Aspects of the Kobe, Loma Prieta, and Northridge Earthquakes*. National Science Foundation, Air Force Office of Scientific Research, Japanese Geotechnical Society (1997).
13. O'Neill, M. W., D. A. Brown, D. G. Anderson, H. El Naggar, F. Townsend, and M. C. McVay. "Static and Dynamic Lateral Loading of Pile Groups," Interim Report for NCHRP Project 24-9. National Cooperative Highway Research Program, Transportation Research Board (1997).
14. Budek, A. M., M. J. N. Priestley, and G. Benzoni. "The Inelastic Seismic Response of Bridge Drilled-Shaft RC Pile/Columns," *Journal of Structural Engineering*, ASCE, Vol. 126, No. 4 (2000); pp. 510–517.
15. Davisson, M. T. "Lateral Load Capacity of Piles," *Highway Research Record 333*, Highway Research Board, National Research Council (1970); pp. 104–112.
16. *Foundations and Earth Structures—Design Manual 7.2*. NAVFAC DM-7.2. Department of the Navy, Naval Facilities Engineering Command (1982).
17. *Canadian Foundation Engineering Manual* (2nd Edition). Canadian Geotechnical Society, Bitech Publishers Ltd. (1985).
18. *AASHTO Bridge Design Specifications*. American Association of State Highway and Transportation Officials (1996).
19. *Design of Pile Foundations—Technical Engineering and Design Guides No. 1*. ASCE, adapted from the U.S. Army Corps of Engineers (1993).
20. Poulos, H. G., and E. H. Davis. *Pile Foundations Analysis and Design*. Wiley (1980).
21. PoLam, I., and G. R. Martin. *Seismic Design of Highway Bridge Foundations, Volume II: Design Procedures and Guidelines*, Report No. FHWA/RD-86/102. U.S.DOT, FHWA (1986).
22. *Improved Seismic Design Criteria for California Bridges* (ATC-32), Contract 59N203. Applied Technology Council (1996).
23. Williams, M. E., C. Fernandes Jr., and M. I. Hoit. "Comparison of Dynamic Analysis Methods for Bridge Piers," *Journal of Bridge Engineering*, ASCE, in review (2001).
24. PoLam, I., M. Kapuskar, and D. Chaudhuri. *Modeling of Pile Footings and Drilled Shafts for Seismic Design*, Technical Report MCEER-98-0018. Multidisciplinary Center for Earthquake Engineering Research, State University of New York at Buffalo (1998).
25. Reese, L. C., and S. T. Wang. *Computer Program LPILE Plus*, Version 3.0, Technical Manual. Ensoft, Inc. (1997).
26. *PAR: Pile Analysis Routines: Theoretical and User's Manuals*. PMB Engineering, Inc. (1988).
27. *Design Manual for Foundation Stiffnesses Under Seismic Loading*. Prepared for Washington State DOT by Geospectra (1997).
28. Schnabel, P. B., J. Lysmer, and H. B. Seed. *SHAKE: A Computer Program for Earthquake Response Analysis of Horizontally Layered Sites*, Report EERC 72-12. University of California Earthquake Engineering Research Center (1972).
29. Norris, G. M. "Seismic Bridge Pile Foundation Behavior," in *Proceedings, International Conference on Design and Construction of Bridge Foundations*, FHWA, Vol. 1 (1994); pp. 27–136.
30. Ashour, M. A., G. Norris, and P. Pilling. "Lateral Loading of a Pile in Layered Soil Using the Strain Wedge Model," *Journal of Geotechnical and Geoenvironmental Engineering*, ASCE, Vol. 124, No. 4 (1998); pp. 303–315.
31. Ashour, M. A., and G. Norris. "Modeling Lateral Soil-Pile Response Based on Soil-Pile Interaction," *Journal of Geotechnical and Geoenvironmental Engineering*, ASCE, Vol. 126, No. 5 (2000); pp. 420−428.
32. Peterson, K., and K. M. Rollins. *Static and Dynamic Lateral Load Testing of a Full-Scale Pile Group in Clay*, Research

Report CEG.96-02. Department of Civil Engineering, Brigham Young University (1996).
33. McVay, M., C. Hays, and M. Hoit. *User's Manual for Florida Pier*, Version 5.1. Department of Civil Engineering, University of Florida (1996).
34. Dobry, R., A. Abdoun, and T. D. O'Rourke. "Evaluation of Pile Response Due to Liquefaction Induced Lateral Spreading of the Ground," in *Proceedings, 4th Caltrans Seismic Design Workshop*, Sacramento (1996).
35. Wilson, D. W., R. W. Boulanger, B. L. Kutter, and A. Abghari. "Soil-Pile Superstructure Interaction Experiments with Liquefiable Sand in the Centrifuge," in *Proceedings, 4th Caltrans Seismic Design Workshop*, Sacramento (1996).
36. Ashford, S. A., and K. Rollins. "Full-Scale Behavior of Laterally Loaded Deep Foundations in Liquefied Sand: Preliminary Test Results," Preliminary Report. Department of Structural Engineering, University of California, San Diego (1999).
37. Randolph, M. F., and H. G. Poulos. "Estimating the Flexibility of Offshore Pile Groups," in *Proceedings, 2nd International Conference on Numerical Methods in Offshore Piling*, Austin (1982); pp. 313–328.
38. Bathe, K. J. *ADINA User's Manual*, ADINA R and D, Inc. (1998).
39. *General Finite Element Analysis Program*, Version 5.4. ANSYS, Inc. (1996).
40. El Naggar, M. H., and M. Novak. "Nonlinear Analysis for Dynamic Lateral Pile Response," *Journal of Soil Dynamics and Earthquake Engineering*, Vol. 15, No. 4 (1996); pp. 233–244.
41. "Recommended Practice for Planning, Designing and Constructing Fixed Offshore Platforms," *API Recommended Practice 2A* (19th edition). American Petroleum Institute (1991); pp. 47–55.
42. Matlock, H. "Correlations for Design of Laterally Loaded Piles in Soft Clays," *Proceedings, Second Annual Offshore Technology Conference*, Houston (1970); pp. 578–588.
43. Reese, L. C., W. R. Cox, and F. C. Koop. "Analysis of Laterally Loaded Piles in Sand," *Proceeding, Offshore Technology Conference*, Houston (1974); pp. 473–484.
44. Sowers, G. F., and T. L. Richardson. "Residual Soils of the Piedmont and Blue Ridge." *Transportation Research Record No. 919.* Transportation Research Board, National Research Council (1983); pp. 10–16.
45. Randolph, M. F. *PIGLET: A Computer Program for the Analysis and Design of Pile Groups Under General Loading Conditions*, Soil Report TR91 CUED/D. Cambridge University (1980); (currently available from the Department of Civil Engineering, University of Western Australia).

APPENDIX A

COMPARATIVE BEHAVIOR OF LATERALLY LOADED GROUPS OF BORED AND DRIVEN PILES

INTRODUCTION

The soil modeling approach that has been adopted in this research is to simulate lateral group behavior by (1) using *p-y* curves for statically loaded single piles from well-known criteria (e.g., *1, 2*)—these criteria are resident in many design-level computer codes and are easy for the designer to implement (e.g., *3–5*); (2) converting the static *p-y* curves into dynamic *p-y* curves if seismic or impact loading is being modeled (see Appendix B); and (3) modifying single-pile curves for lateral group action by using a *p*-multiplier, which may be either a static factor (as discussed in this appendix) or a dynamic factor (as discussed in Appendix B). The *p*-multiplier approach is used in the Florida Pier Program (FLPIER) (*4, 5*), modified for dynamic loading as described in Appendix C.

Values for *p*-multipliers have been evaluated through detailed numerical or analytical modeling or by performing load tests on pile groups, or by a combination of both numerical or analytical modeling and field or centrifuge tests (*6–10*). However, none of these studies has been specific to the construction method that is used to install the piles. The contribution of this appendix is to describe a major field load test program in which the effect of the piling construction method on *p*-multipliers was evaluated.

TEST SITE AND TEST ARRANGEMENT

Site Conditions

In planning for the construction of foundations for numerous viaducts to support rail traffic through the west central coastal plain of Taiwan, the High Speed Rail Authority of Taiwan contracted with several universities, consulting firms, and contractors to construct and load test two large, full-scale pile groups. The west central coastal plain of Taiwan is in a geographical area that is prone to large seismic events, and it was considered necessary to design the viaducts to resist large horizontal loads.

The objective of the test program was to measure the capacity and stiffness of groups of vertical piles of different designs that were loaded laterally with a quasi-static ground-line shear. Two test groups were selected for construction and testing. The cost of construction for each group was estimated to be approximately equal. These groups were constructed and loaded to the capacity of the loading system, 1000 metric tons ("T") (9.8 MN). One pile group consisted of bored piles (drilled shafts), and one consisted of round, displacement-type prestressed concrete piles, which were driven into position.

The test site was located about 5 km west of the town of Chaiyi, Taiwan, on a flat coastal plain. Soil conditions at the test site are summarized in Figure A-1. The ground surface shown in that figure is the elevation of the ground surface at the base of the pile caps of the tested groups after minor excavation. Detailed soil data are available in Reference 11. Made on the test site, within 5 m of each test group, were numerous geophysical tests; soil borings; and cone penetration test (CPT), standard penetration test (SPT), and dilatometer test (DMT) soundings. The Unified classifications of the soil layers and the various parameters listed in the "Properties" column of Figure A-1 were deduced from the borings and soundings (*11*). The piezometric surface was located at 3 m below the ground surface. The soils in the top 8 m of the profile are considered to be "sands" with a relative density of 50 to 60 percent in the following analysis.

Testing Arrangement

The layouts of the test groups are shown in Figures A-2 and A-3. All piles were plumb to the tolerances permitted by the High Speed Rail Authority (i.e., 2 percent). The lateral load tests were conducted essentially by jacking the two test groups apart. That is, the test groups served as mutual reactions for each other.

Bored Pile Group

The bored pile group (see Figure A-2) consisted of six 1.5-m-diameter piles installed to a depth of 33 to 34 m below the ground surface. All six of the group piles were constructed using the slurry displacement method of construction, in which a bentonite slurry was used to maintain borehole stability. Several other bored piles were constructed, as shown in Figure A-2. Piles B1 and B2 served as reference piles for lateral loading (tested as single, isolated piles). They were tested individually with free heads. Pile B10 served as a reference pile for axial loading. (Piles B9 and B11 served as anchor piles for the axial loading test on Pile B10. The group cap served as the reaction for the lateral load tests on Piles B1 and B2.) Only Pile B1 was constructed by the slurry displacement method, as per the group piles. Piles B2 and B10 (which are highlighted in Figure A-2 with boldface) were constructed using the oscillated casing method, in which casing is oscillated into the soil continuously for the full depth of the borehole, and the soil within the casing is excavated while maintaining a balance on the water head at the base of the casing

Depth m	Boring Log	Description	SPT N averaged	Properties
0	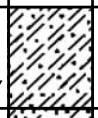	Fine sandy silt; yellowish brown loose with some clayey silts (SM)	5	$k = 27.14$ MN/m^3 $\phi = 35°$ $\gamma = 19$ kN/m^3
3 ▽		Silty fine sand; grey; medium dense; occasionally with sandy silt layers. (SM)	6	$k = 18.86$ MN/m^3 $\phi = 35°$ $\gamma' = 9.2$ kN/m^3
8		Silty clay; greyish brown; medium stiff, occasionally with coarse sand seams (2–3 mm) (CL)	10	$S_u = 60$ kN/m^2 $\varepsilon_{50} = 0.007$ $\gamma' = 9.2$ kN/m^3
12		Silty fine sand; grey; loose with fine sandy silt layer (SM)	10	$k = 18.32$ MN/m^3 $\phi = 34°$ $\gamma' = 9.4$ kN/m^3
17		Clayey silts; grey; medium dense with little sandy silts (ML/CL) Silty clay; grey; medium dense with silty fine sand layer	17	$k = 20.36$ MN/m^3 $\phi = 34°$ $\gamma' = 9.2$ kN/m^3
25		Silty clay; grey; very stiff with little fine sand (CL)	18	$S_u = 115$ kN/m^2 $\varepsilon_{50} = 0.005$ $\gamma' = 9.2$ kN/m^3
32		Silty clay; grey; very stiff with silty fine sand layer (SM/CL)	19	$S_u = 121.3$ kN/m^2 $\varepsilon_{50} = 0.005$ $\gamma' = 9.2$ kN/m^3
43			45	

Figure A-1. Subsurface profile at Chaiyi, Taiwan, test site.

throughout the process. The reinforcing steel is then set, and the borehole is concreted using temie techniques as the casing is withdrawn, similar to the way in which a borehole is concreted during the construction of bored piles by the slurry displacement method. Because Pile B2 was constructed in a manner different from the group piles, results from the test on Pile B1 were used exclusively in the analysis that is described in this appendix. The axial load test results on Pile B10 were used only in a general way to confirm the approximate correctness of the axial load model that is needed for the analysis of laterally loaded pile groups with nonpinned heads.

A potentially important detail is the order in which the piles were installed. In very general terms, the bored piles in the group were installed from the front, or leading, row (i.e., first) to the back, or trailing, row (i.e., last). It is speculated that this installation order might have resulted in reduced effective stresses in the coarse-grained soil surrounding the piles that were installed first—those in the leading row—by the later installation of piles behind the leading row. Reduced effective

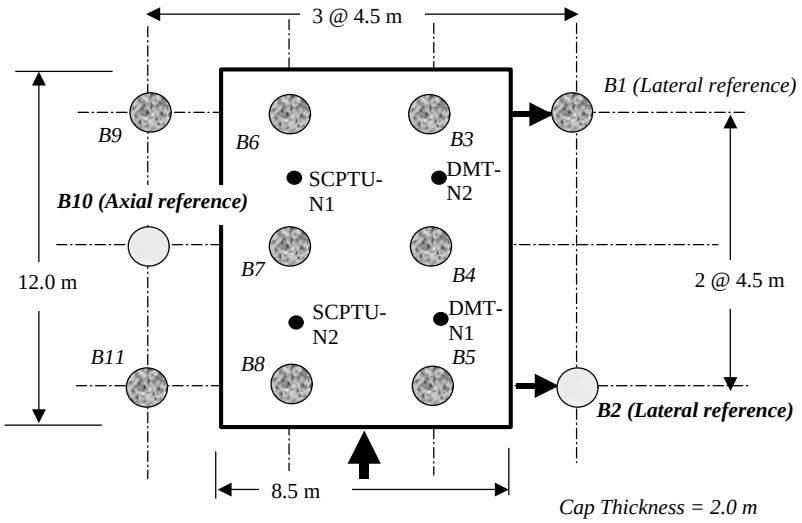

(a) Bored pile group layout.

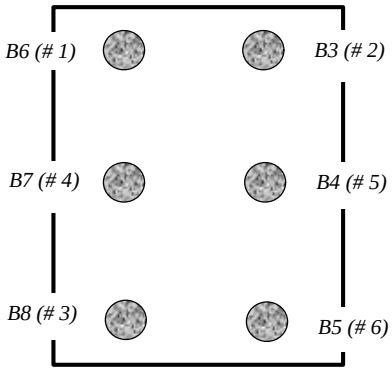

(b) Order of installation for bored piles in test group.

Figure A-2. Plan view of test group for bored piles and reference piles (not to scale).

stresses in the soil mass around the front-row piles should have produced softer soil response behavior of the leading-row piles compared with the behavior that might have occurred if the leading row of piles had been installed last.

Driven Pile Group

The driven pile group consisted of 12 0.80-m-diameter, closed-toe, hollow, circular prestressed concrete piles. They were also driven to a penetration of 33 to 34 m. These piles can be considered to be "displacement piles." The hollow core of each pile was filled with an instrument package and concrete after all of the piles were installed. A single, isolated pile, denoted P13 in Figure A-3, was tested laterally in a free-headed state by reacting off the group pile cap. Before the cap was constructed, Piles P6 and P7 were subjected to axial load tests. Because of the assumptions concerning head fixity in the driven pile group, which is discussed later, it was not necessary to model the axial load behavior of the group piles with close accuracy.

The installation order of the driven piles is also shown in Figure A-3. The order of installation was more random than that of the bored pile group; however, in general, the piles on the leading row were installed prior to the piles on the second (i.e., first trailing) row, which were in turn installed prior to the piles in the third (i.e., second trailing) row. The piles on the fourth (i.e., third trailing) row were installed last. With displacement-type piles in coarse-grained soil, it can be speculated that the effect of installing the leading row first was opposite to the effect of installing the leading row first in the bored pile group. That is, installing displacement piles in a row behind a row of piles already installed would increase effective stresses around the piles already installed and would

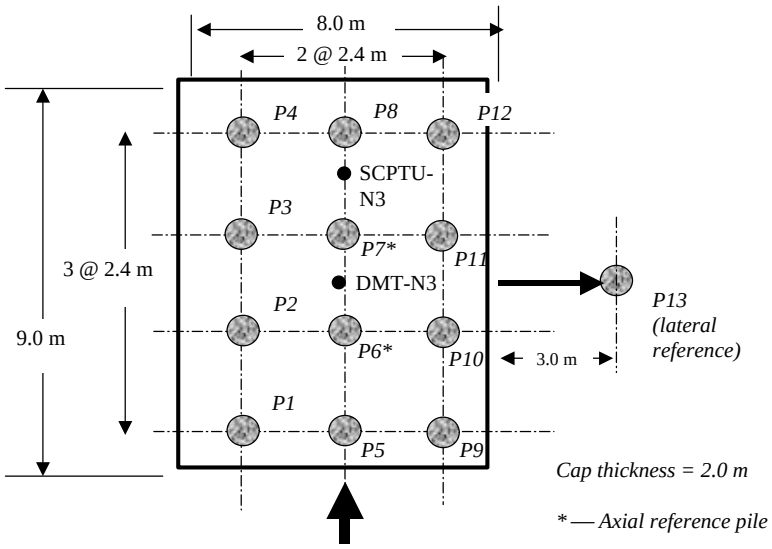

(a) Driven pile group layout.

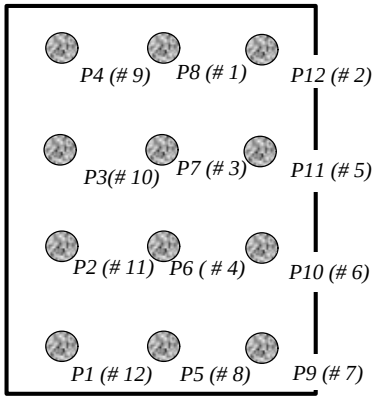

(b) Order of installation for driven piles in test group.

Figure A-3. Plan view of test group for driven piles and reference piles (not to scale).

result in stiffer soil response in those piles than in the piles installed later.

Instrumentation

Both the bored and driven piles were instrumented thoroughly. The piles that were subjected to individual pile axial load tests were instrumented with a toe load cell, a family of telltales and rebar stress meters (referred to in the United States as "sister bars"). The piles that were subjected to lateral load tests, including all of the group piles and the lateral reference piles, were instrumented with inclinometer tubing on approximately the neutral axis of the pile. Deviations in lateral deflection from the pile toes (which are considered to be stationary) were measured with precision inclinometers during the load tests. Some of the piles that were loaded laterally also contained sister bars. The translations and rotations of the group caps were measured by using linear variable differential transformers suspended from reference frames supported in the soil as far from the test groups as possible. The load was applied to the group by multiple hydraulic jacks whose loads were controlled in order to "steer" the group on an approximately straight path. Each jack was equipped with a calibrated electronic load cell.

The instruments for the bored piles were affixed to the reinforcing steel cages prior to inserting the cages into the boreholes and concreting the piles. The instruments for the driven piles were installed in the hollow core of each pile by attaching the instruments to a carrier and lowering the carrier into the core after the piles were driven. The operation was completed by concreting the instruments into the core.

The interpretations given here are based on the jack load cell, cap-deflection, and inclinometer readings. Sister-bar readings, although available, were not used because not all piles had sister bars and because initial review of the readings revealed some inconsistencies that could not be explained by the individuals reviewing the data.

More information on the instrumentation and pile-group arrangements can be found in Reference 12 (*12*).

Single-Pile Tests

General Description

The single-reference piles (i.e., B1, B2, and P13) were all tested statically, free-headed, by applying a horizontal load approximately 0.5 m above the ground surface. The geomaterials from that level to the ground surface were removed in the analyses that follow. The individual test piles were all subjected to forced vibration tests to load amplitudes as high as 44.5 kN (5 tons) prior to the static load tests. Because these loads were comparatively small, it has been assumed that they had minimal effect on the load-movement behavior that was measured in the static tests. The loads were applied to the single piles by reacting off the respective group pile caps, prior to loading the pile groups, in a direction perpendicular to the direction of group loading. Again, it was assumed that the loading of the single piles in this manner had no effect on the measured response of the pile groups.

The single pile load tests were performed from May 29 through 31, 1997, approximately 5 months after the piles were installed. Loads were applied semi-monotonically. That is, loads were applied in increments until the load reached approximately one-seventh of the expected capacity, at which time the load was removed. The process was repeated for loads equal to about two-sevenths of the expected capacity, three-sevenths of the expected capacity, and so forth, until the final capacity was reached. Readings that were made near the peak loads on each cycle are reported in this appendix as it was assumed that the lateral pile response at such loads was not significantly influenced by cycling at lower load amplitudes.

The load deformation depth relations that were measured for Piles B1 (i.e., the reference for the bored pile group test) and P13 (i.e., the reference for the driven pile group test) are shown in Figures A-4 and A-5, respectively. In these figures, the symbol "T" represents metric tons (or tonnes) rather than U.S. tons, where 1 T = 9.8 kN. As stated previously, Pile B2 was not used as a reference because it was installed using the oscillated casing procedure rather than using the slurry displacement procedure, which was used for all of the group piles. As would be expected, the bored pile, B1, carried considerably more load at a given head deflection than did the driven pile, P13, because of B1's much larger moment of inertia. For the same reason, significant lateral pile movement occurred to a greater depth in the reference bored pile (about 7 m) than in the reference driven pile (about 5 m).

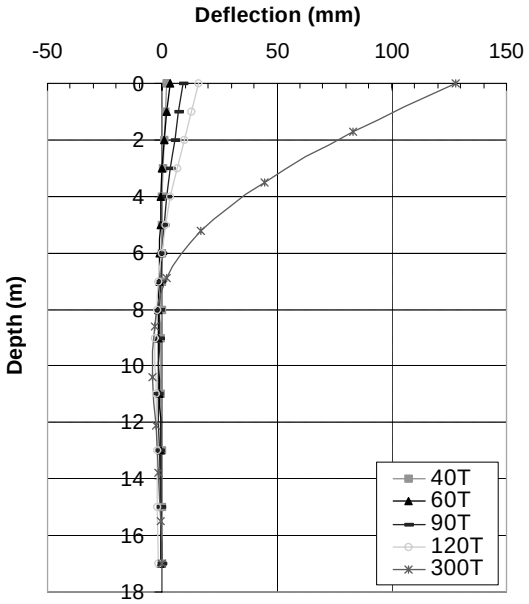

Figure A-4. Measured load deflection depth relations for Pile B1.

Analysis of Single Pile–Test Results

From the perspective of this appendix's objective, the main purpose of the single-pile tests was to establish site-specific, pile geometry–specific, and construction method–specific *p-y* curves for the reference piles. The pile-and-soil profile that was assumed for the analysis of the single pile–load tests is shown in Figure A-6. The soil was modeled initially by using standard *p-y* curve formulations—that of Reese et al. (*1*) for

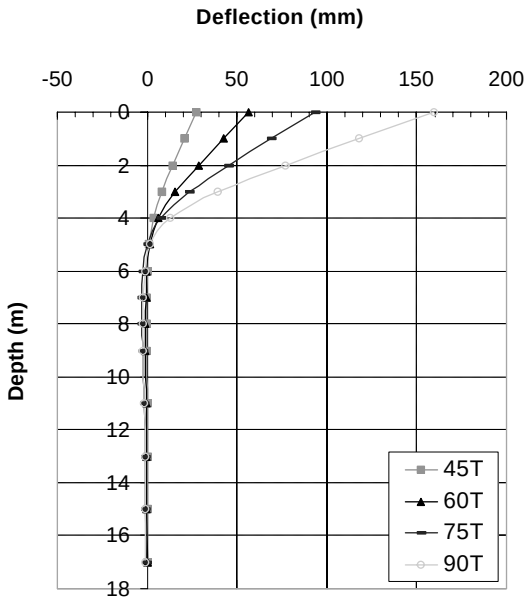

Figure A-5. Measured load deflection depth relations for Pile P13.

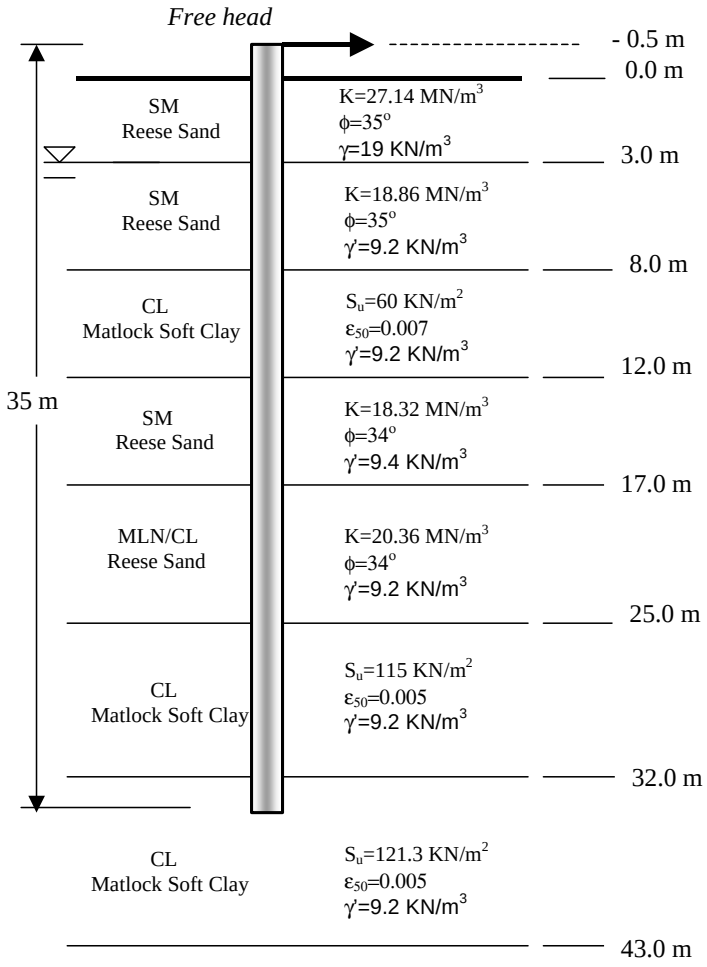

Figure A-6. Soil properties used in developing initial p-y *curves.*

coarse-grained soil layers (i.e., sand) and that of Matlock (*13*) for fine-grained (i.e., clay) soil layers. In preliminary analyses, the Murchison and O'Neill (*2*) *p-y* criterion was also used for the sand layers, in place of the Reese et al. criterion; however, the predictions of deformed pile shape was better with the Reese et al. criterion, so the Reese et al. criterion was used as the starting point for the analysis.

Modeling of the structural properties of the piles is at least as important as modeling the resistance-deformation behavior of the soil (i.e., through *p-y* curves). Simplified design drawings for a typical bored pile and a typical driven (prestressed concrete) pile are shown in Figures A-7 and A-8, respectively. Material properties of the concrete and steel are given in Table A-1. (These were the target properties that were verified from concrete cylinder tests for cast-in-place concrete and steel coupon tests on reinforcing steel. No verification was available for the properties of the concrete in the prestressed outer shell of the driven piles or for the prestressing steel.) The concrete–steel model was the model proposed by Andrade (*14*) and implemented in the version of FLPIER used in this study (*15*). This model computes bending stiffness along the pile by first computing strains across the cross section of a bending element (representing the pile) and assigns corresponding stresses based on uniaxial stress-strain curves for concrete and steel in compression and tension. The gapping-unloading-reloading (hysteretic) structural model described in Appendix C was not resident in the version of FLPIER used in these analyses (i.e., Version 5.1); however, because of the procedure by which the tests were conducted, the gapping-unloading-reloading phenomenon should have had little effect on the pile deflections at the loads at which the tests, both single-pile and group, were analyzed (at or near the peak load in a cycle).

When the tests were first analyzed with FLPIER using the Reese et al. (*1*) and Matlock (*13*) *p-y* criteria for the soil and the Andrade (*14*) structural model for the piles, relatively poor comparisons with the measurements were achieved. Modifications to the *p-y* criteria in the upper 12.0 m of the soil profile were then made in order to improve the match in measured versus computed displaced configuration at several selected loads; that is, site-specific *p-y* curves were determined. The diameters of all bored piles (including the group piles discussed later) were increased in FLPIER from 1.5 to 1.60 m

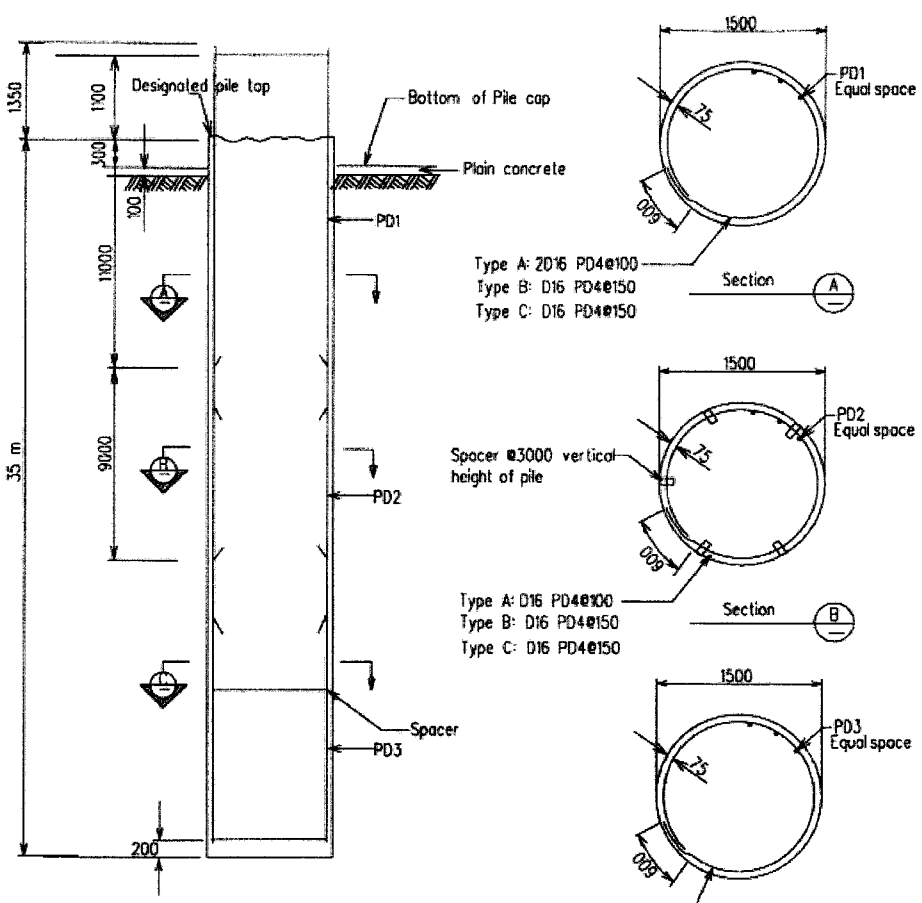

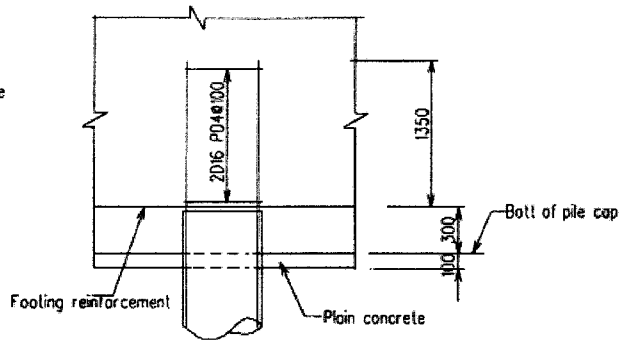

Pile&Pile Cap Connection Detail

Table of Reinforcement A,B,C

NO.	Nominal Diameter	Reinforcement Type	Remark
PD1	D32	———	Type A: 26x3 B: 34 C: 26
PD2	D32	———	Type A: 26x2 B: 34 C: 26
PD3	D32	———	Type A: 26 B: 17 C: 13
PD4	D16	○	

Notes

1 unit: mm except those denoted

2 f_c of concrete=27500 kN/m² ; f_y of steel =411600 kN/m²

3 The reinforcement of bored piles B3-B8 & 12,13 is type A;
B1,2,9&11 is type B; B10 is type C

4 L: the length of bored piles were described inconsistentiy in the series of reports of this project, in this analysis, they are assumed to be 35 m for the single bored pile and 1.5 m shorter for the group piles according to the graphs in the data report.

5 E_c =2x10⁸ kN/m² ; E_s =2.5x10⁷ kN/m²

Figure A-7. Structural details for bored piles.

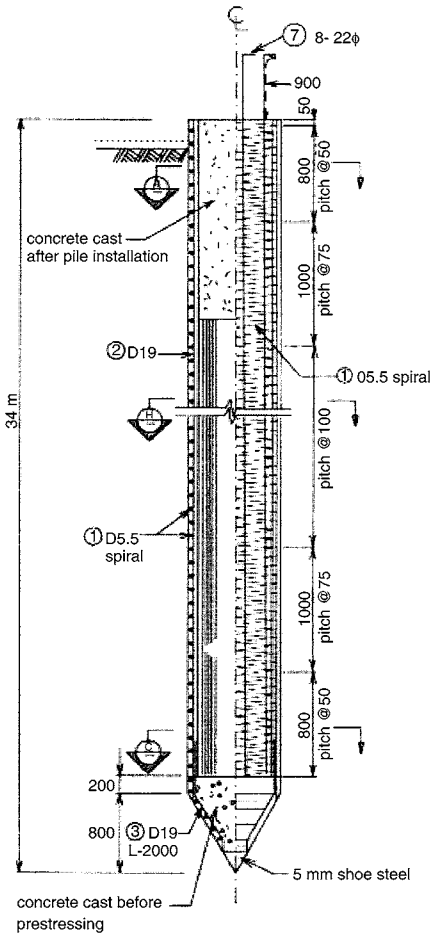

Prestressed Pile Details

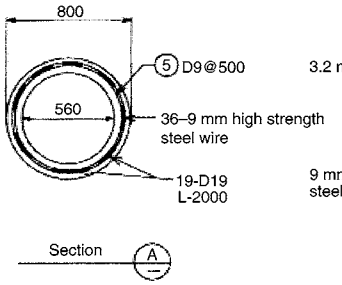

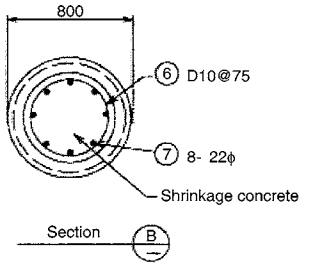

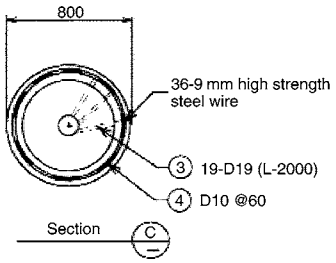

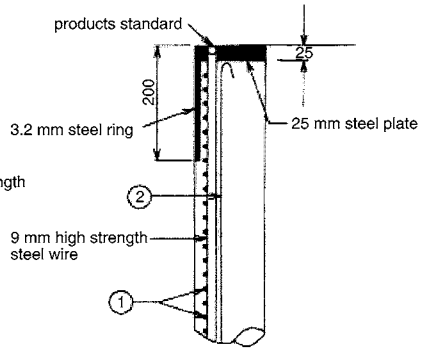

Pile Top Detail

Table of Reinforcement

NO.	Nominal Diameter	Reinforcement Type	Remark
①	D5.5		
②	D19		19
③	D19		19
④	D10		@60
⑤	D9		@500
⑥	D10		@75
⑦	D22		8

Notes

1 PC piles of this project are pretensioned spun concrete piles

2 Ib of concrete: outer material 800 kg/cm^2 (78400 kN/m^2)
core material 210 kg/cm^2 (20580 kN/m^2)

3 Tension strength of 9 mm steel wire area f_w = 14500 kg/cm^2 (1421000 kN/m^2)
f_g = 12500 kg/cm^2 (1225000 kN/m^2)

4 Effective stress transferred to concrete = 80 kg/cm^2 (7840 kN/m^2)

5 L = 34m

6 Es = 2 x 10^3 kN/m^2; Ec = 3.35 x 10^7 kN/m^2

Figure A-8. Structural details for driven (prestressed concrete) piles.

TABLE A-1 Concrete and steel properties for Chaiyi load tests

Property	Bored Piles and Cap	Prestressed Concrete Piles
f'_c (concrete)	27.5 MN/m^2	78.4 MN/m^2 (shell) 20.59 MN/m^2 (core)
E_c (concrete)	2.5 X 10^4 MN/m^2	3.35 X 10^4 MN/m^2 (shell) No data for core (2.0 X 10^4 MN/m^2 used)
f_y (steel)	411.6 MN/m^2	1421 MN/m^2 (cable)
E_s (steel)	199.8 GN/m^2	199.8 GN/m^2

to account for the oversizing of the borehole that commonly occurs when excavating a bored pile in coarse-grained soil under a drilling slurry. The *p-y* curves derived from the original published criteria are compared with the modified *p-y* criteria that were necessary to provide acceptable matches with the measured data in Figures A-9, A-10, and A-11 for Piles B1, B2, and P13, respectively.

One modification to the *p-y* curves was to prescribe a non-zero resistance at the soil surface. This modification is contrary to the Reese et al. sand criterion, which provides for zero soil resistance at the surface. It is not clear what physical phenomenon this change reflected. The surface soil (see Figure A-1) was described as a "sandy silt with some clayey silts," even though it classified as an SM (i.e., silty sand) according to the Unified classification system. It is possible that the need to give the soil surface resistance could reflect a cohesion component to shear strength of the soils not reflected by the Reese et al. sand criteria. A more likely condition, however, was that the bored piles were greater than 1.6 m in diameter at the surface because of the effects of auger drilling and that the need to give the soil non-zero surface resistance actually simulated increased bending stiffness in a pile with a "mushroom" top. The salutary effect of using a non-zero surface resistance *p-y* curve, as shown at the soil surface in Figures A-9 through A-11, versus using null *p-y* curves at the surface, is demonstrated in Figure A-12.

The original and modified *p-y* curves necessary to model Pile B2 (see Figure A-10) were included, even though the data

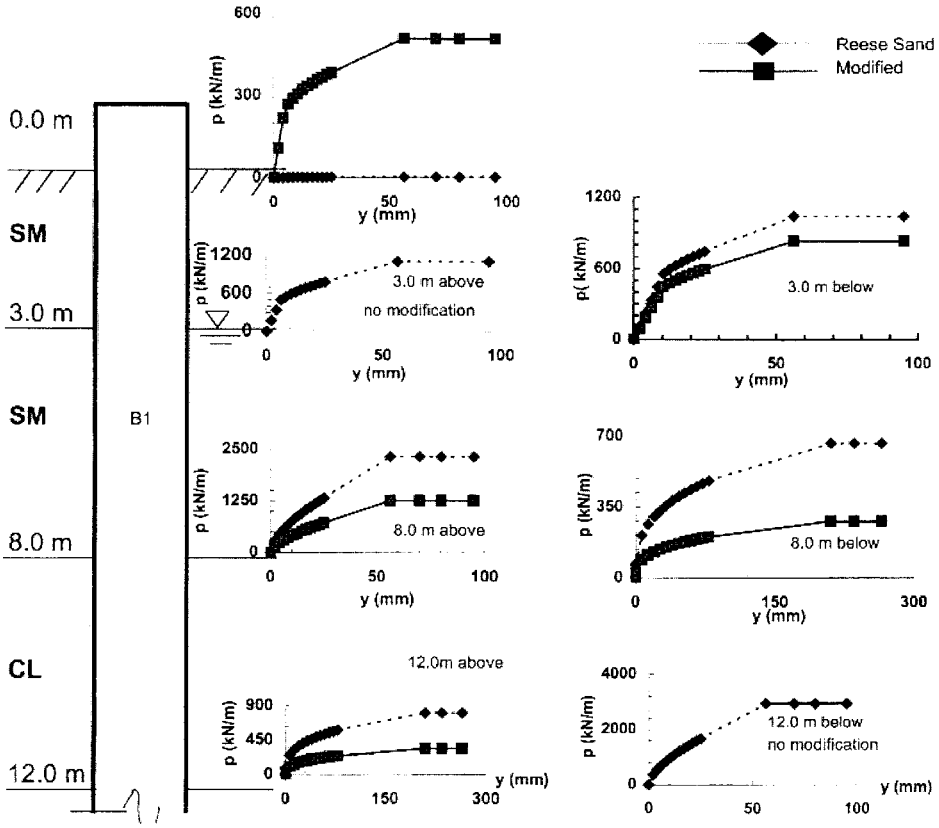

Figure A-9. Original and modified p-y *curves for Bored Pile B-1 (slurry drilled).*

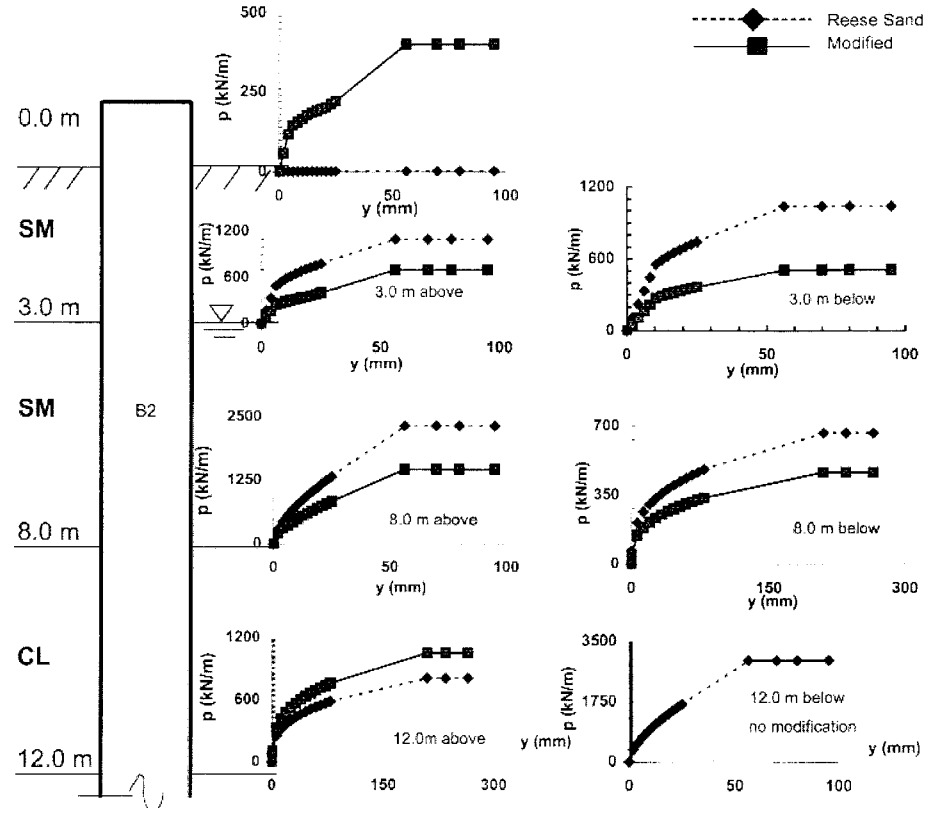

Figure A-10. Original and modified p-y *curves for Bored Pile B2 (full-depth casing).*

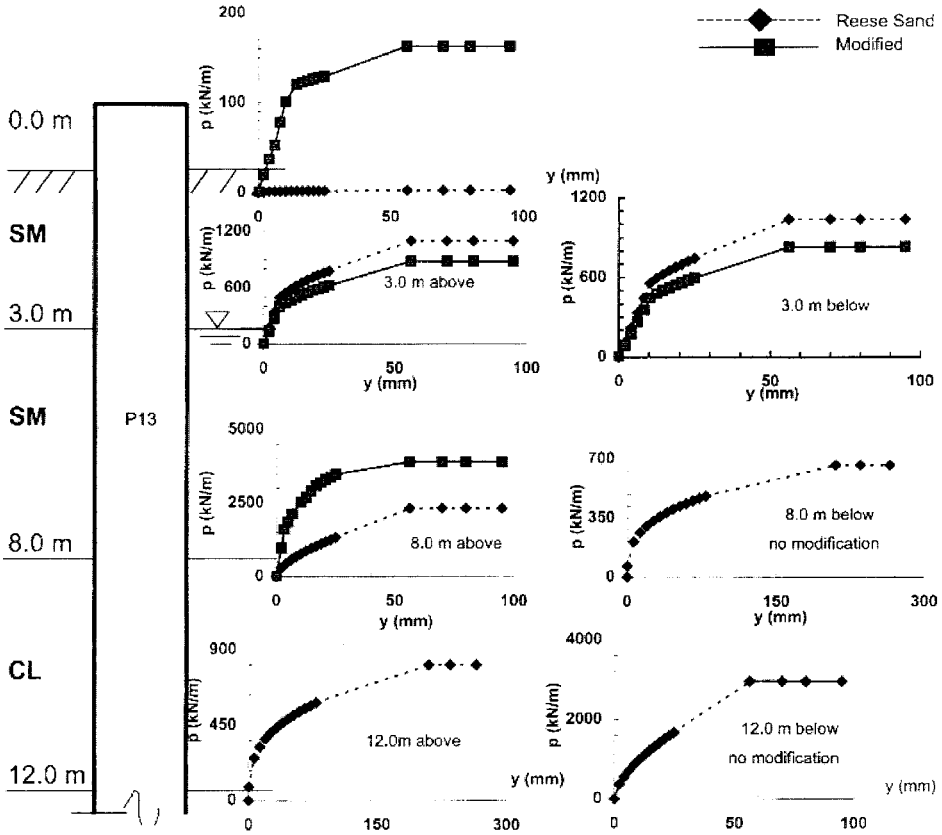

Figure A-11. Original and modified p-y *curves for Driven Pile P13 (prestressed concrete).*

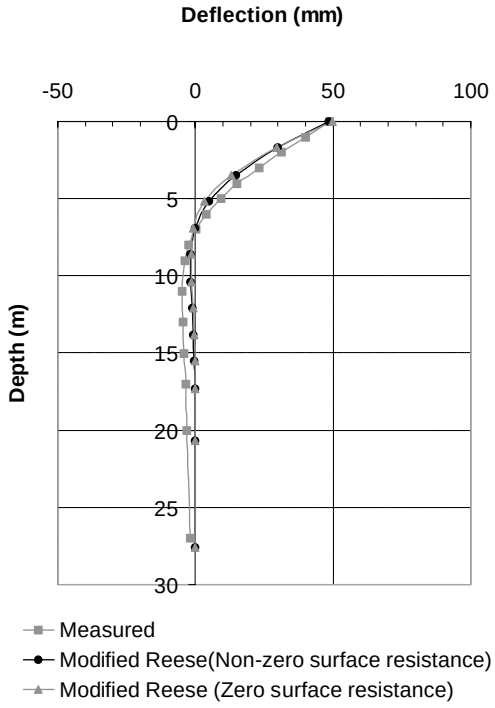

Figure A-12. Effect of p-y *formulation on deflected shape of Bored Pile B1—load = 200 T (1.96 MN).*

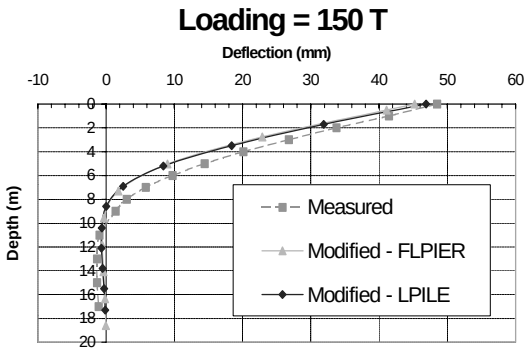

Figure A-13. Predictions of deflected shape of Bored Pile B2 using FLPIER and LPILE plus with modified p-y *criteria—load = 150 T (1.47 MN).*

from Pile B2 were not used in modeling the bored pile group, because a comparison of Figure A-9 for the slurry bored pile with Figure A-10 for the full depth–casing pile shows that, although there are local, depthwise differences in the *p-y* curve corrections, the mean correction is about equal for both methods of construction. This suggests that there was no advantage from the point of view of maintaining soil properties around the piles in using one construction method over the other.

On the other hand, a comparison of Figures A-9 (Bored Pile B1) and A-11 (Driven Pile P13) indicates that smaller modifications had to be made to the *p-y* curves for the driven piles than had to be made for the bored piles. The modifications that were made were generally to stiffen the *p-y* curves for the driven piles whereas the *p-y* curves had to be softened, in general, for the bored piles.

Two numerical models (i.e., computer codes) were used to analyze the single pile–test results: LPILE (*3*) and FLPIER (*15*). Both codes simulate nonlinear bending and axial load effects in laterally loaded concrete piles using similar procedures, and both use *p-y* curves to represent the soil in an identical manner. The results from both codes were essentially identical, as is demonstrated for Pile B2 in Figure A-13. However, FLPIER was selected for further use in this study because it was desired ultimately to develop *p*-multipliers that could be used in FLPIER.

The modified *p-y* curves shown in Figures A-9 through A-11 were accepted as the correct set of *p-y* curves for the test site for bored and driven piles, respectively, of the sizes used in the test groups. The *p-y* curves below a depth of 12 m were taken as the curves predicted by the standard *p-y* criteria. These curves were used without any site-specific modifications. Any deviations from these families of *p-y* curves that were needed to model the group tests were considered to be the results of (a) pile group construction, including installation order; and (b) pile-soil-pile interaction during lateral loading.

Pile Group Tests

Effects of Pile Construction on Soil Property Indexes

When the pile group construction was completed, but prior to load testing of the groups, soundings were made though small access holes in the pile caps to assess the index properties of the soil within the pile groups compared with index properties before the piles were installed. Several different types of probes were used. Two will be considered here: the seismic piezocone (SCPTU) and the DMT. Locations of the probes within each group are shown in Figures A-2 and A-3. Changes from initial values prior to construction to values obtained by probing the soil within the groups for q_c (i.e., cone-tip reading corrected for pore pressure) and E_d (i.e., the dilatometer modulus) are shown in Figures A-14 through A-17 for both the bored pile group and the driven pile group (*16*). The differences in initial and post-construction readings are denoted by the symbol "Δ" in those figures.

In comparing Figures A-14 and A-15, it is obvious that there was a tendency for q_c to decrease because of pile installation in the upper 12 m in the bored pile group; in the same depth range in the driven pile group, the tendency was for q_c to increase because of pile installation. Similarly, in comparing Figures A-16 and A-17, it is seen that the dilatometer modulus decreased within the bored pile group, while there was a slight tendency for it to increase in the driven pile group above a depth of 12 m. These data strongly suggest that the installation

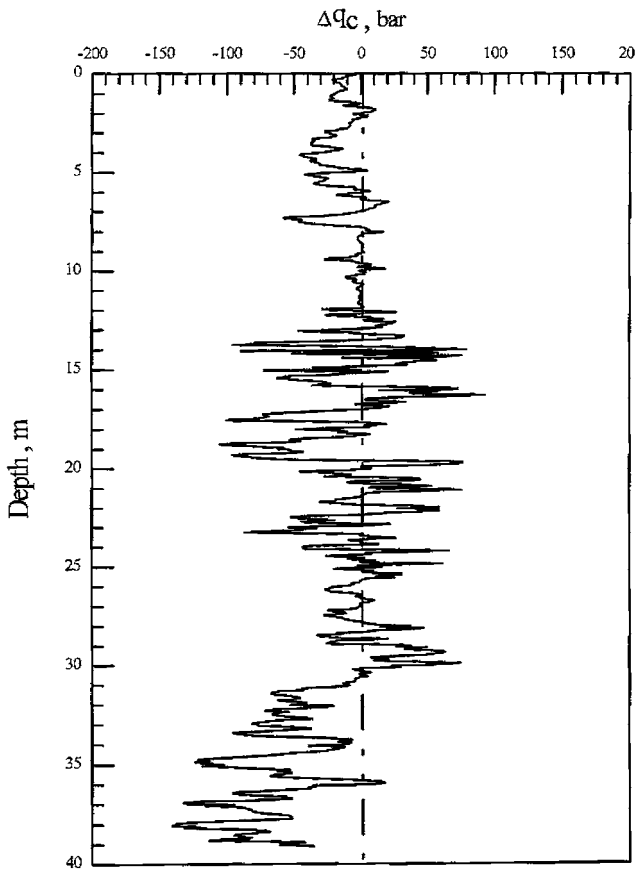

Figure A-14. Change in cone-tip reading (q_c) within bored pile group from preinstallation value to value obtained after piles installed (SCPTU-N1) (after Huang [16]).

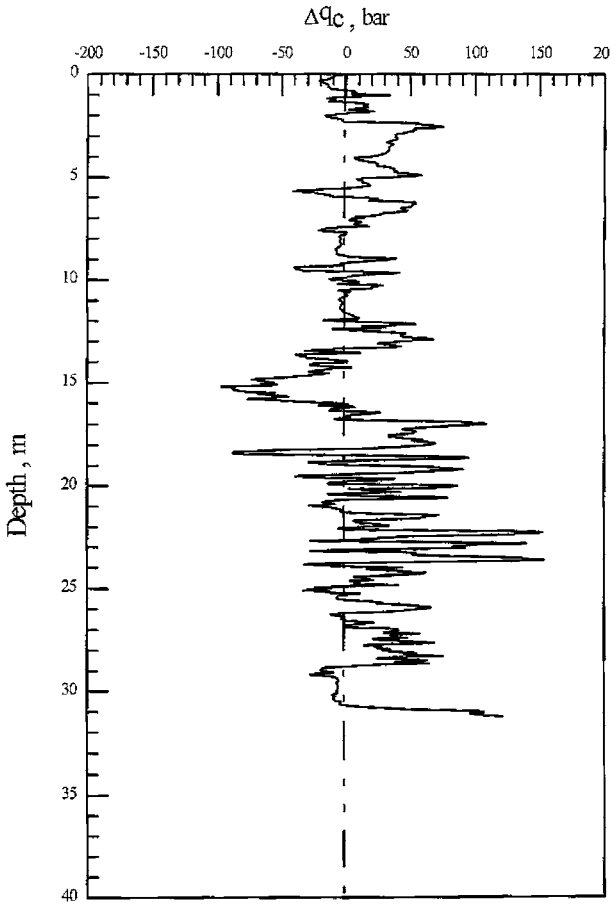

Figure A-15. Change in cone-tip reading (q_c) within driven pile group from preinstallation value to value obtained after piles installed (SCPTU-N3) (after Huang [16]).

of bored piles loosened the soil between the piles within the bored pile group or, perhaps, reduced lateral effective stresses, or both. On the other hand, the installation of the driven piles increased the soil density or lateral effective stresses, or both. These data suggest that the *p*-multipliers that are necessary to simulate group behavior using the site-specific (modified) single-pile *p-y* curves as a baseline will likely be different in the two groups.

Lateral Load Tests

The groups were tested approximately 2 months after the single reference piles were tested, using a quasi-monotonic loading procedure that was very similar to the procedure used for the single piles. The groups were loaded by essentially jacking them apart. The results of the load tests, in terms of cap translation versus lateral load (applied 0.5 m above the ground surface), are shown in Figures A-18 and A-19. A maximum load of 1000 tonnes (17.8 MN) was applied to each group. It is obvious that the bored pile group, consisting of six 1.5-m-diameter piles, was much stiffer than the driven pile group, consisting of twelve 0.8-m-diameter piles, despite the fact that the installation method seemed to weaken the soil around the bored piles within the group.

This seemingly anomalous behavior (from a soil-mechanics perspective) was likely caused by two important factors. First, the bored piles were tied into the pile cap through heavy, hooked rebars, with full development lengths extending into the pile cap, which were assumed to provide a moment connection between the pile cap and the pile heads. No such moment connection existed between the pile cap and the driven piles, in which the cast-in-place concrete for the steel-reinforced pile cap was merely poured over the extended heads of the driven piles. The driven group piles therefore behaved more as free- or pinned-headed piles than as fixed-headed piles. Moment connections stiffen the group response considerably, relative to pinned connections. Second, the sum of the moments of inertia of the 6 bored piles was higher than that of the 12 driven piles, which further stiffened the bored pile group. The fact that the bored pile group was stiffer despite the obvious disadvantages of using bored piles with regard to

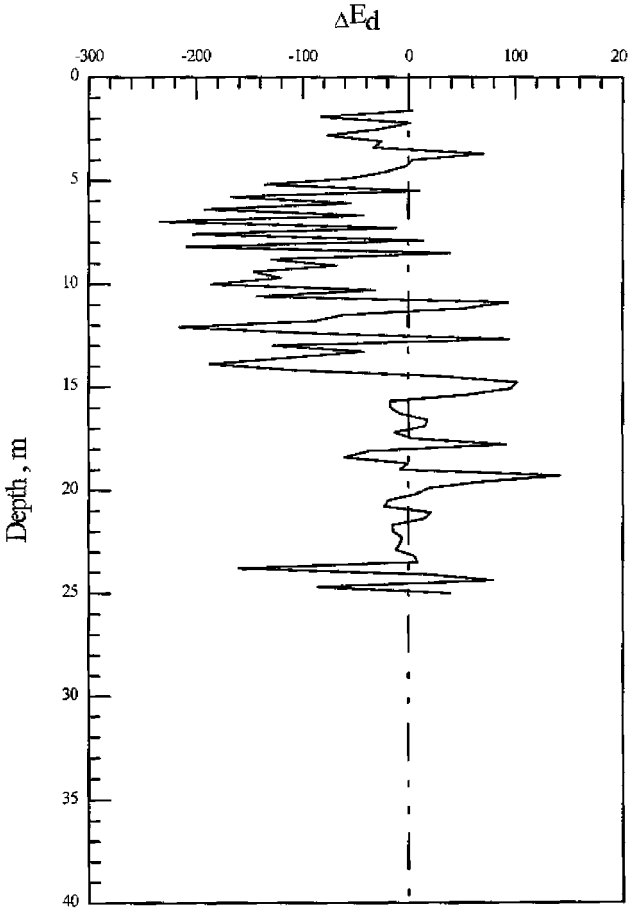

Figure A-16. Change in dilatometer modulus (E_d) within bored pile group from preinstallation value to value obtained after piles installed (DMT-N1) (after Huang [16]).

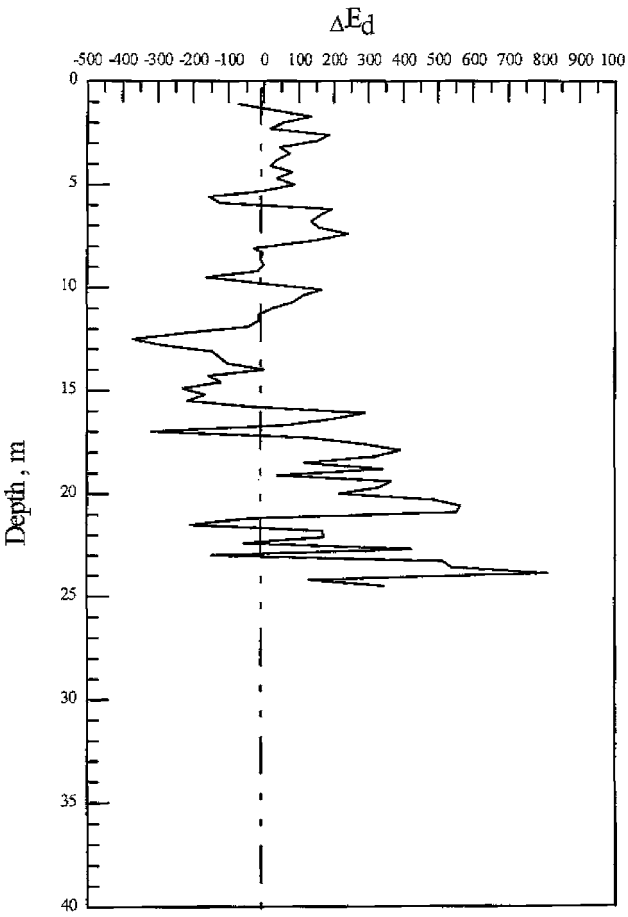

Figure A-17. Change in dilatometer modulus (E_d) within driven pile group from preinstallation value to value obtained after piles installed (DMT-N3) (after Huang [16]).

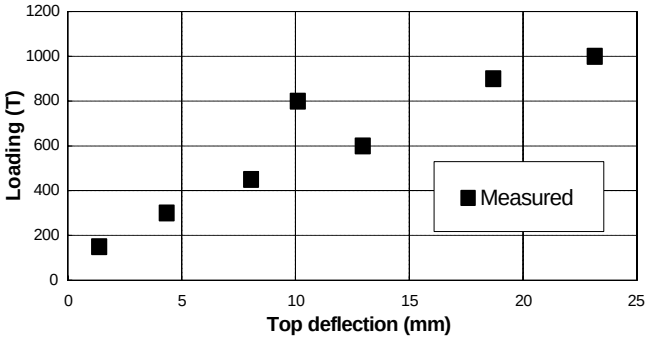

Figure A-18. Cap shear load versus lateral cap deflection—bored pile group.

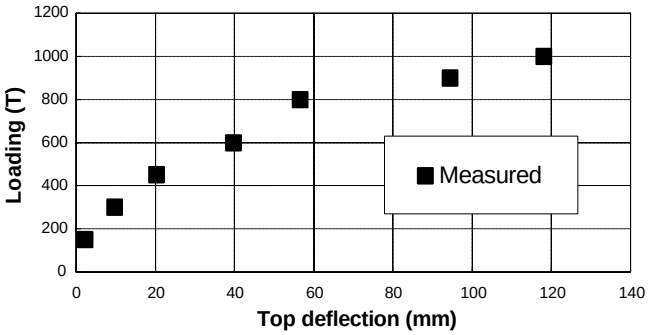

Figure A-19. Cap shear load versus lateral cap deflection—driven pile group.

the stiffness of the soil between the piles indicates the significance of the behavior of the structural components of the pile-soil-cap system and the importance of modeling correctly the structural performance of the pile group system.

On the other hand, a measure of the effects of soil softening caused by lateral pile group action in both groups is evident in Figures A-20 and A-21. The depths of significant lateral pile deflection are much deeper in these figures, from the group tests, than in the corresponding figures for the single-pile tests, Figures A-4 and A-5. The loads shown in Figures A-4 and A-5 are loads per pile whereas those shown in Figures A-20 and A-21 are loads for the entire group. Note that there is some discrepancy in measured head deflections among piles in Figure A-20. The lateral deflections at the head of each pile (at the base of pile cap) should be equal; hence, the differences in head deflections in Figures A-20 and A-21 are indications of the reliability of the deflection readings, which seemed to be comparable in both groups.

Modeling Group Behavior

Both group tests were modeled in a preliminary step using Program GROUP 4.0 (*17*) and FLPIER Version 5.1. Both codes gave similar results for the group load tests at small loads; however, it is necessary to model nonlinear bending in the piles at higher loads, which is not done automatically in GROUP 4.0. This nonlinearity made it difficult to account for the effects of the prestress on the bending stiffness of the driven piles at higher loads. The prestressing force is applied as a uniform axial load along the pile in FLPIER. This force retards the onset of tensile cracking and the resulting reduced bending stiffness in the piles. Eventually, however, the piles develop tensile cracks, which reduce bending stiffness. FLPIER handles this effect automatically. GROUP 4.0 gave a stiffer response than did FLPIER for the bored pile group at higher loads because GROUP 4.0 did not automatically adjust pile stiffness when cracking moments were applied. (In the cases of both bored and driven piles, bending stiffness can be reduced by the user in GROUP 4.0, making multiple runs when combinations of computed bending moments and axial loads indicate that there will be cracking in the cross section; however, this process is slow and inconvenient compared with using FLPIER, which makes the stiffness adjustments for flexural cracking automatically.) FLPIER also allows the user to model the bending flexibility of the pile cap whereas GROUP 4.0 assumes that the pile cap undergoes rigid body motion. Because the pile diameters in the bored pile group were large relative to the thickness of the cap, cap bending was a possibility, and the ability to simulate this phenomenon was a virtue in the group model. For these reasons, and because it

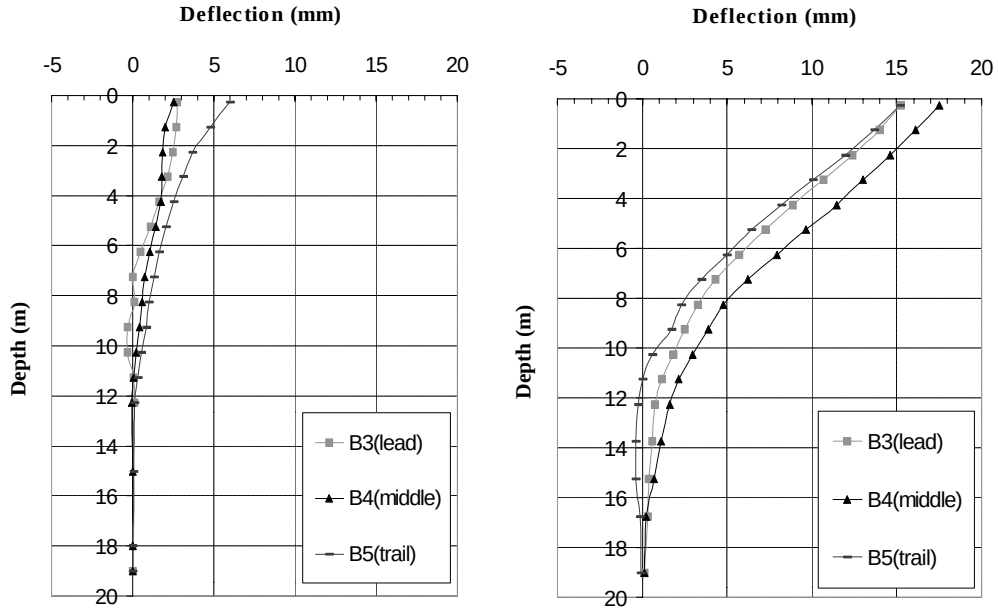

(a) Load = 300 T. *(b) Load = 800 T.*

Figure A-20. Measured deflected shapes along selected piles in bored pile group.

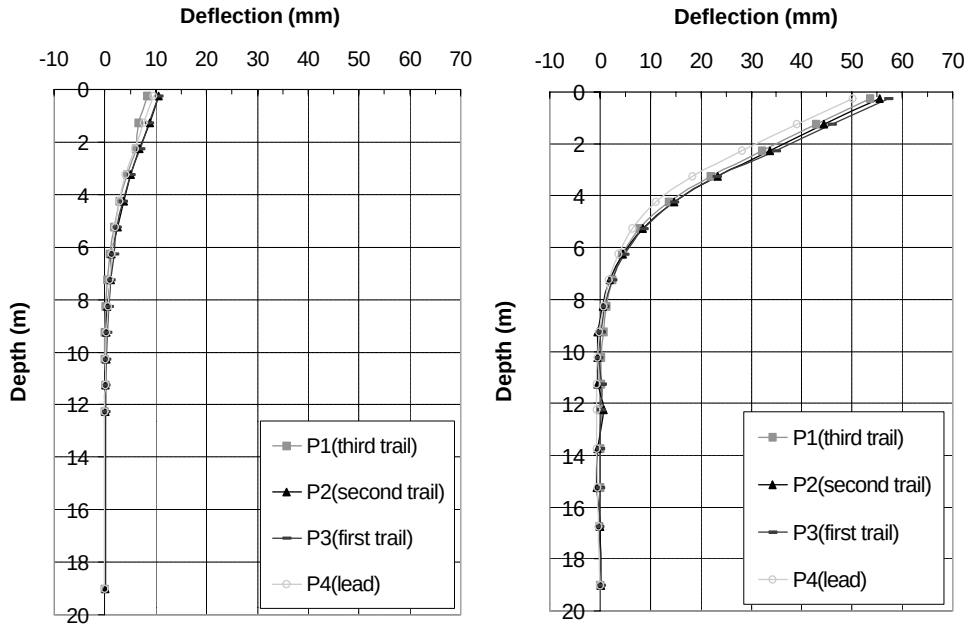

(a) Load = 300 T. *(b) Load = 800 T.*

Figure A-21. Measured deflected shapes along selected piles in driven pile group.

was desired to compute the *p*-multipliers directly for FLPIER, further work with GROUP 4.0 was abandoned.

The pile-head and group-cap conditions that were modeled by FLPIER are shown in Figures A-22 and A-23. All soil that had surrounded the bottom parts of the pile caps was removed physically prior to the tests so that there was no passive resistance or side shearing resistance against either cap. However, both caps were cast on the ground. No measurements of the shearing stresses between the bottoms of the caps and the soil were made, and no reliable measurements of shear load distribution among the piles were available. It was assumed, therefore, that the contribution of cap base shear to the total group

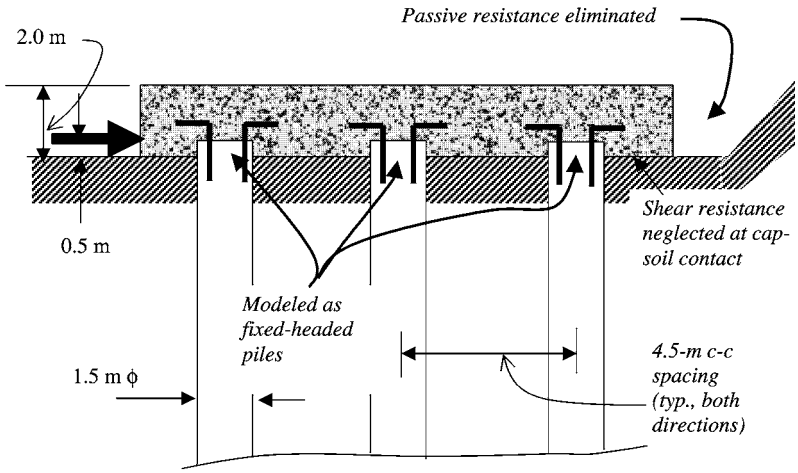

Figure A-22. FLPIER modeling for arrangement for bored pile group.

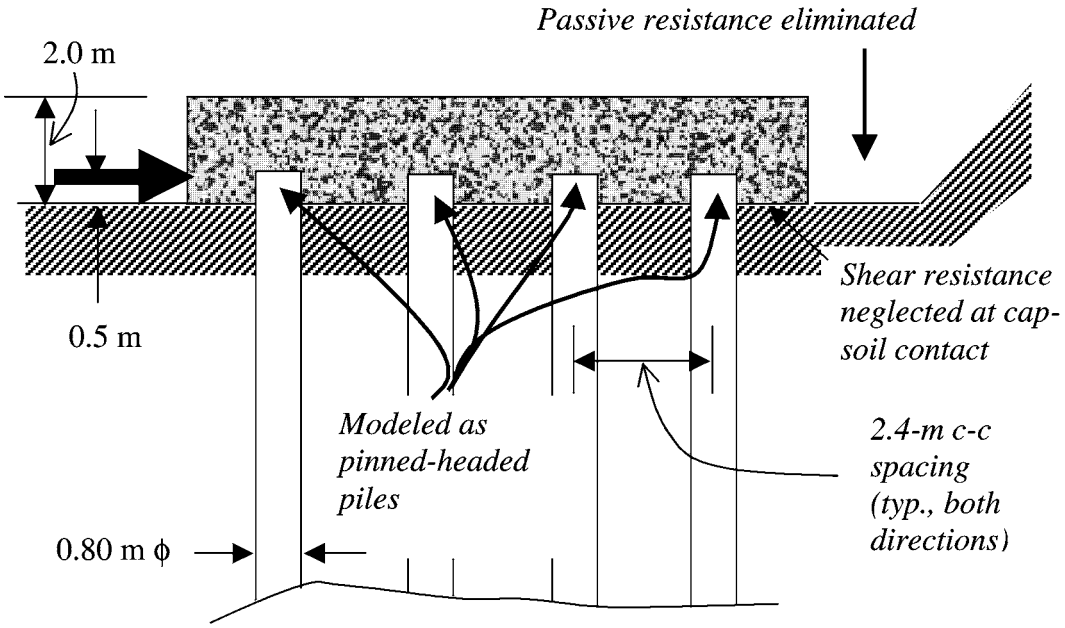

Figure A-23. FLPIER modeling arrangement for driven pile group.

resistance was very small, and it was neglected in the FLPIER analyses.

A less obvious, but no less important, phenomenon that had to be modeled with FLPIER in the simulation of the behavior of the fixed-headed bored pile group was the rotational stiffness of the group, or the axial "push–pull" couples that resist the applied moment (applied load times 0.5 m, as shown in Figures A-22 and A-23) and the "fixing" moments that are produced at the pile heads as the cap translates. These latter moments cause the cap to rotate and the fixing moments to relax, thus softening the lateral response of the pile group. The degree to which the cap rotates under loading from the fixing moments depends upon the stiffness of the group piles in the axial push–pull mode. It is therefore important to model the axial stiffnesses of the piles when the pile heads are assumed to be fixed into the pile cap because these stiffnesses directly influence the *p-y* curves that are required to be used to provide a match with the lateral deflection measurements.

Unfortunately, the only axial load test that was available for direct determination of unit axial load transfer curves for the bored piles, which can also be supplied to FLPIER to simulate axial pile stiffness, was the test on Pile B10. That pile, however, was installed using the full depth–casing technique, rather than the direct-slurry-displacement technique used in the group piles. Unit axial load transfer curves (sometimes called "*t-z*" and "*q-z*" curves), therefore, were generated using an internal routine in FLPIER, which uses an approximate method based on principles given by Randolph and Wroth (*18*). The axial stiffness calculations are carried out by using a simple discrete element model to which *t-z* and *q-z* springs are attached. In order to generate the *t-z* and *q-z* curves in FLPIER, it is only necessary to specify a value of soil shear modulus in the free field, *G*, and the ultimate value of unit side shear f_{max} and of base resistance q_{max}. *G* was estimated in the coarse-grained soil layers from Equations A-1 and A-2:

$$G = \frac{E}{2(1 + \nu)}, \tag{A-1}$$

where

E (force/length^2 in pounds per square foot [psf]) = 10,000 N_{60}. (A-2)

In Equation A-2, N_{60} is the standardized SPT blow count (the average value in a given layer). Poisson's ratio (ν) was taken to be 0.3. For fine-grained soil layers, Equation A-1 was used to estimate *G* whereas *E* was obtained from Equations A-3 and A-4:

$$G = \frac{50\, s_u}{(1 + \nu)}, \tag{A-3}$$

where

$$s_u(\text{in tsf}) = 15N_{60}. \tag{A-4}$$

In Equation A-4, s_u is the undrained shear strength of the fine-grained soil. Poisson's ratio (ν) was taken to be 0.5.

The ultimate unit side and base resistances were obtained from the American Petroleum Institute (API) (*19*), which are strictly valid only for driven piles but which were assumed to give appropriate values for bored piles, as well. In coarse-grained soils, f_{max} is set equal to $\sigma'_v K \tan\delta \le f_{max}$ (limit), where σ'_v is the vertical effective stress at the center of a given soil

layer; K is an earth pressure coefficient taken equal to 0.8; and δ is an angle of pile-soil wall friction prescribed by API Recommended Practice 2A (API RP2A) (*19*), based on the fines content and relative density of the soil. f_{max} (limit) is based on the same properties. q_{max} in compression is defined by σ'_v (base) N_q, where N_q is a function of fines content and relative density $\leq q_{max}$ (limit). q_{max} (limit) is likewise given by API to be a function of fines content and relative density and is set equal to zero for uplift loading.

In fine-grained soils, f_{max} is determined in API RP2A from the ratio of s_u to σ'_v. q_{max} is taken to be 9 s_u at the base of the pile for compression loading and zero for uplift loading.

Once the axial load–movement behavior of single piles was simulated in FLPIER, that value was used for each bored pile in the group without modification for axial group effects. The argument for making this simplifying assumption was that the front (i.e., leading) row of piles would settle, the back (i.e., trailing) row of piles would go into tension, and the middle row of piles would essentially remain stationary axially. The tendency for one pile on the front row to soften the behavior of its neighbor on that row is approximately offset by the tendency for the uplift in both piles in the back row to stiffen the behavior of the piles on the front row, with similar effects for piles on the back row.

No strong concern about modeling of axial behavior existed for the driven pile group because no fixing moments develop with pinned-headed piles, and the lateral stiffness is essentially decoupled from the axial push–pull behavior. Nonetheless, the same procedure was used for simulating axial response in the driven pile group as that used for the bored pile group.

With the modeling of axial behavior accomplished, the main effort in modeling the test groups with FLPIER was to determine how the site-modified, single-pile *p-y* curves (Figures A-9 and A-11) were required to be modified again to produce the *p-y* curves best suited to modeling group behavior. The second-step modification (for group action) was made by multiplying the site-modified *p-y* curves in Figures A-9 (for the bored piles) and A-11 (for the driven piles) by appropriate *p*-multipliers specific to each row of piles, from the leading row to the last trailing row.

The concept of the *p*-multiplier, as applied in this study, is briefly explained in Figure A-24. For each pile on a given row in the group (leading, first-trailing, second-trailing, and so forth), all of the *p*-values on all of the *p-y* curves at every depth are multiplied by a single factor, ρ (i.e., the *p*-multiplier for that row in the group). ρ was varied in the FLPIER model until an acceptable match was found between the computed and measured load-deformation behavior of the pile cap for both group tests. By following the procedure outlined in this appendix, the factor ρ describes the combined effect of group construction and group loading on lateral pile group action.

The ρ values (i.e., *p*-multipliers) were ascertained by varying ρ on a row-by-row basis and comparing the computed cap translations at seven values of cap load, ranging from 150 T (1.47 MN) to 1000 T (9.8 MN). The number of loads at which the absolute value of the computed deflection minus the measured deflection divided by the measured value of deflection exceeded 15 percent was considered a measure of the accuracy of the selected family of ρ values. The results of a subset of analyses of the effects of families of ρ values on cap displacement in the bored pile group are summarized in Table A-2. The most accurate family of ρ values for the bored pile group is shown in Column 8 of Table A-2 although the families of values in Columns 2 and 10 are essentially of equal accuracy.

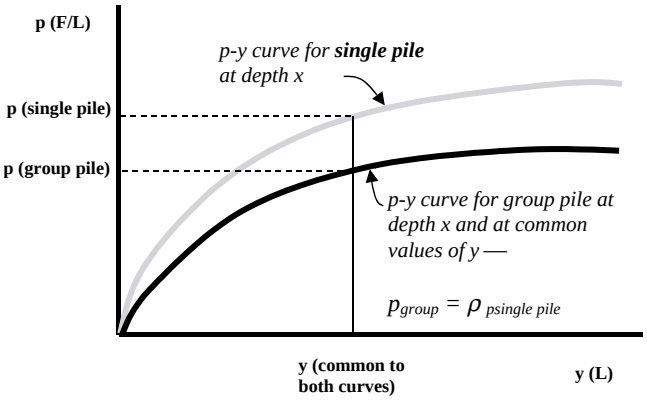

Figure A-24. Definition of the p*-multiplier (*ρ*) for simulating lateral group behavior.*

The optimum set of ρ values (i.e., *p*-multipliers) for each group is presented in Table A-3. Also shown in Table A-3 are values that have been cited by Peterson and Rollins (*8*) as being appropriate for laterally loaded pile groups based on information available in 1996. The *p*-multipliers for the bored pile group in the current study were, on the average, lower than those cited by Peterson and Rollins; the *p*-multipliers for the driven pile group were higher, row by row and on the average, than those of Peterson and Rollins. Considering the independent soil data of Huang (*16*) in Figures A-14 through A-17, these trends appear to be clearly related to installation methods.

The measured lateral load versus lateral-translation relations for both pile groups are compared with the relations predicted by FLPIER using the site-specific (modified) *p-y* curves for both bored and driven piles (see Figures A-9 and A-11, respectively). The *p*-multipliers tabulated in Table A-3 are shown in Figure A-25. The predictions are excellent.

Finally, a typical comparison of computed and measured deflected shapes for group piles is shown in Figure A-26. The FLPIER model with the modified *p-y* curves and the deduced *p*-multipliers appears to give good predictions of pile shape under loading. Further details on the field tests and the analysis of the field tests can be found in Reference 20 (*20*).

CONCLUSIONS AND RECOMMENDATIONS

Conclusions

Although the knowledge obtained from the Chaiyi field tests and their analysis is site specific, the general conclusions stated below are expected to be valid for other sites at which similar

TABLE A-2 Effect of varying *p*-multipliers on cap deflection for the bored pile group

Load (T)	Measured cap deflection (mm)	Computed cap deflection (mm) (1)	(2)	(3)	(4)	(5)	(6)	(7)	(8)	(9)	(10)	(11)	(12)
		0.8	0.6	0.6	0.6	0.7	0.7	0.5	**0.5**	0.5	0.5	0.65	0.55
		0.4	0.3	0.3	0.2	0.2	0.3	0.3	**0.4**	0.4	0.3	0.35	0.47
		0.333	0.3	0.2	0.3	0.3	0.2	0.3	**0.3**	0.2	0.4	0.2	0.13
150	1.38	1.81	2.15	2.32	2.31	2.19	2.20	2.28	**2.14**	2.31	2.13	2.18	2.26
		+31%	+55%	+68%	+67%	+59%	+59%	+65%	**+55%**	+67%	+54%	+58%	+64%
300	4.34	3.48	4.17	4.58	4.56	4.24	4.27	4.57	**4.22**	4.61	4.20	4.24	4.51
		-20%	-4%	+6%	+5%	-2%	-2%	+5%	**-3%**	+6%	-3%	-2%	+4%
450	8.05	6.09	7.55	8.21	8.17	7.62	7.65	8.06	**7.49**	8.19	7.43	7.65	7.95
		-24%	-6%	+2%	+2%	-5%	-5%	+0%	**-7%**	+2%	-8%	-5%	-1%
600	12.96	7.85	9.8	10.8	10.8	10.0	10.0	10.6	9.7	10.7	9.67	10.0	10.4
		-39%	-24%	-17%	-17%	-23%	-23%	-18%	-25%	-17%	-25%	-23%	-20%
800	10.1	11.8	15.3	17.0	17.0	15.6	15.7	16.7	**15.2**	16.9	15.2	15.5	16.4
		+17%	+52%	+68%	+68%	+55%	+55%	+65%	**+50%**	+67%	+50%	+55%	+62%
900	18.69	14.6	19.1	21.5	21.5	19.5	19.5	21.1	**18.9**	21.3	18.9	19.3	20.5
		-22%	+2%	+15%	+15%	+4%	+4%	+13%	**+1%**	+14%	+1%	+3%	+10%
1000	23.15	19.5	26.6	30.1	30.1	27.2	27.2	29.6	**26.4**	29.9	26.4	27.0	29
		-16%	+15%	+30%	+30%	+18%	+18%	+28%	**+14%**	+29%	+14%	+17%	+25%
Average difference ratio		-10%	+13%	+25%	+24%	+15%	+15%	+23%	**+12%**	+24%	+12%	+15%	+21%
Error probability		7/7	3/7	4/7	4/7	4/7	4/7	4/7	**3/7**	4/7	3/7	4/7	4/7

NOTE: The percentage below each computed deflection is the ratio of the difference between a computed and measured deflection to the measured deflection; "Average difference ratio" is the value of the sum of all the difference ratios in a column divided by the number of total loads (i.e., 7); "Error probability" is defined as the ratio of the number of the loads whose corresponding difference ratios exceed ±15% to the number of total loads.

soil conditions exist (loose to medium-dense silty sands and sandy silts near the surface) and at which piles are installed with a similar geometry (rectangular groups with 3-diameter, center-to-center pile spacing) by casting the piles in place or by driving displacement piles. Please note that these conclusions cannot be extended to sites at which liquefaction will occur, nor is it likely that these conclusions apply to predominantly clay sites. The conclusions can be stated as follows:

1. Single-pile *p-y* curves needed to be softer (i.e., reduced *p*-values for given values of *y*) than the prescribed curves (i.e., Reese et al. [*1*] criteria for sand layers; Matlock [*13*] criteria for clay layers) for large-diameter (1.5-m) bored piles. See Figure A-9.
2. Single-pile *p-y* curves did not require overall softening relative to the prescribed curves (i.e., Reese et al. [*1*] criteria for sand layers; Matlock [*13*] criteria for clay layers) for smaller-diameter (0.80-m) driven displacement piles; however, some modification—both softening and stiffening—at individual depths was needed to optimize the simulation of measured single-pile behavior. See Figure A-11.
3. The ratio of the deduced *p*-multipliers for the quasi-static loading of bored piles, averaged over all rows, was

TABLE A-3 *p*-Multipliers for Chaiyi lateral group load tests

Pile Row	Inferred *p*-Multipliers from Chaiyi Load Tests: Bored Pile Group	Inferred *p*-Multipliers from Chaiyi Load Tests: Driven Pile Group	*p*-Multipliers from Peterson and Rollins (*8*) *S / D* = 3	Default *p*-Multipliers from FLPIER (*15*) *S / D* = 3
Lead	0.5	0.9	0.6	0.8
First Trail	0.4	0.7	0.4	0.4
Second Trail	0.3	0.5	0.4	0.2
Third Trail	–	0.4	–	0.3
Average	*0.4*	*0.63*	*0.47*	*0.43*

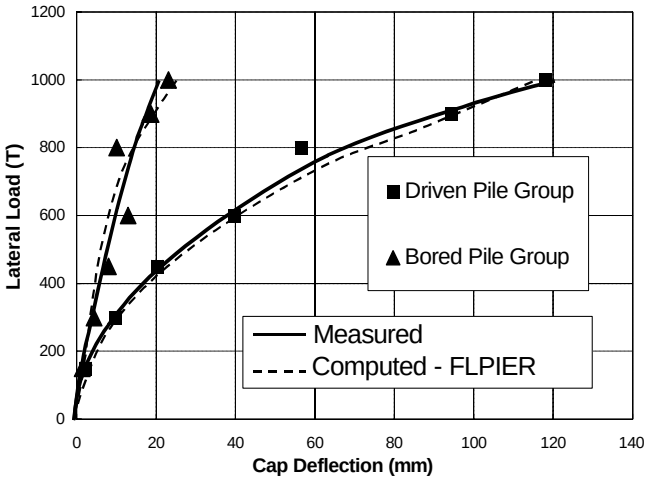

Figure A-25. Measured lateral load-cap deflection relationships for driven and bored pile groups.

approximately 0.65 times that for the quasi-static loading of driven displacement piles. The ratio of the average *p*-multiplier for the bored piles to the average "standard" value recommended by Peterson and Rollins (*8*) was 0.85; the ratio of the average *p*-multiplier for the driven displacement piles was 1.33 times the value recommended by Peterson and Rollins. See Table A-3.

4. The row-wise pattern of *p*-multipliers for both the driven and bored pile groups, tabulated in Table A-3, was similar to that observed by others. That is, the highest values appeared on the leading (i.e., front) row, the next highest on the first trailing row, and so forth. (When the extreme-event loading has a predictable direction, it is appropriate to use row-wise *p*-multipliers in the design process. In seismic events, however, loading direction likely varies, and loading is cyclic, making it more reasonable from a design perspective to use average *p*-multipliers for all piles in the group.) The exact row-to-row ratios of *p*-multipliers is likely a function of the order of pile installation. In this study, the installation order was generally from front (i.e., leading) row to back (i.e., last trailing) row.
5. Apparently, the differences in *p*-multipliers for bored and driven piles largely reflect the effects of the differing effects of boring and driving displacement piles on the density and stress state in the mass of soil within the pile group.
6. The reduced soil stiffness around the bored piles was overshadowed by the effects of head fixity and pile diameter (i.e., the higher moment of inertia) in the bored pile group.

The applicability of the results summarized in this appendix to *p*-multipliers for dynamic loading (see Appendix B) is not clear. However, the results suggest that for low frequencies of seismic loading (low predominant frequency of the seismic event), the average *p*-multiplier for groups of bored piles should be lower than those for driven displacement piles by a factor in the range of 0.65.

Recommendations for Further Research

The following additional research is recommended:

1. Further research is needed to understand the frequency range to which the ratio of *p*-multipliers for bored piles to those for driven piles, deduced from static tests such as these tests, applies.
2. It is possible that *p*-multipliers will be different for bored piles installed with continuous, full-depth casing

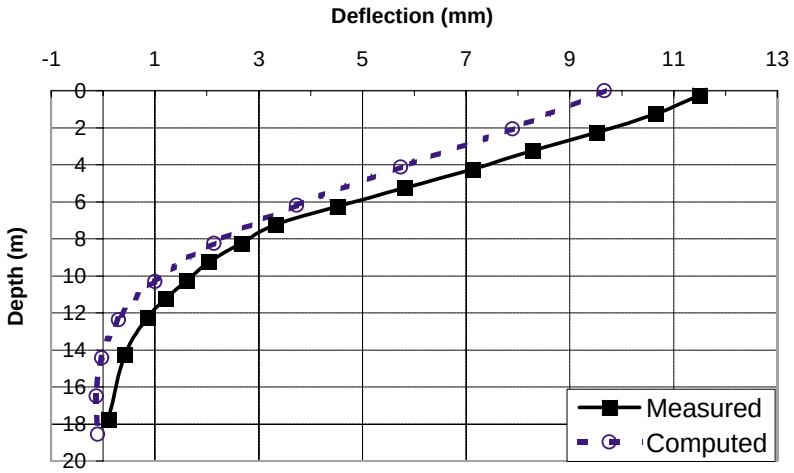

Figure A-26. Measured and predicted deformed shape of Pile B3 on leading row of the bored pile group—load = 600 T.

than for bored piles installed by slurry displacement. Further research into this phenomenon is warranted if full depth–casing construction methods become common on department of transportation projects in the United States.

REFERENCES—APPENDIX A

1. Reese, L. C., W. R. Cox, and F. C. Koop. "Analysis of Laterally Loaded Piles in Sand," *Proceedings, Offshore Technology Conference*, Houston (1974); pp. 473–484.
2. Murchison, J., and M. W. O'Neill. "Evaluation of p-y Relationships in Cohesionless Soil," *Analysis and Design of Pile Foundations*, J. R. Meyer (ed.); ASCE (1984); pp. 174–191.
3. Reese, L. C., and S. T. Wang. *Computer Program LPILE Plus, Version 3.0—A Program for the Analysis of Piles and Drilled Shafts Under Lateral Loads, Technical Manual.* Ensoft, Inc. (1997).
4. Hoit, M., C. Hays, and M. McVay. "The Florida Pier Analysis Program: Methods and Models for Pier Analysis and Design," *Transportation Research Record No. 1569*, Transportation Research Board, National Research Council (1997); pp. 1–7.
5. *PAR: Pile Analysis Routines, Theoretical and User's Manuals.* PMB Engineering, Inc. (1988).
6. Brown, D. A., C. Morrison, and L. C. Reese. "Lateral Load Behavior of Pile Group in Sand," *Journal of Geotechnical Engineering*, ASCE, Vol. 114, No. 11 (1988); pp. 1326–1343.
7. McVay, M., R. Casper, and T.-I. Shang. "Lateral Response of Three-Row Groups in Loose to Dense Sands at 3D and 5D Pile Spacing," *Journal of Geotechnical Engineering*, ASCE, Vol. 121, No. 5 (1995); pp. 436–441.
8. Peterson, K., and K. M. Rollins. *Static and Dynamic Lateral Load Testing of a Full-Scale Pile Group in Clay*, Research Report CEG.96-02. Brigham Young University (1996).
9. Pinto, P., M. McVay, M. Hoit, and P. Lai. "Centrifuge Testing of Plumb and Battered Pile Groups in Sand," *Transportation Research Record No. 1569.* Transportation Research Board, National Research Council (1997); pp. 8–16.
10. Brown, D. A., and C. F. Shie. "Modification of p-y Curves to Account for Group Effects on Laterally Loaded Piles," *Geotechnical Special Publication No. 27*, ASCE, Vol. 2 (1991); pp. 479–490.
11. Chen, C.-H. "Data for Planned Pile Group Tests at Chaiyi Test Site," *Workshop Report.* National Taiwan University (1996).
12. Huang, A. B. *Midterm Report of the Lateral Test of Group Piles.* National Chao-Tung University (Taiwan) (1997).
13. Matlock, H. "Correlations for Design of Laterally Loaded Piles in Soft Clays," *Proceedings, Second Annual Offshore Technology Conference*, Houston, (1970); pp. 578–588.
14. Andrade, P. *Materially and Geometrically Nonlinear Analysis of Laterally Loaded Piles Using a Discrete Element Technique, Final Report.* University of Florida (1994).
15. McVay, M., C. Hays, and M. Hoit. *User's Manual for Florida Pier, Version 5.1.* University of Florida (1996).
16. Huang, A. B. *The Effect of the Installation of Group Piles on the Properties of the Soil in the Vicinity, Final Report.* National Chao-Tung University (Taiwan) (1997).
17. Reese, L. C., and S. T. Wang. *GROUP 4.0 for Windows: Technical Manual.* Ensoft, Inc. (1996).
18. Randolph, M. F., and C. P. Wroth. "Analysis of Deformation of Vertically Loaded Piles," *Journal of the Geotechnical Engineering Division*, ASCE, Vol. 104, No. GT12 (1978); pp. 1465–1488.
19. *Recommended Practice for Planning, Designing and Constructing Fixed Offshore Platforms—API Recommended Practice 2A* (RP2A), 17th Edition. American Petroleum Institute (1993).
20. Zhang, X. "Comparison of Lateral Group Effect between Bored and PC Driven Pile Groups in Sand," M.S. thesis. Department of Civil and Environmental Engineering, University of Houston (1999).

APPENDIX B

DYNAMIC RESPONSE OF PILES TO EARTHQUAKE LOADING—ANALYTICAL

INTRODUCTION

Catastrophic damage resulting from recent earthquakes has raised concerns about the current codes and approaches used for the design of structures and foundations. In the past, free-field accelerations, velocities, and displacements have been used as input ground motions for the seismic design of structures without considering the kinematic interaction of the foundation or the site effects that have resulted from the soil stratigraphy and the introduction of piles. Depending on the pile or pile group configuration and soil profile, free-field response may underestimate or overestimate actual in situ conditions that will result in radically changed foundation and structural behavior and, therefore, in impact design criteria.

The behavior of pile foundations during an earthquake event is influenced by the interaction of the pile foundation with the surrounding soil medium. This interaction can be categorized into (1) kinematic interaction and (2) inertial interaction. The former characterizes the response of piles to the seismic loading through the soil; the latter describes the pile-soil interaction caused by the inertial loading from the superstructure applied at the pile head. The characteristics of the pile-soil interaction in these two types of loading are different; therefore, the kinematic interaction and the inertial interaction are addressed separately.

KINEMATIC RESPONSE OF PILES

Recent destructive earthquakes have highlighted the need for increased research into the revamping of design codes and building regulations to prevent further catastrophic losses in terms of human life and economic assets. The present study investigated the response of single piles to kinematic seismic loading using the three-dimensional finite element program ANSYS (*1*).

The objectives of this study were twofold:

1. Develop a finite element model that can accurately model the kinematic soil-structure interaction of piles, accounting for the nonlinear behavior of the soil, discontinuity conditions at the pile-soil interface, energy dissipation, and wave propagation.
2. Use the developed model to evaluate the kinematic interaction effects on the pile response with respect to the input ground motion. The results of a number of studies on the kinematic interaction of pile groups reported in the literature are also included.

Assumptions and Restrictions

The problem to be addressed is shown in Figure B-1. As shown, the actual system consists of a pile foundation supporting a typical bridge pier. Current design codes use the free-field motion as the input ground motion at the foundation level. The analysis described herein attempted to evaluate the interaction of the pile-soil system and how it alters the free-field motion and modifies the ground motion at the foundation level.

The dynamic loading was applied to the rigid underlying bedrock (see Figure B-1) as one-dimensional horizontal acceleration (X-direction in finite element model), and only horizontal response was ascertained. Vertical accelerations were ignored because the margins of safety against static vertical forces usually provide adequate resistance to dynamic forces induced by vertical accelerations. Wu and Finn (*2*), using a three-dimensional elastic model, found that deformations in the vertical direction and normal to the direction of shaking are negligible compared with the deformations in the direction of horizontal shaking.

Although the finite element analysis used in this study includes important features such as soil nonlinearity and gapping at the pile-soil interface, it does not account for buildup of pore pressure because of cyclic loading. Thus, neither the potential for liquefaction nor the dilatational effect of clays and the compaction of loose sands in the vicinity of piles is accounted for in the current analysis. Furthermore, the inertial interaction between the superstructure and the pile-foundation system is not considered here. The analysis is limited to the response of free-headed piles with no external forces from the superstructure ("D'Alembert forces") to understand better the kinematic interaction effects in seismic events.

Three-Dimensional Finite Element Model

Model Formulation

Full three-dimensional geometric models were used to represent the pile-soil systems. Exploiting symmetry, only one-half of the actual model was built, thus significantly reducing computing time and cost. Figure B-2 depicts the pile-soil system considered in the analysis, showing an isometric view of the half of the model used. Figures B-2 and B-3 show the finite element mesh (Mesh No. 3) used in the analysis.

The pile and soil were modeled using eight-noded block elements. Each node had three translational degrees of freedom (i.e., *X, Y* and *Z* coordinates), as shown in Figure B-4. A three-

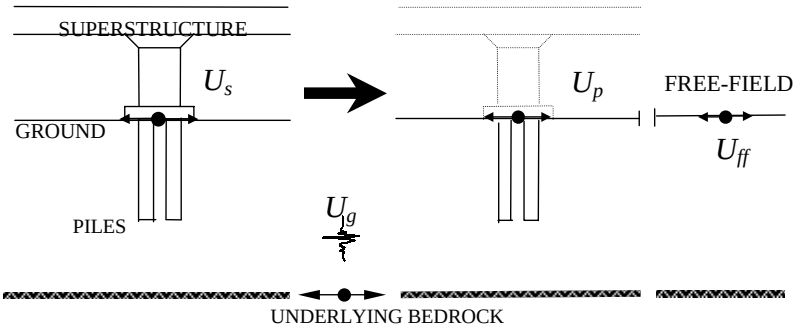

Figure B-1. Definition of the problem and terminology (actual acceleration, U_s*; acceleration due to kinematic interaction only,* U_p*; bedrock acceleration,* U_g*; and free-field acceleration,* U_{ff}*).*

dimensional point-to-surface contact element was used at the pile-soil interface to allow for sliding and separation in tension, but ensured compatibility in compression. The contact element had five nodes with three degrees of freedom at each node (i.e., translations in the *X*, *Y* and *Z* directions), as shown in Figure B-4b. Transmitting boundaries were used to allow for wave propagation and to eliminate the "box effect" (i.e., the reflection of waves back into the model at the boundaries) during dynamic loading. The element used to model the transmitting boundary consisted of a spring and a dashpot arranged in parallel, as illustrated in Figure B-4c.

Soil Properties

To evaluate the effect of soil plasticity on the pile response, the soil was modeled using two approaches: a homogeneous elastic medium and an elastoplastic material using the Drucker–Prager failure criteria. For cases involving plasticity, the angle of dilatancy was assumed to be equal to the angle of internal friction (associated flow rule). There was no strain hardening; therefore, no progressive yielding was considered. Because pore pressures were not considered in this

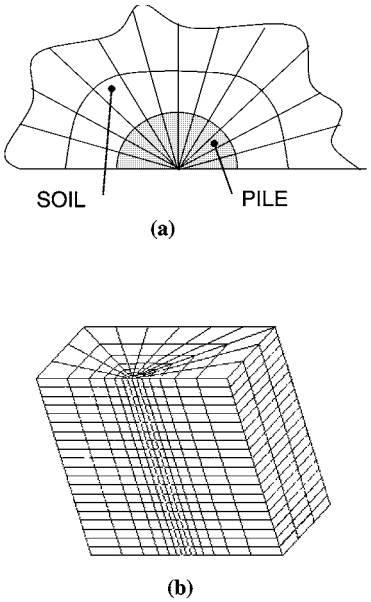

Figure B-2. Pile-soil system. (a) Detail of wedge-shaped pile elements surrounded by soil elements (plan view). (b) Isometric view of soil and pile mesh model.

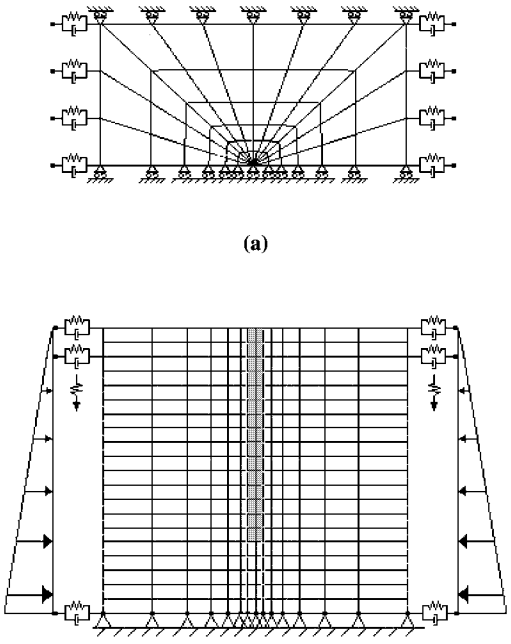

Figure B-3. Finite element mesh (Mesh No. 3) showing boundary conditions. (a) Plan view. (b) Front cross-section view with geostatic pressure distribution.

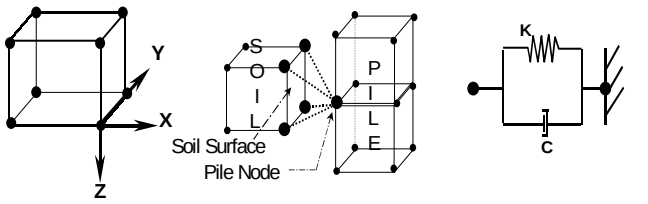

(a) - 8 noded block element, DOF: X, Y, Z **(b) - 5 noded contact element, DOF: X, Y, Z** **(c) - 2 noded boundary element, DOF: X, Y, Z**

Figure B-4. Soil and pile model elements: (a) block element used for soil and pile; (b) surface contact element used between pile and soil to allow for slippage and separation; (c) transmitting boundary element consisting of "spring(K)" and "dashpot(C)" to allow for radiating boundaries.

analysis, effective stress parameters and drained conditions were assumed. The material damping ratio of the soil, β, was assumed to be 5 percent (i.e., $D = 10$ percent). This soil material damping ratio is compatible with the expected strain level under earthquake loading. The governing equations of the system are given by

$$[M]\{\ddot{u}\} + [C]\{\dot{u}\} + [K]\{u\} = \{F(t)\}, \qquad \text{(B-1)}$$

where $\{\ddot{u}\}$, $\{\dot{u}\}$, and $\{u\}$ are the acceleration, velocity and displacement vectors, respectively, and $[M]$, $[C]$, and $[K]$ are the global mass, damping, and stiffness matrixes. The damping matrix is given by $[C] = \zeta [K]$, in which the damping coefficient, ζ, is $2\beta/\omega_0$, and ω_0 is the predominant frequency of the loading (rad/s). Material damping was assumed to be constant throughout the entire seismic event, although the damping ratio varies with the strain level.

Pile Properties

Cylindrical reinforced concrete piles with linear elastic properties were considered in this study. The piles were modeled using eight-noded brick elements. The cylindrical geometry was approximately modeled using wedge-shaped elements (see Figure B-2a). No damping was considered within the piles, and relevant parameters are listed in Figure B-5.

Pile-Soil Interface

Modeling of the pile-soil interface is crucial because of its significant effect on the response of piles to lateral loading (*3*). Two cases were considered in the analysis:

1. The pile and soil were perfectly bonded, in which case the perimeter nodes of the piles coincided with the soil nodes (elastic with no separation).
2. The pile and soil were connected by frictional interface elements that are described below.

The contact surface (i.e., the pile) is said to be in contact with the target surface (i.e., the soil) when the pile node penetrates the soil surface. A very small tolerance was assumed to prevent penetration and to achieve instant contact as pile nodes attempt to penetrate the soil nodes (or vice versa). Coulomb friction was employed between the pile and soil along the

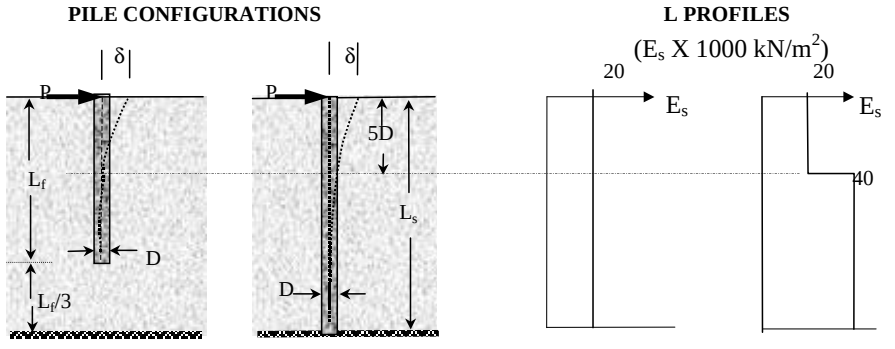

E_s= Soil Young's Modulus
δ = Horizontal deflection
P = Horizontal load
V_s = Shear wave velocity = 60-120 m/s
c' = 34 kPa, $\phi = \Psi = 16.5°$ (Plasticity)

E_p= Pile Young's Modulus = $2*10^7$kPa
ρ_s = Soil submerged unit weight = 11.8 kN/m^3
ρ_p = Pile mass density = 2.3 Mg/m^3
ν_s = Soil Poisson's ratio = 0.45
ν_p = Pile Poisson's ratio = 0.30

Figure B-5. Two-dimensional representation of floating and socketed pile in either homogeneous (used for verification) or layered soil profile.

entire pile length as well as to the pile tip (for floating piles). The coefficient of friction relating shear stress to the normal stress was chosen according to American Petroleum Institute (API) recommendations (*4*) and was assumed to be 0.7. The contact surface coordinates and forces were fully updated to accommodate any large or small deflections that may occur. The penalty function method was used to represent contact with a normal contact stiffness (K_n). K_n allowed the interface element to deform elastically before slippage occurred and was chosen to be equal to the shear modulus of the soil. Convergence was achieved, and over-penetration was prevented using K_n = 6800 kN/m (numerically equal to the shear modulus of the soil).

Boundary Conditions

Boundary conditions varied depending on the type of loading. For static loading, the bottom of the mesh (representing the top of the bedrock layer) was always fixed in all directions. All symmetry faces were fixed against displacement normal to the symmetry plane, but were free to move on the surface of the plane. The nodes along the top surface of the mesh were free to move in all directions. The nodes along the sides of the model were free to move vertically, but were constrained in the horizontal direction by a Kelvin element in order to represent a horizontally infinite soil medium during static and dynamic analyses. The constants were calculated using the solution due to Novak and Mitwally (*5*), given by

$$k_r = \frac{G}{r_0}\left[S_1(a_0, \nu, \zeta) + iS_2(a_0, \nu, \zeta)\right], \qquad \text{(B-2)}$$

where

k_r = total stiffness,
G = soil shear modulus,
r_0 = distance to finite element boundary,
S_1 and S_2 = dimensionless parameters from closed form solutions,
ν = Poisson's ratio,
a_0 = dimensionless frequency equal to $r_0\omega/V_s$,
ω = circular frequency of loading, and
V_s = shear wave velocity of the soil.

The real and imaginary parts of Equation B-2 represent the stiffness (K) and damping (C), respectively, that is

$$K = \frac{GS_1}{r_0} \text{ and } C = \frac{GS_2}{\omega r_0}. \qquad \text{(B-3)}$$

To determine the stiffness and damping of the Kelvin elements, the constants given in Equation B-3 were multiplied by the area of the element face (normal to the direction of loading) because they assume constant unit area of contact. For static loading (i.e., zero frequency), the damping term vanishes, and the element reduces to a spring only.

For dynamic loading, ω was taken as the predominant frequency of the earthquake load and was determined from a discrete Fourier transform of the time history of the input motion. Figure B-6 shows the Fourier amplitude (c_n) versus frequency (ω_n) content for the strong motion record used in the study. It is evident that a narrow spectrum exists at a dominant frequency of approximately 2 Hz.

Time-dependent displacements were applied to the stratum base to simulate seismic loading. All other boundary conditions remained unchanged and are portrayed in Figure B-3.

Loading Conditions

Initial Loading

The state of stress in the pile-soil system in actual in situ conditions was replicated as an initial loading condition prior to any additional dynamic or static external load. That is, geostatic stresses were modeled by applying a global gravitational acceleration, g, to replicate vertically increasing stress with depth. A linearly increasing pressure with depth was applied to the periphery of the soil block to replicate horizontal stresses as shown in Figure B-3b. A coefficient of lateral earth pressure, K_o = 0.65, typical of many geological conditions, was used. Because of the difference in density and stiffness for the pile and soil, the soil tended to settle more than the pile in the vertical direction, resulting in premature slippage at the pile-soil interface. To eliminate this false representation of initial conditions, the difference between the relative displacement between the soil and the pile was accounted for by adding

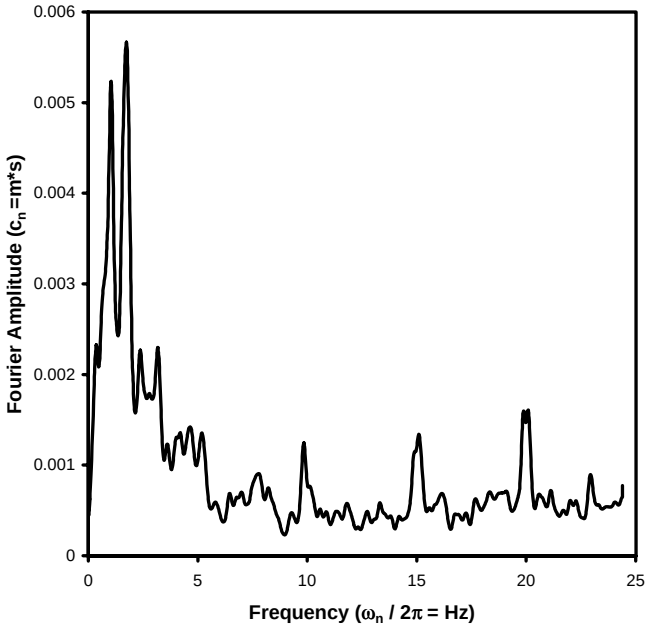

Figure B-6. Fourier amplitude spectrum for earthquake loading at the bedrock level.

a corresponding body load to the pile. The resulting mesh represented in situ conditions, especially for drilled shafts.

Static Loading

All static loads were applied as distributed loads along the perimeter of the pile head that was level with the ground surface. Only one-half of the total load was applied to the pile in the finite element analysis because of the symmetric geometry of a full circular pile.

Dynamic Loading

Strong motion records from the 1989 Loma Prieta earthquake in California ($M_L = 7.1$) were used in the finite element study. The accelerogram and displacement data used were from the Yerba Buena Island rock outcrop station in Santa Cruz Mountain (*6*). The measured displacements were applied to the top of the rigid bedrock layer at 0.02-s intervals. Considering that the maximum acceleration of the measured one-dimensional motion was 0.03 g, the accelerations were multiplied by a factor of seven to simulate a PHA (peak horizontal acceleration) of approximately 0.2 g for the bedrock input motion. It is important to note that the acceleration data were for bedrock motions and not for free-field motions that can either increase or decrease in terms of PHA because of the site effects. Motions of a 20-s duration were modeled to include all of the important features of the earthquake. The predominant frequency was approximately 2 Hz, which is typical of destructive earthquakes (*7*).

Verification of the Finite Element Model

The verification process followed incremental steps to ensure that pile, soil, and boundary conditions were separately accounted for in order to minimize error accumulation. The size of the mesh was mainly dependent on the loading conditions (static or dynamic) and geometry of the piles. The mesh was refined near the pile to account for the severe stress gradients and plasticity encountered in the soil, with a gradual transition to a coarser mesh away from the pile in the horizontal X and Y directions. The vertical Z-direction subdivisions were kept constant to allow for an even distribution of vertically propagating SH-waves. The maximum element size, E_{max}, was less than one-fifth to one-eighth of the shortest wavelength (λ) to ensure accuracy (*7*), that is,

$$E_{max} < (1.5 - 1.8) \times \lambda, \qquad \text{(B-4)}$$

where λ is V_s/f, V_s is the soil shear wave velocity, and f is the excitation frequency in Hz. The minimum V_s was 60 m/s, and the dynamic loading had a cut-off frequency equal to 20 Hz. Thus, a maximum element length of 0.5 m was adopted. The proposed element division was verified using results from a sensitivity study focussing on vertical pile shaft discretization by El Sharnouby and Novak (*8*), who found that using 12 to 20 elements gave accurate results with a minimum of computational effort. Thus, that range was adopted for this study.

The pile mesh was first verified by considering the pile as a fixed cantilever in air (no soil). Lateral deflections resulting from a static load for three different pile mesh sizes were compared with one-dimensional beam flexure theory, and the maximum difference was 8 percent. The results were very close; the small differences, however, could be explained by the fact that beam theory is not exact (it ignores shear deformations), and the finite model was not a perfect cylinder. Since the maximum number of elements (6,000) and nodes (11,000) available was limited, 180 elements were used to model the pile (accuracy within 8 percent of theoretical solutions). When soil and boundary elements were added, the total number of elements was close to the limit.

The soil was added to the model assuming a homogeneous soil stratum (see Figure B-5). The elastic responses of socketed and floating single piles in the homogeneous soil stratum were compared with the results from two different analyses: (1) the results from Poulos and Davis (*9*) using Mindlin's equations and enforcing pile-soil compatibility; and (2) the results presented by Trochanis et al. (*3*) using a three-dimensional finite element analysis, although their pile had a square cross section but the same flexural rigidity. Three different soil meshes were built with increasing refinement to determine an acceptable level of accuracy while maintaining a computationally efficient model. Mesh No. 1 consisted of 1,080 elements, Mesh No. 2 consisted of 2,640 elements, and Mesh No. 3 had 3,280 elements. Other meshes with a total number of elements equal to 6,000 were also tested, but were not used because of unreasonable computer processing time.

The results for the linear elastic response under lateral loading at the pile head are shown in Figure B-7a. The mesh that yielded the closest match (Mesh No. 3, depicted in Figures B-2 and B-3) was used in the analysis. The deflections obtained in this study were slightly greater than those from Poulos and Davis (*9*). However, those authors pointed out that their solution might underestimate the response of long piles in soft soils. Figures B-7b and B-7c show pile-head deflections considering separation at the pile-soil interface and soil plasticity, respectively. It can be seen that good agreement exists with the results from Trochanis et al. (*3*). The differences in the plastic soil case may be attributed to the use of a different model for soil plasticity (a modified Drucker–Prager model). Figures B-8a and B-8b show the elastic soil surface displacements away from the pile compared with results from elastic theory by Poulos and Davis (*9*) and other finite element analyses (*3*). It can be seen from Figures B-8a and B-8b that the results obtained using Mesh No. 3 agree well with both solutions, especially close to the pile. The pressure distribution in the soil agreed equally well.

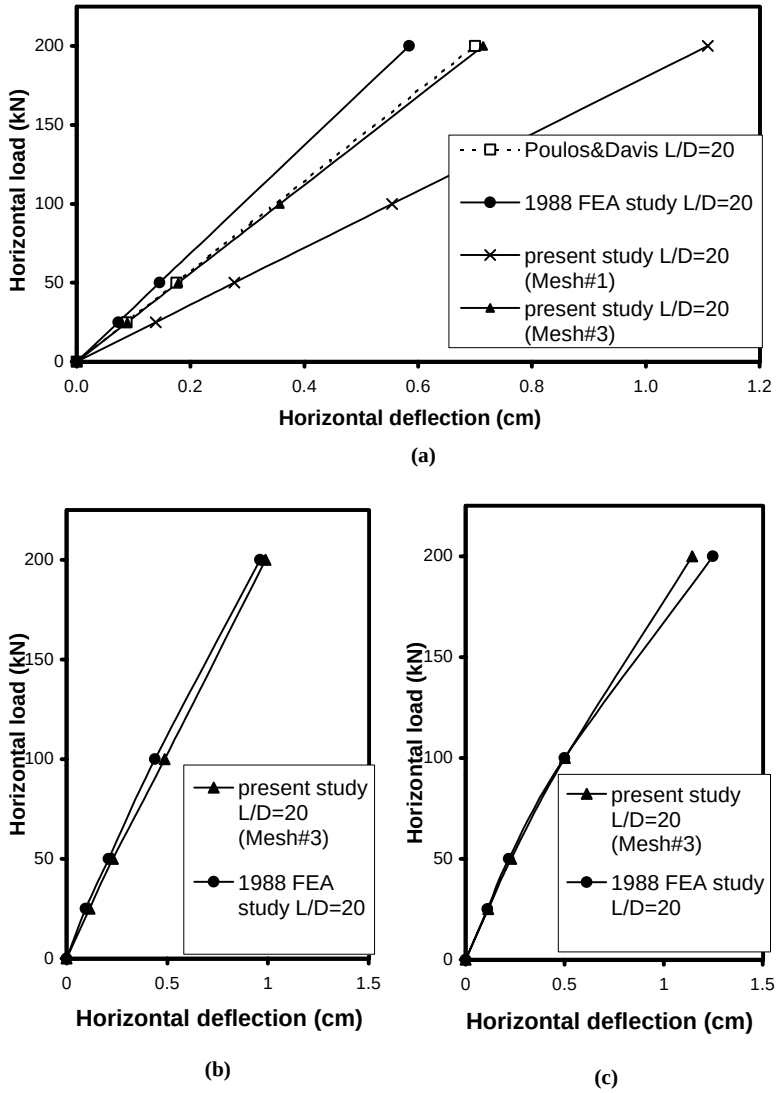

Figure B-7. Response of single socketed pile for (a) elastic, (b) elastic-gapping, (c) plastic-gapping.

The final step in the verification process was accomplished by solving the ground response to an earthquake signal using the finite element model and comparing the elastic free-field response with that obtained using the program SHAKE91 (*10*). Considering that SHAKE91 is a one-dimensional analysis, constraints were applied to the finite model to allow only displacements in the direction of shaking (1 degree of freedom per node) to replicate one-dimensional results. The results from the finite element analysis and SHAKE91 are plotted in Figure B-9 for elastic response using the same parameters. A constant shear modulus and material damping ratio were used in both the SHAKE91 and the finite element analysis models. It can be seen from Figure B-9 that the agreement is good along the entire time period considered. The maximum free-field accelerations for the finite element analyses and SHAKE91 were amplified to approximately 0.6 g from 0.2 g (bedrock input motion) and are compared with bedrock accelerations in Figure B-10. The same finite element analysis model was modified to allow for three-dimensional response, and the free-field response is plotted against the one-dimensional results in Figure B-11. The maximum free-field acceleration obtained from three-dimensional analysis was only 0.35 g (see Figure B-11). The accelerations calculated from the three-dimensional analysis are closer to those observed during actual seismic events. Hence, it was concluded that the three-dimensional analysis resulted in realistic acceleration magnitudes; therefore, all further models discussed herein assumed full three-dimensional capability.

Numerical Study for Kinematic Interaction

The kinematic effects of piles in a homogeneous soil medium were evaluated by comparing acceleration time histories and Fourier spectra of the pile head and the free-field.

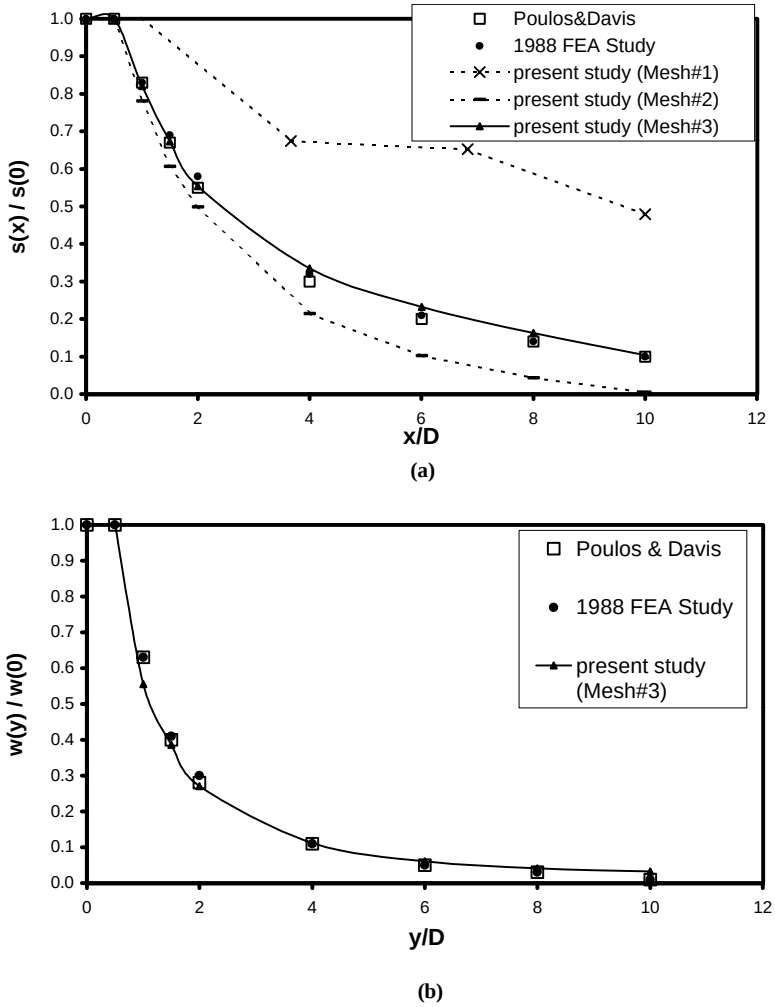

Figure B-8. Elastic soil surface displacements. (a) Comparison of soil displacements' long line of loading, s(x)*, relative to pile-head displacement,* s(0)*. (b) Comparison of soil displacements normal to direction of loading,* w(y)*, relative to pile-head displacement,* w(0)*.*

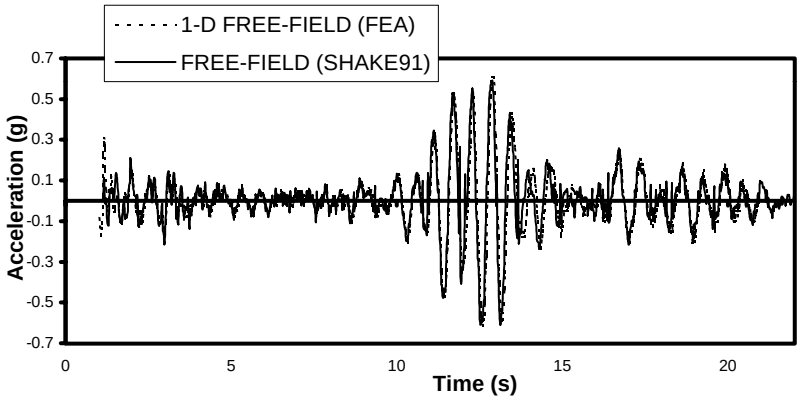

Figure B-9. One-dimensional verification of finite element analysis (FEA using ANSYS) with SHAKE91.

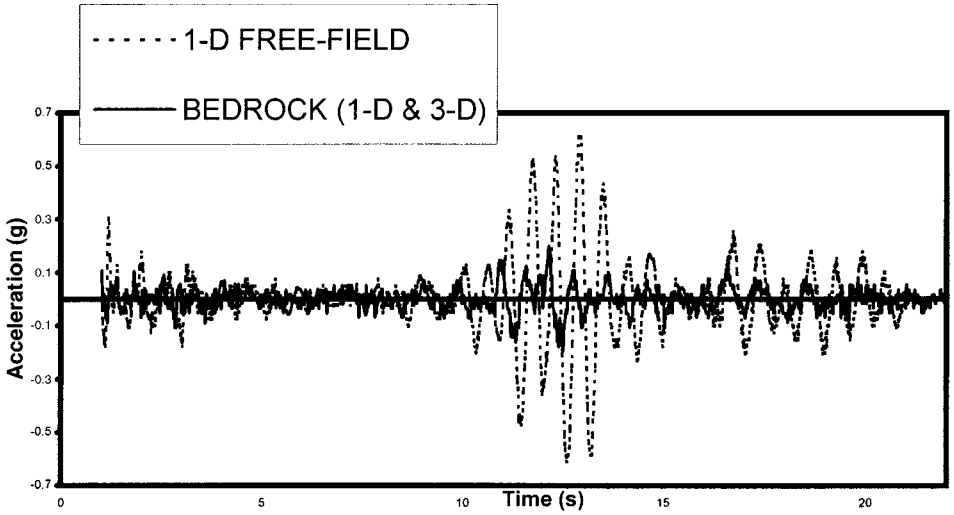

Figure B-10. Response of underlying bedrock and free-field for homogeneous soil (using one-dimensional finite element analysis).

The same dynamic loading was applied in all cases (i.e., Loma Prieta data) to the underlying bedrock for a homogeneous soil profile. Results from seven different pile-soil configurations were obtained and are referred to in Figures B-12 through B-18. The following notation is used throughout the graphs and literature to identify each test case (see Figure B-5 for soil and pile parameters):

- **EFH** (**e**lastic, **f**ree-field, **h**omogeneous)—refers to the free-field response using linear isotropic viscoelastic constitutive relations.
- **PFH** (**p**lastic, **f**ree-field, **h**omogeneous)—refers to the free-field response using a perfect elastic-plastic soil model, Drucker–Prager criteria.
- **ESNFH** (**e**lastic, **s**ingle pile, **n**o separation, **f**loating, **h**omogeneous)—refers to the floating single pile–head response using a linear isotropic viscoelastic soil with no separation at the pile-soil interface, $L/D = 15$, $E_p/E_s = 1{,}000$.
- **ESNSH** (**e**lastic, **s**ingle pile, **n**o separation, **s**ocketed, **h**omogeneous)—refers to the socketed single pile–head response using a linear isotropic viscoelastic soil with no separation at the pile-soil interface, $L/D = 20$, $E_p/E_s = 1{,}000$.
- **ESSFH** (**e**lastic, **s**ingle pile, **s**eparation, **f**loating, **h**omogeneous)—same as the ESNFH case, but allows for separation at the pile-soil interface.
- **PSSFH** (**p**lastic, **s**ingle pile, **s**eparation, **f**loating, **h**omogeneous)—refers to the floating single pile–head response using a perfect plastic-elastic soil model with separation allowed at the pile-soil interface, $L/D = 15$, $E_p/E_s = 1{,}000$, $c' = 34$ kPa, $\psi = 16.5°$.

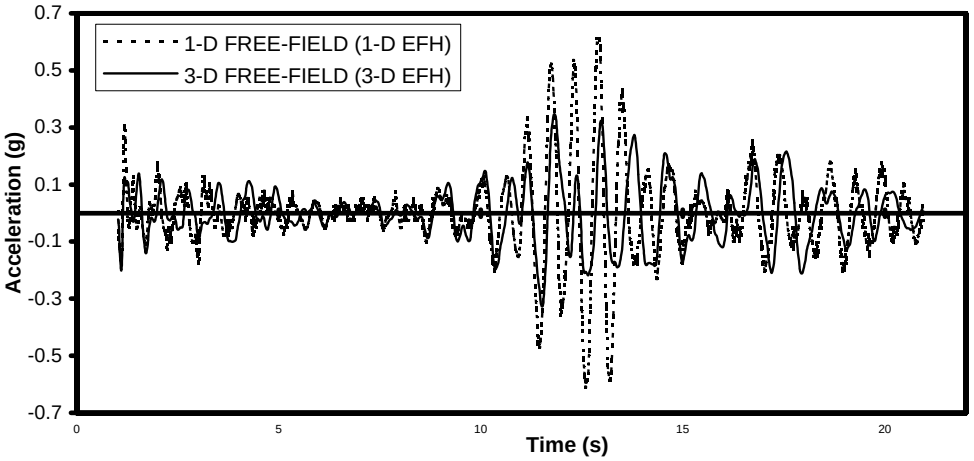

Figure B-11. Elastic free-field response for homogeneous soil (EFH) for one- and three-dimensional analysis.

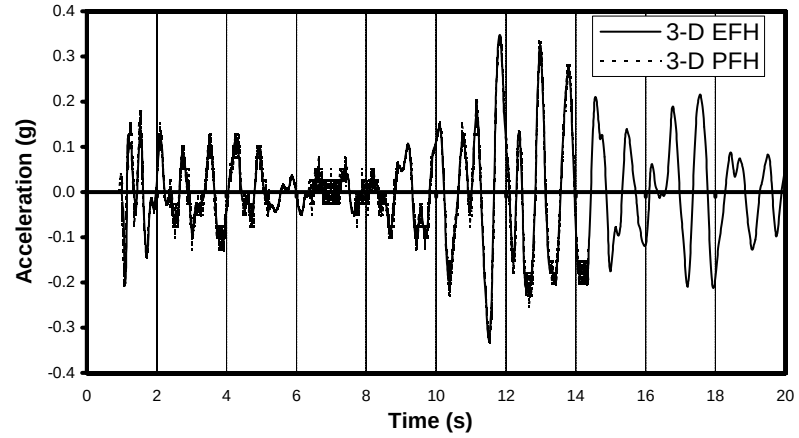

(a)

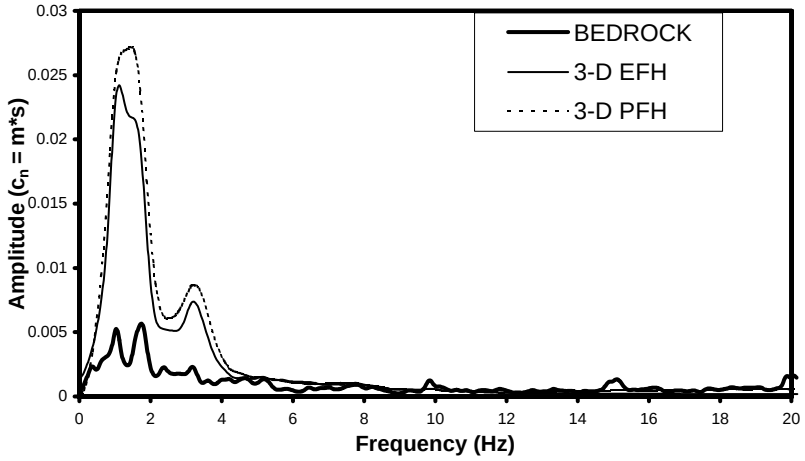

(b)

Figure B-12. Comparisons of the free-field response for the elastic and plastic soil cases and the Fourier spectra for elastic and plastic soil profiles against the input bedrock spectrum. (a) Comparison between calculated accelerations for elastic free-field (EFH) and plastic free-field (PFH) using the Drucker–Prager criteria for a homogeneous soil profile. (b) Fourier spectrum for the response at the bedrock level, elastic soil free-field and plastic soil free-field.

- **PSSSH** (**p**lastic, **s**ingle pile, **s**eparation, **s**ocketed, **h**omogeneous)—refers to the socketed single pile–head response using a perfect plastic-elastic soil model with separation allowed at the pile-soil interface, $L/D = 20$, $E_p/E_s = 1{,}000$, $c' = 34$ kPa, $\psi = 16.5°$.

Results

Figure B-12a compares the free-field response for the elastic and plastic soil cases. The difference between the two cases is not evident over the 20-s duration, but a more detailed evaluation is presented in Figure B-15 for the 2- through 10-s interval. The acceleration response is slightly amplified using a plastic soil model. This can be attributed to the limiting ultimate effective stress and limiting shear strength. Figure B-12b compares the Fourier spectra for elastic and plastic soil profiles against the input bedrock spectrum using a cut-off frequency of 20 Hz. It is evident from the figure that there is an amplification of the Fourier amplitudes for the free-field response compared with the bedrock. There is a notable increase in amplitude for the plastic soil model over the elastic soil model, suggesting that the reduction in soil stiffness reduces the natural frequency of the homogeneous layer. The increase in acceleration and amplitude may be attributed to the fact that the first natural frequency of the elastic homogenous layer is

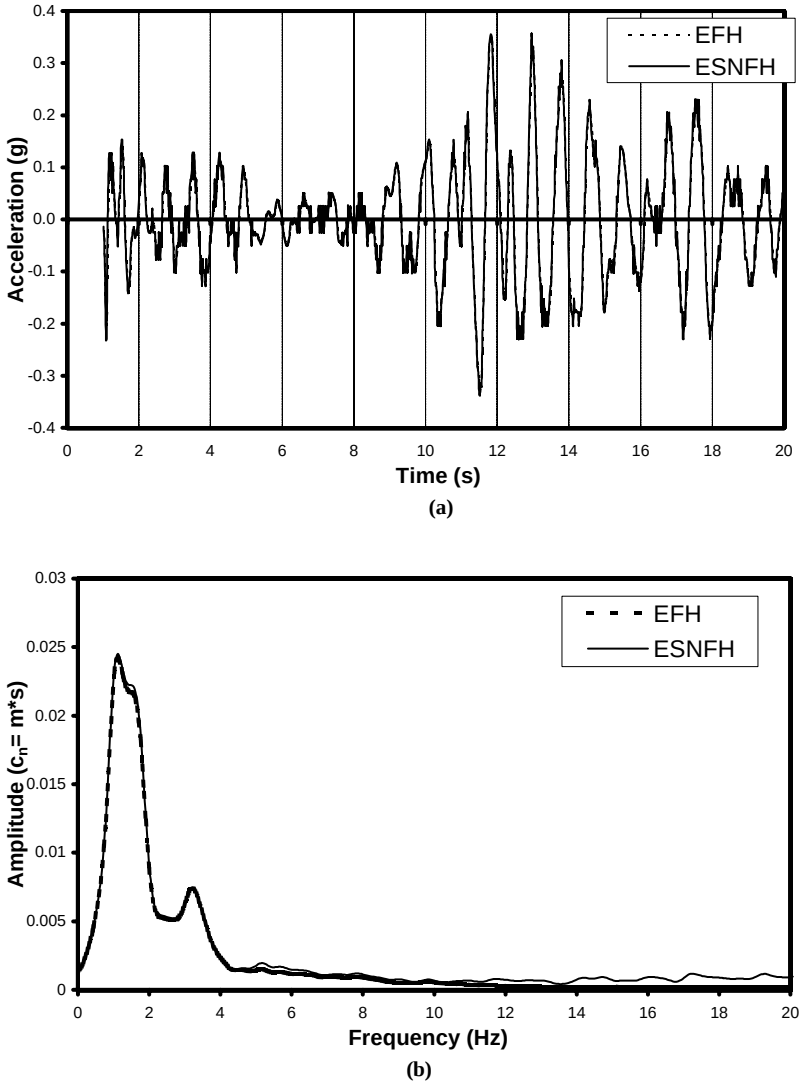

Figure B-13. The corresponding acceleration and Fourier spectrum for ESNFH compared with EFH. (a) Comparison between calculated accelerations for elastic free-field (EFH) and floating pile head (ESNFH) for a homogeneous elastic soil profile. (b) Fourier spectrum for the response of the elastic soil free-field and floating pile head.

slightly greater than 2 Hz, whereas the natural frequency of the plastic soil layer is slightly decreased and became closer to the predominant frequency at the free-field (approximately 1.5 Hz). For higher frequencies (see Figure B-11b), the small amplitude peaks seen at the bedrock level diminish as the seismic waves propagate throughout the soil until they reach the free-field. Both the elastic and plastic free-field amplitudes diminish at frequencies higher than 10 Hz, above which little response is induced in most structures.

Similar results for the floating and socketed pile-head response are plotted in Figures B-13 and B-14. Figures B-13a and B-13b represent the corresponding acceleration and Fourier spectrum for ESNFH compared with EFH. The diagrams are almost identical, except the Fourier amplitudes are slightly greater for the floating pile (especially for a frequency above 5 Hz). Figure B-14 shows the response of the ESNSH socketed pile case. Again, the overall acceleration of the pile head is similar to that of the elastic free-field. The Fourier amplitudes of the socketed pile (no separation) show both a decrease and an increase in magnitude over the elastic free-field, depending on the frequency range. At the predominant frequency amplitude (2 Hz), ESNSH seems to slightly decrease compared with EFH, and at frequencies above and below the predominant frequency, the amplitudes are increased. The increased stiffness of the system caused by the socketed pile may be responsible for the increased amplitude at higher frequency ranges compared with that of the free-field.

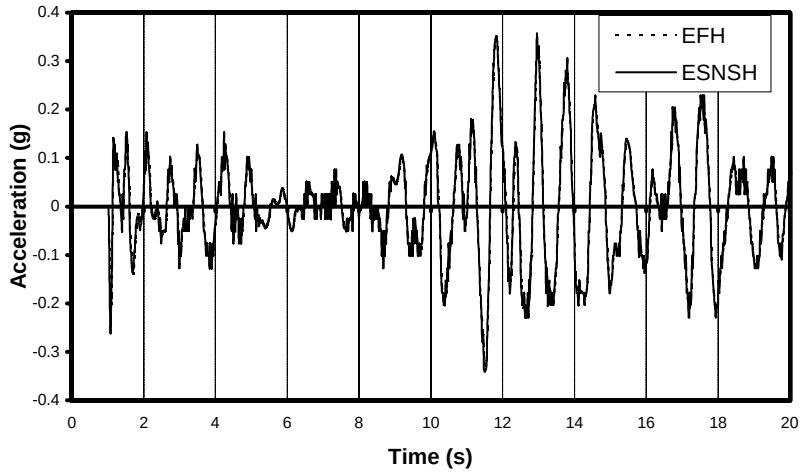

(a)

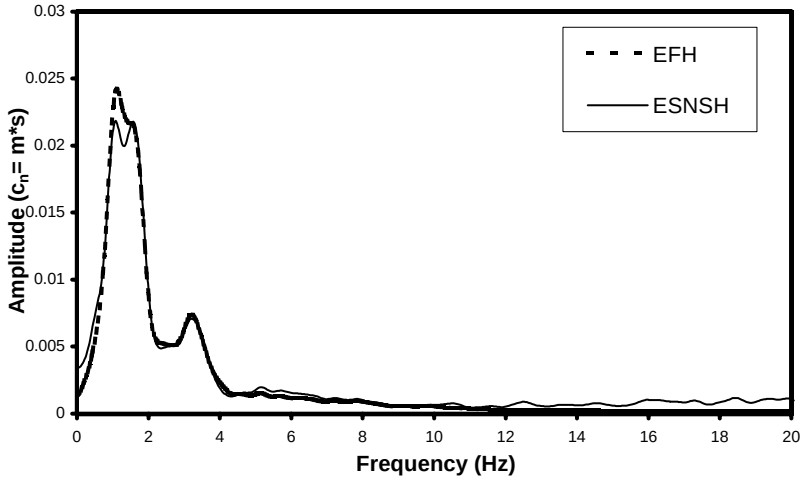

(b)

Figure B-14. Response of the ESNSH socketed pile case. (a) Comparison between calculated accelerations for elastic free-field (EFH) and socketed pile (ESNSH) for a homogeneous soil profile. (b) Fourier spectrum for the response at the plastic soil free-field and socketed pile head.

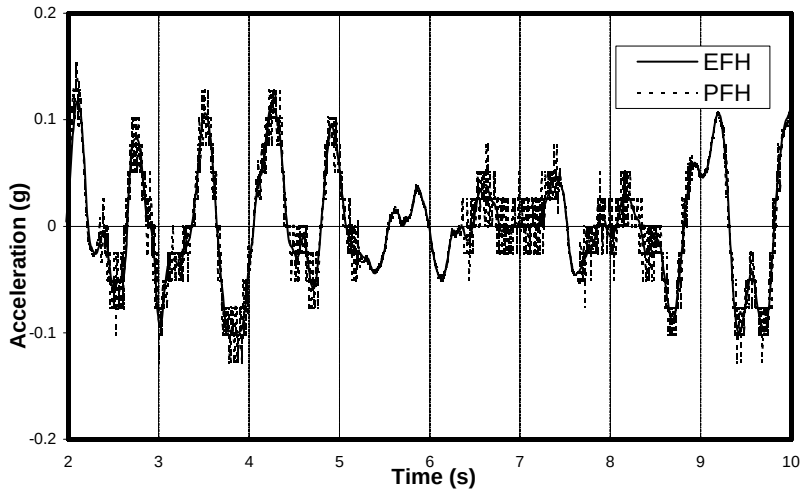

Figure B-15. EFH and PFH response (elastic and plastic free-field, E_s = 20 000 kPa).

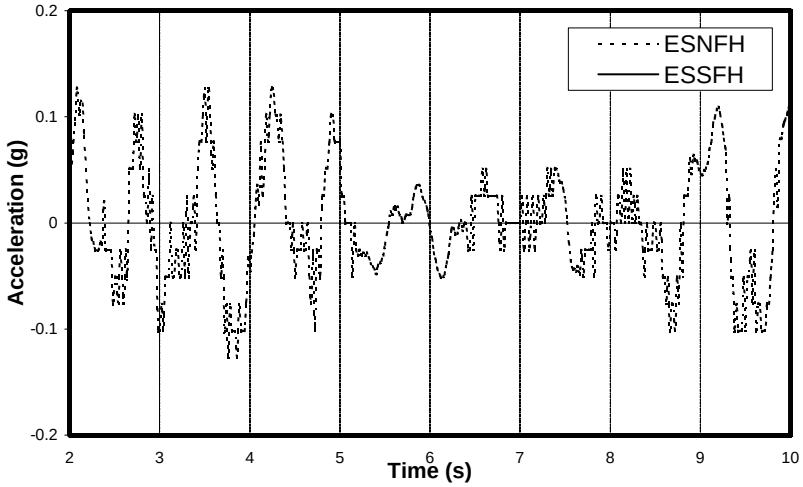

Figure B-16. Pile-head response for floating pile (elastic, elastic with gapping).

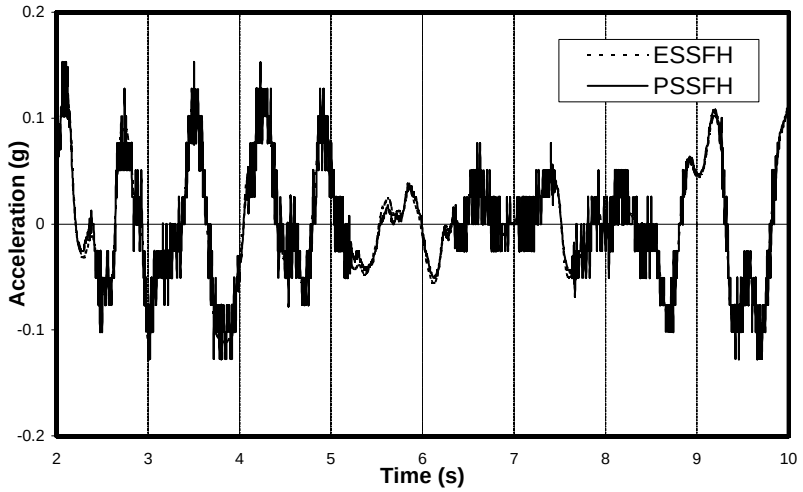

Figure B-17. Pile-head response for floating pile (elastic gapping, plastic gapping).

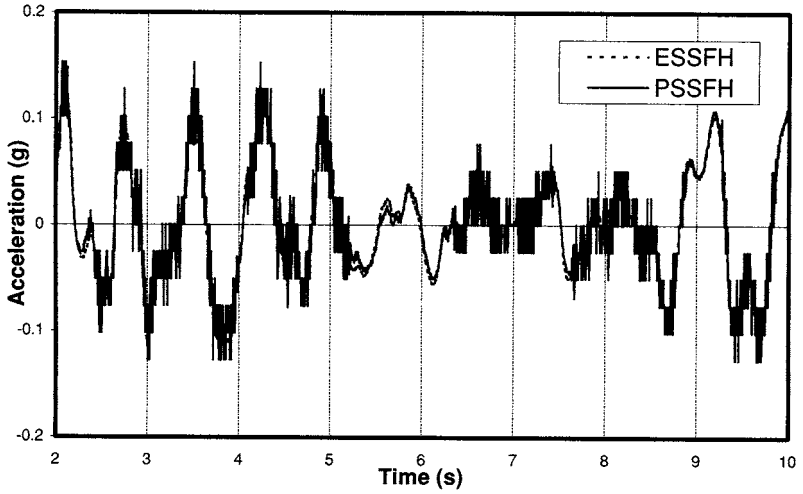

Figure B-18. Pile-head response for floating and socketed pile (plastic gapping).

Figure B-16 introduces the effects of separation between the pile and soil for the floating pile case. Only the 2- through 10-s interval is shown to provide a more detailed analysis. The overall response is very similar for both cases shown in Figure B-16. The floating pile with gapping seems to eliminate small fluctuations of acceleration seen when no gapping was allowed.

Figure B-17 introduces the effects of the soil plasticity in addition to separation for the floating pile. PSSFH is compared with the elastic model (ESSFH), and the results are very similar. The random scatter shown by introducing plasticity may be attributed to the solution procedure used in the finite element program. For convergence reasons, smaller time steps had to be used for the plastic soil model, which led to numerical instabilities. Figure B-18 compares the floating and socketed pile-head response including both separation and soil nonlinearity. The floating pile showed slightly higher peaks over the socketed pile, but the response remained almost identical.

Kinematic Interaction in Pile Groups

Modeling the kinematic response of pile groups, accounting rigorously for all the factors that influence the response, is a formidable task; therefore, most of the investigations on the seismic soil-pile interactions use linear analyses or simple idealized systems.

Analyses of the kinematic response of a single pile and of pile groups have been reported by Takemiya and Yamada (*11*), Flores-Berrones and Whitman (*12*), Gazetas (*13*) and Tazoh et al. (*14*). These studies, however, had very limited parametric results. Ahmad and Mamoon (*15*) and Fan et al. (*16*) attempted to fill this gap by providing comprehensive parametric studies for the kinematic response of piles. The results of these two studies are summarized herein.

Ahmad and Mamoon (*15*) examined the response of single piles under vertically and obliquely incident SH, SV, and P harmonic waves using a hybrid boundary element formulation. The piles were modeled using compressible beam-column elements, and the soil was modeled as a hysteretic viscoelastic half-space. They found that the pile-soil stiffness ratio, angle of incidence, and excitation frequency have significant influence on the seismic responses of piles. The results from the limited cases considered in their study suggested that in the low-frequency range, piles essentially follow the ground motion. This conclusion is similar to what was observed from the analyses presented earlier in this appendix. Ahmad and Mamoon also found that at higher frequencies, piles seem to remain relatively still while the free-field soil mass moves considerably. This filtering effect was found to be severe for a vertically incident wave, gradually diminishing for a more obliquely incident one. Furthermore, they found that flexible piles undergo significant bending under seismic excitation whereas rigid piles tend to show almost low, uniform rigid body motion. Obliquely incident waves produce higher displacement than did a vertically incident one throughout the pile depth. In the low-frequency range, vertically incident waves produce higher rotations of the pile head, but in the higher-frequency range, the opposite trend was observed.

Fan et al. (*16*) performed an extensive parametric study using the boundary element solution proposed by Kaynia and Kausel (*17*) to develop dimensionless graphs for pile-head deflections versus the free-field response for various soil profiles subjected to vertically propagating harmonic waves. Fan et al. (*16*) also used the approach developed by Makris and Gazetas (*18*), in which free-field accelerations are applied to a one-dimensional Beam-on-Dynamic-Winkler-Foundation model with frequency-dependent springs and dashpots to analyze the response of floating single piles and pile groups. Both approaches are essentially linear (or equivalent linear) analyses.

Makris and Gazetas (*18*) studied the kinematic response of single piles, one-row pile groups, and square groups of piles. They considered soil profiles with constant soil modulus, linearly increasing soil modulus with depth, and two distinct constant values above and below a depth $z = L/2$. Each pile-foundation-soil system was excited by vertically propagating harmonic shear free-field waves.

The results of the analyses were portrayed in the form of kinematic displacement factors (plotted versus dimensionless frequency, a_0) defined as the response of the pile cap normalized by the free-field motion. The investigated parameters were the ratio of the effective pile modulus to the soil modulus, the piles spacing-to-diameter ratio, and the pile's slenderness ratio. Inspection of the results revealed the following trends:

1. The general shape of the kinematic displacement factor, I_u, consists of three fairly distinct regions in the frequency range of greatest interest ($a_0 < 0.5$):
   - A low-frequency region ($0 < a_0 < 0.1$–0.3) in which $I_u \approx 1$, meaning the piles follow closely the deformations of the ground.
   - An intermediate-frequency region (0.1–$0.2 < a_0 < 0.3$–0.4) characterized by I_u declining rapidly with frequency, which showed increasing incompatibility between the movement of a pile and the surrounding soil.
   - A relatively high-frequency region ($a_0 > 0.3$–0.4) in which I_u fluctuates around an essentially constant value of about 0.2–0.4.
2. For the low- and intermediate-frequency regions, pile-soil-pile interaction effects on kinematic loading are not significant, but they are significant for pile-head loading (inertial interaction).

Summary and Conclusions—Kinematic Action

A three-dimensional finite element analysis was performed to investigate site effects and pile kinematic interaction effects

from seismic loading for a single pile. The analysis considered floating and socketed piles, including nonlinear soil properties, slippage and gapping at the pile-soil interface, and dissipation of energy through damping. Based on the results from the kinematic interaction study, it was concluded that the pile-head response (floating and socketed) closely resembled the free-field response for the low predominant frequency seismic loading. Fan et al. (*16*) reached a similar conclusion from their parametric study using a boundary element solution.

The following specific conclusions can be drawn:

- The effect of allowing a three-dimensional behavior as opposed to a one-dimensional behavior, with seismic loading applied in one dimension, was to decrease the acceleration amplitudes by a factor of 1.6 for the soil profiles considered.
- The effect of soil plasticity was to increase the Fourier amplitudes at the predominant frequency, but to slightly decrease the maximum acceleration amplitudes.
- The elastic kinematic interaction of single piles (both floating and socketed) has slightly amplified the bedrock motion when compared with the free-field response and has slightly decreased the Fourier amplitudes of all frequencies considered (0 through 20 Hz).
- Overall, the kinematic interaction response, including soil plasticity, slippage and gapping at the pile-soil interface, and damping, is equivalent to the free-field response. The conclusions, however, are limited to the pile and soil parameters and to the earthquake loading used in the analysis.
- For the frequency range of interest, pile-soil-pile interaction effects on kinematic loading are not significant, but are significant for pile-head loading (inertial interaction).

INERTIAL LOADING AND DYNAMIC *p-y* CURVES

Introduction

Most building and bridge codes use factored static loads to account for the dynamic effects of pile foundations. Although very low-frequency vibrations may be accurately modeled using factored loads, the introduction of nonlinearity, damping, and pile-soil interaction during transient loading may significantly alter the response. The typical frequency range of interest for earthquake loading is 0 to 10 Hz; therefore, the emphasis in the current study is on that range.

Novak et al. (*19*) developed a frequency-dependent pile-soil interaction model; however, the model assumes strictly linear or equivalent linear soil properties. Gazetas and Dobry (*20*) introduced a simplified linear method to predict fixed-head pile response accounting for both material and radiation damping and using available static stiffness (derived from finite element or any other accepted method). This method is not suitable for the seismic response analysis because of the linearity assumptions. In general, there is much controversy over advanced linear solutions (frequency domain), as they do not account for permanent deformation or gapping at the pile-soil interface.

Nogami et al. (*21*) developed a time domain analysis method for single piles and pile groups by integrating plane strain solutions with a nonlinear zone around each pile using *p-y* curves. El Naggar and Novak (*22, 23*) also developed a computationally efficient model for evaluating the lateral response of piles and pile groups based on the Winkler hypothesis, accounting for nonlinearity using a hyperbolic stress-strain relationship and slippage and gapping at the pile-soil interface. The model also accounts for the propagation of waves away from the pile and energy dissipation through both material and geometric damping.

The *p-y* curve (unit load transfer curve) approach is a widely accepted method for predicting pile response under static loads because of its simplicity and practical accuracy. In the present study, the model proposed by El Naggar and Novak (*23*) was modified to use existing or developed cyclic or static *p-y* curves to represent the nonlinear behavior of the soil adjacent to the pile. The model uses unit load transfer curves in the time domain to model nonlinearity and incorporates both material and radiation damping to generate dynamic *p-y* curves.

Model Description

Pile Model

The pile is assumed to be vertical and flexible with a circular cross section. Noncylindrical piles are represented by cylindrical piles with equivalent radius to accommodate any pier-pile configurations. The pile and the surrounding soil are subdivided into *n* segments, with pile nodes corresponding to soil nodes at the same elevation. The standard bending stiffness matrix of beam elements models the structural stiffness matrix for each pile element. The pile global stiffness matrix is then assembled from the element stiffness matrixes and is condensed to give horizontal translations at each layer and the rotational degree of freedom at the pile head.

Soil Model: Hyperbolic Stress-Strain Relationship

The soil is divided into *n* layers with different soil properties assigned to each layer according to the soil profile considered. Within each layer, the soil medium is divided into two annular regions as shown in Figure B-19. The first region is an inner zone adjacent to the pile that accounts for the soil nonlinearity. The second region is the outer zone that allows for wave propagation away from the pile and provides for the radiation damping in the soil medium. The soil reactions and the pile-soil interface conditions are modeled separately on both sides of the pile to account for slippage, gapping, and state of stress as the load direction changes.

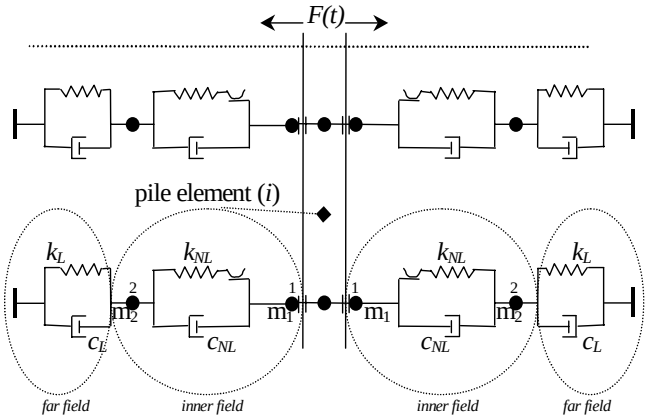

Figure B-19. Element representation of proposed model.

Inner Field Element. The inner field is modeled with a nonlinear spring to represent the stiffness and a dashpot to simulate material (hysteretic) damping. The stiffness is calculated assuming plane strain conditions. The inner field is a homogeneous isotropic viscoelastic, massless medium. The pile is rigid and circular. There is no separation at the soil-pile interface. Displacements are small. Novak and Sheta (*24*) obtained the stiffness (k_{NL}) under these conditions as

$$k_{NL} = \frac{8\pi G_m(1-\nu)(3-4\nu)\left[(r_0/r_1)^2+1\right]}{(r_0/r_1)^2+(3-4\nu)^2\left[(r_0/r_1)^2+1\right]\ln(r_1/r_0)-1}, \qquad \text{(B-5)}$$

where r_0 is the pile radius, r_1 is the outer radius of the inner zone, and ν is the Poisson's ratio of the soil stratum. The ratio r_1/r_0 depends on the extent of nonlinearity, which depends on the level of loading and on the pile's size. A parametric study showed that r_1/r_0 of 1.1 to 2 yielded good agreement between the stiffness of the composite medium (inner zone and outer zone) and the stiffness of a homogeneous medium (no inner zone) under small strain (linear) conditions. G_m is the modified shear modulus of the soil and is approximated, according to the strain level, by a hyperbolic law as

$$G_m = G_{\max}\left(\frac{1-\eta}{1+\eta}\right). \qquad \text{(B-6)}$$

$G_{\max}$ is the maximum shear modulus (small strain modulus) of the soil according to laboratory or field tests; η is a parameter = P/P_u (see Equation B-8). In the absence of actual measurements, maximum shear modulus for any soil layer can be calculated in this model by using the equation of Hardin and Black (*25*):

$$G_{\max} = \frac{3230(2.97-e)^2}{1+e}\,\sigma_0^{0.5} \qquad \text{kN/m}^2, \qquad \text{(B-7)}$$

where e is the void ratio, and σ_0 (kN/m^2) is the mean principal effective stress in the soil layer.

The parameter $\eta = P/P_u$ is the ratio of the horizontal soil reaction in the soil spring, P, to the ultimate resistance of the soil element, P_u. The ultimate resistance of the soil element is calculated using standard relations given by API (*4*). For clay, the ultimate resistance is given as a force per unit length of pile by

$$P_u = 3c_u d + \gamma x d + Jc_u x \qquad \text{or} \qquad \text{(B-8)}$$

$$P_u = 9c_u d, \qquad \text{(B-9)}$$

where

P_u = the minimum of the resistances calculated by Equations B-8 and B-9,
c_u = the undrained shear strength,
d = the diameter of the pile,
γ = the effective unit weight of the soil, and
J = an empirical coefficient dependent on the shear strength.

A value of $J = 0.5$ was used for soft clays (*26*) and $J = 1.5$ for stiff clays (*27*).

The corresponding criteria for the ultimate lateral resistance of sands at shallow depths P_{u1} or at large depths P_{u2} are as follows (*4*):

$$P_{u1} = A\left\{\gamma X\left[\frac{K_0 X\tan\phi\sin\beta}{\tan(\beta-\phi)\cos\alpha} + \frac{\tan\beta}{\tan(\beta-\phi)}(d + X\tan\beta\tan\alpha)\right]\right\} + A\gamma X\left\{K_0 X\tan\beta(\tan\phi\sin\beta-\tan\alpha) - K_a d\right\} \qquad \text{(B-10)}$$

$$P_{u2} = A\gamma X d\left[K_a(\tan^8\beta - 1) + K_0\tan\phi\tan^4\beta\right], \qquad \text{(B-11)}$$

where

A = an empirical adjustment factor dependent on the depth from the soil surface,
K_0 = the earth pressure coefficient at rest,
ϕ = the effective friction angle of the sand,
$\beta = \phi/2 + 45°$,
$\alpha = \phi/2$, and
K_a = the Rankine minimum active earth pressure coefficient defined as $K_a = \tan^2(45° - \phi/2)$.

In the derivation of Equation B-5, the inner field was assumed to be massless (*24*); therefore, the mass of the inner field is lumped equally at two nodes on each side of the pile: Node 1 adjacent to the pile and Node 2 adjacent to the outer field, as shown in Figure B-19.

Far-Field Element. The outer (i.e., far) field is modeled with a linear spring in parallel with a dashpot to represent the linear stiffness and damping (mainly radiation damping). The outer zone allows for the propagation of waves to infin-

ity. The complex stiffness, *K*, of a unit length of a cylinder embedded in a linear viscoelastic soil medium is given by Novak et al. (*19*):

$$K = G_{\max}[S_{u1}(a_0, \nu, D) + iS_{u2}(a_0, \nu, D)], \quad \text{(B-12)}$$

where $a_0 = \omega r_1/V_s$ is the dimensionless frequency: ω is the frequency of loading, V_s is the shear wave velocity of the soil layer, and D is the material damping constant of the soil layer. Figure B-20 shows the general variations of S_{u1} and S_{u2} with Poisson's ratio and material damping. Rewriting Equation B-12, the complex stiffness, *K*, can be represented by a spring coefficient, k_L, and a damping coefficient, c_L, as

$$K = k_L + ia_0c_L. \quad \text{(B-13)}$$

It can be noted from Figure B-20 that for the dimensionless frequency range between 0.05 and 1.5, S_{u1} maintains a constant value, and S_{u2} increases linearly with a_0. The predominant frequency of destructive earthquake loading falls within this range; therefore, for the purpose of a time domain analysis, the spring and dashpot constants, S_{u1} and S_{u2}, respectively, can be considered frequency independent and to depend only on Poisson's ratio. They are given as

$$k_L = G_{\max}S_{u1}(\nu) \quad \text{and} \quad \text{(B-14)}$$

$$c_L = \frac{2G_{\max}r_1}{V_s} S_{u2}(a_0 = 0.5, \nu). \quad \text{(B-15)}$$

Soil-Pile Interface

The soil-pile interface is modeled separately on each side of the pile, thus allowing gapping and slippage to occur independently on each side. The soil and pile nodes in each layer are connected using a no-tension spring. That is, the pile and soil will remain connected and will have equal displacement for compressive stresses. The spring is disconnected if tensile stress is detected in the soil spring to allow a gap to develop. This separation or gapping results in permanent displacement of the soil node that is dependent on the magnitude of the load. The development of such gaps is often observed in experiments, during offshore loading, and after earthquake excitation in clays. These gaps eventually fill in again over time until the next episode of lateral dynamic loading. The pile-soil interface for sands does not allow for gap formation, but instead the sand caves in, resulting in the virtual back-filling of sand particles around the pile during repeated dynamic loading. When the pile is unloaded, the sand on the tension side of the pile follows the pile with zero stiffness instead of remaining permanently displaced as in the clay model. In the unloading phase, the stiffness of the inner field spring is assumed to be linear in both the clay and sand models.

Group Effect

Because each pile in a group is affected not only by its own load, but also by the load and deflection of other piles in the group, the response of a pile group is greatly affected by the interaction between piles. For piles subjected to earthquake loading, this effect is important when considering the inertial loading, as has been pointed out by Fan et al. (*16*). For this reason, the group effect was also investigated in this study. As large displacements, pile-soil separation, and soil nonlinearity are expected to occur during earthquake events, the model developed by El Naggar and Novak (*23*), which is capable of these factors, was used in this study.

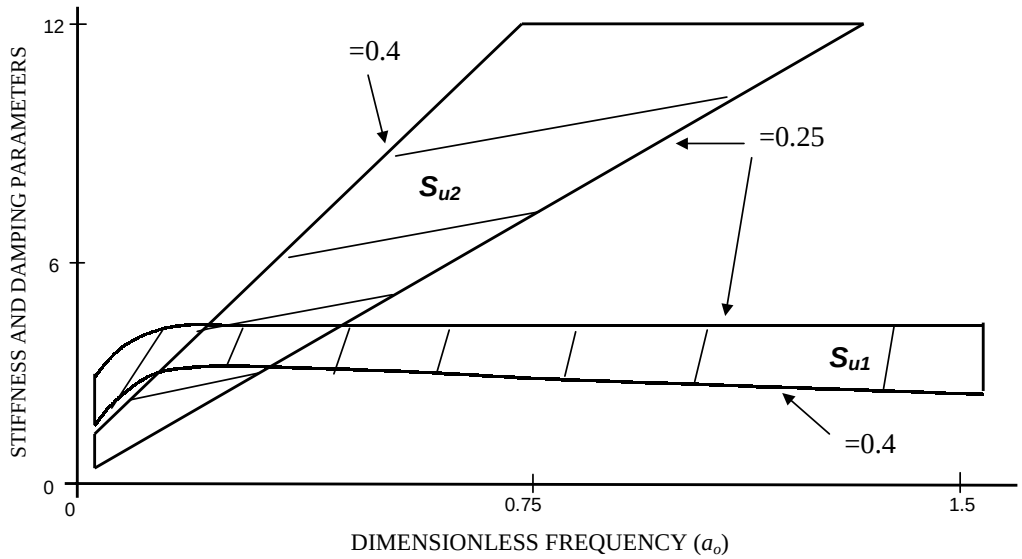

Figure B-20. Envelope of variations of horizontal stiffness and damping stiffness parameters for ν = 0.25–0.40 (after Novak et al. [19]).

Soil Model: p-y *Curve Approach*

The soil reaction to transient loading consists of stiffness and damping. The stiffness is established using the *p-y* curve approach, and the damping is established from analytical solutions that account for wave propagation. A similar approach was suggested by Nogami et al. (*21*) using *p-y* curves.

Based on physical tests, *p-y* curves can be used to relate pile deflections to the corresponding soil reaction at any depth (element) below the ground surface. The *p-y* curve represents the total soil reaction to the pile motion (i.e., the inner and outer zones' reactions combined). The total stiffness, k_{py}, derived from the *p-y* curve is equivalent to the true stiffness (real part of the complex stiffness) of the soil medium. Thus, referring to the hyperbolic law model, the combined inner zone stiffness (k_{NL}) and outer zone stiffness (k_L) can be replaced by a unified equivalent stiffness zone (k_{py}) as shown in Figure B-21a. Hence, to ensure that the true stiffness is the same for the two soil models, the flexibility of the two models is equated, that is,

$$\frac{1}{k_{py}} = \frac{1}{k_L} + \frac{1}{k_{NL}}. \tag{B-16}$$

The stiffness of the nonlinear strength is then calculated as

$$k_{NL} = \frac{(k_{py})(k_L)}{(k_L - k_{py})}. \tag{B-17}$$

The constant of the linear elastic spring, k_L, is established from the plane strain solution (i.e., Equation B-14). The static soil stiffness, k_{py} represents the relationship between the static soil reaction, *p*, and the pile deflection, *y*, for a given *p-y* curve at a specific load level. The *p-y* curves are established using empirical equations (*26, 28, 29*) or curve fit to measured data using an accepted method such as the modified Ramberg–Osgood model (*30*). In the present study, internally generated static *p-y* curves are established based on commonly used empirical correlations for a range of soil types.

Damping

The damping (imaginary part of the complex stiffness) is incorporated into both the *p-y* approach and the hyperbolic model to allow for energy dissipation throughout the soil. The nonlinearity in the vicinity of the pile, however, drastically reduces the geometric damping in the inner field; therefore, both material and geometric (radiation) damping are modeled in the outer field. A dashpot is connected in parallel to the far-field spring, and its constant is derived from Equation B-15. If the material damping in the inner zone is to be considered, a parallel dashpot with a constant c_{NL} to be suitably chosen may be added as shown in Figure B-21b. The addition of the damping resistance to static resistance represented by the static unit load transfer (the *p-y* curve) tends to increase the total resistance as shown in Figure B-22.

Static p-y *Curve Generation for Clay*

The general procedure for computing *p-y* curves in clays both above and below the groundwater table and corresponding parameters are recommended by Matlock (*26*) and Bhushan et al. (*27*), respectively. The *p-y* relationship was based on the following equation:

$$\frac{p}{P_u} = 0.5\left(\frac{y}{y_{50}}\right)^n, \tag{B-18}$$

where

p = soil resistance,
y = deflection corresponding to p,
P_u = ultimate soil resistance from Equations B-8 and B-9,
n = a constant relating soil resistance to pier-pile deflection, and
y_{50} = corrected deflection at one-half the ultimate soil reaction determined from laboratory tests.

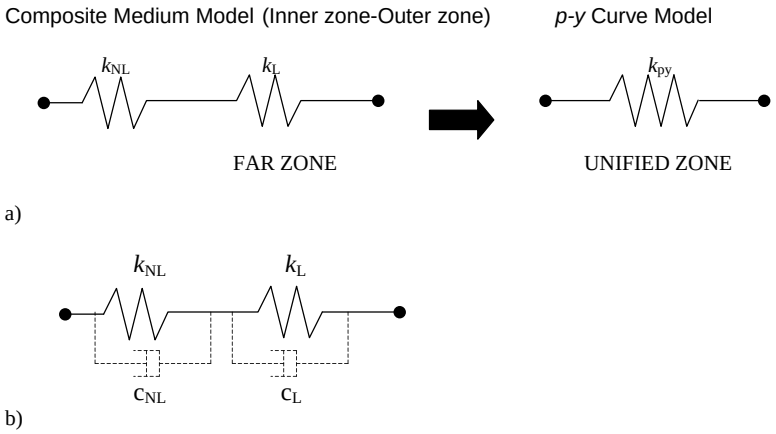

Figure B-21. Soil model: (a) composite medium and p-y *curve; (b) inclusion of damping.*

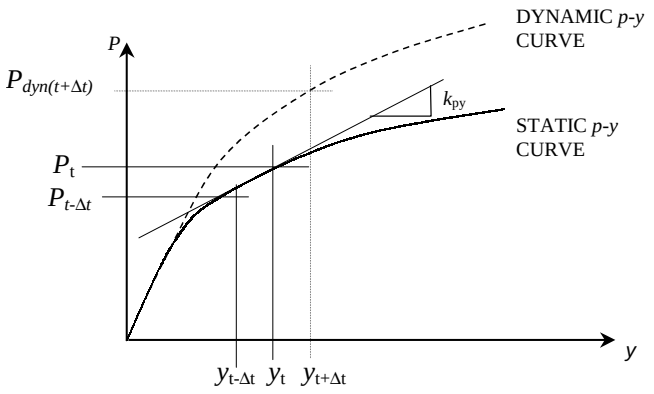

Figure B-22. Determination of stiffness (k_{py}) from an internally generated static p-y *curve to produce a dynamic* p-y *curve (including damping).*

The tangent stiffness constant, k_{py}, of any soil element at time step $t + \Delta t$ is given by the slope of the tangent to the *p-y* curve at the specific load level, as shown in Figure B-22. This slope is established from the soil deflections at time steps t and $t - \Delta t$ and from the corresponding soil reactions calculated from Equation B-18, that is,

$$k_{py(t+\Delta t)} = \frac{p_t - p_{t-\Delta t}}{y_t - y_{t-\Delta t}} . \qquad \text{(B-19)}$$

Therefore, Equations B-14 and B-19 can be substituted into Equation B-17 to obtain the nonlinear stiffness representing the inner field element in the analysis. Thus, the linear and nonlinear qualities of the unit load transfer curves have been logically incorporated into the outer and inner zones, respectively.

Static p-y *Curve Generation for Sand*

Several methods have been used to experimentally obtain *p-y* curves for sandy soils. Abendroth and Greimann (*31*) performed 11 scaled pile tests and used a modified Ramberg–Osgood model to approximate the nonlinear soil resistance and displacement behavior for loose and dense sand. The most commonly used criteria for development of *p-y* curves for sand were proposed by Reese et al. (*32*), but tend to give very conservative results. Bhushan et al. (*33*) and Bhushan and Askari (*34*) used a different procedure based on full-scale load test results to obtain nonlinear *p-y* curves for saturated and unsaturated sand. A step-by-step procedure for developing *p-y* curves in sands, based on Bhushan and Haley (*35*) and Bhushan et al. (*33*), was used to estimate the static unit load transfer curves for different sands below and above the water table. The procedure used to generate *p-y* curves for sand differs from that suggested for clays. The secant modulus approach is used to approximate soil reactions at specified lateral displacements. The soil resistance in the static *p-y* curve model can be calculated using the following equation:

$$p = (k)(x)(y)(F1)(F2) , \qquad \text{(B-20)}$$

where k is a constant that depends on the lateral deflection y (i.e. k decreases as y increases) and relates the secant modulus of soil for a given value of y to depth ($E_s = kx$), and x is the depth at which the *p-y* curve is being generated. $F1$ and $F2$ are density and groundwater (saturated or unsaturated) factors, respectively, and can be determined from Meyer and Reese (*36*). The main factors affecting k are the relative density of the sand (loose or dense) and the level of lateral displacement. The secant modulus decreases with increasing displacement, and, thus, the nonlinearity of the sand can be modeled accurately. This analysis assumes linear increase of the soil modulus with depth (but varies nonlinearly with displacement at each depth), which is typical for many sands.

Equation B-20 was used to establish the *p-y* curve at a given depth. The tangent stiffness k_{py} (needed in the time domain analysis), which represents the tangent to the *p-y* curve at the specific load level, was then calculated using Equation B-19, based on calculated soil reactions from the corresponding pile displacements for two consecutive time steps (using Equation B-20).

Degradation of Soil Stiffness

Transient loading, especially cyclic loading, may result in a buildup of pore water pressures, or a change of the soil structure, or both. Both pore pressures and structural changes can cause the shear strain amplitudes of the soil to increase with increasing number of cycles (*37*). Idriss et al. (*37*) reported that the shear stress amplitude decreased with increasing number of cycles for harmonically loaded clay and saturated sand specimens under strain-controlled undrained conditions. These studies suggest that repeated cyclic loading results in the degradation of the soil stiffness. For cohesive soils, the value of the shear modulus after N cycles, G_N, can be related to its value in the first cycle, G_{max}, by

$$G_N = \delta G_{max} , \qquad \text{(B-21)}$$

where the degradation index, δ, is given by $\delta = N^{-t}$, and t is the degradation parameter defined by Idriss et al. (*37*). This is incorporated into the proposed model by updating the nonlinear stiffness, k_{NL}, by an appropriate factor in each loading cycle.

Time Domain Analysis and Equations of Motion

The time domain analysis was used in order to include all aspects of nonlinearity and to examine the transient response logically and realistically. The governing equation of motion is given by

$$[M]\{\ddot{u}\} + [C]\{\dot{u}\} + [K]\{u\} = \{F(t)\}, \quad \text{(B-22)}$$

where $[M]$, $[C]$, and $[K]$ are the global mass, damping, and stiffness matrixes, and $\{\ddot{u}\}$, $\{\dot{u}\}$, $\{u\}$, and $F(t)$ are acceleration, velocity, displacement, and external load vectors, respectively. In Figure B-19, the equations of motion at Node 1 (adjacent to the inner field) and Node 2 (adjacent to the outer field) are

$$m_1\ddot{u}_1 + c_{NL}(\dot{u}_1 - \dot{u}_2) + k_{NL}(u_1 - u_2) = F_1 \quad \text{(B-23)}$$

$$m_2\ddot{u}_2 - c_{NL}(\dot{u}_1 - \dot{u}_2) - k_{NL}(u_1 - u_2) = F_2, \quad \text{(B-24)}$$

where u_1 and u_2 are displacements of Nodes 1 and 2, F_1 is the force in the nonlinear spring including the confining pressure, and F_2 is the soil resistance at Node 2. The equation of motion for the outer field is written as

$$c\ddot{u}_2 + k_L u_2 = -F_2. \quad \text{(B-25)}$$

Assuming compatibility and equilibrium at the interface between the inner and outer zones leads to the following equation, which is valid for both sides of the pile:

$$\begin{vmatrix} F_1 \\ 0 \end{vmatrix} = \begin{vmatrix} Am_1 + B(c_L + c_{NL}) + k_{NL} & -k_{NL} - Bc_{NL} \\ -k_{NL} - Bc_{NL} & k_{NL} + Am_2 + B(c_L + c_{NL}) + k_L \end{vmatrix} \begin{vmatrix} u_1 \\ u_2 \end{vmatrix} + \begin{vmatrix} F_1^{i-1} \\ F_2^{i-1} \end{vmatrix}, \quad \text{(B-26)}$$

where F_1^{i-1} and F_2^{i-1} are the sums of inertia forces and soil reactions at Nodes 1 and 2, respectively. The values A and B are constants of numerical integration for inertia and damping, and m is mass.

The linear acceleration assumption was used, and the Newmark β method was implemented for direct time integration of the equations of motion. The modified Newton–Raphson iteration scheme was used to solve the nonlinear equilibrium equations.

Verification of the Analytical Model

Verification of Clay Model

Different soil profiles were considered in the analysis. Figure B-23 shows the typical pile-soil system and the soil profiles considered including linear and parabolic soil profiles. The *p-y* model was first verified against the hyperbolic model (*12*). Figures B-24 and B-25 compare the dynamic soil reaction and pile-head response for both the hyperbolic and *p-y* curve models for a single reinforced concrete pile in soft clay. A pile 0.5 m in diameter and 15 m long was used with an elastic modulus (E_p) equal to 35 GPa. A parabolic soil profile with the ratio E_p/E_s = 1,000 at the pile base was assumed. The undrained shear strength of the clay was assumed to be 25 kPa. Figure B-24 shows the calculated dynamic soil reactions for a prescribed harmonic displacement of an amplitude equal to 0.03d at a frequency of 2 Hz at the pile head. It can be noted from Figure B-24 that the soil reactions obtained from the two models are very similar and approach stability after five cycles. The pattern shown in Figure B-24 is also similar to that obtained by Nogami et al. (*21*), showing an increasing gap and stability after approximately five cycles. Figure B-25 shows the displacement-time history of the pile head installed in the same soil profile. The load was applied at the pile head and was equal to approximately 10 percent of the ultimate lateral loading capacity of the pile. The hyperbolic and *p-y* curve models show very similar responses at the pile head, and both stabilize after approximately five cycles.

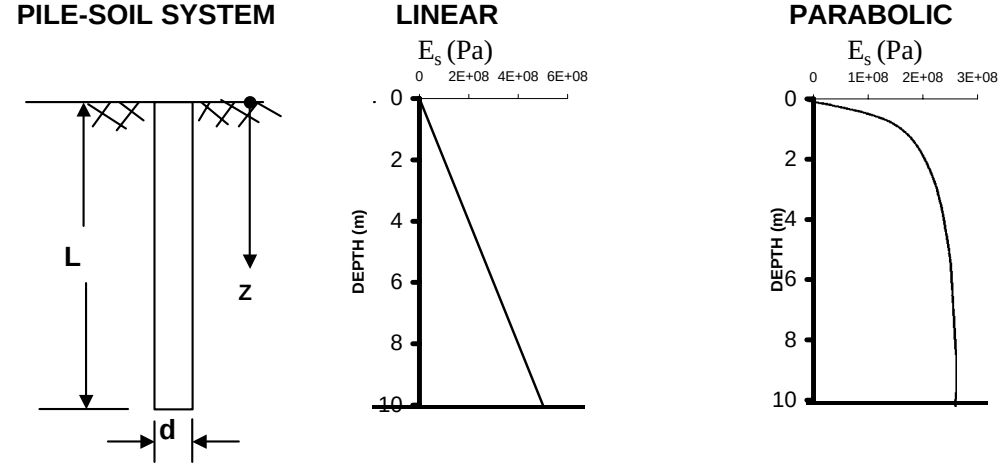

Figure B-23. Soil modulus variation for profiles considered in the analysis.

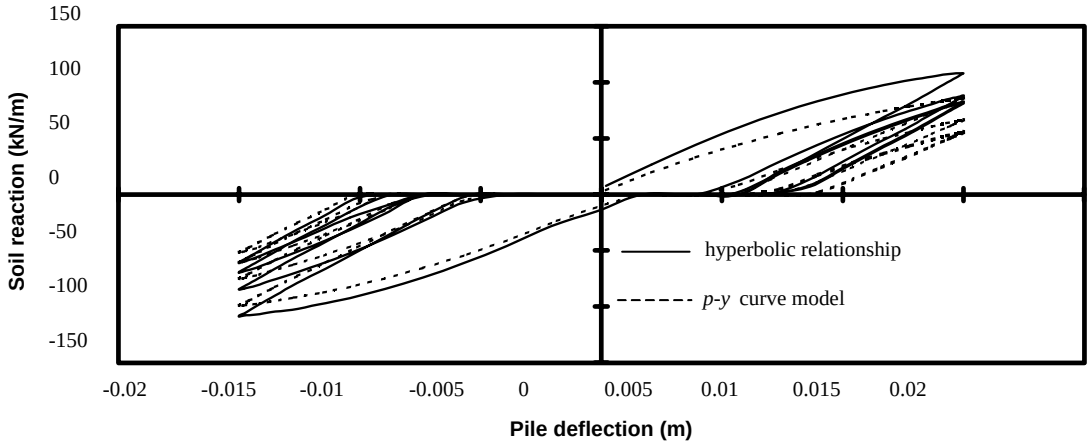

Figure B-24. Calculated dynamic soil reactions at 1.0-m depth (for a prescribed harmonic displacement at pile head with amplitude = 0.015 m, L/d = *30).*

The dynamic soil reactions are, in general, larger than the static reactions because of the contribution from damping. Employing the same definition used for static *p-y* curves, dynamic *p-y* curves can be established to relate pile deflections to the corresponding dynamic soil reaction at any depth below the ground surface. The proposed dynamic *p-y* curves are frequency dependent. These dynamic *p-y* curves can be used in other static analyses that are based on the *p-y* curve approach to account approximately for the dynamic effects on the soil reactions to transient loading.

Figures B-26 and B-27 show dynamic *p-y* curves established at two different clay depths for a prescribed harmonic displacement at the pile head with an amplitude equal to 0.05 d, for a frequency range from 0 to 10 Hz. The shear modulus of the soil was assumed to increase parabolically along the pile length. A concrete pile 12.5 m in length and 0.5 m in diameter was considered in the analysis. The elastic modulus of the pile material was assumed to be 35 GPa and the ratio E_p/E_s = 1,000 (at the pile base). Both the *p-y* curve and hyperbolic models were used to analyze the pile response. The dynamic soil reaction (normalized by the ultimate pile capacity, P_{ult}) obtained from the *p-y* curve model compared well with that obtained from the hyperbolic relationship model, especially for lower frequencies, as can be noted from Figures B-26 and B-27. It can also be observed from Figures B-26 and B-27 that the soil reaction increased as the frequency increased. This increase was more evident in the results obtained from the *p-y* curve model.

Verification of Sand Model

The *p-y* curve and hyperbolic models were used to analyze the response of piles installed in sand. The sand was assumed to be unsaturated, and a linear soil modulus profile was adopted. The same pile as was used in the previous case was considered. Figure B-28 shows the calculated dynamic soil reactions at a 1-m depth for a prescribed harmonic dis-

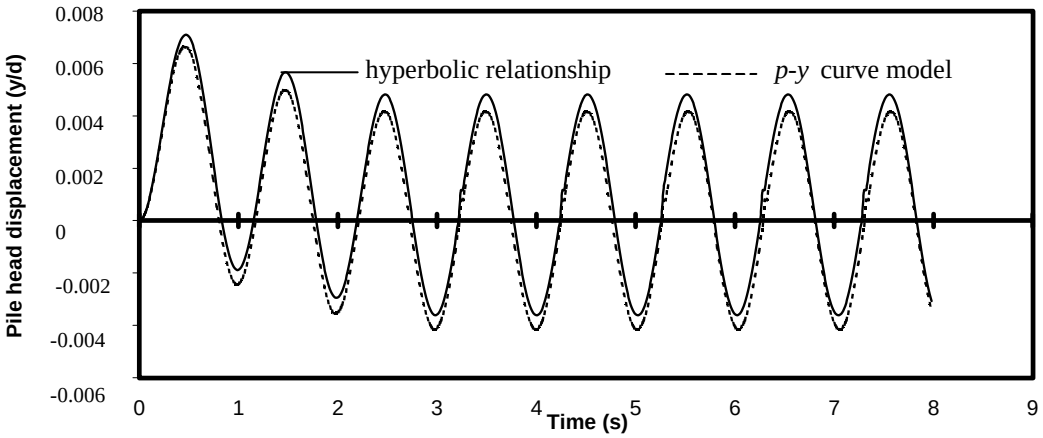

*Figure B-25. Pile-head response under applied harmonic load with amplitude equal to 10 percent of the ultimate load (*L/d = *30,* E_p/E_s (L) = *1000, linear profile).*

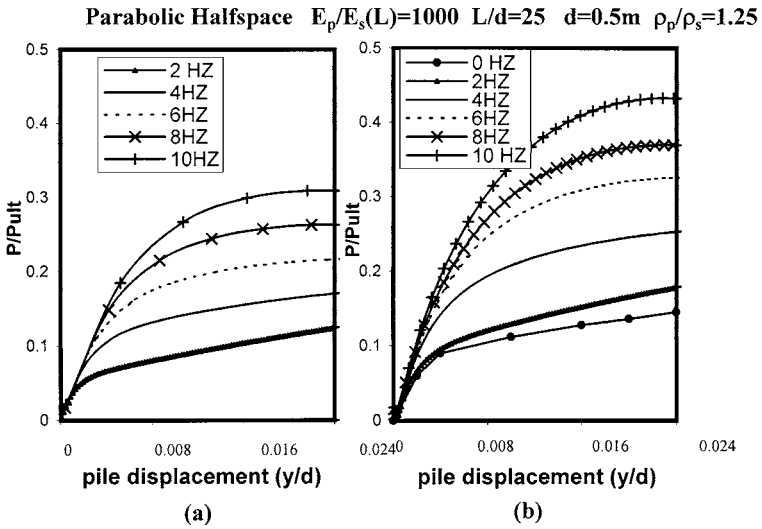

Figure B-26. Calculated dynamic p-y *curves at 1.5-m depth (for a prescribed harmonic displacement at pile head with amplitude equal to 0.05 d) using (a) hyperbolic model and (b)* p-y *curve model.*

placement with an amplitude equal to 0.0375 d at the pile head with a frequency of 2 Hz. As can be seen in Figure B-28, the two models feature very similar dynamic soil reactions. It should be noted that the soil reactions at both sides of the pile are traced independently. The upper part of the curve in Figure B-28 represents the reactions for the soil element adjacent to the right face of the pile when it is loaded rightward. The lower part represents the reactions of the soil element adjacent to the left face of the pile as it is loaded leftward. Both elements offer zero resistance to the pile movement when tensile stresses are detected in the nonlinear soil spring during unloading of the soil element on either side. The soil nodes, however, remain attached to the pile node at the same level, allowing the sand to "cave in" and fill the gap. Observations from field and laboratory pile testing have confirmed that, unlike clays, sands usually do not experience gapping during harmonic loading. Thus, both analyses realistically and logically model the physical behavior of the soil.

The pile-head displacement time histories obtained from the *p-y* curve and hyperbolic models for a pile installed in a sand with linearly varying elastic modulus caused by an applied harmonic load are shown in Figure B-29. It can be noted that good agreement exists between the results from the *p-y* curve model and hyperbolic model.

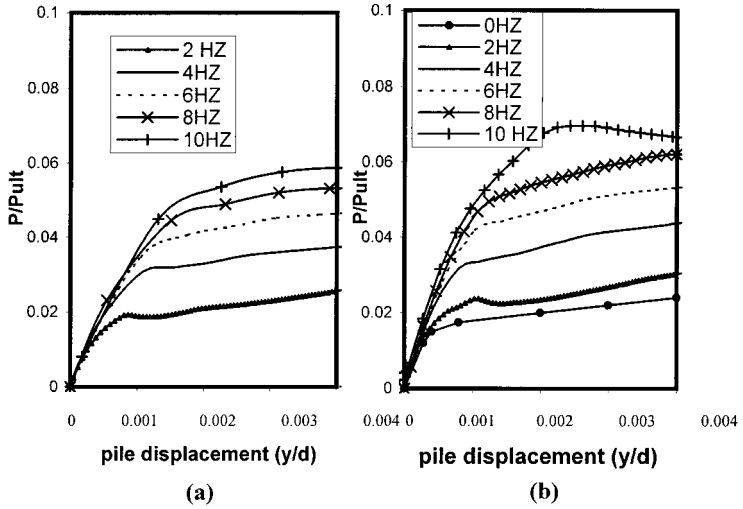

Figure B-27. Calculated dynamic p-y *curves at 3.0-m depth (for a prescribed harmonic displacement at pile head with amplitude equal to 0.05 d) using (a) hyperbolic model and (b)* p-y *curve model.*

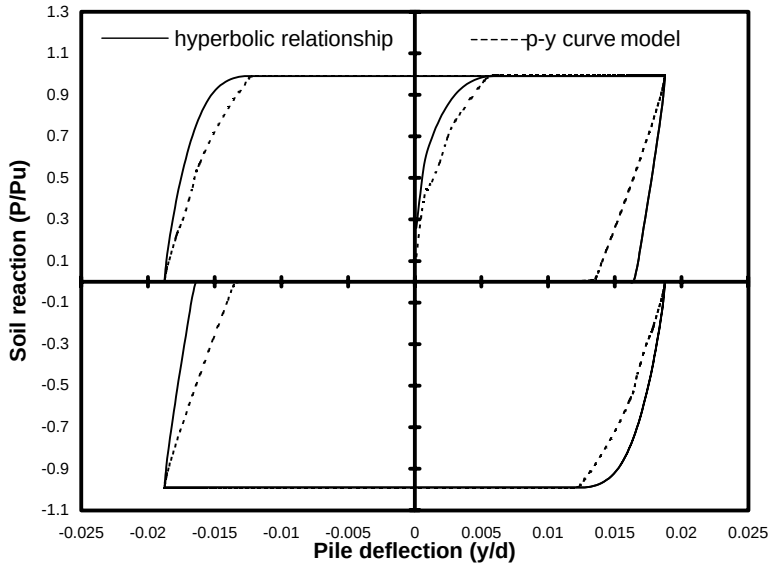

Figure B-28. Calculated dynamic soil reactions at 1.0-m depth (for a prescribed harmonic displacement at pile head with amplitude equal to 0.0375 d, L/d = *25, and* E_p/E_s [L] = *1000).*

Figures B-30 and B-31 show dynamic *p-y* curves established at two different depths for a prescribed harmonic displacement equal to 0.05 d at the pile head for a steel pile driven in sand for a frequency range from 0 to 10 Hz. The results from both the *p-y* curve and hyperbolic models displayed the same trend, as can be noted from Figures B-30 and B-31.

Validation of Dynamic Model with Lateral Statnamic Tests

In order to verify that the *p-y* curve model can accurately predict dynamic response, the model was employed to analyze a lateral Statnamic load test, and the computed response was compared with measured values.

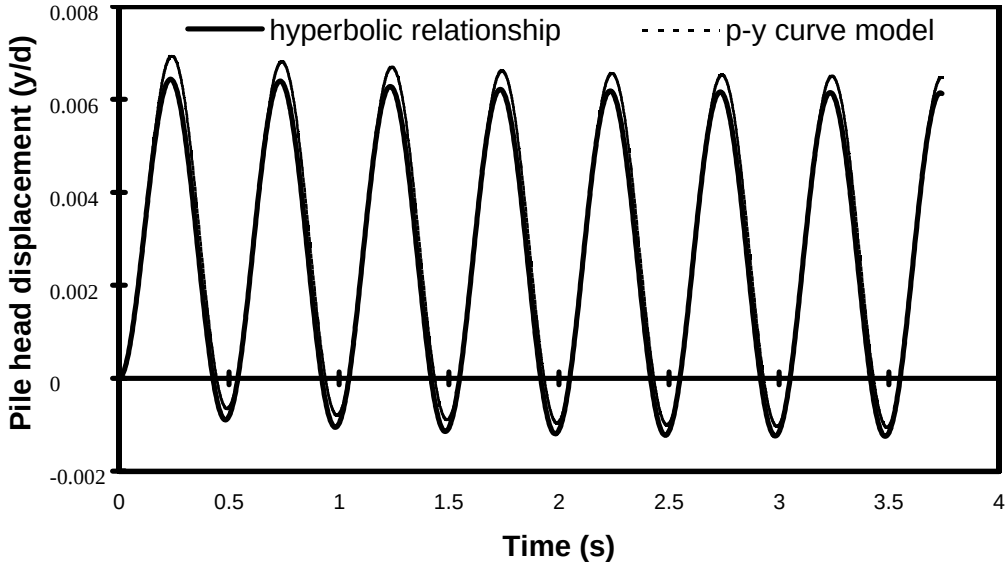

*Figure B-29. Pile-head response to applied harmonic load with an amplitude equal to 8 percent of the ultimate load (*L/d = *25,* E_p/E_s (L) = *1000, linear profile).*

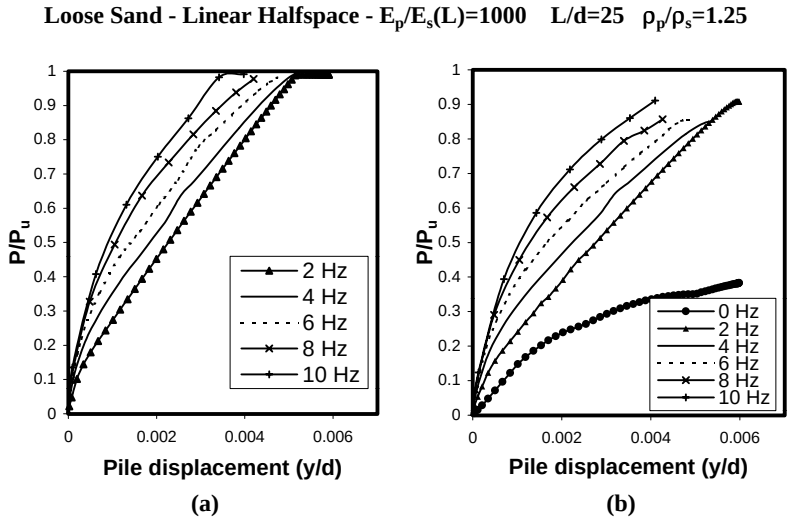

Figure B-30. Calculated dynamic p-y *curves at 3.0-m depth (for a prescribed harmonic displacement at pile head with amplitude equal to 0.05 d) using (a) hyperbolic model and (b)* p-y *curve model.*

The test site was located north of the New River at the Kiwi manoeuvres area of Camp Johnson in Jacksonville, North Carolina. The soil profile is shown in Figure B-32 and consists of medium-dense sand extending to the water table, underlain by a very weak, gray silty clay. There was a layer of gray sand at a depth of 7 m and a calcified sand stratum underlying that layer. The pile tested at this site was a cast-in-place reinforced concrete shaft with steel casing having an outer diameter of 0.61 m and a casing wall thickness of 13 mm. More details on the soil and pile properties and the loading procedure are presented by El Naggar (*38*). Statnamic testing was conducted on the pile 2 weeks after lateral static testing was performed. Statnamic loading tests were performed by M. James and P. Bermingham, both of Berminghammer Foundation Equipment, Hamilton, Ontario.

The computed lateral response of the pile head is compared with the measured response in Figure B-33 for two separate tests with peak load amplitudes of 350 kN and 470 kN. The agreement between the measured and computed values was excellent, especially for the first load test. The initial displace-

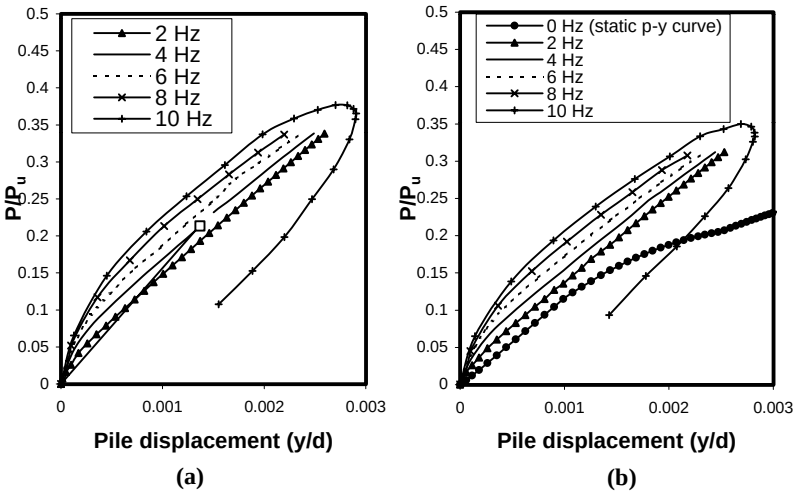

Figure B-31. Calculated dynamic p-y *curves at 4.0-m depth (for a prescribed harmonic displacement at pile head with amplitude equal to 0.05 d) using (a) hyperbolic model and (b)* p-y *curve model.*

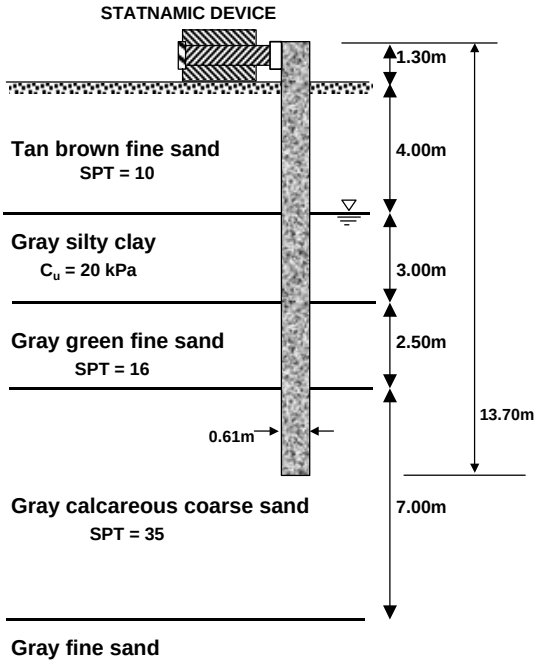

Figure B-32. Soil profile and Statnamic pile test set-up at Camp Johnson, Jacksonville.

ment was slightly adjusted for the computer-generated model to accommodate initial gapping that occurred because of the previous static test performed on the pile. The static *p-y* curve for the top soil layer was reduced significantly in order to model the loss of resistance caused by permanent gap developed near the surface.

Dynamic *p-y* Curve Generation

The dynamic *p-y* curves presented in Figures B-26 through B-28, B-30, and B-31 showed that a typical family of curves exists related to depth, much like the static *p-y* curve relationships. Thus, dynamic *p-y* curves could be established at any depth and be representative of the soil resistance at this specific depth. In this study, they were obtained at a depth equal to 1.5 mm, which was found to illustrate the characteristics of the dynamic *p-y* curves.

More dynamic *p-y* curves were generated using prescribed harmonic displacements applied at the pile head that allowed for the development of plastic deformation in the soil along the top quarter of the pile length. Steel pipe piles were considered in the analysis. It was assumed that sand had a linear soil profile and that the clay had a parabolic profile in order to match the soil profile employed to derive the static *p-y* curves used in the analysis. The soil shear wave velocity profiles and the pile properties are given in Figure B-34. The tests were divided into two separate cases involving clays (Case I) and sandy soils (Case II). Table B-1 summarizes the characteristics of each case and relevant pile and soil parameters. The dynamic *p-y* curves were generated over a frequency range of 0 to 10 Hz (2-Hz intervals) for different classifications of sand and clay based on standard laboratory and field measurements (standard penetration test–value, relative density, c_u, etc.). All results were obtained after one or two cycles of harmonic loading.

Results and Discussion

The results from the computational model showed a general trend of increasing soil resistance with an increase in the load frequency. The dynamic *p-y* curves obtained seem to have three distinct stages or regions. The initial stage (at small displacements) shows an increase in the soil resistance (compared with the static *p-y* curve) that corresponds to increasing the velocity of the pile to a maximum. This increase in the soil resistance is larger for higher frequencies. In the second stage, the dynamic *p-y* curves have almost the same slope as the static *p-y* curve for the same displacement. This stage occurs when velocity is fairly constant and, consequently, the damping contribution is also constant. The third stage of the dynamic *p-y* curve is characterized by a slope approaching zero as plastic deformations start to occur (similar to the static *p-y* curve at the same displacement). There is also a tendency for the dynamic curves to converge at higher resistance levels approaching the ultimate lateral resistance of the soil at depth *x*, P_u (determined from API research [*4*]).

The overall relationship between the dynamic soil resistance and loading frequency for each test was established in the form of a generic equation. The equation was developed from regression analysis relating the static *p-y* curve, frequency, and apparent velocity (ωy), so that

$$P_d = P_s\left[\alpha + \beta a_0^2 + \kappa a_0\left(\frac{\omega y}{d}\right)^n\right], P_d \le P_u \text{ at depth } x, \quad \text{(B-27)}$$

where

P_d = dynamic value of "*p*" on the *p-y* curve at depth *x* (N/m),
P_s = corresponding static soil reaction (obtained from the static *p-y* curve) at depth *x* (N/m),
a_0 = dimensionless frequency = $\omega r_0/V_s$,
ω = frequency of loading (rad/s),
d = pile diameter (m),
y = lateral pile deflection at depth *x* when soil and pile are in contact during loading (m), and
α, β, κ, and n = constants determined from curve fitting Equation B-27 to the computed dynamic *p-y* curves from all cases considered in this study.

A summary of the best-fit values for the constants is provided in Table B-2. The constant α is taken equal to unity to ensure that $P_d = P_s$, for $\omega = 0$. For large frequencies or displacements, the maximum dynamic soil resistance is limited to the ultimate static lateral resistance of the soil, P_u.

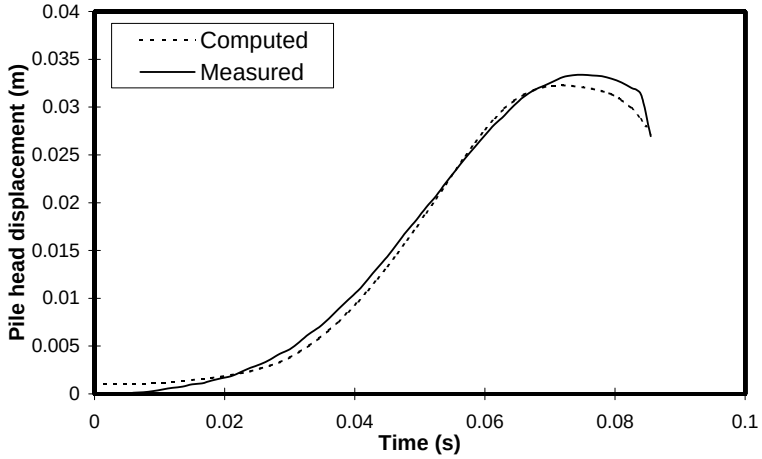

(a)

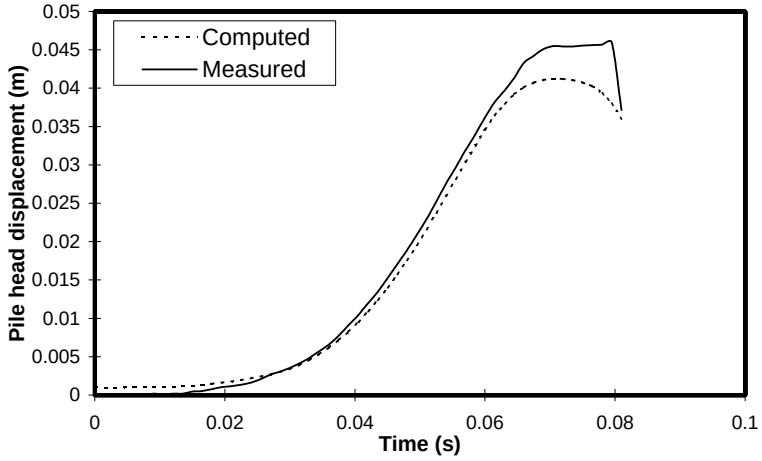

(b)

Figure B-33. Pile-head displacement for Statnamic test with peak load equal to (a) 350 kN and (b) 470 kN.

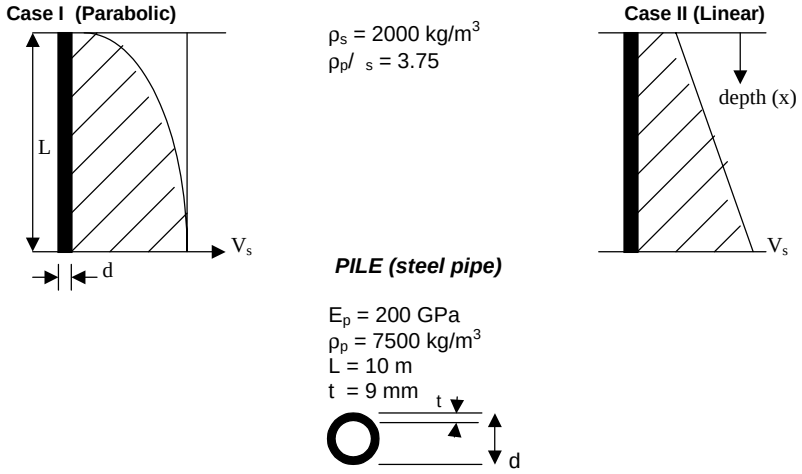

Figure B-34. Description of soil and pile properties for Case I and Case II.

TABLE B-1 Description of parameters used for each test case

CASE I (clays)	SOIL TYPE	C_u (kPa)	ν	*d* (m)	*L/d*	E_p/E_s	G_{max} (kPa)	V_s (m/s)
C1	SOFT CLAY	< 50	0.45	0.25	40	10000	6.6e6	70
C2	MEDIUM CLAY	80	0.45	0.25	40	4500	1.6e7	150
C3	STIFF CLAY	>100	0.45	0.25	40	1600	8.3e7	200

CASE II (sands)	SOIL TYPE	D_r (%)	ϕ	ν	*d* (m)	*L/d*	E_p/E_s	G_{max} (kPa)	V_s (m/s)
S4	LOOSE SAND (saturated)	35	32	0.3	0.25	40	6300	1.2e7	70
S5	MEDIUM SAND (saturated)	50	34	0.3	0.25	40	3800	2.0e7	100
S6	MEDIUM SAND (saturated)	50	34	0.3	0.50	20	3800	2.0e7	100
S8	DENSE SAND (saturated)	90	38	0.3	0.25	40	1580	4.7e7	150
S9	DENSE SAND (unsaturated)	90	38	0.3	0.25	40	790	9.7e7	220

NOTE: All values represent those calculated at a depth of 1.5 m.

TABLE B-2 Dynamic *p-y* curve parameter constants for a range of soil types*

SOIL TYPE	DESCRIPTION	α	β		κ	*n*
			a_o < 0.025	a_o > 0.025		
SOFT CLAY	C_u < 50 kPa V_s < 125 m/s	1	–180	–200	80	0.18
MEDIUM CLAY	50 < C_u < 100 kPa 125 < V_s < 175 m/s	1	–120	–360	84	0.19
STIFF CLAY	C_u > 100 kPa V_s >175 m/s	1	–2900	–828	100	0.19
MEDIUM-DENSE SAND (saturated)	50 < D_r < 85 % 125 < V_s < 175 m/s	1	3320	1640	–100	0.1
MEDIUM-DENSE SAND (unsaturated)	50 <D_r < 85 % 125 < V_s < 175 m/s	1	1960	960	–20	0.1
DENSE SAND (saturated)	D_r > 85 % V_s > 175 m/s	1	6000	1876	–100	0.15

* (d = 0.25, L/d = 40, 0.015 < $a_o = \omega r_o/V_s$ < 0.225); $P_d = P_s\left[\alpha + \beta a_o^{\,2} + \kappa a_o\left(\frac{\omega y}{d}\right)^n\right]$

Figures B-35 and B-36 show dynamic *p-y* curves established using Equation B-27 and the best-fit constants (as dashed lines). The approximate dynamic *p-y* curves established from Equation B-27 represented soft/medium clays and loose to medium-dense sands reasonably well. However, the accuracy is less for stiffer soils (higher V_s values). The precision of the fitted curves also increases with frequency ($\omega \geq 4$ Hz) where the dynamic effects are important. The low accuracy at a lower frequency ($a_0 < 0.02$) may be attributed to the application of the plane strain assumption in the dynamic analysis. This assumption is suitable for higher frequencies as the dynamic stiffness of the outer field model vanishes for $a_0 < 0.02$ because of the assumption of plane strain. Case C1 was also used to obtain dynamic *p-y* curves at depths of 1.0 m and 2.0 m to examine the validity of Equation B-27 to describe the dynamic soil reactions at other depths along the soil profile. The results showed that Equation B-27 (using the constants in Table B-2) predicted the dynamic soil reactions reasonably well.

Development of a Simplified Model

For many structural dynamics programs, soil-structure interaction is modeled using static *p-y* curves to represent the soil reactions along the pile length. However, the use of static *p-y* curves for dynamic analysis does not include the effects of velocity-dependent damping forces. The dynamic *p-y* curves established using Equation B-27 and the parameters given in Table B-2 allow for the generation of different dynamic *p-y* curves based on the frequency of loading and soil profile. Substituting dynamic *p-y* curves in place of traditional static *p-y* curves for analysis should result in better estimates of the response of structures to dynamic loading.

Alternatively, the dynamic soil reactions can be represented using a simple spring and dashpot model. This model can still capture the important characteristics of the nonlinear dynamic soil reactions. A simplified dynamic model that can be easily implemented into any general finite element program is proposed herein.

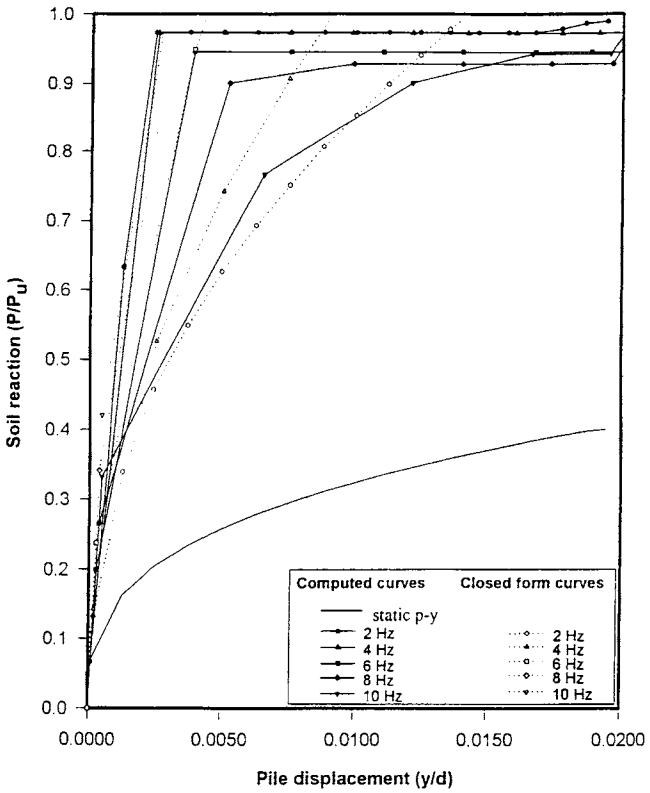

Figure B-35. Dynamic p-y *curves and static* p-y *curve for Case C1 (depth = 1.0 m).*

Complex Stiffness Model

As discussed previously, Equation B-27 can be used directly to represent the dynamic relationship between a soil reaction and a corresponding pile displacement. The total dynamic soil reaction at any depth is represented by a nonlinear spring whose stiffness is frequency dependent.

A more conventional and widely accepted method of calculating dynamic stiffness is through the development of the complex stiffness. The complex stiffness has a real part, K_1, and an imaginary part, K_2, that is,

$$P_d = Ky = (K_1 + iK_2)y \tag{B-28}$$

The real part, K_1 represents the true stiffness, *k;* the imaginary part of the complex stiffness, K_2, describes the out-of-phase component and represents the damping caused by the energy dissipation in the soil element. Because this damping component generally grows with frequency (resembling viscous damping), it can also be defined in terms of the constant of equivalent viscous damping (the dashpot constant) given by $c = K_2/\omega$. The dynamic *p-y* curve relation can be described as

$$P_d = (k + i\omega c)y = ky + c\dot{y}\,, \tag{B-29}$$

in which both *k* and *c* are real and represent the spring and dashpot constants, respectively, and $\dot{y} = dy/dt$ is velocity. Using Equation B-27, the dynamic *p-y* curve can be written in the form of Equation B-28, that is,

$$P_d = (K_1 + iK_2)y$$

$$= \left\{ \frac{P_s \alpha}{y} + i \frac{P_s\left(\beta a_0^2 + \kappa a_0 \left(\frac{\omega y}{d}\right)^n\right)}{y} \right\} y. \tag{B-30}$$

The stiffness and damping constants are then calculated as

$$k = K_1 = \frac{P_s \alpha}{y} \quad \text{and} \tag{B-31}$$

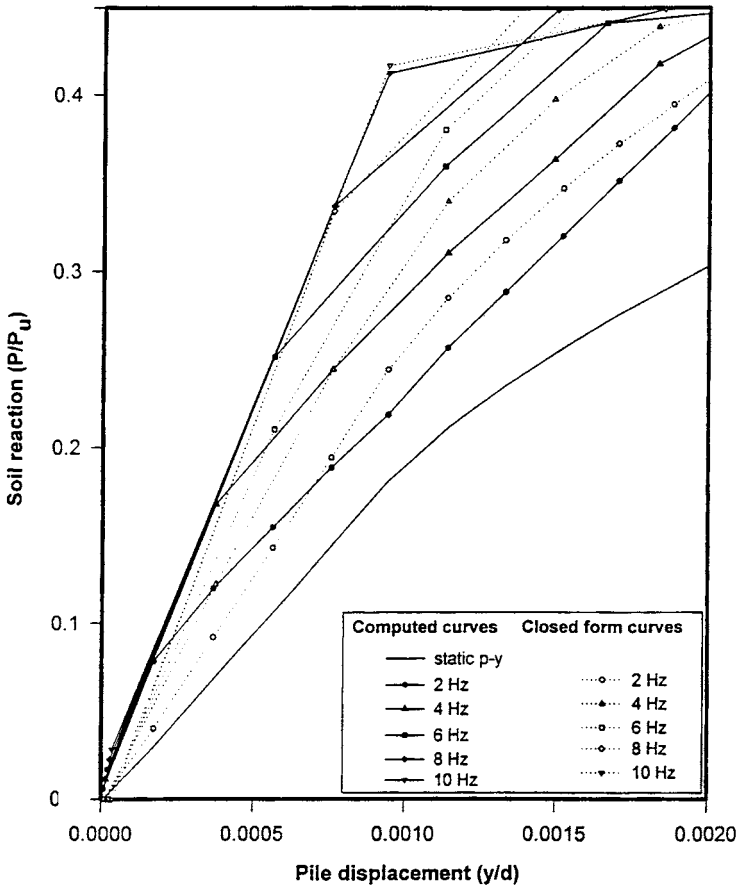

Figure B-36. Dynamic p-y *curves and static* p-y *curve for Case S5 (depth = 1.5 m).*

$$c = \frac{K_2}{\omega} = \frac{P_s\left(\beta a_0^2 + \kappa a_0\left(\frac{\omega y}{d}\right)^n\right)}{\omega y}. \qquad \text{(B-32)}$$

The complex stiffness can be generated at any depth along the pile using the static *p-y* curves and Equations B-31 and B-32.

Complex Stiffness Constants—Soft Clay Example

The complex stiffness constants were calculated for Test C1 (see Table B-2) using the method described in the previous section. The values of the true stiffness, *k*, were obtained for the range of displacements experienced by the pile for the frequency range from 0 to10 Hz. The stiffness parameter $(S_1)_{py}$ was defined as

$$(S_1)_{py} = \frac{k_{py}}{G_{\max}}. \qquad \text{(B-33)}$$

The constant of equivalent damping, *c*, was obtained by averaging the value from Equation B-32 for the range of velocities experienced by the pile for each frequency of loading. Then, the equivalent damping parameter $(S_2)_{py}$ was defined as

$$(S_2)_{py} = \frac{cV_s\omega}{G_{\max}r_0}. \qquad \text{(B-34)}$$

Figure B-37 shows the true stiffness calculated from the static *p-y* curve, and it can be noted that this stiffness is identical at all loading frequencies considered. There is a definite trend of decreasing stiffness with increased displacement because of the soil nonlinearity. The constant of equivalent damping presented in Figure B-38 shows a decreasing pattern with frequency that can be attributed to separation at the pile-soil interface. The values from Figures B-37 and B-38 can be directly input into a finite element program as spring and dashpot constants to obtain the approximate dynamic stiffness of a soil profile similar to Test C1.

Implementing Dynamic p-y *Curves in ANSYS*

A pile-and-soil system similar to Test C1 was modeled using *ANSYS* (*1*) to verify the applicability and accuracy of

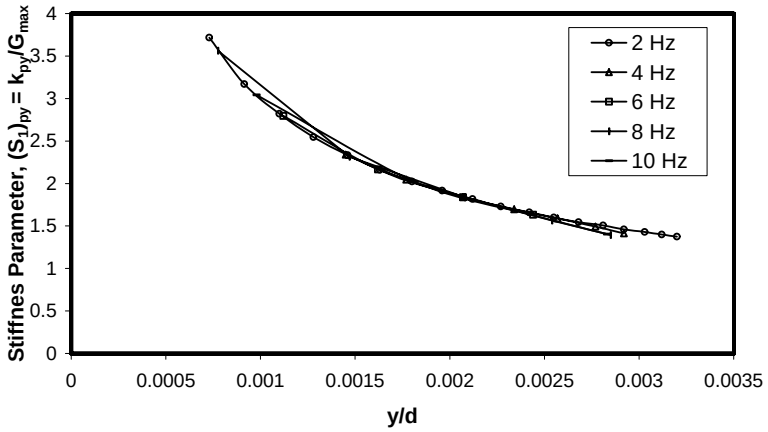

Figure B-37. True stiffness parameter for Test C1 (soft clay).

the dynamic *p-y* curve model in a standard structural analysis program. A dynamic harmonic load with peak amplitude of 100 kN at a frequency of 6 Hz was applied to the head of the same steel-pipe pile used in Test C1. The soil stiffness was modeled using three procedures: (1) static *p-y* curves; (2) dynamic *p-y* curves using Equation B-27; and (3) complex stiffness method using equivalent damping constants. The pile-head response for each test was obtained and compared with the results from the two-dimensional *p-y* curve model.

The pile was modeled using two-noded beam elements and was discretized into 10 elements that increased in length with depth. At each pile node, a spring or a spring and a dashpot were attached to both sides of the pile to represent the appropriate loading condition at the pile-soil interface. The pile and soil remained connected and had equal displacement for compressive stresses. The spring or the spring-and-dashpot model disconnects if tensile stress is detected in the soil, allowing a gap to develop.

The soil was first modeled using nonlinear springs with force displacement relationships calculated directly from static *p-y* curves. The soil stiffness was then modeled using the approximate dynamic *p-y* curve relationship calculated for Test C1 using Table B-2. The last computational test considered a spring and a dashpot in parallel.

The pile-head response for each computational test is shown in Figures B-39 and B-40, along with the calculated response from the two-dimensional analytical *p-y* model. Figure B-39a shows that the static *p-y* curves model computed larger displacements with increasing amplitudes as the number of cycles increased. Figure B-39b shows that the response computed using the dynamic *p-y* curve model was in good agreement with the response computed using the two-dimensional analytical model. The results obtained using the complex stiffness model are presented in Figure B-40a and show a decrease in displacement amplitude. The overdamped response can be attributed to using an average damping constant, which

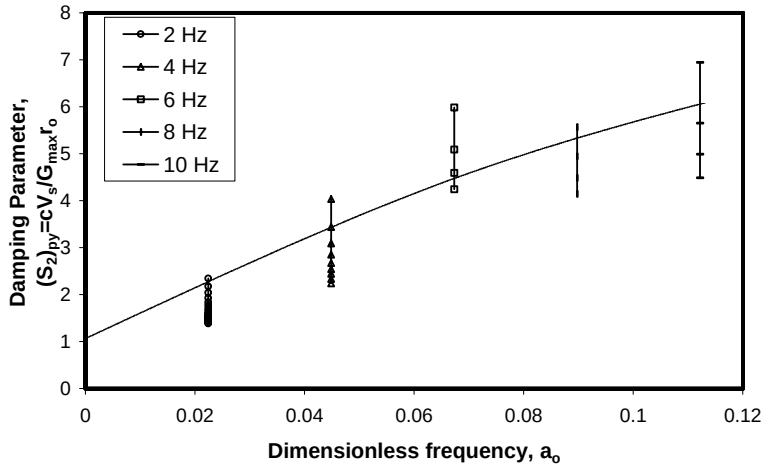

Figure B-38. Equivalent damping parameter for Test C1 (soft clay) with dimensionless frequency.

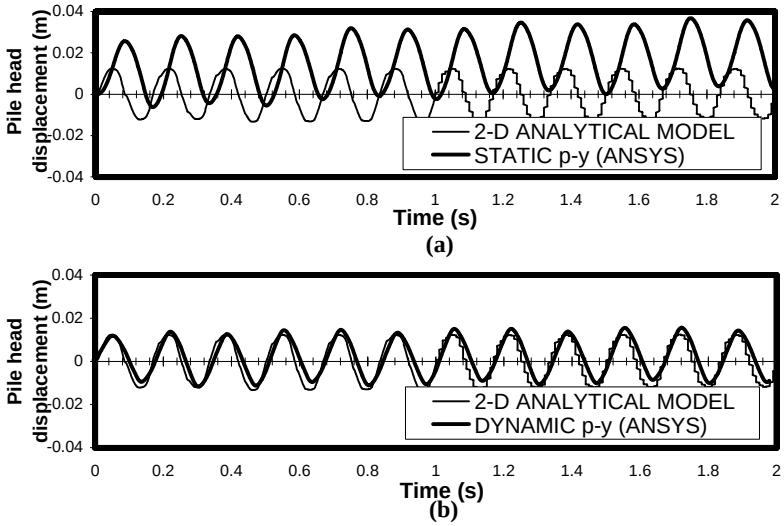

Figure B-39. Calculated pile-head response using two-dimensional analytic model compared with ANSYS using (a) static p-y *curves and (b) dynamic* p-y *curves.*

overestimates the damping at higher frequencies and large nonlinearity. Figure B-40b shows the response of the two-dimensional model compared with the complex stiffness approach with the average damping constant reduced by 50 percent. The results show that the response in this case is in good agreement with the response computed using the two-dimensional analytical model.

DYNAMIC *p*-MULTIPLIERS

One reasonable approach to account for pile-soil-pile interaction for piles in a group would be to predict the loss in soil resistance relative to that of an isolated single pile. Poulos and Davis (*9*) introduced the interaction-factors concept to reduce the soil stiffness in the context of linear elastic analysis. Focht and Koch (*39*) extended that linear elastic procedure to introduce the nonlinearity of soil into the evaluation of group interaction factors by applying a *y*-multiplier to "stretch" *p-y* curves. Cox et al. (*40*) described an alternate approach to account approximately for the group effect, in which a "*p*-factor" would be used to "shrink" the *p*-values on the *p-y* curve rather than to stretch the *y*-values.

The *p*-multiplier concept was formalized by Brown et al. (*41*) and Brown and Bollman (*42*). This concept states that lat-

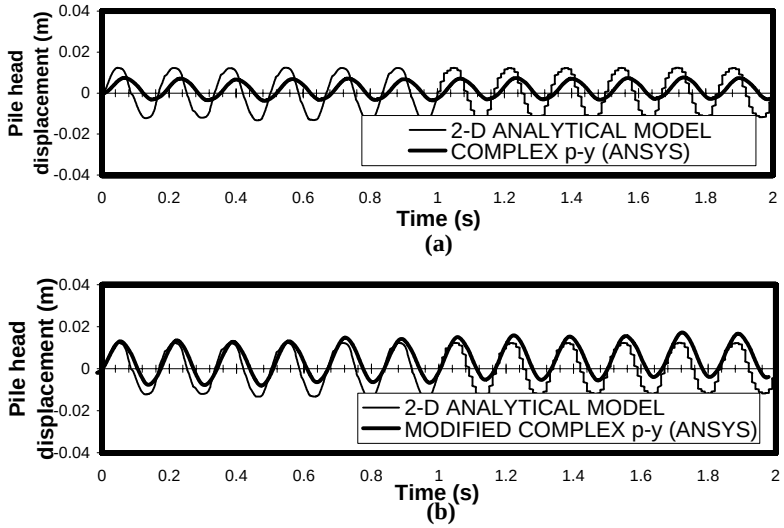

Figure B-40. Calculated pile-head response, two-dimensional analytic model, compared with ANSYS using (a) complex stiffness and (b) modified complex stiffness.

eral group action reduces the *p*-value on the *p-y* curve at every point on every *p-y* curve for a given pile (based on its geometric position in the group) by the same amount, regardless of pile deflection. In this manner, the *p*-multiplier provides a means for expressing the elastic interaction that appears in the interaction factors plus an actual reduction in ultimate soil resistance. The *p*-multiplier assumes a different value depending upon whether a pile is in a leading position or in a trailing position and the angle between the line connecting the two piles and the load direction, θ. Using the *p*-multipliers would allow the analysis of the lateral response of a pile group as an ensemble of individual piles. The soil resistance to the movement of each of these individual piles would be represented by *p-y* curves with *p*-values reduced by properly chosen *p*-multipliers. For example, the Florida Pier Program (FLPIER; see Appendix C) uses *p*-multipliers as an option for considering lateral group action. The *p*-multipliers found in the literature are given either by row (i.e., the same *p*-multiplier value for all piles in the same row) or by assuming different values for each pile. In the latter case, the total *p*-multiplier for any pile is obtained by multiplying (rather than by summing) the *p*-multipliers due to all the piles in the group.

The *p*-multipliers reported in the literature were developed from the analysis of static or cyclic load tests on single piles and pile groups. These tests, however, do not represent the dynamic loading conditions during an earthquake event; therefore, it is necessary to check the validity of the *p*-multiplier concept under dynamic loading conditions and develop, if possible, *p*-multipliers from dynamic loading events. This was a major objective of the overall project. The following section describes the results of an exploratory investigation into dynamic *p*-multipliers, independent of the analysis of the load tests conducted explicitly for this project (see Appendix D).

The approach suggested by El Naggar and Novak (*23*) to account for the group effect, along with the analytical model described above for the analysis of a single pile's response, was used to analyze the response of a single pile and groups of two piles to a prescribed harmonic displacement at the pile heads. Thus, dynamic *p*-multipliers could be established by comparing the soil resistance for a pile in a group of two piles with that of a single pile. At this point, a limited parametric study was considered for piles in cohesionless soil with different densities (e.g., loose, medium, and dense sand profiles). The parameters whose influence on *p*-multipliers is investigated in this study for a given pile-and-soil profile include

- The ratio of the spacing between the two piles to the diameter of the piles, *S/d;*
- The pile-head displacement ratio, *y/d;*
- The dimensionless frequency, a_0; and
- The angle between the line connecting the two piles and the load direction, θ.

To establish the *p*-multiplier, two loading cases were considered separately: a pile loaded individually and a group of two identical piles. In both loading cases, a prescribed harmonic displacement with specified peak amplitude was applied at the pile head, the response was analyzed, and the force at the pile head was calculated. The *p*-multiplier was approximated by the peak pile-head force at one pile in the two-pile group divided by the peak force for the single pile. The loading starts from zero, and the forces are established after five loading cycles. The response was found to stabilize almost completely after this number of cycles.

The *p*-multiplier was plotted versus the peak of the applied harmonic displacement, as a ratio of the pile diameter. Figure B-41 shows the *p*-multipliers for piles installed in loose sand (S4 in Table B-1), and θ equals 0°. It can be noted from Figure B-41 that the main factors that affect the *p*-multipliers in this case are the spacing ratio, *S/d,* and the pile-head displacement ratio, *y/d.* The *p*-multiplier increased as *S/d* increased, meaning that the group effect decreased. The *p*-multipliers also increased as the *y/d* increased. This means that during a dynamic loading event, which is characterised by large pile-head displacement, the pile-soil-pile interaction decreases, and the piles tend to behave as individual piles. This may be attributed to the concentration of soil deformations in the vicinity of the pile at higher displacements. Comparing the *p*-multipliers in Figure B-41 obtained for different loading frequencies, it can be seen that the effect of the frequency on the *p*-multipliers is small and that there is no clear trend for it.

Figures B-42 and B-43 show the *p*-multipliers for piles installed in medium-dense and dense sand, respectively. Similar observations can be made for both cases. The *p*-multipliers increased as both *S/d* and *y/d* increased, and the effect of the frequency is negligible. It must be emphasised, however, that these observations are based on limited results. Further investigations should be done before these observations can be asserted. Also, the behavior of piles in clay is different and is currently under investigation.

The *p*-multipliers shown in Figures B-42 and B-43 (and similar ones for other soil profiles) could be curve fitted. The best curve-fit function would be in the form

$$p\text{-multiplier} = f\,(S/d, y/d, a_0, \theta) \qquad \text{(B-35)}$$

This function can then be evaluated to yield the *p*-multiplier according to *S/d,* θ values for each two piles in the group, and the expected *y/d* and a_0 for a specific event.

SUMMARY, CONCLUSIONS, AND RECOMMENDATIONS FOR IMPROVEMENTS

Summary and Conclusions

A simple, two-dimensional analysis method was developed to model the response of piles to dynamic loads. The model was formulated in the time domain and developed to model transient nonlinear response of the pile-soil system efficiently. Static *p-y* curves were used to generate the nonlinear

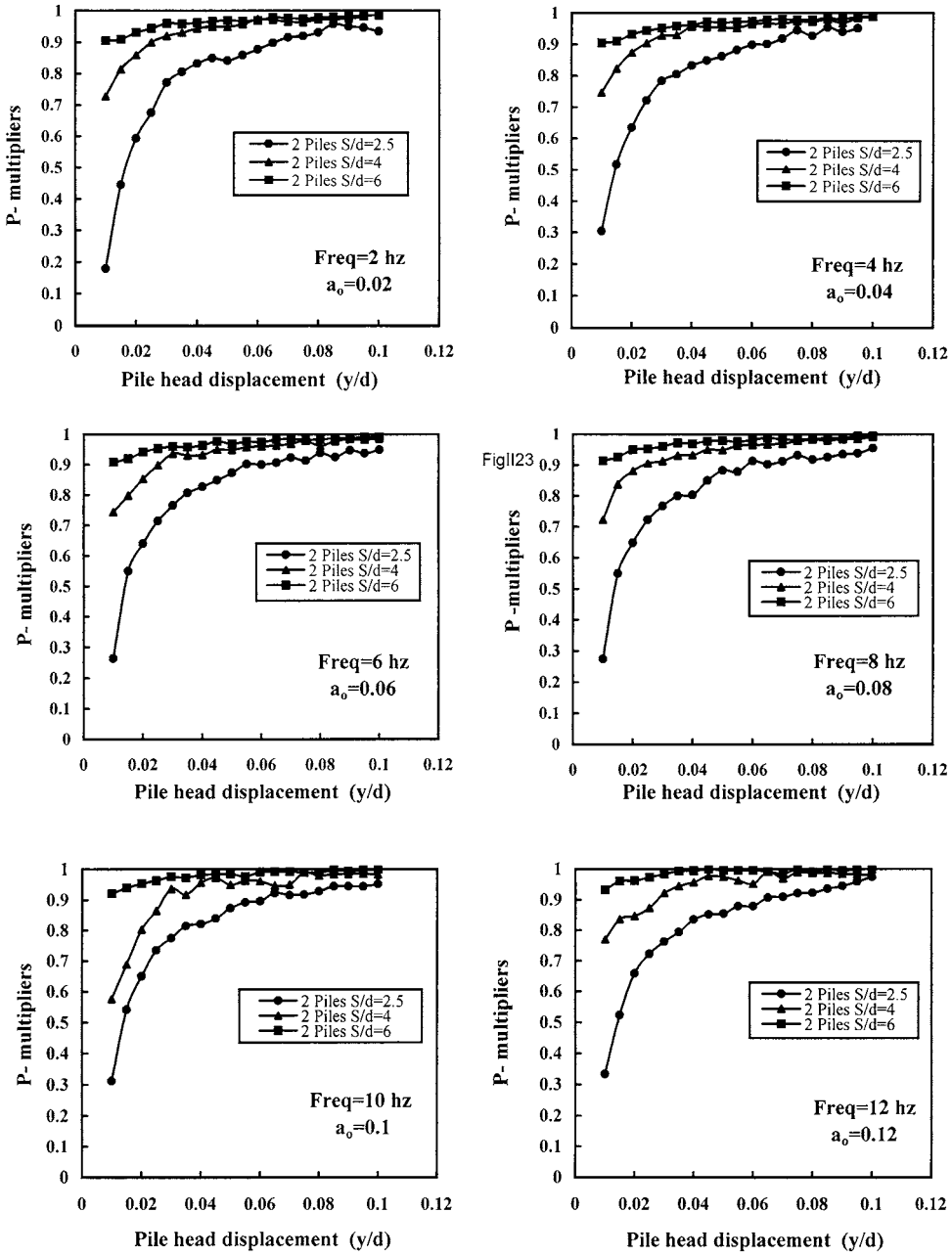

Figure B-41. p-*Multipliers versus pile-head displacement for loose sand.*

soil stiffness in the context of a Winkler model. The piles were assumed to be vertical and circular, although piles with other cross sections can be modeled by simply computing an equivalent radius r_0 for the noncircular pile. The piles were modeled using standard beam elements. A practically accurate and computationally efficient model was developed to represent the soil reactions. This model accounted for soil nonlinearity, slippage and gapping at the pile-soil interface, and viscous and material damping.

Dynamic soil reactions (dynamic *p-y* curves) were generated for a range of soil types and harmonic loading with varying frequencies applied at the pile head. Closed-form solutions were derived from regression analysis relating the static *p-y* curve, dimensionless frequency, and apparent velocity of the soil particles. That model is summarized in Equation B-27, which converts a static *p-y* model into an approximate dynamic model by multiplying *p*-values on the static *p-y* curve (such as the API sand curve) by a factor that is dependent upon both frequency and lateral pile displacement relative to the pile diameter. Several curve-fitting parameters that were necessary to write Equation B-27 in closed form from the results of numerous numerical solutions are given in Table B-2.

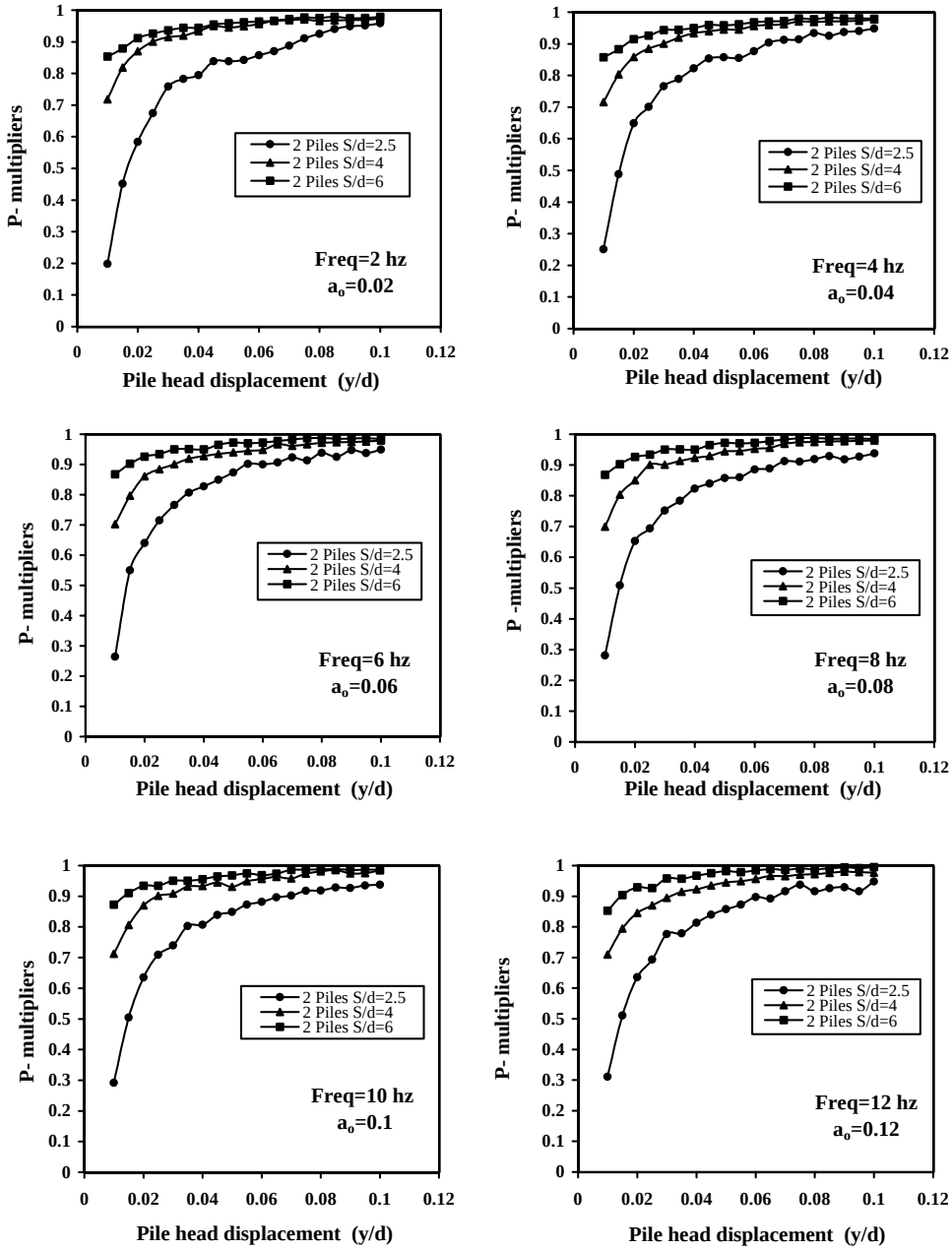

Figure B-42. p-*Multipliers versus pile-head displacement for medium-dense sand.*

Although the dynamic *p-y* curves are frequency dependent, they are approximately frequency independent for frequencies above about 10 Hz (ω = 62.8 radians). This model is included in FLPIER (see Appendix C), although verification against full-scale or centrifuge tests on piles using this relationship was not accomplished with FLPIER within the timeframe limitations of this project.

A simple spring-and-dashpot model was also proposed whose constants were established by splitting the dynamic *p-y* curves into real (stiffness) and imaginary (damping) components. The model is summarized in Equation B-29, in which a displacement-dependent soil stiffness, *k*, is determined from Equation B-31 and displacement- and frequency-dependent damping is determined from Equation B-32. This model appears to be most accurate for dimensionless frequencies ($a_0 = \omega r_0/V_s$) > 0.02. This model is intended to be used in programs that employ equivalent linear analyses for harmonic loading at the pile head.

The proposed dynamic *p-y* curves and the spring-and-dashpot model were incorporated into a commercial finite element program (ANSYS) that was used to compute the response of a laterally loaded pile. The computed responses

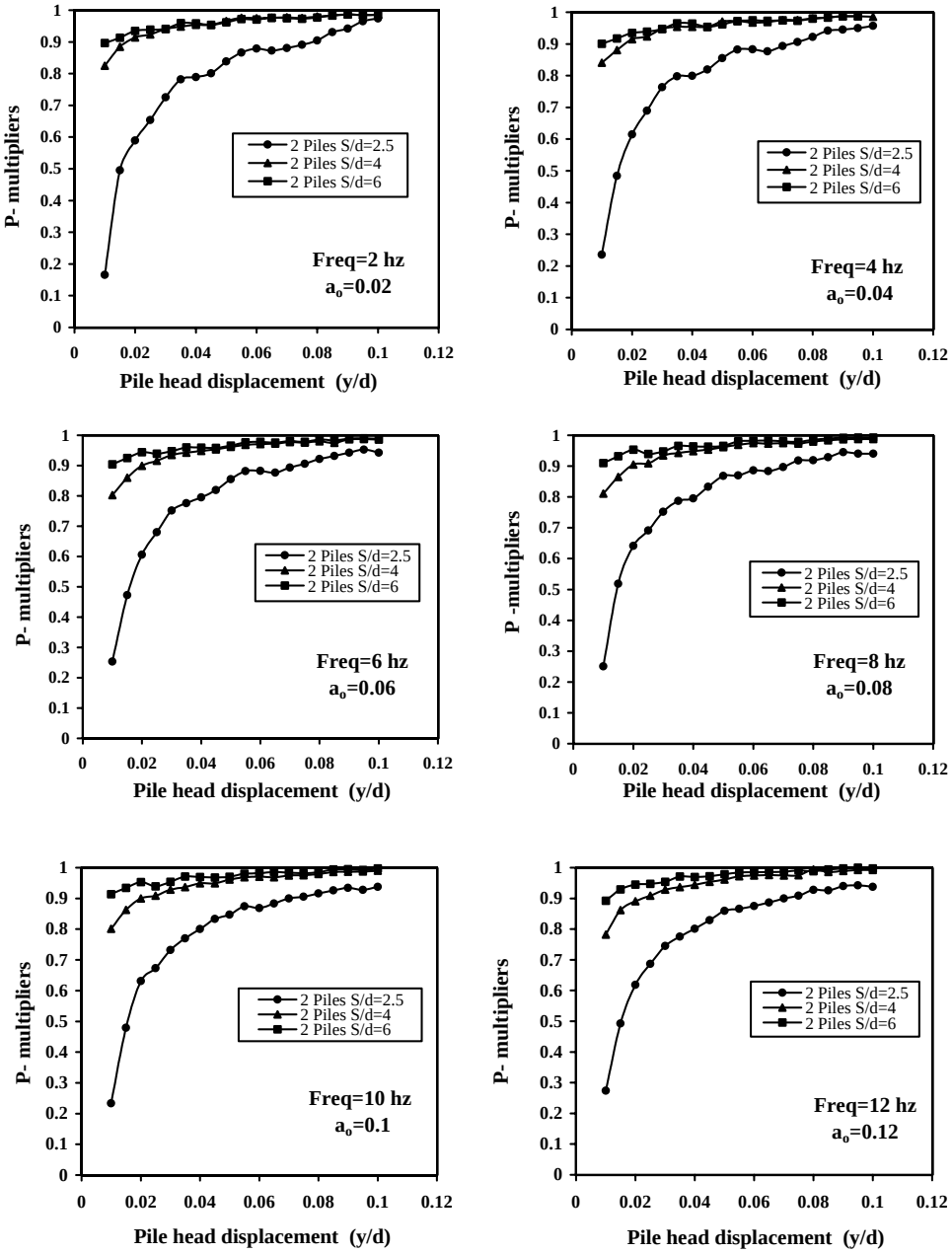

Figure B-43. p-*Multipliers versus pile-head displacement for dense sand.*

compared well with the predictions of the two-dimensional analysis.

The group effect (lateral pile-soil-pile interaction through the soil) was considered in the analysis, and a procedure for the development of dynamic *p*-multipliers for sand profiles was proposed. Like the *p-y* curves, the *p*-multipliers are frequency dependent; however, based on limited evidence given herein (see Figures B-41 through B-43), the *p*-multipliers for loose through dense sand can be treated in design practice as frequency independent in the frequency range $a_0 = \omega r_0 / V_s = 0.02$ to 0.12, especially for pile-head displacements (y) equal to or greater than 0.2 d, where d is the pile diameter (or equivalent diameter for noncircular piles). Such displacements are typical of those for which solutions are needed for extreme-event loading.

For relatively low frequencies, the predominant frequency of the earthquake motion being modeled can be used to compute the values on the *p-y* curves. However, for cases in which inertial behavior is stronger than kinematic behavior (the piles are driven by inertial superstructure feedback rather than the kinematic motion of the surrounding soil), the natural frequency of the structure being modeled may be the controlling predominant frequency, ω, to be used in evaluating the dynamic *p-y* curves and *p*-multipliers. Selec-

tion of a value for ω must therefore be done carefully by the user of the model (Equations B-27, B-29, B-30, and B-32). If the user decides that the primary frequency at the pile head will be 10 Hz or greater, the *p-y* model can be evaluated by setting ω = 62.8 radians/s in the expression for a_0, and the curve can be treated as frequency independent.

The dynamic *p-y* curves and the dynamic *p*-multipliers can then be used to model the dynamic lateral behavior of pile groups approximately, either in FLPIER or in other software that uses *p-y* models for the soil.

Recommendations for Further Development

The dynamic *p*-multipliers have been developed exclusively for sand profiles (in which strength and stiffness increase with depth). Time and resources did not permit a corresponding development for clay profiles. Further development of the model should include the development of *p*-multipliers for clay profiles (uniform strength stiffness with depth) and for mixed soil profiles. The model should also be used directly in FLPIER (see Appendix C) to ensure that it is performing properly in the context of that computer code.

REFERENCES—APPENDIX B

1. *General Finite Element Analysis Program*, Version 5.4. ANSYS, Inc. (1996).
2. Wu, G., and W. D. L. Finn. "Dynamic Nonlinear Analysis of Pile Foundations Using Finite Element Method in the Time Domain," *Canadian Geotechnical Journal*, Vol. 34 (1996); pp. 44–52.
3. Trochanis, A. M., J. Bielak, and P. Christiano. "A Three-Dimensional Nonlinear Study of Piles Leading to the Development of a Simplified Model," Technical Report National Science Foundation Grant No. ECE-86/1060, Carnegie Mellon University (1988).
4. "Recommended Practice for Planning, Designing and Constructing Fixed Offshore Platforms," *API Recommended Practice 2A* (19th edition). American Petroleum Institute (1991); pp. 47–55.
5. Novak, M., and H. Mitwally. "Transmitting Boundary for Axisymmetrical Dilation Problems." *Journal of Engineering Mechanics*, ASCE, Vol. 114, No. 1, (1988); pp. 181–187.
6. National Center for Earthquake Engineering Research Information Service, State University of New York at Buffalo website: nceer.eng.buffalo.edu (1998).
7. Kramer, S. L. *Geotechnical Earthquake Engineering.* Prentice-Hall (1996).
8. El Sharnouby, B., and M. Novak. "Static and Low Frequency Response of Pile Groups," *Canadian Geotechnical Journal*, Vol. 22, No. 2 (1985); pp. 79–84.
9. Poulos, H. G., and E. H. Davis. *Pile Foundation Analysis and Design.* John Wiley and Sons (1980).
10. Idriss, I. M., and J. I. Sun. "Modifications to SHAKE Program Published in Dec. 1972 by Schnabel, Lysmer & Seed," *User's Manual for SHAKE91* (with Accompanying Program), Center for Geotechnical Modeling, University of California at Berkeley (1992).
11. Takemiya, H., and Y. Yamada. "Layered Soil-Pile-Structure Interaction," *Earthquake Engineering and Structural Dynamics*, Vol. 9 (1981); pp. 437–457.
12. Flores-Berrones, R., and R. V. Whitman. "Seismic Responses of End-Bearing Piles," *Journal of Geotechnical Engineering*, ASCE, Vol. 108 (1982); pp. 555–569.
13. Gazetas, G. "Seismic Response of End-Bearing Piles," *International Journal of Soil Dynamics and Earthquake Engineering*, Vol. 3, No. 2 (1984); pp. 82–93.
14. Tazoh, T., T. Wakahara, and K. Shimizu. "Effective Motion of Group Pile Foundation," *Proceedings, 9th World Conference on Earthquake Engineering*, Vol. III (1988).
15. Ahmad, S., and S. M. Mamoon. "Seismic Response of Floating Piles to Obliquely Incident Waves," *Proceedings, 2nd International Conference on Recent Advances in Geotechnical Earthquake Engineering and Soil Dynamics*, Vol. I, St. Louis, MO (1991); pp. 805–813.
16. Fan, K., G. Gazetas, A. Kaynia, E. Kausel, and S. Ahmad. "Kinematic Seismic Response of Single Piles and Pile Groups," *Journal of Geotechnical Engineering*, ASCE, Vol. 117, No. 12, (1991); pp. 1860–1879.
17. Kaynia, A. M., and E. Kausel. "Dynamic Stiffnesses and Seismic Response of Pile Groups," *Research Report.* Massachusetts Institute of Technology (1982).
18. Makris, N., and G. Gazetas. "Dynamic Pile-Soil-Pile Interaction, Part II: Lateral and Seismic Response," *Earthquake Engineering and Structural Dynamics*, Vol. 21 (1992); pp. 145–162.
19. Novak, M., T. Nogami, and F. Aboul-Ella. "Dynamic Soil Reactions for Plane Strain Case," *Journal of the Engineering Mechanics Division*, ASCE, Vol. 104 (1978); pp. 953–959.
20. Gazetas, G., and R. Dobry. "Horizontal Response of Piles in Layered Soils," *Journal of Geotechnical Engineering*, ASCE, Vol. 110, No. 1 (1984); pp. 20–40.
21. Nogami, T., K. Konagai, J. Otani, and H. L. Chen. "Nonlinear Soil-Pile Interaction Model for Dynamic Lateral Motion," *Journal of Geotechnical Engineering*, ASCE, Vol. 118, No. 1 (1992); pp. 106–116.
22. El Naggar, M. H., and M. Novak. "Nonlinear Lateral Interaction in Pile Dynamics," *Journal of Soil Dynamics and Earthquake Engineering*, Vol. 14, No. 3 (1995); pp. 141–157.
23. El Naggar, M. H., and M. Novak. "Nonlinear Analysis for Dynamic Lateral Pile Response," *Journal of Soil Dynamics and Earthquake Engineering*, Vol. 15, No. 4 (1996); pp. 233–244.
24. Novak, M., and M. Sheta. "Dynamic Response of Piles and Pile Groups," *Proceedings, 2nd International Conference on Numerical Methods in Offshore Piling*, Austin (1982); pp. 489–507.
25. Hardin, B. O., and W. L. Black. "Vibration Modulus of Normally Consolidated Clay," *Journal of the Soil Mechanics and Foundations Division*, ASCE, Vol. 94, No. SM2 (1968); pp. 353–369.
26. Matlock, H. "Correlations for Design of Laterally Loaded Piles in Soft Clay," *Proceedings, 2nd Offshore Technology Conference*, Vol. 1, Houston (1970); pp. 577–588.
27. Bhushan, K., S. C. Haley, and P. T. Fong. "Lateral Load Tests on Drilled Piers in Stiff Clays," *Journal of the Geotechnical Engineering Division*, ASCE, Vol. 105, No. GT8 (1979); pp. 969–985.

28. Reese, L. C., and R. C. Welch. "Lateral Loading of Deep Foundations in Stiff Clay," *Journal of the Geotechnical Engineering Division,* ASCE, Vol. 101, No. GT7 (1975); pp. 633–649.
29. Reese, L. C., W. R. Cox, and F. D. Koop. "Field Testing and Analysis of Laterally Loaded Piles in Stiff Clay," *Proceedings, 7th Annual Offshore Technology Conference,* Vol. 2, Houston (1975); pp. 671–690.
30. Desai, C. S., and T. H. Wu. "A General Function for Stress-Strain Curves," *Proceedings, 2nd International Conference on Numerical Methods in Geomechanics,* ASCE, Vol. 1 (1976); pp. 306–318.
31. Abendroth, R. E., and L. F. Greimann. "Pile Behavior Established from Model Tests" *Journal of Geotechnical Engineering,* ASCE, Vol. 116, No. 4 (1990); pp. 571–588.
32. Reese, L. C., W. R. Cox, and F. D. Koop. "Analysis of Laterally Loaded Piles in Sand," *Proceedings, 6th Annual Offshore Technology Conference,* Vol. 2, Houston (1974); pp. 473–483.
33. Bhushan, K., L. J. Lee, and D. B. Grime. "Lateral Load Tests on Drilled Piers in Sand," *Drilled Piers and Caissons,* M. W. O'Neill (ed.); ASCE (1981); pp. 131–143.
34. Bhushan, K., and S. Askari. "Lateral Load Tests on Drilled Pier Foundations for Solar Plant Heliostats" Laterally Loaded Piles, *ASTM STP 835,* J. A. Langer (ed.), ASTM (1984); pp. 141–155.
35. Bhushan, K., and S. C. Haley. "Development of Computer Program Using P-Y Data from Load Test Results for Lateral Load Design of Drilled Piers," Research report prepared for Woodward-Clyde Consultants Professional Development Committee (1980).
36. Meyer, B. J., and L. C. Reese. "Analysis of Single Piles Under Lateral Loading" *Research Report 244-1,* Center for Highway Research, University of Texas at Austin (1979) pp. 1–145.
37. Idriss, I. M., R. Dobry, and R. D. Singh. "Nonlinear Behavior of Soft Clays During Cyclic Loading," *Journal of the Geotechnical Engineering Division,* ASCE, Vol. 104, No. GT12 (1978); pp. 1427–1447.
38. El Naggar, M. H. "Interpretation of Lateral Statnamic Load Test Results" *Geotechnical Testing Journal,* ASTM, Vol. 21, No. 3 (1998); pp. 169–179.
39. Focht, J. A., Jr., and K. J. Koch. "Rational Analysis of the Lateral Performance of Offshore Pile Groups," *Proceedings, Offshore Technology Conference,* Dallas (1973).
40. Cox, W. R., D. A. Dixon, and B. S. Murphy. "Lateral Load Tests on 25.4-mm (1-in.) Diameter Piles in Very Soft Clay in Side-by-Side and In-Line Groups," *STP 835,* ASTM (1984); pp. 122–139.
41. Brown, D. A., C. Morrison, and L. C. Reese. "Lateral Load Behaviour of Pile Group in Sand," *Journal of Geotechnical Engineering,* ASCE, Vol. 114, No. 11 (1988); pp. 1326–1343.
42. Brown, D. A., and H. Bollman. "Pile Group Design for Lateral Loading Using COM 624," *Proceedings, Conference on the Design of Bridges for Extreme Events,* U.S. DOT, FHWA (1996).

APPENDIXES C THROUGH F

UNPUBLISHED MATERIAL

Appendixes C through F contained in the research agency's final report are not published herein. For a limited time, loan copies are available on request to NCHRP, Transportation Research Board, Box 289, Washington, D.C., 20055. The appendixes are titled as follows:

- Appendix C: Dynamic Model for Laterally Loaded Pile Groups—Computational Model (FLPIER);
- Appendix D: Testing at Wilmington, North Carolina;
- Appendix E: Testing at Spring Villa NGES, Alabama; and
- Appendix F: Calibration of Strain Gauges and Correction of Raw Strain Data.

The **Transportation Research Board** is a unit of the National Research Council, which serves the National Academy of Sciences and the National Academy of Engineering. The Board's mission is to promote innovation and progress in transportation by stimulating and conducting research, facilitating the dissemination of information, and encouraging the implementation of research results. The Board's varied activities annually draw on approximately 4,000 engineers, scientists, and other transportation researchers and practitioners from the public and private sectors and academia, all of whom contribute their expertise in the public interest. The program is supported by state transportation departments, federal agencies including the component administrations of the U.S. Department of Transportation, and other organizations and individuals interested in the development of transportation.

The National Academy of Sciences is a private, nonprofit, self-perpetuating society of distinguished scholars engaged in scientific and engineering research, dedicated to the furtherance of science and technology and to their use for the general welfare. Upon the authority of the charter granted to it by the Congress in 1863, the Academy has a mandate that requires it to advise the federal government on scientific and technical matters. Dr. Bruce M. Alberts is president of the National Academy of Sciences.

The National Academy of Engineering was established in 1964, under the charter of the National Academy of Sciences, as a parallel organization of outstanding engineers. It is autonomous in its administration and in the selection of its members, sharing with the National Academy of Sciences the responsibility for advising the federal government. The National Academy of Engineering also sponsors engineering programs aimed at meeting national needs, encourages education and research, and recognizes the superior achievements of engineers. Dr. William A. Wulf is president of the National Academy of Engineering.

The Institute of Medicine was established in 1970 by the National Academy of Sciences to secure the services of eminent members of appropriate professions in the examination of policy matters pertaining to the health of the public. The Institute acts under the responsibility given to the National Academy of Sciences by its congressional charter to be an adviser to the federal government and, upon its own initiative, to identify issues of medical care, research, and education. Dr. Kenneth I. Shine is president of the Institute of Medicine.

The National Research Council was organized by the National Academy of Sciences in 1916 to associate the broad community of science and technology with the Academy's purpose of furthering knowledge and advising the federal government. Functioning in accordance with general policies determined by the Academy, the Council has become the principal operating agency of both the National Academy of Sciences and the National Academy of Engineering in providing services to the government, the public, and the scientific and engineering communities. The Council is administered jointly by both the Academies and the Institute of Medicine. Dr. Bruce M. Alberts and Dr. William A. Wulf are chairman and vice chairman, respectively, of the National Research Council.

Abbreviations used without definitions in TRB publications:

AASHO	American Association of State Highway Officials
AASHTO	American Association of State Highway and Transportation Officials
ASCE	American Society of Civil Engineers
ASME	American Society of Mechanical Engineers
ASTM	American Society for Testing and Materials
FAA	Federal Aviation Administration
FHWA	Federal Highway Administration
FRA	Federal Railroad Administration
FTA	Federal Transit Administration
IEEE	Institute of Electrical and Electronics Engineers
ITE	Institute of Transportation Engineers
NCHRP	National Cooperative Highway Research Program
NCTRP	National Cooperative Transit Research and Development Program
NHTSA	National Highway Traffic Safety Administration
SAE	Society of Automotive Engineers
TCRP	Transit Cooperative Research Program
TRB	Transportation Research Board
U.S.DOT	United States Department of Transportation

THE NATIONAL ACADEMIES

Advisers to the Nation on Science, Engineering, and Medicine

National Academy of Sciences
National Academy of Engineering
Institute of Medicine
National Research Council